

**The deep structure of  
Gaussian scale space images**

## Colophon

The image of the cover is a photograph by Helma Kuijper of one of her “topological” spatial objects, entitled *untitled*. It was recognised by the author of this thesis as an attempt to popularise the deep structure of Gaussian scale space, and in particular scale space critical curves. He consequently baptised the scene (being the art work), as well as the image (sic!), as *Natural Trees Spanning Artificial Critical Curves*.

This thesis was prepared using the  $\text{\LaTeX}$  2<sub>ε</sub> typesetting language. The main body of the text was set using a 11-points Times Roman font at A4 paper size. Figures were obtained using Mathematica (a product of Wolfram Research Inc.) and converted to Encapsulated PostScript (registered trademark of Adobe Systems inc.). The final PostScript version was converted to Portable Document Format (PDF), B5 paper size, and transferred to film for printing.

Copyright © 2002 by Arjan Kuijper. All rights reserved. No part of this publication may be reproduced or transmitted in any form or by any means, electronic or mechanical, including photocopy, recording, or any information storage and retrieval system, without permission in writing from the author.

ISBN 90–393–3061–1

Printed by PrintPartners Ipskamp B.V., Enschede.

# **The deep structure of Gaussian scale space images**

De diepe structuur van Gaussische schaalruimte beelden  
(met een samenvatting in het Nederlands)

PROEFSCHRIFT

TER VERKRIJGING VAN DE GRAAD VAN DOCTOR AAN DE UNIVERSITEIT UTRECHT OP  
GEZAG VAN DE RECTOR MAGNIFICUS, PROF. DR W.H. GISPEN, INGEVOLGE HET BESLUIT  
VAN HET COLLEGE VOOR PROMOTIES IN HET OPENBAAR TE VERDEDIGEN OP MAANDAG  
17 JUNI 2002 DES MIDDAGS TE 16.15 UUR

DOOR

**Arjan Kuijper**

GEBOREN OP 23 DECEMBER 1970, TE ALKMAAR

promotor: Prof. dr ir M.A. Viergever  
Faculteit Wiskunde en Informatica  
Universiteit Utrecht

copromotor: Dr L.M.J. Florack  
Faculteit Biomedische Technologie  
Technische Universiteit Eindhoven

The research described in this thesis was carried out at the Image Sciences Institute, Institute of Information and Computing Sciences, Faculty of Mathematics and Computer Science, Utrecht University (Utrecht, the Netherlands), under the auspices of ImagO, the Graduate School for Biomedical Image Sciences.

Financial support for publication of this thesis was kindly provided by ImagO and Utrecht University.

The challenge is to understand the image  
really on all the levels simultaneously,  
and not as an unrelated set of derived images  
at different levels of blurring.

J.J. KOENDERINK

Commissie: Prof. dr ir B.M. ter Haar Romeny  
Faculteit Biomedische Technologie  
Biomedische Beeldverwerking, Technische Universiteit Eindhoven

Prof. dr P. Johansen  
Faculty of Natural Sciences  
Department of Computer Science, University of Copenhagen, Denmark

Prof. dr ir M.H. Overmars  
Faculteit Wiskunde en Informatica,  
Instituut voor Informatica en Informatiekunde, Universiteit Utrecht

Prof. dr D. Siersma  
Faculteit Wiskunde en Informatica,  
Mathematisch Instituut, Universiteit Utrecht

Prof. dr J. Weickert  
Faculty of Mathematics and Computer Science  
Saarland University, Saarbrücken, Germany

---

# Contents

---

<b>Contents</b>	<b>vii</b>
<b>1 Introduction and Summary</b>	<b>1</b>
1.1 Introduction . . . . .	1
1.1.1 Images . . . . .	2
1.1.2 Image Formation . . . . .	2
1.1.3 Image Analysis . . . . .	3
1.1.4 More and More Data . . . . .	3
1.1.5 About Trees and a Forest . . . . .	4
1.1.6 The Combination is More than the Sum of the Parts . . . . .	4
1.2 Summary of this Thesis . . . . .	5
1.2.1 Chapter 2 . . . . .	5
1.2.2 A Deep Thought on Deep Structure . . . . .	6
1.2.3 Chapter 3 . . . . .	6
1.2.4 Chapter 4 . . . . .	6
1.2.5 Chapter 5 . . . . .	7
1.2.6 Chapter 6 . . . . .	8
1.2.7 Chapter 7 . . . . .	8
1.2.8 Chapter 8 . . . . .	8
1.3 Conclusions . . . . .	9
<b>2 Gaussian Scale Space</b>	<b>11</b>
2.1 Scale Space Basics . . . . .	12
2.1.1 The Beginning . . . . .	12
2.1.2 Physical Properties . . . . .	13
2.1.3 Theory of Distributions . . . . .	14
2.1.4 Uncommittedness . . . . .	14

2.1.5	Regularisation . . . . .	16
2.1.6	Entropy . . . . .	16
2.2	Differential Equations . . . . .	17
2.2.1	Heat Equation . . . . .	17
2.2.2	Partial Differential Equations . . . . .	18
2.3	Biological Inspiration . . . . .	19
2.4	Hierarchies . . . . .	19
2.4.1	Multi-Scale Watershed . . . . .	20
2.5	Two Decades of Linear Scale Space . . . . .	20
2.5.1	Sub-Structures . . . . .	21
2.5.2	Deep Structure . . . . .	21
2.5.3	Poisson Scale Space . . . . .	21
<b>3</b>	<b>Saddle Points in 2D</b>	<b>23</b>
3.1	Introduction . . . . .	23
3.2	Critical Points: Continuous versus Discrete . . . . .	23
3.2.1	The Euler Number . . . . .	24
3.3	Neighbourhoods . . . . .	24
3.3.1	Rectangular Grids . . . . .	24
3.3.2	Hexagonal Grids . . . . .	25
3.4	Construction of a Hexagonal Lattice . . . . .	25
3.4.1	Horn . . . . .	26
3.4.2	Blom . . . . .	26
3.4.3	Types of Hexagonal Grid Points . . . . .	26
3.5	Conclusions . . . . .	28
<b>4</b>	<b>Topological Structure</b>	<b>29</b>
4.1	Introduction . . . . .	30
4.1.1	Historical Background . . . . .	30
4.1.2	Scale and Topology . . . . .	30
4.1.3	Deep Structure . . . . .	30
4.1.4	Catastrophe Theory . . . . .	30
4.1.5	Canonical versus Covariant Formalism . . . . .	31
4.2	Theory . . . . .	31
4.2.1	Catastrophe Theory . . . . .	31
4.2.2	Catastrophe Theory and the Scale Space Paradigm . . . . .	32
4.2.3	Canonical Formalism . . . . .	33
4.2.4	Covariant Formalism . . . . .	35
4.3	Experimental Results . . . . .	44
4.3.1	Visualisation of $\mathbf{z}^T$ and $\bar{\mathbf{w}}$ . . . . .	44
4.3.2	Location of the Catastrophe . . . . .	44
4.3.3	Fraction of the Area Where $\det \mathbf{M} > 0$ . . . . .	47
4.3.4	Estimation of the Area Where $\det \mathbf{M} > 0$ . . . . .	49
4.4	Conclusion and Discussion . . . . .	50



4.5	Appendix: Determinants and Cofactor Matrices . . . . .	51
<b>5</b>	<b>Scale Space Hierarchy</b>	<b>53</b>
5.1	Introduction . . . . .	53
5.1.1	Scale Space . . . . .	53
5.1.2	Deep Structure . . . . .	54
5.1.3	Related Work . . . . .	54
5.1.4	Aim . . . . .	54
5.2	Theory . . . . .	55
5.2.1	Deep Structure in Gaussian Scale Space . . . . .	56
5.2.2	Scale Space Critical Points . . . . .	57
5.2.3	Properties of Critical Curves in Scale Space . . . . .	59
5.2.4	The Structure of Iso-Intensity Manifolds . . . . .	61
5.3	Scale Space Hierarchy and Pre-Segmentation . . . . .	62
5.3.1	Scale Space Hierarchy . . . . .	62
5.3.2	Segmentation . . . . .	66
5.4	Applications . . . . .	67
5.4.1	1D Signals . . . . .	67
5.4.2	2D Images . . . . .	67
5.5	Conclusions and Discussion . . . . .	77
5.6	Appendix: Critical Curves and Manifolds . . . . .	77
<b>6</b>	<b>The Application of Catastrophe Theory</b>	<b>81</b>
6.1	Introduction . . . . .	81
6.1.1	Scale Space . . . . .	81
6.1.2	Deep Structure . . . . .	82
6.1.3	Related Work . . . . .	82
6.1.4	Aim . . . . .	83
6.2	Theory . . . . .	83
6.2.1	Gaussian Scale Space . . . . .	84
6.2.2	Scale Space Saddles . . . . .	85
6.2.3	Catastrophe Theory . . . . .	85
6.2.4	Scale Space Hierarchy . . . . .	88
6.3	Scale Space Catastrophes and Scale Space Saddles . . . . .	89
6.3.1	1D Images . . . . .	89
6.3.2	$n$ -D Images, $n > 1$ . . . . .	92
6.3.3	Morsification Summary . . . . .	100
6.4	Applications . . . . .	101
6.4.1	Artificial Image . . . . .	101
6.4.2	Simulated MR Image . . . . .	102
6.5	Summary and Discussion . . . . .	103

<b>7</b>	<b>Modelling Non-Generic Events</b>	<b>105</b>
7.1	Introduction . . . . .	105
7.1.1	Scale Space History . . . . .	106
7.1.2	Deep Structure . . . . .	106
7.1.3	Related Work . . . . .	106
7.1.4	Aim . . . . .	107
7.2	Theory . . . . .	107
7.2.1	Gaussian Scale Space . . . . .	107
7.2.2	Catastrophe Theory . . . . .	108
7.2.3	Catastrophes and Scale Space . . . . .	109
7.3	Scale Space Catastrophe Models . . . . .	112
7.3.1	$A_2$ Fold Catastrophe . . . . .	113
7.3.2	$A_3$ Cusp Catastrophe . . . . .	113
7.3.3	$D_4^\pm$ Umbilic Catastrophes . . . . .	114
7.3.4	$D_5^\pm$ Parabolic Umbilic Catastrophes . . . . .	119
7.3.5	$D_6^\pm$ Second Umbilic Catastrophes . . . . .	119
7.3.6	Other Non-Generic Catastrophes . . . . .	122
7.3.7	Morsification Summary . . . . .	123
7.4	Applications . . . . .	123
7.4.1	$D_4^-$ Catastrophe . . . . .	123
7.4.2	$D_6^-$ Catastrophe . . . . .	124
7.5	Discussion . . . . .	127
<b>8</b>	<b>Logical Filtering</b>	<b>129</b>
8.1	Introduction . . . . .	129
8.2	Theory . . . . .	130
8.2.1	Gaussian Scale Space . . . . .	130
8.2.2	Scale Space Hierarchy . . . . .	132
8.2.3	Logical Filtering . . . . .	133
8.3	Properties of the Vector Field . . . . .	133
8.3.1	Local Environment . . . . .	135
8.3.2	Morse Critical Points . . . . .	135
8.3.3	Critical Points at Catastrophes . . . . .	137
8.3.4	Critical Points with Vanishing Laplacean . . . . .	137
8.3.5	Non-Critical Points with Vanishing Laplacean . . . . .	137
8.3.6	Examples . . . . .	137
8.4	Deep Structure . . . . .	141
8.4.1	Manifolds and Segments . . . . .	141
8.4.2	Hierarchy Algorithm . . . . .	148
8.4.3	Visualisation and Simplification . . . . .	149
8.5	Results . . . . .	150
8.5.1	Blob Image . . . . .	150
8.5.2	MR Image . . . . .	152
8.6	Summary and Discussion . . . . .	158

<b>Bibliography</b>	<b>161</b>
<b>Publications</b>	<b>179</b>
<b>Inleiding en samenvatting</b>	<b>181</b>
<b>Dankwoord</b>	<b>191</b>
<b>Curriculum Vitae</b>	<b>195</b>



# CHAPTER 1

---

## Introduction and Summary

---

There is inherent in nature a hidden harmony that reflects itself in our minds under the image of simple mathematical laws. That then is the reason why events in nature are predictable by a combination of observation and mathematical analysis. Again and again in the history of physics this conviction, or should I say this dream, of harmony in nature has found fulfilments beyond our expectations.

---

HERMANN WEIL

### 1.1 Introduction

In this computer era, a huge number of images of them emerge from computers<sup>1</sup>. Computers offer great advantages for images in the way of derivation, storage, manipulation, multiplication, transmission, and so on.

---

<sup>1</sup>Even the one on the cover of this thesis.

### 1.1.1 Images

In general, a human inspector knows both the content of the image and its purpose. In this sense images serve only as *additional* information of the written story. The contrary, however, is also possible: the image may be the *subject* that needs clarification. An intriguing question is whether it is possible to manipulate the computer data such that its content, or meaning, becomes clearer or more explicit with as few human-machine interactions as possible. In order to achieve this, several observations have to be taken into consideration:

- There is “something” in the real world that is captured by the image, for instance persons, planes, stars, or brain tumours.
- “It” is only digitally present on the computer. Only combinations of “zeros and ones” are present and organised such that “it” can be visualised.
- “Something” needs to be done with “it”, for example: Emphasise or extract more relevant parts.
- Whatever is done, should be done in a meaningful and reproducible way. It is not difficult to play around with images, sweep parts out, and draw moustaches, but that is obviously not what is wanted.
- The outcome of what is done should be presented in a efficacious manner.

The reader is of course free to add extra requirements.

The acquisition of computer data, shortly named *image formation*, as well as the analysis of the computer data representing “something”, shortly named *image analysis*, involve interactions with multiple scientific disciplines, varying from mathematics, via *e.g.* biology and computer science, to physics. For instance, in the early years of image analysis most investigation took place on signals like radar and sonar by the electric engineering society, whereas nowadays medical imaging is topic of a large part of the research.

### 1.1.2 Image Formation

How real life scenes are captured by “observation machines”, like CCD cameras, MR scanners, or telescopes, can be described by *physical “laws”*. These laws are rules dictated by the intrinsic properties of the observation machine. Generally they do not have any what so ever a priori relation to the real life scene itself. So although we can take images of everything, the image formation is not related to details of the *outside* “scene”.

However, the initial images, also called (raw) data, are obtained by the observation machines and thus heavily depend on the settings of the parameters *inside* the observation machine. For instance, a close-up picture can not be extended to a panoramic picture. The same holds for the opposite if the same resolution is wanted. The outcome of an MR scan contains extra information, like “T1” or “T2” weighted, yielding information about the way the measurement is taken. This doesn’t only imply that physics lies on the base of images, but also generates a loss of information, in the sense that the derived data only *partially* represents the real life scene. If the observation machine parameters are set properly, this is not really something to bother about, although it signals the limited value of further outcomes: if we want a close-up, we should simply take action beforehand. Another type of loss is implied in

the wish to obtain the data in an *organised, digitised* way in order to be able to make them accessible for computer storage, calculations, and representation. Although all observation machines have their physical limitations (photographic granularity, photon densities, magnetic spin), usually a fixed specific resolution and grid is set to obtain such sizes on the data, that they can still be handled. The real life scene is thus reduced to a set of single measurements nicely ordered on some grid.

### 1.1.3 Image Analysis

The next stage in a lot of cases is to *do* something with the data: they are obtained with some purpose. They are output of an image formation procedure, and in turn input to some image analysis task. So parts of the data may contain more relevant information than other parts and they need to be restored, emphasised or extracted. For instance: new milky ways, black holes, or planets with the possibility of life in astronomic data; brain tumours, aneurysms, or weak bones in medical images; license plates or possible suspects in forensic data; and so on. Here, obviously, a lot of human understanding and interpretation comes into sight. Mathematical models based on the assumed distortion of the image, on the intrinsic properties of the interesting objects, or *e.g.* on biological or medical knowledge are proposed, and implemented as computer algorithms. The outcome is validated and either used or rejected. In the latter case the model is adjusted, implemented, validated, and so on.

Here a remarkable fact comes clear. The validation may signal whether a model is good or bad – within the framework of the assumptions –, the rejection or usage of the results is often based on the human interpreter looking at the outcome. This judgement is clearly based on visual inspection of the resulting data, based on the interpreters skills and experience. For the models to produce well, they need to meet some kind of coherence to human vision and interpretation. Alternatively, the models need to simulate the human way of looking and interpreting in some sense. Therefore, also the field (neuro-)biology contributes in image analysis, investigating which mechanisms are involved in looking, transporting data to the brains and interpreting these data (and giving feedback to the eyes).

### 1.1.4 More and More Data

The exponential increase of computing facilities in the last decades of the previous century has led to a tremendous increase of data, both from observations – the image formation – and from the proposed models – the image analysis tasks. On the input side several reasons can be found:

- The number of acquisitions increased.
- The size of single acquisitions increased.
- The acquisitions became more complicated.

This was obviously enabled by the continuous increase free amount of storage space. In the field of medical imaging one can think of increasing number of MR images, with precision increased by a factor 2, 4 or more, and moving from two dimensional images to three dimensional images, and even time-sequences of them. On the output side also an increase took place. Computing time puts a heavy constraint on possible algorithms. Consequently, the algorithms in the early years of image analysis were simple and often based on one-step *filters*, a single operation on the two dimensional image in a rectangular grid. One can think of *edge detection* and *noise suppression*.

Increasing CPU speed led to an increasing *number* of proposed mathematical models and an increased *complexity*. Instead of one-step filters, multi-step filters were needed to represent the proposed models: a series of complicated operations on an image yields the output image. The models describe a desired situation of the image given some constraint(s), for example the requirement of both edge enhancement and noise suppression.

Also new tasks popped up, based on image *retrieval* from this tremendous number of available images. For example: “Find a picture of Rembrandt’s Homecoming of the Prodigal Son on the Internet.” Or: “Given an image of a needle, find its location (or similar ones) in a (hay) stack of images: an image database.” This kind of tasks naturally lead to the development of digital image management systems. Such systems are often referred to as Picture Archiving and Communication Systems (PACS). They are, for example, emerging in clinical and radiological environments.

Another new task is image *matching*: Do two images describe the same scene in some pre-described sense? And in stereo vision: can we reconstruct the three dimensional scene as best as possible given the two images of the left and the right eye.

### 1.1.5 About Trees and a Forest

This explosive growth of in- and output data urges for proper and transparent mathematical methods regulating them and prohibiting wild-growth: everything is possible, but not everything is useful. Even more (worse?), mathematical models and algorithms have a tendency to function as “black boxes”, whose output can be tuned with some parameters. Problems rose in several ways. To mention some:

- It is not always clear what kind of behaviour is to be expected when certain models are applied.
- The choice of the parameter tuning depends on the person working with the images and model, and the relation between the outcome and the parameter setting is not clear.
- It is sometimes not even clear what parameters “mean”, or what a combination of them imply.
- A slight change in the parameters sometimes leads to large differences in the output image.
- The raw data obviously consists of a discrete set of numbers. Thus it is not straightforward to apply continuous mathematical models to them.

The first three points mention the *ad-hoc nature*, the fourth item points out the so-called *ill-posedness*, and the last one signals a *conceptual problem*. In the last decade of the previous millennium the number of mathematicians interested in computer vision grew rapidly, since these problems can typically be explained by mathematical investigation of the models used. Computer vision appears to be a promising field of application for mathematics, even when the latter uses highly abstract theories that are not clear at all for non-mathematicians.

### 1.1.6 The Combination is More than the Sum of the Parts

Summarising, within the field of image analysis the combination of knowledge from physics, electric engineering, mathematics, (neuro-)biology and computer science, together with acquaintance of the field of the application of the particular image analysis task, is necessary to obtain meaningful results. The reader can guess that this huge area of science can impossibly be covered in one thesis.



## 1.2 Summary of this Thesis

In this thesis I restrict myself to the mathematics around the raw data, the initial image, that is digitally stored. I do not bother how these data are obtained, this is taken for granted. Neither is it known what they represent or what kind of special items might be present. Consequently, validation of results with respect to a specified high-level task like segmentation is *not* applicable, simply because I assume that there is no specified high-level task. The validation takes place on a different field. The *methods* and *models* used and derived should have a “meaning”. Consequently, the outcome should be predictable and understandable based on the methods and models. One may call this a specified low-level task based on the data, not on the image.

The following sections shortly describe the chapters of this thesis. Since the chapters (will) appear as articles, one will find some overlap in the descriptions of scale space and catastrophe theory in the “introduction” and “theory” sections of the various chapters. In order to maintain the readability of the chapters separately this was not altered.

### 1.2.1 Chapter 2

Chapter 2 discusses in more detail approaches to the last problem mentioned above, about the discrepancy between discrete data and continuous models. Mathematically this discrepancy is tackled by Schwartz’ “Theory of Distributions”. A physical approach, based on the “Pi theorem”, boils down to the idea of introducing the necessary parameter *scale*. Or better: the discovery of scale. Points of the image can only be interpreted, and dealt with, by scale. Under some assumptions, for instance that “nothing is known about the image”, solutions satisfying the mathematical requirements are found. Since there is no a priori preferred scale, all possible scales can (and must) be taken into account. The image is therefore extended with an extra dimension, scale, and this new image forms a *scale space*.

One of the solutions boils down to convolution of the initial image with a Gaussian profile whose width is related to scale. This scale space is therefore called *Gaussian scale space*. Furthermore, taking scale as a time parameter, this profile is the general solution of the so-called “*Diffusion Equation*”, or “*Heat Equation*”. This equation describes the spread of heat during time when a homogeneous plate is initially heated at several spots. As one can imagine, at the end (if we wait “infinitely” long) the whole plate has constant temperature. The same holds for the scale space image: at “infinite” coarse scale the image has constant value. Increasing scale thus yields blurring. An important property is its linearity, for which reason this scale space is a *linear scale space*.

From the end-user’s point of view, when using only single scale images, applying a scale space may reduce the amount of noise, but it blurs (away) everything, which may make it useless for *e.g.* segmenting tasks. Using all scales, on the other hand, is redundant. For this reason, also the other way round is taken: with the diffusion equation as a *starting* point, one may investigate its use for image analysis. Consequently, one may also investigate non-linear versions of it. Task specific information may be used for modelling, for which this approach is then denominated “*geometry driven diffusion*”. Going further, any partial derivative equation (PDE) can be used, yielding the infinite series of PDE-approaches. As mentioned before, then these approaches merely “are doing something for some purpose” with the data.

Returning to the linear diffusion equation, the relevance with respect to *biological modelling* of (stages of) vision comes into question. It appears that in the first stages of vision, light coming into the eye and the transportation of the visual stimulus to the brain, both Laplacean profiles and blurring occur.

This signals the possibility of using a Gaussian scale space as model for front-end vision. The scale space can be visualised by a stack of simplified versions of the image. During simplifying, regions disappear in a cascading way. Theoretically a *hierarchical structure* can be found: there are regions within regions.

A short review of some results of investigations of *Gaussian scale space* with respect to image analysis and its intrinsic properties in the last decades concludes this chapter. Readers familiar with (Gaussian) scale space can skip this chapter. In the following chapters I will assume familiarity with the scale space paradigm.

### 1.2.2 A Deep Thought on Deep Structure

Knowing that scale is important and that taking one single scale is not appropriate is one thing, it still doesn't *comprise* the notion of scale space. The relevance lies in investing Gaussian scale space *itself*, *i.e.* at all scales simultaneously. This has been called the *deep structure* of Gaussian scale space. The task is to investigate – and hopefully understand – what happens between two different scales, what mechanisms occur in gradually changing scale. That is the subject of the rest of this thesis.

Regarding the image as a height function, I restrict myself to the most elementary properties of this function: its critical points and some subsets of points with the same value. These points give an adequate description of an image, *cf.* a two dimensional image with its critical points (the minima, maxima, and saddles) and isophotes through the saddles. The latter enclose regions in the image.

### 1.2.3 Chapter 3

Having said this, one still encounters difficulties on applying mathematical actions (finding its critical points) on a discrete grid. In chapter 3, a short inter-mezzo, I explain problems that arise when using a *rectangular* grid: The horizontal and vertical neighbourhood relation, as well as its extension with the double diagonal neighbourhood relation give rise to mathematical and practical difficulties. A *hexagonal* grid solves these problems. It is also something that is present within the human vision system. And consequently something I will use, explaining how the present rectangular grid can be regarded as hexagonal.

### 1.2.4 Chapter 4

Once being able to detect critical points, it is time to *trace* them over scale. An important result coming from the mathematical field of singularity theory, shows that when increasing scale, spatial critical points can annihilate only pairwise. In two (and higher) dimensional images also creations of such pairs can occur. So if we look at a blurred series of images, we see the number of spatial critical points change. The locations in scale space where these annihilations and creations take place are called *catastrophe points*. In chapter 4 the movement of spatial critical points in scale space is investigated. In a single image at a calculated scale, critical points generally “lie between the grid points” (*i.e.* sub-pixel) and only their neighbouring points are found. Ideally, the movement is found using the tangent vector of the scale space critical path that they traverse. In the discrete case their movement can be estimated using perturbation theory yielding vectors in scale space pointing to the position of the critical point on a coarser scale with sub-pixel precision. By using also scale information, the location is predicted more precisely than only using spatial information. Things get complicated when the catastrophe points are involved. Then the

formulation used for critical points no longer hold and a more complicated expression is needed and given.

All expressions are given in an arbitrary co-ordinate system, the *covariant formulation*. This is an important notion, since all theoretical results are stated in so-called *canonical coordinates*. These coordinates are chosen such, that the system is nice and easy to describe and understand. In reality, however, one will almost never encounter this situation, because the coordinate system is typically chosen *beforehand* and not adapted to the particular local image configuration. Each catastrophe, however, can locally be transformed to this canonical description. The determinant of the matrix involved in the expression for finding catastrophe points is at the same time an indicator of whether the catastrophe point is a creation or an annihilation. Experiments show that the fraction of space where creations are “allowed” due to this sign of the determinant, is relatively small. This meets intuition, since it is known that more annihilations than creations are to be expected, due to the fact that all-but-one extrema are to vanish while increasing scale. Examples of the theory are given for two dimensional images.

### 1.2.5 Chapter 5

In Chapter 5 these results are used to build critical curves in scale space: the spatial critical points of the image at increasing scales are calculated and linked, thus forming critical branches of extrema and saddle points. The branches are connected at the catastrophe points thus forming the critical curves. Within the scale space image, catastrophe points are regular points. I show that the only critical points in scale space are *scale space saddle points*, lying on the saddle branches. Tracing the intensities of the critical points over scale, one finds that maxima decrease monotonically and minima increase monotonically. Saddle branches, however, can have local extrema with respect to the intensity. I show that these local extrema occur at the scale space saddles.

Using this property that extrema are suppressed due to the diffusion equation, it is obtained that iso-intensity manifolds in scale space that intersect the extremum branch are dome-shaped. If the manifold does not intersect a saddle branch, it encapsulates a closed region in scale space with its top at the intersection of the manifold with the extremum branch. Each extremum branch intersects a manifold that contains only one saddle, either a spatial saddle at the initial image, or a scale space saddle. This “*critical*” manifold forms the boundary of a nesting of closed regions. Consequently, to all extrema that annihilate a critical region can be assigned.

Due to the nesting property of Gaussian scale space, a hierarchy procedure follows in a straightforward manner. The regions define a “*pre-segmentation*” of the initial image. This special segmentation is obtained without any knowledge of the image in contrast to the usual definition of an arbitrary segmentation. It is a “complete” segmentation in the sense that all structurally (topologically) meaningful segments are accounted for. In practice it is typically an “over-segmentation”, since the entire image is divided into parts and several pre-segments will typically belong to a single “semantical” segments, *e.g.* a single tissue type in a MR image. It is conjectured – and this is at the same time its true significance – that a pre-segmentation is never an “under-segmentation”, for splitting up a pre-segment has no justification from the data evidence point of view. Of course, an expert user may impose his / her will by using external knowledge so as to force such a splitting nevertheless.

Note that the pre-segmentation is solely derived from the fact that a Gaussian scale space follows from the necessity of scale. I give examples of the described procedure and results.

### 1.2.6 Chapter 6

The aforementioned procedure uses the *generic* catastrophes: events with exactly two critical points. Sometimes it is necessary to assume that *non-generic* catastrophes occur, in which multiple critical points interact. This is the case when of three critical points only one remains, and one is not able to identify which pair annihilates. Sometimes one doesn't want to identify them, for instance if the image contains local symmetry. The extension of the hierarchical algorithm that is able to handle this special case is presented in chapter 6. Main advantage is that it *stabilises* the hierarchy tree. More symmetries – think of a checkerboard – can be implemented in a similar fashion.

I also discuss the *irrelevance* of the creation of critical points with respect to the tree and the pre-segmentation. From the notion of critical curves this is clear, since they only form protuberances of the critical curve in scale space. Finally, modelling non-generic local symmetry reveals that a single saddle branch can contain *multiple* scale space saddles. Since the critical region assigned to an extremum is obtained by the first manifold containing a saddle, of the multiple saddles on a saddle branch only one is relevant: in case of a minimum, the saddle with the lowest intensity value, in case of an extremum the one with the highest intensity value.

Some tests show the application of this theory.

### 1.2.7 Chapter 7

In the previous section I mentioned that creations “*only form protuberances of the critical curve in scale space*”. This fact needs a discussion in more detail. For that purpose an important result from “Catastrophe Theory” is used, namely a list polynomials describing catastrophes and their difficulty. The latter is represented by a number of parameters needed to remove a catastrophe point. Regarding scale as a parameter, it is clear that the usual catastrophe in scale space requires exactly one parameter. For the catastrophes mentioned in the previous section, multiple parameters are needed, *e.g.* for perturbing the local symmetry. In chapter 7, I investigate the list and adjust it such, that it satisfies the diffusion equation and is thus a scale space polynomial expression. The adjustment of polynomials with multiple parameters yields one special, namely scale. I show that by this adjustment *non-generic events* in scale space can be modelled. This yields not only multiple annihilations in case of symmetries, but also a description of the protuberances of the critical curves.

Moreover, regarding polynomials in spatial variables and one scale parameter, the critical curve itself is modelled. Now two remarkable facts become clear. Firstly, the protuberances are *not* very stable: a small perturbation doesn't harm them, but a larger one removes them from the critical curve. This is exactly what intuition tells – when blurring, things disappear, so creations are not really to be expected –, but what was mathematically proven to be *locally* wrong for critical points. Secondly, critical curves can also appear in *closed loops*, created at some scale and annihilated at some coarser scale. These curves one would complete miss if one would only trace the critical curves starting at the initial image. Calculations on images indeed show the predicted behaviour for the critical curves.

### 1.2.8 Chapter 8

Now it is time to return to the hierarchy structure. In chapter 5, I described the presence of domes in the scale space image, but there is more. As I mentioned, these domes are the critical “onion skin” around a series of extremum domes. The critical one contains a saddle, mostly a scale space one, but sometimes a

spatial saddle – then it is the one in the initial image. In chapter 8, I investigate the other part connected at the saddle. This easily boils down to investigation the structure of *iso-intensity manifolds* in scale space and their nesting. In an ordinary two dimensional image isophotes are nested, circle around extrema and only intersect themselves at saddles. So a curve through a saddle contains two parts. In scale space images a similar result holds. On part is known, namely the critical dome. Intriguing question is what information is held by the *other* part.

I investigate the behaviour of the manifolds and show that taking into account the other part of the manifold containing the critical dome, one elegantly obtains an unambiguous scale space intensity based hierarchy that encapsulates the one mentioned in Chapter 5, but is much more *robust*. The hierarchy can be visualised by a binary tree, a tree in which each node has one parent and two children. One of the children is the dome of Chapter 5, the other child is equal to the parent. It can even be reduced to a sequence of nestings, where each node is represented by a pair of parentheses. Within the parentheses the children are put, and the parentheses are labelled by the dome-child. This allows one to apply a “*logical filter*”: children in the tree that are less significant in scale space, can be swept out by simplifying the tree: just cut off the smallest branches. And from the other side of the tree: the most significant scale space parts are the strongest, the thickest (or largest) branches. One thus obtains a structure of the scale space image that is implicitly present, but only needs to be extracted.

### 1.3 Conclusions

This brings us to the end of this thesis. Its main contribution is that it starts the investigation of the deep structure of Gaussian scale *space*. In the various chapters it gives novel insights in the behaviour of spatial critical points under the influence of the scale parameter, yielding critical curves with not only generic catastrophe points, but also scale space saddle points. Modelling non-generic catastrophes give insight in the structure of critical curves, *e.g.* the presence of those forming closed loops.

Another novel insight lies in the iso-intensity manifolds in scale space. An appropriate selection of them, partially based on those through the scale space saddles, uniquely separate the scale space image – and thus the original image – in “regions of influence” organised by the spatial extrema. One thus gets for free a hierarchy of the image and the ability of uncommitted “pre-segmentation”.

Going further, also uncommitted imaging tasks like registration, coding, compression, clustering, simplification, transmission, and comparison – to mention some – are possible. Keyword in all these applications is *uncommitted*. The applications boil easily down from the fact that a uniquely defined hierarchy is available.

This is *completely different* from any user-defined task – which is the general case: the hierarchy is (implicitly) present in *the deep structure of Gaussian scale space images*.



---

# Gaussian Scale Space

---

Physics is finished, young man. It's  
a dead-end street.

---

PHILIPP VON JOLLY,  
MAX PLANCK'S TEACHER

This chapter shortly reviews Gaussian scale space, its axioms and known properties. The interested reader may also take a look at some of the present scale space literature.

- Obviously, one can take Koenderink's first seminal paper [139], as well as some of his tutorials [141] or his book [145]. He generally takes the physical and geometrical point of view.
- The first "scale space book" is by Lindeberg [174]. It may nowadays already be a bit dated, lacking the research of the last ten years, but it still gives a lot of information on and insight in the basic ideas, the transfer of continuous concepts to discrete algorithms, some mathematical properties and applications.
- A more mathematical point of view is taken by Florack [65], showing nicely how "heavy" mathematical equipment is a powerful tool proving that Gaussian scale space is the mathematical way to deal with images.
- A forthcoming book by Ter Haar Romeny [104] gives a tutorial introduction, using the interactive software package Mathematica [250], enabling the user to play around with scale space concepts. A strong emphasis is put on the relation between scale and human vision.
- Weickert [245] discusses the Gaussian scale space in the context of the axiomatics leading to use partial differential equations in image processing, see also section 2.2.

- More detailed information can be found in the proceedings of a scale space workshop in 1996 [125], also published as a book [233], and the proceedings of the subsequent scale space conferences in 1997 [106], 1999 [197], and 2001 [136], although these proceedings also contain a lot of Gaussian-scale-space-related papers, a direct consequence of the results we will discuss in section 2.2.
- Finally, the papers of Salden [221, 222] contain detailed information on the axiomatic view and a lot of citations.

In the next sections we will use the line of reasoning of some of these authors, although most of the following arguments is taken from the works by Florack and Ter Haar Romeny. However, it is presented in a strongly reduced way. For details the reader is referred to the literature mentioned in this chapter.

## 2.1 Scale Space Basics

In order to understand why at all one should use a (Gaussian) scale space, the underlying concepts of discrete images, some physics and mathematics are combined yielding unavoidable evidence that a scale space is a necessary concept to be used when dealing with images.

### 2.1.1 The Beginning...

Scale space in the Western literature started in 1983 by a paper of Witkin [249], discussing the blurring properties of one dimensional signals. The extension to more dimensional images was made in 1984 by Koenderink [139]. We will summarise this thought in the following. When blurring an image, each blurred version of the image is caused by the initial image. It is physically not possible that new structures are created (for instance, dark circles or spots in a white area).

This notion of *causality* implies the non-enhancement of local extrema: everything is flattened. So the intensity of maxima decrease and those of minima increase during the blurring process. At these points, all eigenvalues are negative and positive, respectively. The sum of the eigenvalues equals the trace of the Hessian, the matrix with all second order derivatives. Taking for simplicity a 2D image  $L(x, y)$ , the trace of the Hessian becomes  $L_{xx} + L_{yy}$ , shortly denoted as  $\Delta L$ . Then the causality principle states that at maxima  $\Delta L < 0$  (being the sum of the eigenvalues) and  $L_t < 0$  (decreasing intensity for increasing scale). At minima the opposite holds:  $\Delta L > 0$  and  $L_t > 0$ . And thus, in all cases,  $\Delta L \cdot L_t > 0$ .

Obviously, this holds in any dimension. One thus obtains an  $(n + 1)$ -dimensional image  $L(\mathbf{x}, t)$ , with  $\mathbf{x} \in \mathbb{R}^n$ . Imposing linearity between  $\Delta L$  and  $L_t$  yields  $\Delta L = \alpha L_t$ , with  $\alpha > 0$  as a possible ("simplest") solution. We may take  $\alpha = 1$  without loss of generality<sup>1</sup>. This results in the differential equation

$$\begin{cases} L_t(\mathbf{x}, t) = \Delta L(\mathbf{x}, t) \\ \lim_{t \downarrow 0} L(\mathbf{x}, t) = L_0(\mathbf{x}), \end{cases} \quad (2.1)$$

where  $L_0(\mathbf{x})$  denotes the original image. This equation has the general solution

$$L(\mathbf{x}, t) = \int_{-\infty}^{\infty} \frac{1}{\sqrt{4\pi t}^n} \exp\left(-\frac{(\mathbf{x} - \mathbf{x}')^2}{4t}\right) L(\mathbf{x}') d\mathbf{x}'. \quad (2.2)$$

<sup>1</sup>Although one may also encounter  $\alpha = 1/2$ .



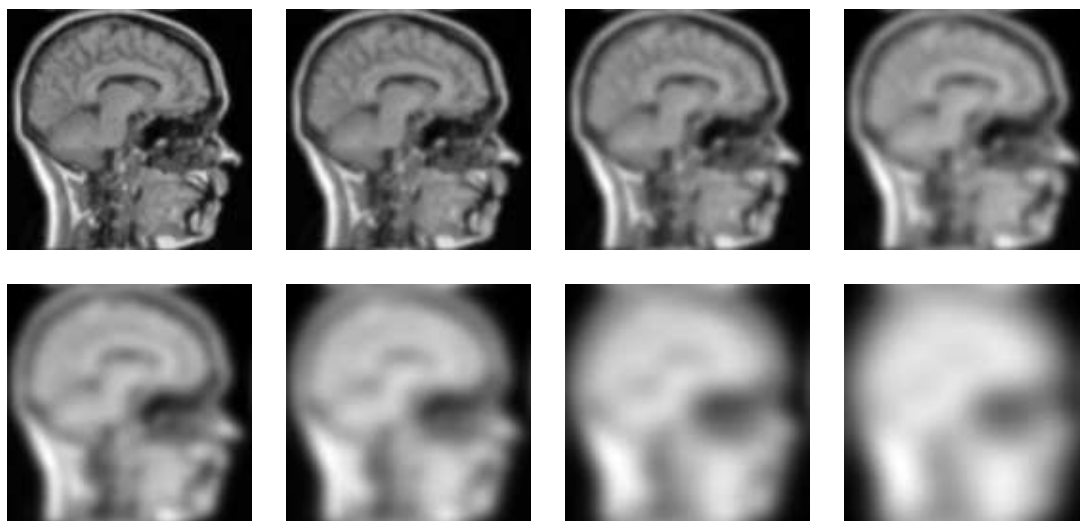


Figure 2.1: An MR image at successive scales  $t = \frac{1}{2}e^i$ , for  $i = 0, \dots, 4.2$  in steps of 0.6.

So the blurred image has to be taken as the convolution of the original image with a Gaussian filter. An example of a series of blurred images is given in Figure 2.1, showing an MR image at increasing scales. The set of *all* blurred images is the Gaussian scale space (image).

### ... and Before

Although the papers of Witkin and Koenderink are the start of scale space in the Western literature, the idea was already twenty years old, as Weickert *et al.* describe [245, 247, 248]. The Japanese Iijima [119] wrote a paper deriving the Gaussian as unique filter. Unfortunately, the paper was in Japanese, as some more interesting literature [208, 257, 258, 259].

But there is more to say than that a Gaussian is to be used for *blurring*. This is based on mathematics and physical properties of the image.

### 2.1.2 Physical Properties

Before applying any algorithm or whatsoever on images, it is firstly necessary to look at the properties of the objects to be described themselves. The observation is that physical units have *dimensions*, like “meters” or “Candela”. In any equation describing the objects, the dimensions need to be correct.

The *Law of Scale Invariance* states that the physical laws must be independent of the choice of the parameters. The *Pi Theorem* [15] relates the number of independent dimensionless combinations of the variables and the dimensions of the variables.

As an example, take the flow of some fluid through a pipe. The behaviour of the flow depends on some of the parameters, like density  $\rho$  (in kilogram per cubic meter), the velocity  $v$  (in meters per second), the diameter of the pipe  $d$  (in meters) and the viscosity of the fluid  $\mu$  (in kilogram per meter per second). In this case the Pi theorem “returns” the combination  $Re = \frac{\rho v d}{\mu}$ , which is the only parameter in

the so-called Navier-Stokes equation describing the flow through a pipe [15].

One can verify that indeed  $Re$  is dimensionless. This number, the Reynolds number, is an indicator whether the flow will be turbulent or stay laminar. So one can double the velocity and to be assured that the properties of the flow remain equal, for instance bisect the diameter of the pipe, or double the viscosity. In both cases  $Re$  remains equal. The strength of this property lies in the fact that it is possible to build and test scaled versions of object with – more or less – the same properties as the real sized object, *e.g.* ships or planes.

What happens when we obtain an image? Obviously, we look at some object by virtue of some light source, through a certain aperture. Then there are the illuminance of the outside world  $L_o$  and the processed image  $L$ , both in Candela per squared meter, as well as the sizes of the aperture  $\sigma$  and the outside word  $\mathbf{x}$ , both in meters. The Pi theorem returns the scale invariances  $\frac{L}{L_o}$  and  $\frac{\mathbf{x}}{\sigma}$ . Clearly, it is *meaningless* to say anything about  $\mathbf{x}$  without specifying  $\sigma$ . That is, ignoring  $\sigma$  boils down to the implicit meaningless choice  $\sigma = 1$ . And consequently, both fractions are related:

$$\frac{L}{L_o} = F\left(\frac{\mathbf{x}}{\sigma}\right). \quad (2.3)$$

To determine this relation more precisely, several axioms are imposed. Firstly a mathematical intermezzo is needed, since we deal with discrete data.

### 2.1.3 Theory of Distributions

The mathematical pre-route to Gaussian scale space follows from Schwartz’ “Theory of Distributions” [224]. Its relevance becomes clear from the following example: Disturb a function  $f(x)$  by a small perturbation  $\epsilon \sin(\delta x)$ ,  $|\epsilon| \ll 1$  and  $\delta$  arbitrary, *e.g.*  $1/\epsilon^2$ . It doesn’t alter  $f(x)$  much. The derivative, however, does:  $f'(x) + \epsilon\delta \cos(\delta x)$  shows large variations, compared to  $f'(x)$ .

This indicates that differentiation is *ill-posed* (in the sense of Hadamard). An operation is well-posed if the solution exists, is uniquely determined and depends *continuously* on the the initial or boundary data. That means: there is one solution and it is stable. So the problem is not the function, but the differentiation performed on it. This gets even worse, when dealing with discontinuous functions: they even cannot be differentiated. And in fact, all computer data *is* discontinuous.

To overcome ill-posedness Schartz introduced the (large) *Schwartz space*, containing smooth test functions. These functions are infinitely differentiable and decrease sufficiently fast at the boundaries. A *regular tempered distribution* is the correlation of a smooth test function and some function (or: discrete image). The outcome is that this regular tempered distribution can be regarded as a *probing* of the image with some mathematically nice filter. Derivatives are obtained as probing with the derivative of the filter and indeed depend continuously on the input image.

Having solved the problem of discontinuity, one now needs to find the proper smooth test function in combination with physical laws and state a number of axioms.

### 2.1.4 Uncommittedness

Concerning the size of the aperture  $\sigma$ , some axioms about *uncommittedness* are desirable. The following axioms state that “we know nothing and have no preference”. We remark that that immediately poses a restriction cancelling out cases in which we *do* know something and want to use that.

- *Spatial homogeneity* means that all locations in the field of view are a priori equivalent. So there is no preferred location that should be measured in a different fashion, *i.e.* there is shift invariance.
- *Spatial isotropy* indicates that there is no a priori preferred orientation in a point (or collection of them). Horizontal and diagonal structures are equally measured.
- *Spatial scale invariance* does not discriminate between large, small, and intermediate objects. There is no reason to emphasize details or large areas.
- *Linearity* is imposed, since there is no preferred way to combine observations. Non-linearity in a system implies “feedback”, *i.e.* memory, or knowledge.

The axioms of linear shift invariance lead to the observation that the image must be a convolution of the original image by the aperture function. Since in the Fourier domain a convolution of functions becomes the product of them, we will turn to it. Stated in Fourier space Eq. (2.3) becomes

$$\mathcal{L}(\omega; \sigma) = \mathcal{L}_0(\omega) \mathcal{F}(\omega; \sigma). \quad (2.4)$$

The Pi theorem states that  $(\omega; \sigma)$  is a function of  $(\omega \sigma)$ . Obviously, there must also be some “hidden” scale  $\epsilon$  in  $\mathcal{L}_0$  such that its argument is likewise dimensionless, say  $\omega \epsilon$ ; this could be something like “pixel scale”. The spatial isotropy implies that  $\mathcal{F}$  only depends on the magnitude  $\Omega = \|\omega \sigma\|^p$ :

$$\mathcal{F}(\omega; \sigma) = \mathcal{F}(\Omega) \quad (2.5)$$

Scale invariance and linearity turn out [65] to require that observing an observed item equals observing it by an aperture size that is a linear combination of the two aperture sizes:

$$\mathcal{F}(\Omega_1) \mathcal{F}(\Omega_2) = \mathcal{F}(\Omega_1 + \Omega_2). \quad (2.6)$$

Eq. (2.6) has the solution  $\mathcal{F}(\Omega) = \exp(\alpha \Omega)$ , so Eq. (2.5) becomes

$$\mathcal{F}(\omega; \sigma) = \exp(\alpha \|\omega \sigma\|^p). \quad (2.7)$$

For a fixed  $\omega$ , the limit for  $\sigma$  to zero has to leave the image un-scaled, which is true. For the limit  $\sigma$  to infinity it has to fully scale the image, *i.e.* averaging it completely. So necessarily  $\alpha < 0$ . For notational purposes (in the diffusion equation as will be shown in section 2.2), we take  $\alpha = -\frac{1}{2}$ , although one might also encounter  $\alpha = -\frac{1}{4}$ , the choice of Lindeberg, see *e.g.* [174] and “followers”.

This leaves only freedom of choosing  $p$ . The additional requirement of *separability* into the spatial dimensions yields  $p = 2$ , although other values for  $p$  still bring up linear scale spaces, albeit non-Gaussian [52]. So we find in the Fourier domain for Eq. (2.7)

$$\mathcal{F}(\omega; \sigma) = \exp\left(-\frac{1}{2} \omega^2 \sigma^2\right) \quad (2.8)$$

and in the spatial domain the inverse Fouriertransform of Eq. 2.8 gives the kernel

$$F(\mathbf{x}; \sigma) = \frac{1}{\sqrt{2\pi\sigma^2}^n} \exp\left(-\frac{\mathbf{x}^2}{2\sigma^2}\right). \quad (2.9)$$

Note that Eq. (2.9) is identical to the convolution kernel of Eq. (2.2) when we set  $t = \frac{1}{2}\sigma^2$ . The name “Gaussian” scale space is obvious. The Gaussian kernel is an element of the Schwartz space, as being a smooth test function: it is infinitely differentiable and it decreases sufficiently fast at the boundaries, just as its derivatives.

### 2.1.5 Regularisation

Another route to Gaussian scale space is due to regularisation. For a full treatment the reader is referred to Nielsen *et al.* [65, 104, 194, 195, 196]. Here we outline this approach. The task is to find a solution  $f$  that is close in the  $L_2$ -norm to some signal  $g$ , given the constraints that all derivatives of  $f$  are also bounded in the  $L_2$ -norm. Using so-called Euler-Lagrange multipliers  $\lambda_i$ , this can be combined to minimisation of the “energy”-functional

$$E[f] = \frac{1}{2} \int_{-\infty}^{\infty} \left( (f - g)^2 + \sum_{i=1}^{\infty} \lambda_i \left( \frac{\partial^i}{\partial x^i} f \right)^2 \right) dx . \quad (2.10)$$

In the Fourier-domain Eq. (2.10) is simplified to

$$E[\hat{f}] = \frac{1}{2} \int_{-\infty}^{\infty} \left( (\hat{f} - \hat{g})^2 + \sum_{i=1}^{\infty} \lambda_i \omega^{2i} \hat{f}^2 \right) d\omega, \quad (2.11)$$

since the Fourier transform  $(\frac{\partial}{\partial x} f(x))^2$  equals  $(-i\omega \hat{f}(\omega))(i\omega \hat{f}(\omega))$ , the product of the complex function with its complex conjugate. Also Parseval's theorem is used, stating that the Fourier transform of  $\int_{-\infty}^{\infty} f^2 dx$  equals  $\int_{-\infty}^{\infty} \hat{f}^2 d\omega$ , with  $\hat{f}(\omega)$  the Fourier transform of  $f(x)$ . The solution of Eq. (2.11) is found by so-called calculus of variations:  $\frac{\delta E}{\delta \hat{f}} = 0$ , yielding

$$\hat{f} - \hat{g} + \sum_{i=1}^{\infty} \lambda_i \omega^{2i} \hat{f} = 0 . \quad (2.12)$$

Consequently, Eq. (2.12) gives the linear system  $\hat{g} = \hat{h}^{-1} \hat{f}$ . The optimal  $\hat{f}$  is thus the linear filtering of  $\hat{g}$  by  $\hat{h}$ . Taking  $\lambda_0 = 1$ , we find the filter

$$\hat{h}^{-1} = \sum_{i=0}^{\infty} \lambda_i \omega^{2i}. \quad (2.13)$$

The Pi Theorem implies that  $\lambda_i \propto \omega^{-2i}$ , since  $\hat{h}$  is dimensionless. Assuming the semi-group property on this filter, such that filters can be added linearly, one obtains  $\lambda_i = t^i / i!$  and thus Eq. (2.13) becomes

$$\hat{h}^{-1} = \sum_{i=0}^{\infty} \frac{t^i}{i!} \omega^{2i} = e^{\omega^2 t}, \quad (2.14)$$

and the Gaussian filter is again obtained, *cf.* Eq. (2.8) with  $t = \frac{1}{2}\sigma^2$ . In this case separability is included. In fact, a series of regularisation filters  $e^{(\omega^2 t)^p}$  can be obtained for  $p \in \mathbb{N}$ . Results hold for multi-dimensional rotationally invariant regularisation.

### 2.1.6 Entropy

Nielsen also gave an alternative route, based on the statistics of the aperture function [104, 194]. A statistical measure for the disorder of this aperture function  $g(x)$  is given by the entropy, defined as

$$H(g) = \int_{-\infty}^{\infty} g(x) \log[g(x)] dx , \quad (2.15)$$

using the natural logarithm. This measurement states something like “there is nothing ordered, ranked”, if it takes its maximum. However, there are some constraints: Firstly, measuring a complete image shouldn’t cause a global enhancement or amplification; the function must be normalised. Secondly, measuring at some point  $x_0$ , we do expect the mean of the measurement to be at  $x_0$ , which we can take equal to zero, since all points are regarded the same. Thirdly, the function has some size, say  $\sigma$ . So the standard deviation of  $g(x)$  is related to this size. Finally, the aperture, as a real object, is positive. These constraints yield

$$\begin{cases} \int_{-\infty}^{\infty} g(x) dx = 1, \\ \int_{-\infty}^{\infty} xg(x) dx = 0, \\ \int_{-\infty}^{\infty} x^2g(x) dx = \sigma^2, \\ g(x) > 0 \end{cases} \quad (2.16)$$

Note that the Pi Theorem requires that one replaces  $g$  by  $g/g_0$  for some dimensionally compatible constant unit  $g_0$ , but this only yields irrelevant constants in Eq. (2.15), given the first constraint. So just as in the previous section, it is the task to maximise  $H(g)$ , Eq. (2.15), given these constraints. This yields, just as in the previous section an Euler-Lagrange equation:

$$E[g] = \int_{-\infty}^{\infty} \left( g(x) \log[g(x)] + \lambda_0 g(x) + \lambda_1 x g(x) + \lambda_2 x^2 g(x) \right) dx$$

Again solving  $\frac{\delta E}{\delta g} = 0$  gives

$$1 + \log[g(x)] + \lambda_0 + \lambda_1 x + \lambda_2 x^2 = 0, \quad (2.17)$$

so obviously

$$g(x) = e^{-(1+\lambda_0+\lambda_1x+\lambda_2x^2)}. \quad (2.18)$$

Checking the constraints, Eq. (2.16), results in  $\lambda_1 = 0$ ,  $\lambda_2 = \frac{1}{2\sigma^2}$ ,  $\lambda_0 = -1 + \frac{1}{4} \log[4\pi^2\sigma^4]$ , yielding

$$g(x) = \frac{1}{\sqrt{2\pi\sigma^2}} e^{-\frac{x^2}{2\sigma^2}}. \quad (2.19)$$

And again we have the Gaussian, Eq. (2.2), which is, from a statistical point of view, not very strange.

## 2.2 Differential Equations

The previous sections reveals the Gaussian kernel as a non-spurious detail generating filter, as a smooth test-function, as an uncommitted resultant, as regularisation filter, and as an orderlessness operator. But one can also investigate it from the point of view of differential equations.

### 2.2.1 Heat Equation

As shown by Koenderink, convolution of the original image with the Gaussian filter is the general solution of the partial differential equation  $L_t = \Delta L$ . Such a solution is called the *Greens function*, or fundamental solution. It is well-known in the field of physical transport processes. For instance in heat and thermodynamics, where this equation describes the evolution of the temperature when e.g. a plate is

locally heated [2]. From this field of physics, the equation has become known as the *Heat* or *Diffusion Equation*.

As a consequence, much effort has been put in investigation of this equation, both theoretically (*e.g.* with respect to remaining spatial maxima, the so-called hot spots [13, 14, 30, 34, 123, 182]) and applied-numerically [2, 28, 254]. Note that “scale” has been replaced by “time”, a minor *conceptual* change.

One even might put the point of view on this side and take the equation as an *axiom* for scale space. Then a scale space image is the result of an initial image under action of time. In general the “converged” image is the only desired image, the scale space is just the way to reach it.

## 2.2.2 Partial Differential Equations

A comprehensive investigation of using several different types of partial differential equations (PDEs) has been made by Weickert [245], where also details can be found. We will only shortly mention some of them, to explain the role of scale space (the Heat Equation) in relation to PDEs.

From the physical background, the heat equation originates from *Ficks law*  $j = -D \cdot \nabla L$ , describing that a flux is caused compensating some concentration gradient by some tensor  $D$ , together with the continuity equation  $L_t = -\nabla \cdot j$ , stating that the diffusion only transports heat. The combination yields  $L_t = \nabla \cdot (D \cdot \nabla L)$ . If  $D$  does not depend on the evolving image, the diffusion is called *linear*. Obviously, Gaussian scale space is obtained by taking  $D = \mathbf{1}_n$ . *Non-linear diffusion*, depending on the image and its geometry, is also known as *geometry driven diffusion*. Investigation of these models becomes harder, since, in general, Greens functions are not known. However, this is not a problem, since usually only the final, converged, image is of interest. This image is supposed to reveal the best solution to the task the equation is setup for, for example segmentation and / or denoising [35].

### Perona Malik

One of the most well-known and relatively simple (but problematic) non-linear scale spaces is obtained by the Perona Malik filter [211], where  $D = g(|\nabla L|^2)$ , for instance  $g(s^2) = 1/(1 + s^2/\lambda^2)$ ,  $\lambda > 0$  and  $g(s^2) = \exp(-s^2/\lambda^2)$ ,  $\lambda > 0$ . The basic idea is that edges should be preserved, while the rest of the image should be smoothed.

### Reaction-Diffusion

These types of PDEs minimise some energy functional under some constraints. Examples leading to Gaussian scale space were given in sections 2.1.5 and 2.1.6. Reaction-Diffusion equations include an extra function describing the (desired) behaviour on edges [245].

### Total Variation

Related to the previous PDEs are Total Variation methods. They minimise (some function of) the absolute value of the gradient of the image under certain conditions of the noise (zero mean and given standard deviation). The converged image is smoothed, while edges are preserved [20].

### Curvature Based

In the image there are isophotes and, perpendicular to them, flow lines. Instead of smoothing both, one may want to smooth only along the isophotes, ending up with *mean curvature motion*. The motion of the curve is known as *Euclidean shortening flow*, or *geometric heat equation* [138]. An adapted variant of it is (among other names) the *affine shortening flow*. Applications appear in context of active contour models (“snakes”) [209].

### Morphology

Morphology in its oldest form yields probing an image with a binary structuring element, an  $n \times n$  window. This is a discrete model applicable to discrete images, as can be found in any elementary book on image processing, *e.g.* [115, 231]. Applying morphological elements in a “clever” way, one can obtain a multi-scale system [1, 192] Using a parabolic structuring element, yields a morphological scale space equivalent to Gaussian scale space [25, 26, 27, 121, 122]. It has been shown that this equivalence can be expressed by a combining PDE. Both cases appear to be the limiting cases of this PDE [68].

## 2.3 Biological Inspiration

The human system is capable of looking around and identifying object of different sizes simultaneously. We can see a building with windows and bricks at the same time. All these objects have different sizes. So the eye and the system behind it is capable of working multi-scale [63, 66, 70, 104, 105, 116, 120, 256]. Besides, not only the eye, also our haptic system is a multi-scale system [183].

Models for describing the so-called *receptive field* in the retina can use Gaussian scale space, as argued by Lindeberg and Florack [174, 178, 179], and Koenderink [140, 142, 146, 147, 148, 149], *cf.* ter Haar Romeny [104].

The Laplacean of the Gaussian, known as the Mexican hat [185], can be used to model the sensitivity profile of a so-called *centre surround receptive field*. As Ter Haar Romeny states “we observe the Laplacian of the world” [104].

These observations, and many more that can be found in the literature mentioned, motivate the investigation of Gaussian scale space from the field of biology. But not only Gaussian scale space. At some visual stage in the brain a large amount of feedback to the eye is found. This implies the use of image structure, or memory, or non-linearity. This argues for the use of geometry driven (non-linear) models [102], as a stage next to linear models.

## 2.4 Hierarchies

An important notion in image analysis is that of a hierarchy: There is some *nesting* of several objects within the image. One can think of a road, containing cars, containing licence-plates, containing numbers and letters. More generally stated: regions within regions. This nesting of regions can be obtained if the regions are known, for instance due to edge detection or segmentations.

One way is to focus solely on the image and to try to build a *graph* [210, 228, 229]. One would like to end up with a tree, *i.e.* a graph without the possibility to walk around and visit parts multiple times.

A *tree structure* is straightforward and simplifies the structure. However, this is not always possible when describing objects within the image, but difficulties can be reduced by using the special technique of Reeb graphs [18, 19, 81, 137, 226, 227].

Early approaches in image analysis used pyramids, where stacks of images (or image primitives) of decreasing size are generated, *e.g.* by averaging four pixels into one in the next level, thus ending up with pyramidal structures. An example of such a structure based on the Laplacean is due to Burt and Adelson [31]. The idea is that global structures will live long in the pyramid, and the successive disappearance of structure returns a hierarchy. In fact, all hierarchy approaches need some stack of images, or image primitives (like the magnitude of the gradient), that simplifies in some sense going up in the tree. Therefore scale space methods and hierarchical approaches are strongly related, see *e.g.* Nacken [192] and Lester and Arridge [166].

### 2.4.1 Multi-Scale Watershed

One example of an image primitive is the magnitude of the gradient, yielding a non-linear approach. It is used in watershed segmentations, a very old principle going back at least one and a half century [32, 187]. The idea is that while flooding a landscape, water will flow into pools. At some specific heights, pools will merge. In Mathematical Morphology watersheds are commonly used [122].

Olsen [203, 204, 205, 206, 207] generated a multi-scale watershed algorithm based on Gaussian derivatives: on each scale the watershed is calculated, yielding a *watershed space*. Interactively a user can select regions and refine (or coarsen) them [44]. Multi-scale watershed algorithms yield usable hierarchical (segmentation driven) algorithms [82, 246].

## 2.5 Two Decades of Linear Scale Space

Since the Gaussian filter has been used for decades in signal processing, *i.e.* the one dimensional case, much effort has been made to investigate its properties. The Laplacean gives information with respect to edges, a reason for investigating its zero crossings (locations where it changes sign) [3, 50, 118, 181, 219, 225, 244, 252]. They can reconstruct the original signal – under certain conditions, see also the series of papers by Johansen (*et al.*) [124, 125, 126, 127, 128, 129].

Emerging since the papers of Koenderink and Witkin, two dimensional investigations started from the image algorithmic point of view [12, 38, 39, 253], including topics like robustness [111, 112] and implementations [21, 22, 23, 24, 213].

In the last decade of the previous century, papers appeared based on the considerations and axioms described in this chapter, *e.g.* by Florack (*et al.*) [67, 69, 75, 76, 77, 78, 79, 80, 107], exploiting the differential structure of scale space, and relations between linear and non-linear scale spaces [68, 73], by Lindeberg (*et al.*), building a hierarchical structure and paying attention to the discrete implementation, [169, 170, 171, 172, 173, 174], and the detection of image entities [175, 176, 177, 180], and by Griffin (*et al.*) [95, 98, 99, 100].

Scale space ideas can also be extended to the uncertainty in grey value detection [92, 96, 97, 150, 151], to optic flow [74], and orientation analysis [133]. Also time can be scaled in a similar fashion (taking into account that time uses a half-axis: the future cannot be modelled!) [65, 108, 143]. A possible tracking of surfaces with the same intensity over scale has been described by Fidrich [60, 61]. From the



mathematical point of view, especially the singularities (special points, to be encountered later on) are interesting [17, 45, 46, 47, 48, 71, 72, 154, 155].

Applications [103] can be found in various fields, *e.g.* stochastics [11], statistics [33], clustering [167, 193], recognition [37], segmentation [113, 132], and image enhancement by deblurring [65, 117, 214]. Medical applications of Gaussian scale space can be found in [42, 43, 110, 168, 180, 199, 200, 201, 202, 218, 230, 237] and in the comprehensive overview by Duncan and Ayache [53]. Already in the early nineties the linear scale space segmentation tool called hyperstack was used for segmentation in medical context, see *e.g.* [94, 152, 153, 201, 202, 240, 241, 242, 243]. It should be noted that it also contains heuristic models in order to provide a segmentation.

Recently, Geusebroek *et al.* applied Gaussian scale space theory to colour images, yielding good segmentations [84, 85, 86, 87, 88, 89, 90, 109].

### 2.5.1 Sub-Structures

Edge detection has been one purpose of image analysis from the beginning. However, edge detection methods do not always yield desired results [58, 59, 62]. Much research has therefore been done on the properties of sub-structures, *i.e.* structure within (scale space) images [134, 234], like curve-linear ones [236], and relative critical sets, like ridges [36, 54, 55, 56, 57, 83] and its extension cores [49], their generic properties and their relations to the medial axis [48, 49, 135], obtained by convolving the original image with  $-\sigma^2 \Delta G$ , with  $G$  the normalised Gaussian.

### 2.5.2 Deep Structure

Most research has been done on *using* scale space, *e.g.* for selecting some proper scale to derive some nice result like edge-detection or segmentation. The emphasis is then put on the *scale* part of scale space. The scale *parameter* gives extra information or an extra degree of freedom to “play around” with the image.

There is, obviously, also the *space* part of scale space. Then the emphasis is on the extra *dimension* that is available due to the scale parameter. The investigation of this extra dimension is the subject of this thesis. In his original paper, Koenderink called this *deep structure*: the image at all scales simultaneously [139].

Related and relevant research that has been done by others on the field of this deep structure, will be discussed in each of the following chapters.

### 2.5.3 Poisson Scale Space

Although linear scale space is often the synonym for Gaussian scale space (and vice versa), *this is not true*. The Gaussian scale space is an instance of a linear scale space. Recently, Duits *et al.* [52] showed that given the axioms of section 2.1.4, also another linear kernel can be used if separability<sup>2</sup> is not required, recall Eq. (2.7). Then there are infinite linear scale spaces, spanned by

$$\mathcal{F}(\omega; \sigma) = \exp(\alpha \|\omega \sigma\|^p). \quad (2.20)$$

---

<sup>2</sup>Note that separability is a coordinate-dependent notion and therefore not a fundamental requirement.

The specific choice  $p = 1$  in  $n$  spatial dimensions yields the kernel

$$F(\mathbf{x}; \sigma) = \frac{\Gamma(\frac{n+1}{2}) \sigma}{\pi^{(n+1)/2} (||\mathbf{x}||^2 + \sigma^2)^{\frac{n+1}{2}}}, \quad (2.21)$$

where  $\Gamma(i)$  is the Euler gamma function, given by  $\int_0^\infty t^{i-1} e^{-t} dt$ . Although  $F$  is a smooth function, it is not an element of the Schwartz space. The kernels and the filtered images are harmonic functions, since Eq. (2.21) is the Greens function of another famous physical equation, given by

$$\Delta L + L_{\sigma\sigma} = 0. \quad (2.22)$$

In mathematics Eq. (2.22) is called “the Poisson equation in half space”, and its kernel “half-space Poisson kernel” [101] and one consequently obtains a Poisson scale space. Taking all derivatives within the  $\Delta$ -operator results in  $\Delta_{\mathbf{x},\sigma} L = 0$ , the “famous” Laplace-equation with Dirichlet boundary condition, *viz.*  $\lim_{\sigma \downarrow 0} L(\mathbf{x}, \sigma) = L(\mathbf{x})$ , is obtained.

Using proper boundary conditions it can be shown that Eq. (2.22) is equivalent to the evolution equation

$$\frac{\partial L}{\partial \sigma} = -\sqrt{-\Delta} L, \quad (2.23)$$

using a fractional power of a derivative operator. In fact, instead of a squareroot, any power between zero and one can be used, see Duits *et al.* [52].

This recent discovery of the infinite set of linear scale spaces may give rise to a revival of investigation of linear scale space properties, both theoretical and practical. Linear scale space isn’t finished. It isn’t a dead-end street<sup>3</sup>.

---

<sup>3</sup>In 1874, at the age of 16, Max Planck entered the University of Munich. Before he began his studies he discussed the prospects of research in physics with Philipp von Jolly, the professor of physics there, and was told that physics was essentially a complete science with little prospect of further developments.

---

## Saddle Points in 2D

---

On a hexagonal tessellation life is easier.

---

BERTHOLD KLAUS PAUL HORN

### 3.1 Introduction

Mathematically, spatial critical points are defined by the zeros of the gradient. Regarding a discrete grid on which the image is embedded, these zeros will in general not coincide with the grid points, but lie somewhere in between them. In this chapter I investigate the influence of the structure of the grid with respect to detecting all critical points

### 3.2 Critical Points: Continuous versus Discrete

Many methods, based on continuous functions, can be applied to find the locations of critical points with sub-pixel precision. For instance, the method of determining the zero crossings of the gradients, in which for each pixel the result is “positive” or “negative” for each partial derivative. Or the method of calculating winding numbers (see *e.g.* Staal *et al.* [234] and Kalitzin *et al.* [131]), based on a local neighbourhood around each pixel. The change of orientation of the gradient vector field on the boundary of that neighbourhood determines the type of each point. These approaches, however, only yield evidence of a pixel being close to (*i.e.* in the neighbourhood of) a critical point. If all critical points are found and uniquely assigned to a pixel, all is well. However, it may occur that two neighbouring pixels give alike output. One (then) may try any sub-pixel precision algorithm, but still need to assign the critical point to one grid point.

Assigning extrema to grid points is fairly trivial: the grid point is an extremum if its value is larger - or, equivalently, smaller - than all its neighbours. For saddle points the situation is more complicated. Keyword in this observation is neighbourhood, to which we will come back.

### 3.2.1 The Euler Number

An important topological entity is the Euler number. In two dimensions in binary images it simply equals the number of objects minus the number of holes, in three dimensions it is more complicated, see Lee *et al.* [164, 165]. So for simplicity we restrict ourselves to two dimensions. The Euler number of an image is related to the winding number [114, 164] mentioned before. It can be expressed in term of the critical points: Let  $\chi(M)$  denote the Euler number of a manifold  $M$  (say the image),  $g$  denote the genus of the manifold (roughly the number of holes, see *e.g.* Koenderink [145] and Milnor [190]),  $m_+$  the number of maxima,  $m_-$  the number of minima, and  $s$  the number of saddles (assume there are no catastrophes/singularities), then

$$m_+ - s + m_- = 2(1 - g) = \chi(M)$$

So calculating the Euler number is just counting the critical points. Another nice property is commonly used in *e.g.* combinatorial and computational topology ([18, 19, 81, 114, 137, 226, 227]). A triangulation of an object, or image, is obtained by taking a number of landmarks (*e.g.* points) and overlay the object with triangles that connect three landmarks. A method that is also commonly used in spline representations of objects. Obviously, this can be generalised to a set of vertices, that are connected by edges thus forming cells (called faces). Then the Euler number is also present here: it equals the number of faces (F) minus the number of edges (E), plus the number of vertices (V):

$$\chi(M) = F - E + V.$$

This Euler number, “popping up everywhere” (Koenderink, [145]) gives a powerful requirement with respect to assigning the critical points of an image to its grid points. Assuming that two adjacent pixels have different values, it is at fore hand clear what the number of saddle points *must* be. Furthermore, the chosen grid (triangulation) should be such, that it does not violate the Euler number.

## 3.3 Neighbourhoods

Having noticed this, it is necessary to determine what “a neighbourhood” means. Golay pointed out that only three types of planar, symmetric, isotropic point grids exist, namely square, hexagonal and triangular ones. The triangular grid can be obtained from the hexagonal one, and is least suited for for neighbourhood investigations [93]. So the other two remain.

### 3.3.1 Rectangular Grids

Using a rectangular grid, as is rather common in image analysis, a first idea would be the so-called 4-neighbour connectivity: For the moment, think of a pixel as a square, connected to its neighbours left, right, up and down, see Figure 3.1a, where the grey blocks denote the neighbours. An alternative is the so-called 8-neighbour connectivity, in which also the corners are taken into account (Figure 3.1b).

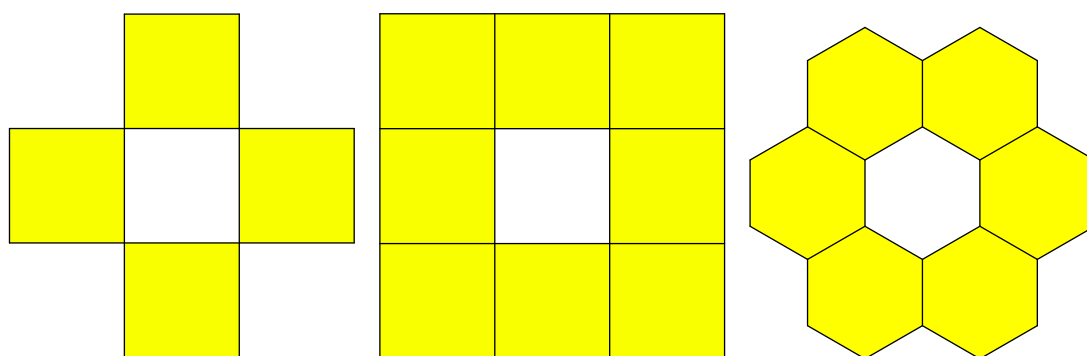


Figure 3.1: Different types of connectivity based on neighbours (in grey) of the centre block: a) 4-neighbour connectivity. b) 8-neighbour connectivity. c) 6-neighbour connectivity.

Here immediately problems rise, as shown by the following example of Deutsch [51]. Assuming that in Figure 3.1a the centre block is background, we have 4 faces. Each has 4 vertices, so in total there are 16 vertices (landmarks), since the four faces are disjoint. Furthermore there are 16 edges, leading to an Euler number of  $4 - 16 + 16 = 4$ , whereas the number of objects minus the number of holes yields  $4 - 1 = 3$ . A problem. For the 8-neighbourhood a similar result holds: In the same Figure 3.1a there are still 4 faces and 16 edges, but now there are 12 vertices. This yields an Euler number of  $4 - 16 + 12 = 0$ , but now the part in the middle isn't a hole: it is connected to the background, so the number of objects minus the number of holes is  $1 - 0 = 1$ . The problem is solved by assuming 4-neighbour connectivity for the objects, and 8-neighbourhood for the background (then counting objects yield  $4 - 0 = 4$ ) or the other way round (obtaining a hole in the middle and  $1 - 1 = 0$ ). This duality between 4- and 8-neighbour connectivity makes it non-trivial to implement it in grey value images instead of binary images.

### 3.3.2 Hexagonal Grids

The problems mentioned in the previous section are avoid when using an hexagonal grid. An example of it is shown in Figure 3.1c, where the grey blocks represent the neighbourhood of the block in the middle. Now there is no problem in connectivity: Assuming again that the centre block is background, we have 24 vertices, 30 edges, and 6 faces so the Euler number  $V - E + F = 24 - 30 + 6 = 0$ , equalling one object minus one hole (the genus is one).

Consequently, from a topological point of view, hexagonal grids (or: lattices) are to be preferred. Middleton and Sivaswamy state that they have been shown to have better efficiency and less aliasing. They exploit the oblique effect in human vision. They can be obtained by staggering the individual square pixels like a brick wall. Generally, a preference has been shown for them in the work due to their consistent connectivity [188].

## 3.4 Construction of a Hexagonal Lattice

The idea of the brick wall is shown in Figure 3.2a, where each brick has six neighbours. Obviously, it takes “the golden way in between” the 4- and 8-neighbourhood connectivity by simply translating rows.

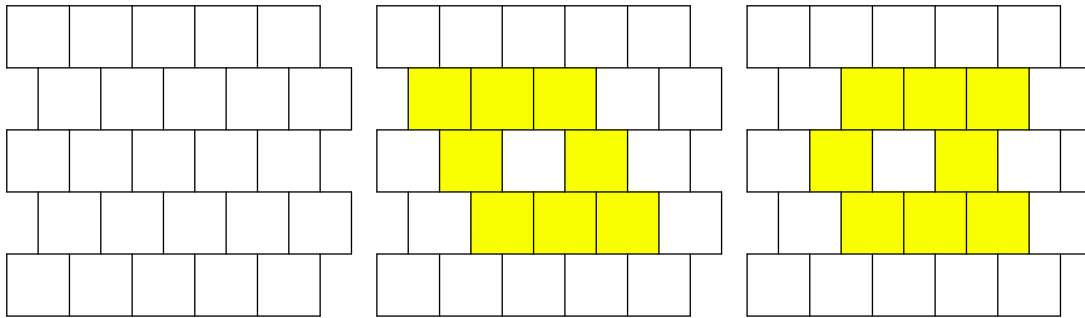


Figure 3.2: A hexagonal lattice. Staggering the individual square pixels like a brick wall (a) and the effect on the 8 neighbours due to the translations of Horn (b) and Blom (c).

It remains to select how to translate, and which pair of neighbouring pixels to select (or deselect) in the original rectangular grid.

### 3.4.1 Horn

Horn [115] suggests two neighbours on the same diagonal, to be obtained by moving the row above a particular cell a half cell to the left and the row below a half cell to the right (or the other way round). An example is shown in Figure 3.2b, where the eight neighbours in the rectangular grid are grey. In this example the neighbours top-left and bottom-right are removed to obtain 6-neighbourhood connectivity.

### 3.4.2 Blom

To locate the critical points uniquely Blom [21] used a translation, which is derived from a usual 2-D grid by shifting each even row a half pixel to the right and leaving odd rows unattached, or of course any similar translation. An example of this translation is shown in Figure 3.2c, where the eight neighbours in the rectangular grid are again grey. In this example the neighbours top-right and bottom-right are removed to obtain the 6-neighbourhood connectivity. So this translation is in fact only half of Horn's translation. The advantage of Blom's approach is found in its relatively simple algorithmic implementation.

### 3.4.3 Types of Hexagonal Grid Points

On this grid each point has 6 neighbours. For each of these neighbours the sign of the difference with respect to the point itself is determined. To determine the class of the point, the number of sign changes walking clockwise along these six neighbours is counted. This leads to 4 typical cases:

- Zero sign changes: The point is an extremum, a maximum iff all signs are negative, a minimum iff all are positive. See Figure 3.3a.
- Two sign changes: The point is a regular point, see *e.g.* Figure 3.3b.
- Four sign changes: the point is a saddle point, see *e.g.* Figure 3.3c.

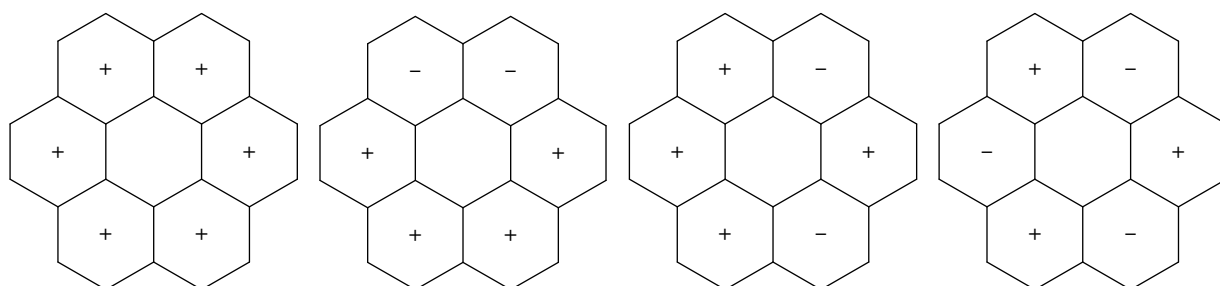


Figure 3.3: The four typical neighbourhoods in a hexagonal lattice. a) An extremum. b) A regular point. c) A saddle point. d) A degenerate saddle point, a so-called monkey saddle.

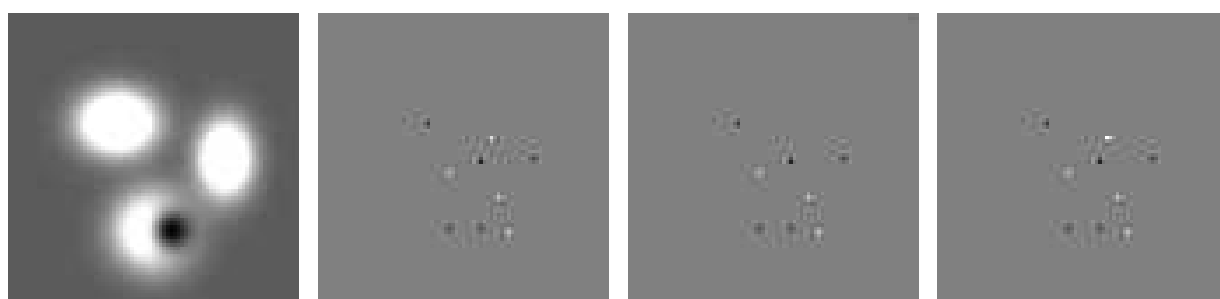


Figure 3.4: a) synthetic image. Type of the pixels (black is extremum, grey is regular, white is saddle) according to: b) Detection at a 6-neighbourhood. c) Detection at a 4-neighbourhood. d) Detection at an 8-neighbourhood.

- Six sign changes: The point is a degenerated saddle point, a so-called monkey-saddle, see Figure 3.3d.

The monkey saddle is non-generic, that is: it is generically not to be found. A monkey saddle can analytically be modelled by the function  $x^3 - 3xy^2$ , which is not stable under a small perturbation.

In the remaining we use Blom's translation, which, we emphasise, holds the Euler number and thus finds all saddle points. A close look at the description of the lattice shows that it can be implemented as the 6 neighbourhood of a point by taking into account the 8 neighbours and disregarding the upper right and lower right neighbour in the even rows, and the upper left and lower left neighbour in the odd rows. Or vice versa.

In Figure 3.4a we show an artificial image containing 5 extrema and -thus- 4 saddle points. The 6-neighbourhood connectivity result is shown in Figure 3.4b. The black pixels are of type 0, *i.e.* extrema, the grey are of type 2, regular, and the white pixels are of type 4, saddle points. A result as desired.

Figure 3.4c shows the result of the 4-neighbourhood connectivity. Now there is one saddle (a pixel of type 4) missing in the middle of the image. Obvious since the 4-neighbourhood connectivity is too rough to detect the saddles. The 8-neighbourhood connectivity is shown in Figure 3.4d. Now the missing saddle is detected, but not unambiguously. It is assigned to two neighbouring pixels.

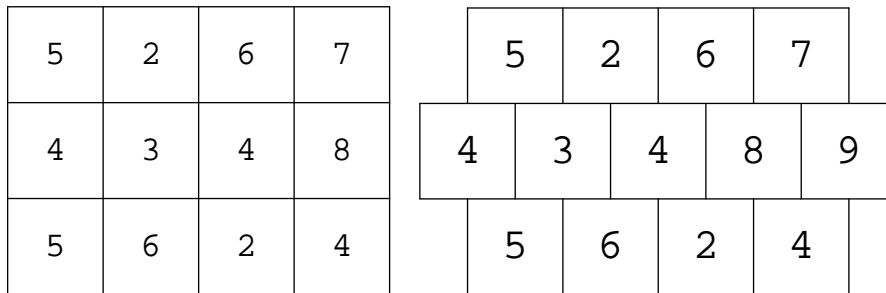


Figure 3.5: Saddle detection: a) Values in the rectangular grid. b) Values in the corresponding hexagonal grid.

This becomes clear from a more detailed investigation around this pixel. The rectangular grid can be represented as Figure 3.5a. Using a 4-neighbourhood connectivity on the two pixels in the middle of the centre row, it becomes evident that both the “3” and the “4” show two sign changes. Starting on top, the “3” has pattern  $- + + +$ , the “4” has pattern  $+ - - +$ . They are thus qualified as regular points. Using an 8-neighbourhood connectivity, however, one finds four sign changes for both pixels: the “3” has pattern  $- + + + + - + +$ , the “4”  $+ - - + - + + +$ . And thus they are qualified as saddle points.

The corresponding 6-neighbourhood connectivity is shown in Figure 3.5b. Now the “3” has pattern (starting top left)  $+ + + + + -$ , thus two sign changes and consequently a regular point. The “4” has pattern  $- - + - + +$  and is thus a saddle. Its neighbour, the “8” is again a regular point.

### 3.5 Conclusions

Concluding we find that a hexagonal grid is highly preferred in finding saddle points in two dimensions, since firstly it respects the Euler number, guaranteeing that all saddles are found, and secondly it assigns the saddles unambiguously to pixels. Quoting Horn [115]: “On a hexagonal tessellation life is easier”.

A disadvantage is that it is only usable in two dimensions. However, attempts for similar tessellations using truncated octahedral and rhombic dodecahedral tillings are made [189].



---

# Topological Structure

---

It is wrong to think that the task of physics is to find out how nature is. Physics concerns what we can say about nature.

---

NIELS BOHR

**abstract** We investigate the “deep structure” of a scale space image. The emphasis is on topology, *i.e.* we concentrate on critical points—points with vanishing gradient—and catastrophe points—critical points with degenerate Hessian—and monitor their displacements, respectively generic morsifications in scale space. Relevant parts of catastrophe theory in the context of the scale space paradigm are briefly reviewed, and subsequently rewritten into coordinate independent form. This enables one to implement topological descriptors using a conveniently defined coordinate system. A description in a user-defined Cartesian coordinate system is stated, as well as results of a straightforward implementation. The location of a catastrophe can be predicted with sub-pixel accuracy. An example of an annihilation is given. Also an upper bound is derived for the area where critical points can be created. Theory is clarified on experimental data of an MR, a CT, and an artificial noise image.

**keywords** scale space, catastrophe theory, critical points, deep structure, image topology.

## 4.1 Introduction

### 4.1.1 Historical Background

A *scale space representation*, the embedding of a image into a one-parameter family of images, is a well-known method to endow an image with a topology. The Gaussian scale space model is one of the simplest among the possible representations. In this model, the parameter encodes scale. Increasing scale pertains to blurring the image. It has been proposed by Iijima [119]. His work remained unnoticed for decades in the English literature, just as other Japanese accounts [208, 257]. A translation of their motivations, as well as other axiomatic approaches yielding Gaussian scale space, can be found in the work of Weickert et al. [248, 247].

The introduction into English literature is due to Witkin [249] and Koenderink [139]. Koenderink's account gives insight in the process of blurring itself. It appears that the Gaussian scale space model pertains to *topological structure*.

### 4.1.2 Scale and Topology

The fact is that *scale provides topology*. Scale is a degree of freedom allowing a hierarchy of topologies that enable transitions between coarse and fine scales. The main problem, a decent topology for images, has been addressed by the mathematical community before. It turns out that the *theory of tempered distributions* by Schwartz [224] and (Gaussian) scale space theory are close-knit, see e.g. [64, 65].

### 4.1.3 Deep Structure

Both Koenderink and Witkin proposed to investigate the structure at all levels of resolution simultaneously, the so-called *deep structure* of the image. Although this deep structure is still a unsolved problem, many widely varying applications have been developed using heuristic approaches: The segmentation or detection algorithms typically use some type of scale selection or linking scheme, cf. Bergholm's edge focusing scheme [16], Lindeberg's feature detection method [174, 175, 176], the scale optimisation criterion used by Niessen et al. [199] and Florack et al. [74] for motion extraction, Vincken's hyperstack segmentation algorithm [242], Olsen's multi-scale watershed segmentation [206], etc. Other approaches focus on high resolution reconstruction aspects, cf. Hummel and Moniot [118], Johansen [129], and Nielsen and Lillholm [198].

These results led to an increasing investigation of a general underpinning of deep structure, that may serve as a common basis for a variety of of schemes. All these bottom-up methods invariably rely on on *catastrophe theory*.

### 4.1.4 Catastrophe Theory

An introduction of Catastrophe Theory as investigated by Thom [238, 239], can be found in several books [6, 91, 212]. It has been pointed out by Koenderink that Thom's classification theorem can be applied to scale space image. This may be expected, since there is one control parameter, the isotropic inner scale. However, the difficulty rises from the fact that scale space is constrained by the isotropic diffusion equation, so the control parameter is a special one.

A comprehensive account on this subject is by Damon [45] and others, like Griffin [98], Johansen [124, 125, 129], Lindeberg [170, 174], and Koenderink [140, 144, 145, 146, 147].

### 4.1.5 Canonical versus Covariant Formalism

The purpose of the present work is threefold: (i) to collect relevant results from the literature on catastrophe theory, (ii) to express these in terms of user-defined coordinates, and (iii) to investigate their usage in practice.

For this purpose covariant expressions for the tangents to the critical curves in scale space, both through Morse as well as non-Morse critical points will be derived, a covariant interpolation scheme for the locations of the latter in scale space will be established, and the curvature of the critical curves (again in covariant form) at the non-Morse critical points will be computed.

The requirement of covariance is a novel and important aspect not covered in the literature. The reason for this requirement is that in practice one is not given the special, so-called “canonical coordinates<sup>1</sup>” in terms of which catastrophe theory is formulated in the literature. They give, due to their simplicity, qualitative insight in understanding the various aspects of the situation, but in the absence of an operational definition they are of little *practical* use.

A covariant formalism—by definition—allows us to use whatever coordinate convention whatsoever. All computations can be carried out in a user-defined coordinate system. In this work this is a Cartesian coordinate system aligned with the grid of the digital image. This means that in order to carry out the computations as described, all that is needed is a small number of image convolutions per level of scale, and some algebraic combinations of the results, as will be clear from the examples.

## 4.2 Theory

Theory is presented as follows. The general plan of catastrophe theory (Section 4.2.1) is outlined and considered in the context of scale space theory (Section 4.2.2). An in-depth analysis is presented in canonical (Section 4.2.3), respectively arbitrary coordinate systems (Section 4.2.4). The first three sections mainly serve as a review of known facts from literature. The remainder covers novel aspects that are useful for exploiting these in practice.

### 4.2.1 Catastrophe Theory

Catastrophe theory is the study of how the critical points –points at which the gradient vanishes– change as the control parameters change.

Typically, critical points are isolated points where the Hessian has nonzero eigenvalues. The *Morse Lemma* states that the qualitative properties of a function at these so-called *Morse critical points* are essentially determined by the quadratic part of the Taylor series (the *Morse canonical form*).

In many practical situations one encounters *families* of functions that depend on *control parameters*. An example of such a control parameter is “scale” in a scale space image.

---

<sup>1</sup>The term “canonical coordinates” is taken from Gilmore [91].

While varying a control parameter continuously, a Morse critical point will move along a *critical curve*. At isolated points on such a curve one of the eigenvalues of the Hessian may become zero, so that the Morse critical point turns into a *non-Morse critical point*.

In situations with several control parameters,  $\ell$  eigenvalues of the Hessian may vanish simultaneously, leaving  $n - \ell$  of them nonzero. Then the *Thom Splitting Lemma* simplifies things: It states that, in order to study the degeneracies, one can simply discard the  $n - \ell$  “nice” variables corresponding to the regular  $(n - \ell) \times (n - \ell)$ -sub-matrix of the Hessian, and thus study only the  $\ell$  “bad” ones [238, 239]. One can thus split up the function into a Morse and a non-Morse part, and study the canonical forms of each separately, because the same splitting result holds in a full neighbourhood of a non-Morse function.

The Morse part can—obviously—be canonically described in terms of the quadratic part of the Taylor series. The non-Morse part can also be put into canonical form, called the *catastrophe germ*. This is a polynomial of order 3 or higher.

The Morse part does not change qualitatively after a small perturbation. Critical points may move and corresponding function values may change, but nothing will happen to their type: if  $i$  eigenvalues of the Hessian are negative prior to perturbation (a “Morse  $i$ -saddle”), then this will still be the case afterwards.

The non-Morse part does change qualitatively due to perturbation. In general, the non-Morse critical point of the catastrophe germ will split either into a non-Morse critical point that can be described by a polynomial of a degree that is lower than the polynomial used before the perturbation, and a number of Morse critical points, or solely into a number of Morse critical points. This state of events is called *morsification*.

The Morse saddle types of the isolated Morse critical points involved in this process are characteristic for the catastrophe. *Thom’s Theorem* provides an exhaustive list of “elementary catastrophes” (1, . . . , 5 control parameters), with canonical formulas for the catastrophe germs as well as for the perturbations needed to describe their morsification [238, 239].

## 4.2.2 Catastrophe Theory and the Scale Space Paradigm

One should not carelessly transfer Thom’s results to scale space, since there is a nontrivial constraint to be satisfied: Any scale space image, together with all admissible perturbations, must satisfy the *isotropic diffusion equation*. Damon has shown how to extend the theory in this case in a systematic way [45].

If we restrict ourselves to *generic* situations only, and consider only “typical” input images that are not subject to special conditions such as symmetries, things are actually fairly simple. Then the only generic morsifications in scale space are *creations* and *annihilations* of pairs of Morse hyper-saddles of opposite *Hessian signature*: they have opposite sign of the Hessian determinant evaluated at the location of the critical point; for a proof, see Damon [45].

The description of topological events in Damon’s account follows the usual line of approach in the literature and relies on an appropriate choice of so-called “canonical coordinates”. These are usually inconvenient in practice, unless an operational scheme relating them to user-defined coordinates is provided. Mathematical accounts fail to be operational in the sense that—in typical cases—canonical coordinates are at best proven to exist. Their mathematical construction often relies on manipulations of the physically void trailing terms of a Taylor series expansion, in other words, on derivatives up to infinite order, and consequently lacks an operational counterpart. Even if one were in the possession of an algorithm one should realize that canonical coordinates are in fact *local* coordinates, with the fiducial

origin placed at the point of interest. Each potential catastrophe in scale space would thus require an independent construction of a canonical frame.

In summary, the *canonical formalism* is a line of approach that exploits suitably chosen coordinates. It provides a way to approach topology if neither metrical relations nor numerical computations are of interest. Thus its role is primarily to *understand* topology. In the next section we give a self-contained summary of the canonical formalism for the generic cases of interest.

### 4.2.3 Canonical Formalism

The two critical points involved in a creation or annihilation event always have opposite Hessian signature, so that this signature may serve to define a conserved “topological charge” intrinsic to these critical points.

It is clear (by definition!) that the charge of Morse critical points can never change, as this would require a zero-crossing of the Hessian determinant, violating the Morse criterion that all Hessian eigenvalues should be nonzero. Thus the interesting events are the interactions of charges within a neighbourhood of a non-Morse critical point.

**Definition 1** *A Morse critical point is assigned a topological charge  $q = \pm 1$  corresponding to the sign of the Hessian determinant evaluated at that point. A regular point has zero topological charge. The topological charge of a non-Morse critical point equals the sum of charges of all Morse critical points involved in the morsification.*

**Definition 2** *Denoting  $\mathbf{x} = (x_1, \dots, x_n)$  for brevity, and identifying the first coordinate to be the “bad” one, we define the catastrophe germs*

$$\begin{aligned} g^A(x_1; t) &\stackrel{\text{def}}{=} x_1^3 + 6x_1t, \\ g^C(x_1, x_2; t) &\stackrel{\text{def}}{=} x_1^3 - 6x_1(x_2^2 + t), \end{aligned}$$

*together with their perturbations*

$$\begin{aligned} f^A(\mathbf{x}; t) &\stackrel{\text{def}}{=} g^A(x_1; t) + Q(\mathbf{x}; t), \\ f^C(\mathbf{x}; t) &\stackrel{\text{def}}{=} g^C(x_1, x_2; t) + Q(\mathbf{x}; t). \end{aligned}$$

*The quadric  $Q(\mathbf{x}; t)$  is actually independent of  $x_1$  and is defined as follows:*

$$Q(\mathbf{x}; t) \stackrel{\text{def}}{=} \sum_{k=2}^n \epsilon_k (x_k^2 + 2t),$$

*in which each  $\epsilon_k$  is either  $+1$  or  $-1$ .*

Note that germs as well as perturbations satisfy the diffusion equation

$$\frac{\partial L}{\partial t} = \Delta L, \tag{4.1}$$

where  $L = L(\mathbf{x}; t)$  and the so-called Laplacean  $\Delta \stackrel{\text{def}}{=} \partial_{x_1}^2 + \partial_{x_2}^2 + \dots + \partial_{x_n}^2$ .

In the canonical formalism it is conjectured that, given a generic event in scale space, one can always set up coordinates in such a way that the qualitative behaviour is summarised by one of the two “canonical forms” given above. Any non-generic event can be perturbed yielding compounds of these generic events.

Since one control parameter is present, the quadric does not depend on  $x_1$ . At the location of the catastrophe exactly one Hessian eigenvalue vanishes.

The forms  $f^A$  and  $f^C$  correspond to an annihilation and a creation event at the origin, respectively. The latter requires  $n \geq 2$ , so creations will not be observed in 1D signals.

Both types of events are referred to as *fold catastrophes*, again due to the fact that they both are obtained by varying one control parameter. The diffusion equation imposes a constraint that manifests itself in the asymmetry of these two canonical forms. In fact, whereas the annihilation event is relatively straightforward, a subtlety can be observed in the creation event, *viz.* the fact that the possibility for creations to occur requires space to be at least two-dimensional.

### The A-Germ

Morsification of the A-germ of Definition 2 entails an annihilation of two critical points of opposite charge as resolution is diminished.

**Result 1** *Recall Definition 2. For  $t < 0$  we have two Morse critical points carrying opposite charge, for  $t > 0$  there are none. At  $t = 0$  the two critical points collide and annihilate. The critical curves are parametrised as follows:*

$$\mathbf{P}_{\pm} : (\mathbf{x}; t)_{\pm} = (\pm\sqrt{-2t}, 0, \dots, 0; t).$$

When defining the velocities of the points by  $\partial_t \mathbf{P}_{\pm}$ , the rate of spatial displacement per unit  $t$  [170], it follows directly that the critical points collide with infinite opposite velocities before they disappear. At the origin both branches of critical curves are tangential to the  $(x_1, t)$ -plane, and in fact approach each other from opposite spatial directions tangential to  $t = 0$ , and—in this canonical case—perpendicular to the zero-crossing of the Hessian determinant.

Thus one must be cautious and take the parametrisation into account if one aims to link corresponding critical points near annihilation in numerical computations. The corresponding critical points are separated by a distance of the order  $\mathcal{O}(\sqrt{\delta t})$  if  $\delta t$  is the “time-to-collision”, with time in the sense of the scale evolution parameter of Eq. (4.1).

For 1D signals this summarises the analysis of generic events in scale space. For images there are other possibilities, which are studied below. In 2D the present case describes the annihilation of a minimum or maximum with a saddle. Minima cannot annihilate maxima, nor can saddles annihilate each other. In 3D one has two distinct types of hyper-saddles, one with a positive and one with a negative topological charge. Also minima and maxima have opposite charges in this case, and so there are various possibilities for annihilation all consistent with charge conservation. However, charge conservation is only a constraint and does *not* permit one to conclude that all events consistent with it will actually occur. In fact, by continuity and genericity one easily appreciates that a Morse  $i$ -saddle can only interact with a  $(i - 1)$ -saddle ( $i = 1, \dots, n$ ), because *one and only one* Hessian eigenvalue is likely to change sign when traversing the non-Morse point (*i.e.* the degenerate critical point) along the critical curve. Genericity implies that sufficiently small perturbations will not affect the annihilation event qualitatively.

It may undergo a small dislocation in scale space, but it is bound to occur. So in 3D images one is likely to find annihilations of maxima with negative hyper-saddles, minima with positive hyper-saddles, and positive hyper-saddles with negative hyper-saddles.

### The C-Germ

Morsification of the C-germ of Definition 2 shows a creation of two critical points of opposite charge as resolution is diminished. Note that this event is generic and doesn't violate the causality principle that is the core of scale space theory [139]. The event of interest here is the one occurring in the immediate vicinity of the origin.

**Result 2** *Recall Definition 2. For  $t < 0$  there are no Morse critical points in the immediate neighbourhood of the origin. At  $t = 0$  two critical points of opposite charge emerge producing two critical curves for  $t > 0$ . The critical curves are parametrised as follows:*

$$\mathbf{P}_{\pm} : (\mathbf{x}; t)_{\pm} = (\pm\sqrt{2t}, 0, \dots, 0; t).$$

Again charges are conserved, and again the emerging critical points escape their point of creation with infinite opposite velocities. Genericity implies that creations will persist despite perturbations, and will suffer at most a small displacement in scale space.

### The Canonical Formalism: Summary

To summarise, creation and annihilation events together complete the list of possible generic catastrophes. The canonical formalism enables a fairly simple description of what can happen topologically. However, canonical coordinates do not coincide with user-defined coordinates, and cease to be useful if one aims to compute metrical properties of critical curves. This limitation led us to develop the covariant formalism, which is presented in the next section.

#### 4.2.4 Covariant Formalism

In practice the separation into “bad” and “nice” coordinate directions is not given. The actual realization of canonical coordinates varies from point to point, a fact that might lead one to believe that it requires an expensive procedure to handle catastrophes in scale space. However, the covariant formalism declines from the explicit construction of canonical coordinates altogether. It allows us (i) to carry out computations in any *user-defined coordinate system*, and (ii) to compute *metrical properties* of topological events (angles, directions, velocities, accelerations, *etc.*). It is often most convenient to employ a *Cartesian coordinate system*, adjusted to the grid of the digital image, and we shall do so at the end of this section in order to illustrate the results obtained. However, wherever we refrain from such an explicit choice the results are valid using any other type of coordinates, as long as they are admissible in the sense of being  $C^{\infty}$ -related to a Cartesian coordinate system by means of a locally defined homeomorphism; for details *cf.* Spivak [232]. Note that this excludes, among others, polar coordinates<sup>2</sup>!

<sup>2</sup>Although inadmissible in the technical sense, polar coordinates can often be employed without problems due to the relatively harmless singularity at the origin. However, our application of perturbation theory in what follows requires strict regularity.

The covariant formalism relies on tensor calculus. The only tensors we shall need are (i) metric tensor  $g_{\mu\nu}$  and its dual  $g^{\mu\nu}$  (the components of which in a Cartesian frame equal the Kronecker symbol  $\delta_{\nu}^{\mu}$ , *i.e.* 1 if  $\mu = \nu$ , otherwise 0), (ii) Levi-Civita tensor  $\varepsilon_{\mu_1 \dots \mu_n}$  and its dual  $\varepsilon^{\mu_1 \dots \mu_n}$  in  $n$  dimensional space, and (iii) *covariant derivatives* of the image. In a Cartesian frame the Levi-Civita tensor is defined as the completely antisymmetric tensor with  $\varepsilon_{1, \dots, n} = 1$ ; from this any other nontrivial component follows from permuting indices and toggling signs. Actually, we will only encounter products containing an even number of Levi-Civita tensors, which can always be rewritten in terms of metric tensors only (see *e.g.* Florack *et al.* [77] for details). One may substitute “partial derivative” for “covariant derivative” as long as one sticks to Cartesian frames or rectilinear coordinates. (This is all we need below.) More details on the abovementioned geometric concepts can be found in Spivak [232]. Wherever possible we will use matrix notation to alleviate theoretical difficulties, so that familiarity with the tensor formalism is not necessary.

(Covariant) derivatives at the fiducial origin can be extracted by linear filtering:

$$L_{\mu_1 \dots \mu_k} \stackrel{\text{def}}{=} (-1)^k \int d\mathbf{z} f(\mathbf{z}) \phi_{\mu_1 \dots \mu_k}(\mathbf{z}). \quad (4.2)$$

Here,  $(-1)^k \phi_{\mu_1 \dots \mu_k}(\mathbf{z})$  is the  $k$ -th order transposed derivative of the normalised Gaussian  $\phi(\mathbf{z})$  with respect to  $z^{\mu_1}, \dots, z^{\mu_k}$ , tuned to the location and scale of interest (these parameters have been left out for notational simplicity),  $d\mathbf{z}$  is the invariant spatial volume element – defined such that  $\int d\mathbf{z} \phi(\mathbf{z}) = 1$  irrespective of scale –, and  $f(\mathbf{z})$  represents the initial image. In particular, the components of the image gradient and Hessian are denoted by  $L_{\mu}$  and  $L_{\mu\nu}$ , respectively.

Distributional differentiation according to Eq. (4.2) is *well-posed* because it is actually integration. Well-posedness admits discretisation and quantisation of Eq. (4.2), and guarantees that other sources of small scale noise are not destructive. Of course the filters need to be realistic; for scale space filters this means that one keeps their scales confined to a physically meaningful interval, and that one keeps their differential order below an appropriate upper bound [24]. Equally important is the observation that Eq. (4.2) makes differentiation operationally *well-defined*. One can actually extract derivatives from an image in the first place, because things are arranged in such a way that, unlike with “classical” differentiation and corresponding numerical differencing schemes, *differentiation precedes discrete sampling*. In practice one will almost always calculate derivatives at all base points  $\mathbf{x}$  in the image domain; in that case Eq. (4.2) is replaced by a *convolution*:  $L_{\mu_1 \dots \mu_k}(\mathbf{x}) = f * \phi_{\mu_1 \dots \mu_k}(\mathbf{x})$ —the minus sign is then implicit.

The ensemble of image derivatives up to  $k$ -th order provides a model of local image structure in a full scale space neighbourhood, known as the *local jet of order k* [80, 91, 142, 148, 149, 212]. It is necessary and sufficient to consider structure up to fourth order at the voxel<sup>3</sup> of interest (the argument is given below):

$$\begin{aligned} \overset{(4)}{L}(\mathbf{x}; t) = & L + L_{\mu} x^{\mu} + \frac{1}{2} L_{\mu\nu} x^{\mu} x^{\nu} + \Delta L t \\ & + \frac{1}{6} L_{\mu\nu\rho} x^{\mu} x^{\nu} x^{\rho} + \Delta L_{\mu} x^{\mu} t + \frac{1}{24} L_{\mu\nu\rho\sigma} x^{\mu} x^{\nu} x^{\rho} x^{\sigma} \\ & + \frac{1}{2} \Delta L_{\mu\nu} x^{\mu} x^{\nu} t + \frac{1}{2} \Delta^2 L t^2. \end{aligned} \quad (4.3)$$

Summation convention applies to pairs of upper and lower indices. In particular, the  $n + 1$  constraints

<sup>3</sup>The term “voxel” refers to the volume element that corresponds to a grid point in scale space.



for the sub-voxel location of a non-Morse critical point can be approximated by

$$\begin{cases} \nabla L^{(4)}(\mathbf{x}; t) \approx 0, \\ \det \nabla \nabla^T L^{(4)}(\mathbf{x}; t) \approx 0. \end{cases} \quad (4.4)$$

It is understood that the coefficients of Eq. (4.3) are evaluated at a grid point somewhere near the non-Morse critical point (such a point is easily found with grid precision, *e.g.* by the method of zero-crossings). For a Morse critical point one simply leaves out the determinant constraint, leaving  $n$  (approximate) equations in  $n$  unknowns (and 1 scale parameter).

Let us investigate the system of Eqs. (4.3–4.4) in the immediate vicinity of a critical point of interest. Assume that  $(\mathbf{x}; t) = (\mathbf{0}; 0)$  labels a fiducial grid point near the desired zero-crossings, *i.e.* the base point for the numerical derivatives in Eqs. (4.2–4.3). Both gradient as well as Hessian determinant at the corresponding (or any neighbouring) voxel will be small, though odds are that they are not exactly zero. Then we know that Eq. (4.4) will be solved for  $(\mathbf{x}; t) \approx (\mathbf{0}; 0)$ , and we may use perturbation theory for interpolation to establish a lowest order sub-voxel solution. Uniqueness is enforced by *linearisation*, a legitimate method provided the assumption of genericity (an isolated creation or annihilation point) is not violated. (The zero-crossings method, by the way, also tells us when we should look for Morse critical points and discard the Hessian degeneracy constraint, *viz.* at voxels containing intersections of the  $n$  gradient zero-crossings, but not on or near a Hessian zero-crossing.)

Returning to the issue of sufficiency and necessity of fourth order, note that (i) *higher orders will not contribute* to the linearisation (sufficiency), whereas (ii) any further truncation will either lead to *loss of essential terms* in the linear system, or to a *violation of the diffusion constraint*, Eq. (4.1), *cf.* [80] (necessity). This readily follows by inspection of the linearisation procedure, the details of which are as follows. Introduce a formal parameter  $\varepsilon \approx 0$  corresponding to the order of magnitude of the left hand sides of Eq. (4.4) at the fiducial origin. Substitute  $(\mathbf{x}; t) = \varepsilon(\mathbf{x}_1; t_1)$  into Eq. (4.4) and collect terms of order  $\mathcal{O}(\varepsilon)$  (the terms of order zero vanish by construction). Absorbing the formal parameter back into the scaled quantities the result is the following linear system:

$$\begin{cases} L_{\mu\nu} x^\nu + \Delta L_\mu t & = -L_\mu, \\ \tilde{L}^{\mu\nu} L_{\mu\nu\rho} x^\rho + \tilde{L}^{\mu\nu} \Delta L_{\mu\nu} t & = -\|L_{\mu\nu}\|, \end{cases} \quad (4.5)$$

in which the  $\tilde{L}^{\mu\nu}$  are the components of the transposed cofactor matrix obtained from the Hessian (*cf.* the appendix), and  $\|L_{\mu\nu}\|$  denotes the Hessian determinant<sup>4</sup>. The determinant constraint (last identity) follows from a basic result in perturbation theory for matrices:

$$\det(\mathbf{A} + \varepsilon \mathbf{B}) = \det \mathbf{A} + \varepsilon \operatorname{tr}(\tilde{\mathbf{A}} \mathbf{B}) + \mathcal{O}(\varepsilon^2).$$

In Eq. (4.5) the coefficients and data on left and right hand sides can be obtained by any discrete implementation of the linear filtering of the initial image as defined by Eq. (4.2), so that we indeed have an operationally defined interpolation scheme for locating critical points within the scale space continuum. It is important to note that the system of Eq. (4.5) holds in any (admissible!) coordinate system (manifest covariance), thus in particular in any Cartesian coordinate system.

<sup>4</sup>This abuse of notation—there are actually *no* free indices in  $\|L_{\mu\nu}\|$ —is common in classical tensor calculus.

The next goal is to invert the system of Eq. (4.5) *while maintaining manifest covariance*. This obviates the need for numerical inversions or the construction of canonical frames for every candidate voxel in scale space, as is done for instance in Lindeberg's approach [170]. Also for conceptual reasons one may prefer explicit solutions over implicit ones that still require an inversion or Hessian eigensystem analysis. The analytical inversion differs qualitatively for Morse and non-Morse critical points and so we discuss the two cases separately.

It is convenient to rewrite Eq. (4.5) in matrix form with the help of the definitions

$$\mathbf{H}_{\mu\nu} \stackrel{\text{def}}{=} L_{\mu\nu}, \quad (4.6)$$

$$\mathbf{w}_\mu \stackrel{\text{def}}{=} \Delta L_\mu, \quad (4.7)$$

$$\mathbf{z}_\mu \stackrel{\text{def}}{=} L_{\mu\nu\rho} \tilde{L}^{\nu\rho}, \quad (4.8)$$

$$\mathbf{g}_\mu \stackrel{\text{def}}{=} L_\mu, \quad (4.9)$$

$$c \stackrel{\text{def}}{=} \Delta L_{\mu\nu} \tilde{L}^{\mu\nu}. \quad (4.10)$$

Note that

$$\mathbf{H} = \nabla \mathbf{g}, \quad (4.11)$$

$$\mathbf{w} = \partial_t \mathbf{g}, \quad (4.12)$$

$$\mathbf{z} = \nabla \det \mathbf{H}, \quad (4.13)$$

$$c = \partial_t \det \mathbf{H}, \quad (4.14)$$

*i.e.* all relevant information is contained in first order spatial and scale derivatives of the image's gradient and Hessian determinant, as it should.

With this notation the  $(n+1) \times (n+1)$  coefficient matrix of Eq. (4.5) becomes

$$\mathbf{M} \stackrel{\text{def}}{=} \begin{bmatrix} \mathbf{H} & \mathbf{w} \\ \mathbf{z}^T & c \end{bmatrix}, \quad (4.15)$$

in terms of which the linear system of Eq. (4.5) can be rewritten as

$$\mathbf{M} \begin{bmatrix} \mathbf{x} \\ t \end{bmatrix} = - \begin{bmatrix} \mathbf{g} \\ \det \mathbf{H} \end{bmatrix}. \quad (4.16)$$

### Morse Critical Points

For Morse critical points at fixed resolution the relevant subsystem in the hyper-plane  $t = 0$  is

$$\mathbf{H}\mathbf{x} = -\mathbf{g}, \quad (4.17)$$

but in fact we obtain a linear approximation of the *critical curve* through the Morse critical point of interest if we allow scale to vary:

$$\mathbf{H}\mathbf{x} = -(\mathbf{g} + \mathbf{w}t). \quad (4.18)$$

This can be easily generalised to any desired order.

From Eq. (4.18) it follows that at level  $t = 0$  the tangent to the critical curve in scale space is given by

$$\begin{bmatrix} \mathbf{x} \\ t \end{bmatrix} = \begin{bmatrix} \mathbf{x}_0 \\ 0 \end{bmatrix} + \begin{bmatrix} \mathbf{v} \\ \beta \end{bmatrix} t \quad (4.19)$$

in which the sub-voxel location of the Morse critical point is given by

$$\mathbf{x}_0 = -\mathbf{H}^{\text{inv}} \mathbf{g}, \quad (4.20)$$

and its instantaneous scale space velocity by

$$\begin{bmatrix} \mathbf{v} \\ \beta \end{bmatrix} = \begin{bmatrix} -\mathbf{H}^{\text{inv}} \mathbf{w} \\ 1 \end{bmatrix}. \quad (4.21)$$

Scale space velocity is an  $(n+1)$ -component quantity to be interpreted in the sense of a combined spatial displacement per unit of  $t$  (first  $n$  components) and a scale displacement per unit of  $t$  (last component), *i.e.* a vector plus a scalar quantity. Note that if scale is identified with  $t$ , then the last component reduces to unity, and the spatial vector coincides with Lindeberg’s “drift velocity” [170]. This is, however, not a good parametrisation at precisely those points that are of interest here (generic catastrophes).

Note that the path followed by Morse critical points is always transversal to the hyper-plane  $t = 0$ , which is why we can set the scale component equal to unity. In other words, such critical points can never vanish “just like that”; they necessarily have to change identity into a non-Morse variety. According to Eq. (4.21), spatial drift velocity  $\mathbf{v}$  becomes infinite as the point moves towards a degeneracy (odds are that  $\mathbf{w}$  remains nonzero), an observation already made by Lindeberg [170].

If we do not identify “time” with scale, but instead re-parametrise  $t = \det \mathbf{H} t'$ , then scale space velocity—now defined as the displacement per unit of  $t'$ —becomes

$$\begin{bmatrix} \mathbf{v}' \\ \beta' \end{bmatrix} = \begin{bmatrix} -\tilde{\mathbf{H}} \mathbf{w} \\ \det \mathbf{H} \end{bmatrix}. \quad (4.22)$$

With this refinement of the scale parameter the singularity is approached “horizontally” from a spatial direction perpendicular to the null-space of the Hessian (note, *e.g.* by diagonalising the Hessian, that  $\tilde{\mathbf{H}}$  becomes singular, yet remains finite when eigenvalues of  $\mathbf{H}$  degenerate). The trajectory of the critical point continues smoothly through the catastrophe point, where its “temporal sense” is reversed. This picture of the generic catastrophe captures the fact that there are always pairs of critical points of opposite Hessian signature that “belong together”, either because they share a common fate (annihilation) or because they have a common cause (creation). The two members of such a pair could therefore be seen as manifestations of a single “topological particle” if one allows for a non-causal interpretation, in much the same way as one can interpret positrons as instances of electrons upon time-reversal. The analogy with particle physics can be pursued further, as Kalitzin points out, by modelling catastrophes in scale space as interactions conserving a topological charge [131]. Indeed, charges are operationally well-defined conserved quantities that add up under point interactions at non-Morse critical points, irrespective their degree of degeneracy. This interpretation has the advantage that one can measure charges from spatial surface integrals around the point of interest (by using Stokes’ theorem), thus obtaining a “summary” of qualitative image structure in the interior irrespective of whether the enclosed critical points are generic

or not, or even detectable as such. So far, however, Kalitzin's approach has not been refined to the sub-voxel domain, and does not give us a local parametrisation of the critical curve.

The perturbative approach can be extended to higher orders without essential difficulties, yielding a local parametrisation of the critical curve of corresponding order. It remains a notorious problem to find the *optimal order* in numerical sense, because it is clear that although the addition of yet another order will *reduce* the formal truncation error due to the smaller Taylor tail discarded, it will at the same time *increment* the amount of intrinsic noise due to the computation of higher order derivatives. It is beyond the scope of this chapter to deal with this issue in detail; a point of departure may be Blom's study of noise propagation under simultaneous differentiation and blurring [24]. We restrict our attention to lowest nontrivial order. For Morse critical points this is apparently third order, for catastrophe points this will be seen to require fourth order derivatives.

If one knows the location of the catastrophe point one can find a similar critical curve parametrisation in terms of the parameter  $t'$ , starting out from this catastrophe point instead of a Morse critical point. In that case we first have to solve the catastrophe point localisation problem. It is clearly of interest to know the parametrisation *at the catastrophe point*, since this will enable us to identify the two corresponding branches of the Morse critical curves that are glued together precisely at this point. Our next objective will be to find the location of the catastrophe point with sub-voxel precision, as well as geometric properties of the critical curve passing through. The additional scale degree of freedom obviously becomes essential, because catastrophe points will typically be located in-between two pre-computed levels of scale.

### Catastrophe Points

For catastrophe points we must consider the full system of Eq. (4.16), since Eq. (4.20) breaks down at degeneracies of the Hessian. A discrete zero-crossings method for  $\mathbf{g}$ , respectively  $\mathbf{g}$  and  $\det \mathbf{H}$ , is to be preferred as a criterion for extracting the scale space voxels of interest, as it preserves connectivity and avoids the arbitrariness of setting a threshold.

Recall Eq. (4.15). Let us rewrite the corresponding cofactor matrix, the Cartesian coefficients of which are defined by (*cf.* the appendix)

$$\widetilde{\mathbf{M}}^{\mu\nu} \stackrel{\text{def}}{=} \frac{1}{n!} \varepsilon^{\mu\mu_1\dots\mu_n} \varepsilon^{\nu\nu_1\dots\nu_n} \mathbf{M}_{\mu_1\nu_1} \dots \mathbf{M}_{\mu_n\nu_n},$$

into a similar block form:

$$\widetilde{\mathbf{M}} \stackrel{\text{def}}{=} \begin{bmatrix} \overline{\mathbf{H}} & \overline{\mathbf{w}} \\ \overline{\mathbf{z}}^T & \overline{c} \end{bmatrix}. \quad (4.23)$$

By substitution one may verify that the defining equation  $\widetilde{\mathbf{M}}\mathbf{M} = \det \mathbf{M} \mathbf{I}_{(n+1)\times(n+1)}$  is satisfied iff the coefficients are defined as follows:

$$\begin{aligned} \overline{\mathbf{H}}^{\mu\nu} &\stackrel{\text{def}}{=} \frac{1}{(n-1)!} \varepsilon^{\mu\mu_1\dots\mu_{n-1}} \varepsilon^{\nu\nu_1\dots\nu_{n-1}} \mathbf{H}_{\mu_1\nu_1} \dots \mathbf{H}_{\mu_{n-2}\nu_{n-2}} \\ &\quad (c \mathbf{H}_{\mu_{n-1}\nu_{n-1}} - (n-1) \mathbf{w}_{\mu_{n-1}} \mathbf{z}_{\nu_{n-1}}), \\ \overline{\mathbf{w}}^\mu &\stackrel{\text{def}}{=} -\frac{1}{(n-1)!} \varepsilon^{\mu\mu_1\dots\mu_{n-1}} \varepsilon^{\nu\nu_1\dots\nu_{n-1}} \mathbf{H}_{\mu_1\nu_1} \dots \mathbf{H}_{\mu_{n-1}\nu_{n-1}} \mathbf{w}_\nu, \\ \overline{\mathbf{z}}^\mu &\stackrel{\text{def}}{=} -\frac{1}{(n-1)!} \varepsilon^{\mu\mu_1\dots\mu_{n-1}} \varepsilon^{\nu\nu_1\dots\nu_{n-1}} \mathbf{H}_{\mu_1\nu_1} \dots \mathbf{H}_{\mu_{n-1}\nu_{n-1}} \mathbf{z}_\mu, \\ \overline{c} &\stackrel{\text{def}}{=} \frac{1}{n!} \varepsilon^{\mu_1\dots\mu_n} \varepsilon^{\nu_1\dots\nu_n} \mathbf{H}_{\mu_1\nu_1} \dots \mathbf{H}_{\mu_n\nu_n}. \end{aligned}$$

In addition we have

$$\det \mathbf{M} = \frac{1}{n!} \varepsilon^{\mu_1 \dots \mu_n} \varepsilon^{\nu_1 \dots \nu_n} \mathbf{H}_{\mu_1 \nu_1} \dots \mathbf{H}_{\mu_{n-1} \nu_{n-1}} (c \mathbf{H}_{\mu_n \nu_n} - n \mathbf{w}_{\mu_n} \mathbf{z}_{\nu_n}).$$

In coordinate-free notation we have

$$\bar{\mathbf{z}} = -\tilde{\mathbf{H}}\mathbf{z}, \quad (4.24)$$

$$\bar{\mathbf{w}} = -\tilde{\mathbf{H}}\mathbf{w}, \quad (4.25)$$

$$\bar{c} = \det \mathbf{H} \quad (4.26)$$

Note that  $(\bar{\mathbf{w}}; \bar{c}) = (\mathbf{v}'; \beta')$ , recall Eq. (4.22). Finally,  $\det \mathbf{M} = c \det \mathbf{H} - \text{tr}(\tilde{\mathbf{H}}\mathbf{w}\mathbf{z}^T)$ . At the location of a critical point this is proportional to the scale space scalar product of the critical point's scale space velocity and the scale space normal to the Hessian zero-crossing (recall Eqs. (4.13–4.14), Eq. (4.22) and the remark above):

$$\det \mathbf{M} = \mathbf{z}^T \bar{\mathbf{w}} + c \bar{c} = \mathbf{w}^T \bar{\mathbf{z}} + c \bar{c}. \quad (4.27)$$

**Theorem 1 (Transversality)** *At a catastrophe point the critical curve intersects the Hessian zero-crossing transversally.*

**Proof of theorem 1** *This readily follows by inspection of the tangent hyper-plane to the Hessian zero-crossing,*

$$\mathbf{z}^T \mathbf{x} + c t = 0, \quad (4.28)$$

*and the critical curve's tangent vector, Eq. (4.22). The cosine of the angle of intersection follows from Eq. (4.27), which is nonzero in the generic case:  $\det \mathbf{M} \neq 0$  at catastrophe points; genericity implies transversality.  $\square$*

With the established results it is now possible to invert the linear system of Eq. (4.16); just note that

$$\mathbf{M}^{\text{inv}} = \frac{1}{\det \mathbf{M}} \tilde{\mathbf{M}}, \quad (4.29)$$

so that

$$\begin{bmatrix} \mathbf{x} \\ t \end{bmatrix} = -\frac{1}{\det \mathbf{M}} \begin{bmatrix} \bar{\mathbf{H}}\mathbf{g} + \bar{\mathbf{w}}\bar{c} \\ \bar{\mathbf{z}}^T \mathbf{g} + \bar{c}^2 \end{bmatrix}.$$

The expression is valid in any coordinate system as required. Note that the sign of  $\det \mathbf{M}$  subdivides the image domain into regions to which all generic catastrophes are confined. In fact, the following lemma holds.

**Lemma 1 (Creations versus Annihilations)** *At annihilations we have  $\det \mathbf{M} < 0$ , at creations  $\det \mathbf{M} > 0$ .*

One way to see this is to note that it holds for the canonical forms  $f^A$  and  $f^C$  of Definition 2. If we now transform these under an arbitrary coordinate transformation, it is easily verified that the sign of  $\det \mathbf{M}$  is preserved. An alternative proof based on geometric reasoning is given below.

**Proof of lemma 1** First consider an annihilation event, and recall Eqs. (4.13–4.14), and the geometric interpretation of Eqs. (4.25) and (4.26) as the scale space velocity given by Eq. (4.22). As the topological particle with positive charge (i.e. the Morse critical point with  $\det \mathbf{H} > 0$ ) moves towards the catastrophe (towards increasing scale), the magnitude of  $\det \mathbf{H}$  must necessarily decrease. By the same token, as the anti-particle ( $\det \mathbf{H} < 0$ ) moves away from the catastrophe (towards decreasing scale), the magnitude of  $\det \mathbf{H}$  must decrease as well. But recall that at the catastrophe  $\det \mathbf{M} = \mathbf{z}^T \bar{\mathbf{w}}$  is just the directional derivative of  $\det \mathbf{H}$  in the direction of motion as indicated. Therefore  $\det \mathbf{M} < 0$ .

Next consider a creation event. The positive particle now escapes the singularity in the positive scale direction, whereas the negative particle approaches it in the negative scale direction, so that along the prescribed path  $\det \mathbf{H}$  must necessarily increase. In other words,  $\det \mathbf{M} > 0$  at the catastrophe. This completes the proof.  $\square$

The lemma is a special case of the following, more general result, which gives us the curvature of the critical curve at the catastrophe.

**Theorem 2 (Critical Path)** At the location of a generic catastrophe the critical curve satisfies

$$t = \frac{1}{2} \frac{1}{\det \mathbf{M}} \left( \mathbf{z}^T \mathbf{x} \right)^2 + \mathcal{O}(\|\mathbf{x}\|^3, \|\mathbf{x}\| t, t^2).$$

The curvature of the critical curve at the catastrophe is given by

$$\kappa_{\text{catastrophe}} = \frac{\det \mathbf{M}}{\bar{\mathbf{w}}^T \bar{\mathbf{w}}}.$$

**Proof of theorem 2** Consider the local 3-jet expansion at the location of a generic catastrophe:

$$\begin{cases} \nabla \overset{(3)}{L}(\mathbf{x}; t) & \approx 0, \\ \det \nabla \nabla^T \overset{(3)}{L}(\mathbf{x}; t) & \approx 0, \end{cases}$$

in which  $L_\mu = 0$  and  $\|L_{\mu\nu}\| = 0$ . From this it follows that along the critical curve through the catastrophe

$$\Delta L_\mu t = -L_{\mu\nu} x^\nu - \frac{1}{2} L_{\mu\nu\rho} x^\nu x^\rho + \mathcal{O}(\|\mathbf{x}\|^3, \|\mathbf{x}\| t, t^2).$$

Contraction with  $\tilde{L}^{\mu\nu}$  and ignoring  $\mathcal{O}$ -terms yields

$$\tilde{L}^{\mu\nu} \Delta L_\mu t = -\tilde{L}^{\mu\nu} L_{\mu\nu} x^\nu - \frac{1}{2} \tilde{L}^{\mu\nu} L_{\mu\nu\rho} x^\nu x^\rho.$$

Noting that  $\tilde{L}^{\mu\nu} L_{\mu\nu} = \det \mathbf{H} \mathbf{I}_{n \times n} = 0$  at the catastrophe and using Eqs. (4.6 - 4.8), and (4.25), we have

$$\bar{\mathbf{w}}^\nu t = \frac{1}{2} (\mathbf{z}_\rho x^\rho) x^\nu.$$

Contraction with  $\mathbf{z}_\nu$ , and using Eq. (4.24) yields

$$\mathbf{z}^T \bar{\mathbf{w}} t_{\text{catastrophe}} = \frac{1}{2} \left( \mathbf{z}^T \mathbf{x} \right)^2.$$

Recall that  $\mathbf{z}^T \bar{\mathbf{w}} = \det \mathbf{M}$  at a catastrophe point, so that the first result follows. Twofold differentiation in  $\bar{\mathbf{w}}$ -direction produces the curvature expression. Note that this is a dimensionless quantity.  $\square$

### Explicit Results from the Covariant Formalism

Having established covariant expressions we have drawn several geometric conclusions that do not follow from the canonical formalism. Here we give a few more examples, using explicit Cartesian coordinates in 2D. Then  $\mathbf{x} = (x, y)$  and

$$\mathbf{H} = \begin{bmatrix} L_{xx} & L_{xy} \\ L_{xy} & L_{yy} \end{bmatrix}, \quad (4.30)$$

$$\mathbf{w} = \begin{bmatrix} L_{xxx} + L_{xyy} \\ L_{xxy} + L_{yyx} \end{bmatrix}, \quad (4.31)$$

$$\mathbf{z} = \begin{bmatrix} L_{xxx}L_{yy} + L_{xx}L_{xyy} - 2L_{xy}L_{xxy} \\ L_{yyy}L_{xx} + L_{yy}L_{xxy} - 2L_{xy}L_{xyy} \end{bmatrix}, \quad (4.32)$$

$$c = L_{xx}(L_{xxy} + L_{yyy}) + L_{yy}(L_{xxx} + L_{xxy}) - 2L_{xy}(L_{xxy} + L_{xyy}), \quad (4.33)$$

and

$$\tilde{\mathbf{H}} = \begin{bmatrix} L_{yy} & -L_{xy} \\ -L_{xy} & L_{xx} \end{bmatrix}. \quad (4.34)$$

Expressions for  $\bar{\mathbf{w}}$ ,  $\bar{\mathbf{z}}$ ,  $\tilde{\mathbf{M}}$ ,  $\bar{\mathbf{M}}$ , and  $\tilde{\mathbf{H}}$  can be calculated straightforwardly.

**Example 1** *At any point on the critical curve—including the catastrophe point—any scale space tangent vector is proportional to the regularised scale space velocity given by Eq. (4.22). In 2D Cartesian coordinates we have*

$$\begin{bmatrix} \mathbf{v}'_x \\ \mathbf{v}'_y \\ \beta' \end{bmatrix} = \begin{bmatrix} (L_{xxy} + L_{yyx})L_{xy} - (L_{xxx} + L_{xyy})L_{yy} \\ (L_{xxx} + L_{xyy})L_{xy} - (L_{xxy} + L_{yyx})L_{xx} \\ L_{xx}L_{yy} - L_{xy}^2 \end{bmatrix}.$$

Recall that the prime indicates that velocity is to be interpreted as the displacement in scale space per unit of re-parametrised scale  $t' = t / \det \mathbf{H}$ .

**Example 2** *In 2D the tangent plane to the Hessian zero-crossing in scale space is given by the following equation in any Cartesian coordinate system:*

$$(L_{xxx}L_{yy} + L_{xx}L_{xyy} - 2L_{xy}L_{xxy})x + (L_{yyy}L_{xx} + L_{yy}L_{xxy} - 2L_{xy}L_{xyy})y + ((L_{xxy} + L_{yyx})L_{xx} + (L_{xxx} + L_{xyy})L_{yy} - 2(L_{xxy} + L_{xyy})L_{xy})t = 0.$$

**Example 3** *In a full (2+1)D scale space neighbourhood of an annihilation (creation) the following differential invariant always has a negative (positive) value:*

$$\begin{aligned} \det \mathbf{M} = & ([L_{xxy} + L_{yyx}]L_{xx} + [L_{xxx} + L_{xyy}]L_{yy} \\ & - 2[L_{xxy} + L_{yyx}]L_{xy})(L_{xx}L_{yy} - L_{xy}^2) \\ & - \{L_{xx}[L_{xxy} + L_{yyx}][L_{yyy}L_{xx} + L_{yy}L_{xxy} - 2L_{xy}L_{xyy}] \\ & + L_{yy}[L_{xxx} + L_{xyy}][L_{xxx}L_{yy} + L_{xx}L_{xyy} - 2L_{xy}L_{xxy}] \\ & - L_{xy}([L_{xxx} + L_{xyy}][L_{yyy}L_{xx} + L_{yy}L_{xxy} - 2L_{xy}L_{xyy}] \\ & + [L_{xxy} + L_{yyx}][L_{xxx}L_{yy} + L_{xx}L_{xyy} - 2L_{xy}L_{xxy}])\} \end{aligned}$$

The expressions in Cartesian coordinate systems are a bit complicated, but nevertheless follow straightforwardly from their condensed covariant counterparts, which at the same time illustrates the power of the covariant formalism. Moreover, they are easily computed in terms of basic algebraic combinations of the outputs of a small number of image convolutions, just recall Eq. (4.2). In the next section we will apply these results to several images.

### 4.3 Experimental Results

In our experiments we used a  $64 \times 64$  sub-images of a  $256 \times 256$  MR scan (Figure 4.1, top row), a CT scan (Figure 4.1, middle row), and a  $64 \times 64$  artificial image containing only  $N(0,10)$  Gaussian noise, *i.e.* zero mean and standard deviation  $\sigma = 10$  (Figure 4.1, bottom row).

#### 4.3.1 Visualisation of $\mathbf{z}^T$ and $\overline{\mathbf{w}}$

As an example of the vectors  $\overline{\mathbf{w}}$  (see Eq. (4.25)) and  $\mathbf{z}^T$  (see Eq. (4.13)) we selected two critical points of the MR image (Figure 4.1b) at scale  $\sigma = 2.46$ . This image with its critical points is shown in Figure 4.2a. Extrema (saddle points) are visualised by the white (black) dots. At the upper middle part of this image a critical isophote generated by a saddle and enclosing two extrema is shown (see also Figure 4.2b). At a larger scale the saddle point will annihilate with the upper one of these extrema. At these two points we have calculated the direction and magnitude of the vectors  $\overline{\mathbf{w}}$  and  $\mathbf{z}^T$ . The vectors are shown on these points at two successive scales  $\sigma = 2.46$  (Figure 4.2c) and  $\sigma = 2.83$  (Figure 4.2d). Indeed the velocity (given by  $\overline{\mathbf{w}}$ ) of the extremum (dark arrow at the white dot) is in the direction of the saddle, and thus in the direction of the point of annihilation. The velocity vector at the saddle has the same direction, as the result of the parametrisation by Eq. (4.25).

Furthermore, since the point where the annihilation takes place (at  $\det \mathbf{H} = 0$ ) is between the two critical points, the vector  $\mathbf{z}^T$ , which is the normal vector (recall Eq. (4.15)) to the zero-crossing of  $\det \mathbf{H}$ , directs from the saddle towards the extremum both at the saddle and the extremum.

Finally, it can be seen that the vectors of  $\mathbf{z}^T$  and  $\overline{\mathbf{w}}$  at the critical points have an angle of more than  $\frac{\pi}{2}$ . Since  $\det \mathbf{M}$  is the inner product of these vectors at a catastrophe (see Eq. (4.27)), this leads to a negative sign of  $\det \mathbf{M}$ , indicating that the two critical points approach each other and disappear eventually.

#### 4.3.2 Location of the Catastrophe

Although the location of the critical points at the image can easily be calculated by using the zero-crossings of the derivatives, the sub-pixel position of the catastrophe point in scale space requires inversion of the complete linear system, Eq. (4.16), yielding Eq. (4.29). As an example we took the same two critical points as in the previous section. The resulting vectors of 4 successive scales for the MR sub-image (Figure 4.2c) are shown in Figure 4.3. At each pixel the projection of the vector on the spatial plane is shown. A bright (dark) arrow denotes a positive (negative) scale-coordinate. The approximate location of the catastrophe can be found with sub-pixel precision by averaging the arrows as shown in Table 4.1. The black dot in Figure 4.3 is located at the estimated position of the catastrophe, the ellipse shows the standard deviation of the estimation.

Below the catastrophe-scale the location is accurate whereas at a scale above it (at  $\sigma = 3.32$ , see Figure 4.3h) the estimated location turns out to be more uncertain. The estimation of the  $t$ -coordinate



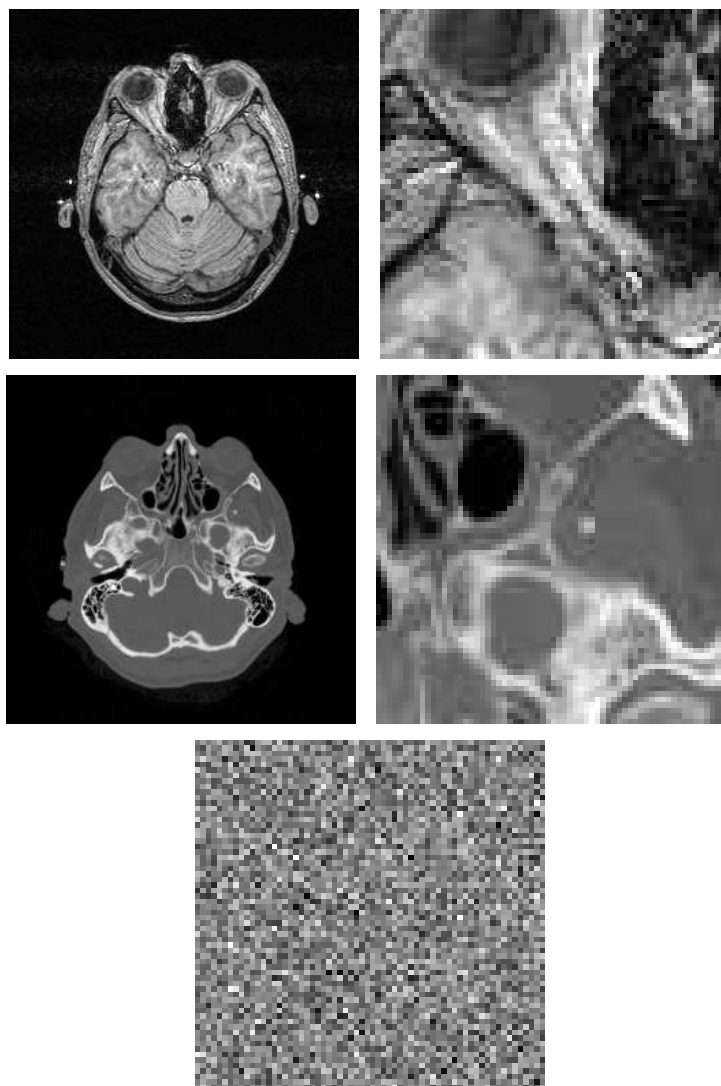


Figure 4.1: Top row: Left) Original  $256 \times 256$  pixel MR image. Right)  $64 \times 64$  pixel sub-image. Middle row: Left) Original  $256 \times 256$  pixel CT image. Right)  $64 \times 64$  pixel sub-image. Bottom row:  $64 \times 64$  artificial Gaussian  $N(0,10)$  noise image.

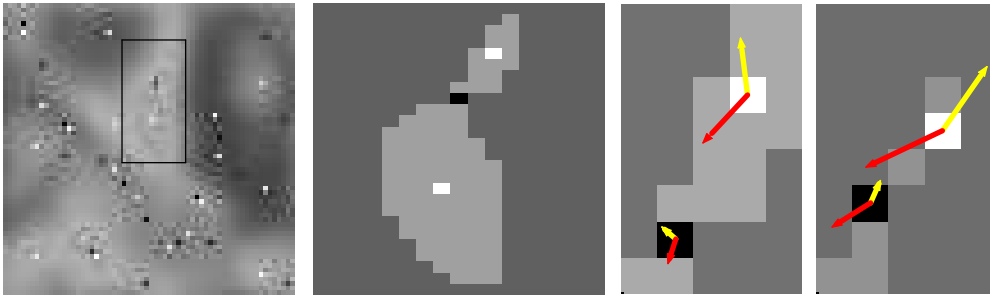


Figure 4.2: a) Critical points (extrema white, saddles black) of Figure 4.1b at scale  $\sigma = 2.46$ . At the field of interest the critical isophote through a saddle is shown; b) sub-image of a, showing the field of interest more clearly. The saddle is about to annihilate with the upper extremum; c) Sub-image of the two annihilating critical points and the vectors of  $\bar{w}$  (dark) and  $z^T$  (bright) at scale  $\sigma = 2.46$ ; d) Same, at scale  $\sigma = 2.83$ .

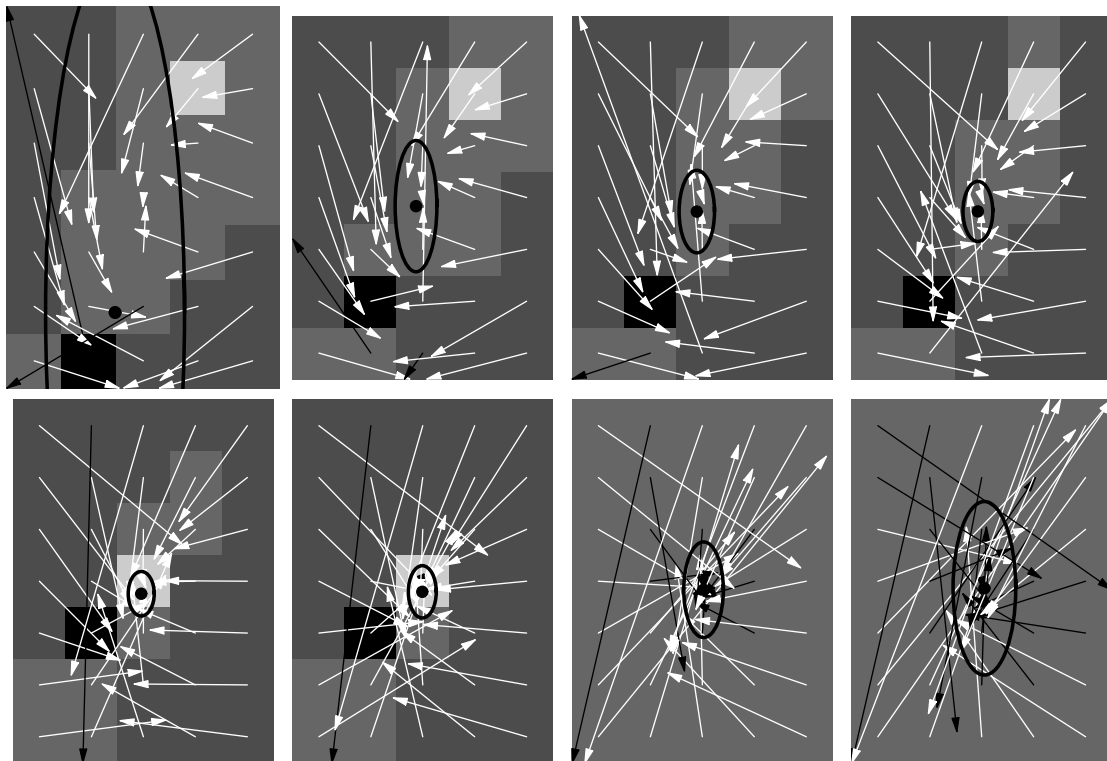


Figure 4.3: Visualisation of Eq. (4.29) of the vector  $(x, y)$ ; a bright (dark) arrow signifies a positive (negative) value of the  $t$ -component. The black dot is located at the mean value of the inner 15 arrows, the ellipse shows the standard deviation (see Table 4.1). First row: a: scale  $\sigma = 2.34$ ; b: scale  $\sigma = 2.46$ ; c: scale  $\sigma = 2.59$ ; d: scale  $\sigma = 2.72$ . Second row: e: scale  $\sigma = 2.86$ ; f: scale  $\sigma = 3.00$ ; g: scale  $\sigma = 3.16$ , a catastrophe has occurred; h: scale  $\sigma = 3.32$ .

scale	x-coordinate	y-coordinate	t-coordinate	estimated scale
2.34	0.48 ± 1.27	-0.11 ± 6.54	0.63 ± 3.76	2.60 ± 1.45
2.46	0.87 ± 0.40	1.83 ± 1.27	1.59 ± 0.66	3.04 ± 0.22
2.59	0.89 ± 0.34	1.73 ± 0.80	1.34 ± 0.45	3.06 ± 0.15
2.72	0.92 ± 0.29	1.73 ± 0.58	1.11 ± 0.43	3.10 ± 0.14
2.86	0.96 ± 0.25	1.76 ± 0.43	0.82 ± 0.48	3.13 ± 0.15
3.00	0.99 ± 0.27	1.80 ± 0.50	0.47 ± 0.60	3.16 ± 0.19
3.16	1.02 ± 0.38	1.84 ± 0.92	-0.0057 ± 0.79	3.16 ± 0.25
3.32	1.05 ± 0.60	1.86 ± 1.67	-0.64 ± 1.11	3.12 ± 0.35

Table 4.1: Estimation of the location of the catastrophe, as an average of the 15 arrows in the rectangle spanned by the two critical points of Figure 4.3a. The origin in the  $(x, y)$ -plane is fixed for all figures at the middle of the saddle (black square) of Figure 4.3a. The average value of the  $t$ -direction is positive below catastrophe scale and negative above it.

is positive below catastrophe-scale and negative above, as expected. The standard deviation is largely influenced by the cells that are distant from the critical curve, which also can be seen in Fig 4.3h. Since the relation between scale  $\sigma$  and coordinate  $t$  is given by  $t = \frac{1}{2}\sigma^2$ , we can easily calculate the estimated scale  $\sigma_{est} = \sqrt{\sigma^2 + 2t_{calc}}$  with error  $\delta\sigma_{est} = \partial_t\sigma_{est} \cdot \delta t_{calc} = \delta t_{calc}/\sigma_{est}$ .

By slightly increasing scales the catastrophe is experimentally found between the scales 3.050 and 3.053, which is covered by all estimated scales in Table 4.1. Since the estimation is a linear approximation of the top of a curve, a small overestimation (*here*: a tenth of a pixel) is expected and indeed found in this case. In summary the location of the catastrophe point can be pinched down by linear estimation with sub-pixel precision.

### 4.3.3 Fraction of the Area Where $\det \mathbf{M} > 0$

Since creations can only occur at  $\det \mathbf{M} > 0$ , we calculated the number of pixels at the three different images (Figures 4.1a, c and e) where this invariant is positive. If we for the moment assume that all elements of the matrix  $\mathbf{M}$  are independent of each other, the distribution of catastrophes is in some sense random in the image, just as the distribution of extrema and saddle points, discriminated by the areas  $\det \mathbf{H} > 0$  and  $\det \mathbf{H} < 0$ , respectively. However, since annihilations are supposed to occur more often and the derivatives up to third and fourth order are not independent since they have to satisfy the heat equation, we expect the area where  $\det \mathbf{M} > 0$  to be small. In the following figures we show this fraction as a percentage of the total area of the image.

For the MR image we see relative areas up to 0.12 (Figure 4.4, top-left). Furthermore the number of critical points decreases logarithmically with scale (Figure 4.4, top-right). The slope is  $-1.76 \pm .01$ . An a priori estimation value is -2, see *e.g.* Florack's monograph [65].

In Figure 4.5 the image of the sign of  $\det \mathbf{M}$  of the MR-subimage (Figure 4.1b) is shown at four successive scales. It appears that the locations of the image where  $\det \mathbf{M}$  is positive are relatively small isolated areas.

For the CT image we see more or less the same results (Figure 4.4, second row): the fraction where  $\det \mathbf{M}$  is positive is a bit higher at small scales ( $\sigma < 2.22$ , the value 40 at the horizontal axis) and a bit

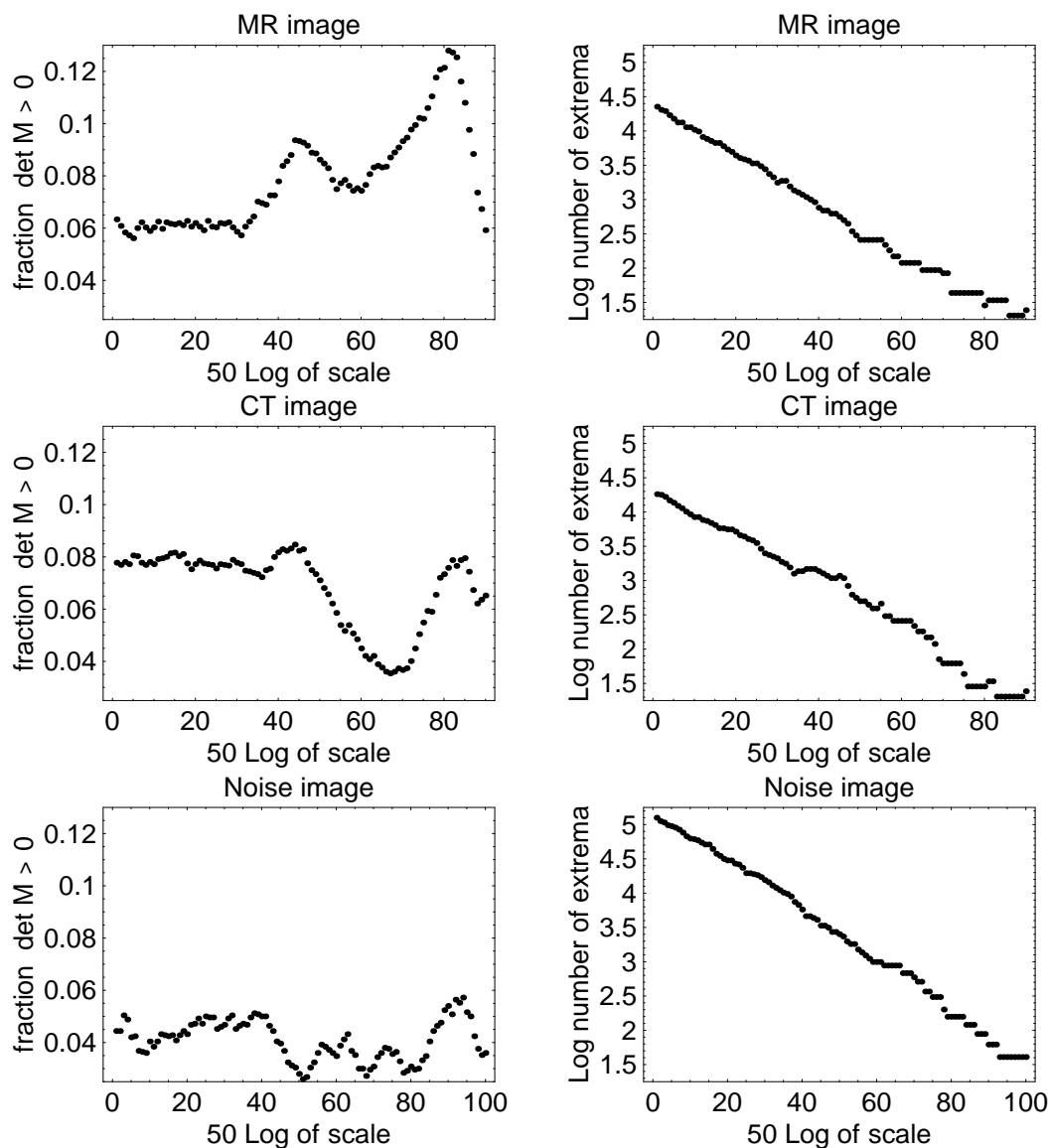


Figure 4.4: Results of calculations; scales vary from  $e^{1/50}$  to  $e^{90/50}$ ; First row: MR image; Second row: CT image; Third row: artificial noise image. First column: Fraction of  $\det M > 0$ , ranging from 0.04 to 0.12 for the MR and CT image, and less for the artificial noise image; Second column: Logarithm of the number of critical points, with slopes  $-1.76 \pm .01$ ,  $-1.74 \pm .02$ , and  $-1.84 \pm .01$ , respectively.

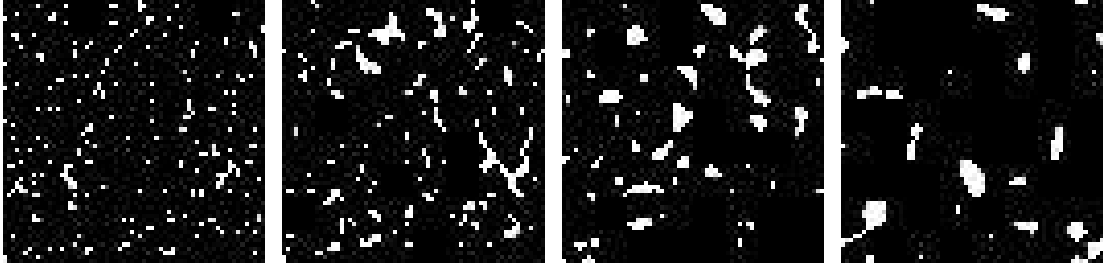


Figure 4.5: In white the area where  $\det \mathbf{M} > 0$ . a) At scale  $\sigma = 1.57$ , corresponding to the value 22.5 on the horizontal axis of Figure 4.4. b) At scale  $\sigma = 2.46$  (value 45). c) At scale  $\sigma = 3.866$  (value 67.5). d) At scale  $\sigma = 6.05$  (value 90).

smaller at high scales. The slope of graph of the logarithm of the number of critical points at increasing scale is found to be  $-1.74 \pm 0.02$ .

At the noise image the relative area where  $\det \mathbf{M} > 0$  is significantly smaller than at the MR and CT images. This might indicate that creations require some semi-global structure (like a ridge), that is very unlikely in a noise image. The logarithm of the number of extrema has a slope of  $-1.84 \pm .01$  (Figure 4.4, bottom-right), which is closer to the expected value -2 than the slope at the MR and CT image. This might also be caused by the lack of structure in the noise image.

#### 4.3.4 Estimation of the Area Where $\det \mathbf{M} > 0$

In the previous section the fraction of the area where  $\det \mathbf{M} > 0$  was found to be ranging from 0.04 to 0.12. A mathematical survey on the sign of  $\det \mathbf{M}$  might show the expectation of creations. At non-Morse points this invariant can be simplified considerably. If the Hessian becomes singular, the rows (or, equivalently the columns) are dependent of each other, *i.e.*  $(L_{xx}, L_{xy}) = \lambda(L_{xy}, L_{yy})$ . Therefore<sup>5</sup>  $L_{xx} = \lambda^2 L_{yy}$  and  $L_{xy} = \lambda L_{yy}$ . So in general, the Hessian and its transposed co-factor matrix at a catastrophe can be described by

$$\mathbf{H} = \begin{bmatrix} \lambda^2 & \lambda \\ \lambda & 1 \end{bmatrix} L_{yy}, \quad \tilde{\mathbf{H}} = \begin{bmatrix} 1 & -\lambda \\ -\lambda & \lambda^2 \end{bmatrix} L_{yy} \quad (4.35)$$

The second order Taylor expansion of the image now reads  $\frac{1}{2}\lambda^2 L_{yy} x^2 + \lambda L_{yy} x y + L_{yy} y^2$  which reduces to  $\frac{1}{2}L_{yy}(\lambda x + y)^2$ . The parameter  $\lambda$  depends on the rotation between the axes of the covariant and the canonical coordinates. If these coincide we have  $\lambda = 0$ , *i.e.* both  $L_{xx}$  and  $L_{xy}$  are zero, see Definition 2). With Eq. (4.35) the explicit form of  $\det \mathbf{M}$  at a catastrophe in 2D reduces significantly to

$$\det \mathbf{M} = L_{yy}^2 (L_{xxx} - 3\lambda L_{xxy} + 3\lambda^2 L_{xyy} - \lambda^3 L_{yyy})(-L_{xxx} + \lambda L_{xxy} - L_{xyy} + \lambda L_{yyy}) \quad (4.36)$$

Equation (4.36) shows that the sign of  $\det \mathbf{M}$  only depends on third order derivatives and the orientation of the critical curve, as determined by  $\lambda$ . If we assume that all third order derivatives are independent, the

<sup>5</sup>The choice of  $L_{yy}$  as leading term is of minor importance, we could just as well have chosen  $\mu(L_{xx}, L_{xy}) = (L_{xy}, L_{yy})$ , leading to  $L_{yy} = \mu^2 L_{xx}$  and  $L_{xy} = \mu L_{xx}$ , which would be particularly prudent if  $L_{yy}$  is close to zero.

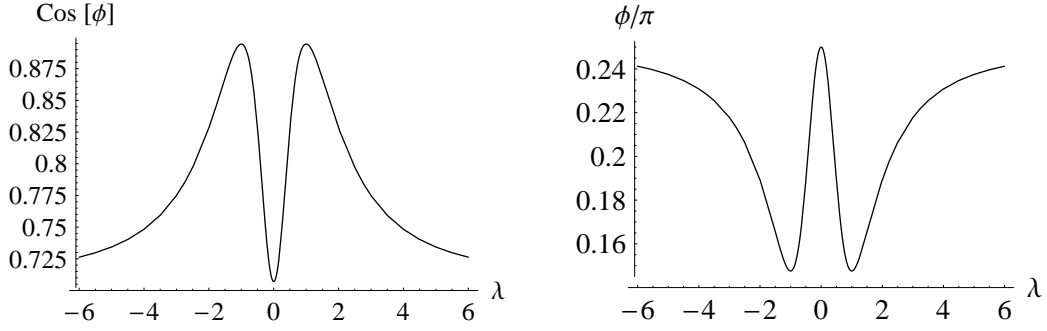


Figure 4.6: Left: Cosine of the angle of planes given by Eq. (4.37). Right: Fraction of the 4D  $(L_{xxx}, L_{xxy}, L_{xyy}, L_{yyy})$ -space where  $\det \mathbf{M}$  is smaller than zero.

zerocrossings of equation (4.36) can be regarded as the union of two linear planes in the 4-dimensional  $(L_{xxx}, L_{xxy}, L_{xyy}, L_{yyy})$  space. The planes divide this space into 4 subspaces where the determinant is either positive or negative, whereas any point on the planes leads to  $\det \mathbf{M} = 0$ . The normal vectors to these planes are given by  $n_1 = (1, -3\lambda, 3\lambda^2, -\lambda^3)$  and  $n_2 = (-1, \lambda, -1, \lambda)$ . The factor  $L_{yy}^2$  does not change the sign of the determinant. By definition we then have

$$\cos \phi = \frac{n_1 \cdot n_2}{\|n_1\| \cdot \|n_2\|} = -\frac{1 + 6\lambda^2 + \lambda^4}{\sqrt{(2 + 2\lambda^2)(1 + 9\lambda^2 + 9\lambda^4 + \lambda^6)}} \quad (4.37)$$

This angle is invariant with respect to the transformations  $\lambda \rightarrow -\lambda$  and  $\lambda \rightarrow \frac{1}{\lambda}$ . Figure 4.6a shows the cosine of the angle for different values of  $\lambda$ .

**Lemma 2** *The fraction  $\mu$  of the space of third order derivatives where creations can occur is bounded by  $\frac{1}{\pi} \arccos(\frac{2}{5}\sqrt{5}) \leq \mu \leq \frac{1}{4}$ .*

**Proof of lemma 2** *The fraction of the space where annihilations can occur is given by the fraction of the image where  $\det \mathbf{M} < 0$  and  $\det \mathbf{H} = 0$ . Since Eq. (4.37) is negative definite and  $\phi \in [0, \pi]$ , the fraction  $\frac{\phi}{\pi}$  gives the fraction of the space where annihilations can occur. This fraction varies from  $\frac{3}{4}$  at both  $\lambda = 0$  and  $\lambda \rightarrow \infty$ , to  $\frac{1}{\pi} \arccos(-\frac{2}{5}\sqrt{5}) \approx 0.852 \dots$  at  $\lambda = 1$ , which follow directly from differentiation, see also Figure 4.6b. Equivalently, creations can occur in at most  $\frac{1}{4}$  of all possible tuples  $(L_{xxx}, L_{xxy}, L_{xyy}, L_{yyy})$ .  $\square$*

The usual generic events, e.g. discussed by Damon [45] and others [124], correspond to the case  $\lambda = 0$ . In the canonical coordinates the equations Definition 2) are found. Then Eq. (4.36) reduces to  $\det \mathbf{M} = -L_{yy}^2 L_{xxx} (L_{xxx} + L_{xxy})$  and it can easily be seen that the fraction of the space is  $\frac{1}{4}$ , i.e. in only a quarter of the possible values of  $L_{xxx}$  and  $L_{xxy}$  a creation can occur.

## 4.4 Conclusion and Discussion

We have described the deep structure of a scale space image in terms of an operational scheme to characterise, detect and localise critical points in scale space. The characterisation pertains to local geometrical

properties of the scale traces of individual critical points (locations, angles, directions, velocities, accelerations), as well as to topological ones. The latter fall into two categories, local and bilocal properties. The characteristic local property of a critical point is determined by its Hessian signature (Morse  $i$ -saddle or catastrophe point), which in turn defines its topological charge. The fact that pairs of critical points of opposite charge can be created or annihilated as resolution decreases determines bilocal connections; such pairs of critical points can be labelled according to their common fate or cause, *i.e.* they can be linked to their corresponding catastrophe (annihilation, respectively creation). Close to such catastrophes, empirically observed properties of the critical points are consistent with the presented theory. The location of catastrophes in scale space can be found with subpixel accuracy. The approximate location of an annihilation and the idea of scale space velocity have been visualised.

The possibility to establish links is probably the most important topological feature provided by the Gaussian scale space paradigm. Because bifurcations in a link-tree ideally reflect the morsifications of the catastrophes in scale space (as these determine the unfolding of topological structure over scale), the results of this study can be used to establish a rigorous mathematical underpinning of various multiresolution techniques that are used in image analysis.

Conceptually a scale space representation is a continuous model imposed on a discrete set of pixel data. The events of topological interest in this scale space representation are clearly the catastrophe points, and the question presents itself whether these discrete events in turn suffice to define a complete and robust discrete representation of the continuous scale space image (possibly up to a trivial invariance). An important role is played by creations. In general, more annihilations than creations are observed, because creations need a “special structure” of the neighbourhood. This is also indicated by the results of the test images. In the 1D case it has been proven to be possible to reconstruct the initial image data from its scale space catastrophe points, at least in principle [129], but the problem of robustness and the extension to higher dimensions is still unsolved. The solution to this problem affects multiresolution schemes for applications beyond image segmentation, such as registration, coding, compression, *etc.* The experimental reconstructions shown by Nielsen and Lillholm [198] are promising results in this context.

## 4.5 Appendix: Determinants and Cofactor Matrices

**Definition 3** Let  $\mathbf{A}$  be a square  $n \times n$  matrix with components  $a_{\mu\nu}$ . Then we define the transposed cofactor matrix  $\tilde{\mathbf{A}}$  as follows. In order to obtain the matrix entry  $\tilde{a}^{\mu\nu}$  skip the  $\mu$ -th column and  $\nu$ -th row of  $\mathbf{A}$ , evaluate the determinant of the resulting submatrix, and multiply by  $(-1)^{\mu+\nu}$  (“checkerboard pattern”). Or, using tensor notation,

$$\tilde{\mathbf{A}}^{\mu\nu} \stackrel{\text{def}}{=} \frac{1}{(n-1)!} \varepsilon^{\mu\mu_1\dots\mu_{n-1}} \varepsilon^{\nu\nu_1\dots\nu_{n-1}} \mathbf{A}_{\mu_1\nu_1} \dots \mathbf{A}_{\mu_{n-1}\nu_{n-1}}.$$

By construction we have  $\mathbf{A}\tilde{\mathbf{A}} = \det \mathbf{A} \mathbf{I}$ . Note that if the components of  $\mathbf{A}$  are indexed by lower indices, then by convention one uses upper indices for those of  $\tilde{\mathbf{A}}$  (*vice versa*). Furthermore, it is important for the considerations in this chapter to observe that the transposed cofactor matrix is always well-defined, and that its components are homogeneous polynomial combinations of those of the original matrix of degree  $n-1$ . In the nonsingular case one has  $\tilde{\mathbf{A}} = \det \mathbf{A} \mathbf{A}^{\text{inv}}$ ; transposed cofactor matrix equals inverse matrix times determinant. See *e.g.* Strang [235].





---

## Scale Space Hierarchy

---

It requires a very unusual mind to undertake the analysis of the obvious.

---

ALFRED NORTH WHITEHEAD

**abstract** We investigate the deep structure of a scale space image. We concentrate on scale space critical points – points with vanishing gradient with respect to both spatial *and* scale direction. We show that these points are always saddle points. They turn out to be extremely useful, since the iso-intensity manifolds through these points provide a scale space hierarchy tree and induce a “pre-segmentation”: a segmentation without a priori knowledge. Furthermore, both these scale space saddles and the so-called catastrophe points form the critical points of the parameterised critical curves – the curves along which the spatial critical points move in scale space. This enables one to localise these two types of special points relatively easy and automatically. Experimental results concerning the hierarchical representation and pre-segmentation are given and show results that correspond to a fair degree to both the mathematical and the intuitive forecast.

### 5.1 Introduction

#### 5.1.1 Scale Space

One way to understand the structure of an image is to embed it in a one-parameter family. If a scale-parametrised Gaussian filter is applied, the parameter can be regarded as the “scale” or the “resolution” at which the image is observed. The resulting structure has become known as *linear*, or *Gaussian, scale*

*space*. In view of the rich literature on this subject we will henceforth assume familiarity with the basics of Gaussian scale-space theory [65, 106, 119, 139, 174, 208, 233, 245, 247, 249].

### 5.1.2 Deep Structure

In their original accounts both Koenderink [139] and Witkin [249] proposed to investigate the “deep structure” of an image, *i.e. structure at all levels of resolution simultaneously*. Encouraged by the results in specific image analysis applications, an increasing interest has recently emerged in trying to establish a generic underpinning of deep structure. This may serve as a basis for a diversity of multiresolution schemes. Such bottom-up approaches often rely on *catastrophe theory* [6, 91, 184, 212, 238, 239], which is now fairly well-established in the context of the scale-space paradigm.

### 5.1.3 Related Work

The application of catastrophe theory in Gaussian scale space has been studied by Damon [45]—probably the most comprehensive account on the subject—as well as by many others [95, 98, 124, 126, 128, 129, 130, 140, 144, 145, 146, 147, 168, 169, 170, 174, 206, 216].

An important stage in using the deep structure is to link image properties of two subsequent resolution scales. Although this may seem obvious, it is a non-trivial task in a discrete scale space. For example, if extrema at different scales correspond to an extremum at the input image, they should be linked. However, extrema may be annihilated or created. Tracking over scale therefore needs a cautious approach.

Koenderink [139] mentioned a possible linking strategy using the properties of the Gaussian scale space. Only a few heuristic attempts have been made to build such multi-scale datastructures.

Vincken *et al.* constructed a hyperstack segmentation algorithm [242]. Simmons *et al.* [230] used the idea of Koenderink’s scheme for building a so-called extremum stack. Their work was an extension of the results by Lifshitz and Pizer [168], who implemented Koenderink’s scheme, mainly focusing on heuristics and the performance of the algorithm.

The idea of tracing critical points and using the location where they vanish as input for a hierarchy tree was also proposed and implemented by Zhao and Iijima [258], cited in [248], and by Wada and Sato [244].

Olsen implemented a segmentation algorithm based on multi-scale watersheds [204, 206, 207].

These datastructures generally use the property of annihilation of extrema at increasing scale. However, the possibility of creations is ignored and consequently not implemented.

As an outcome of the use of catastrophe theory, much effort has been put into investigation of annihilations. It has commonly been accepted that these special points form the crux in understanding the deep structure, although it is not clear how to use them. It has been argued by several authors [113, 139, 168, 170, 174], to use the intensity at the annihilation point. Preliminary results of this chapter were given by Kuijper and Florack in [157].

### 5.1.4 Aim

The aim of this chapter is to investigate the deep structure of Gaussian scale spaces. We show that this results in an unambiguous hierarchical representation of an arbitrary image. For that reason we combine

knowledge from catastrophe theory, the multi-scale linking strategy as suggested by Koenderink [139], and properties of linear scale space. For that reason we introduce the so-called scale space saddles. In section 5.2 we show that these scale space saddles are the key to explore the deep structure of scale space images. They give rise to an unambiguous multi-scale hierarchy describing the image. Images in one dimension fundamentally differ from those in higher dimensions, since only in 1D images the scale space saddles coincide with the catastrophe points. Therefore both cases are discussed separately. In the appendix we clarify the theory by discussing the generic annihilation event and the appearance of scale space saddles in its neighbourhood. The scale space saddle approach leads to a non-heuristic hierarchical multi-scale data structure and a segmentation of images without any a priori knowledge and is presented in Section 5.3. Several examples of our approach on simple artificial images and a 2D MR image are shown in Section 5.4. Main conclusions and results are given in section 5.5.

## 5.2 Theory

The linearity of a Gaussian scale space enables us to treat the scale parameter as a special variable. For that purpose we describe in this section relevant results known from the literature (Section 5.2.1) and present new theory based on the critical points in scale space (Section 5.2.2), critical curves (Section 5.2.3), and iso-intensity manifolds (Section 5.2.4), for which purpose we need the following definitions:

**Definition 4**  $L(\mathbf{x})$ ,  $\mathbf{x} \in \mathbb{R}^n$ , denotes an arbitrary  $n$ -dimensional image. We will refer to this image as the initial image.

**Definition 5**  $L(\mathbf{x}; t)$ ,  $(\mathbf{x}; t) \in (\mathbb{R}^n; \mathbb{R}^+)$  denotes the  $(n + 1)$ -dimensional Gaussian scale space image of  $L(\mathbf{x})$ , i.e.  $\lim_{t \downarrow 0} L(\mathbf{x}; t) = L(\mathbf{x})$ .

**Definition 6** Spatial critical points, i.e. saddles and extrema (maxima or minima), at a certain scale  $t_0$  of  $L(\mathbf{x}; t)$  are defined as the points at fixed scale  $t_0$  where the spatial derivatives vanish:  $\nabla L(\mathbf{x}; t_0) = \mathbf{0}$ . We will refer to these points as spatial critical points to distinguish them from scale space critical points, see Definition 7.

**Definition 7** Scale space critical points of  $L(\mathbf{x}; t)$  are defined as the points where both the spatial derivatives and scale derivative vanish:  $\nabla L(\mathbf{x}; t) = \mathbf{0}$  and  $\partial_t L(\mathbf{x}; t) = 0$ . Since for Gaussian scale spaces the diffusion equation holds, the latter equation equals  $\Delta L(\mathbf{x}; t) = 0$ , denoting a zero Laplacean.

**Definition 8** A critical curve is a one dimensional manifold in the  $(\mathbf{x}; t)$  (scale) space on which  $\nabla L(\mathbf{x}; t) = \mathbf{0}$ .

Note that the intersection of all critical curves with a certain scale space level  $t_0$  results in the spatial critical points of  $L(\mathbf{x}; t_0)$ .

**Definition 9** The Hessian is the matrix of second order spatial derivatives:  $H = \nabla \nabla^T L$ .

**Definition 10** A branch of a critical curve is a subset of a critical curve on which the sign of determinant of the Hessian doesn't change.

**Definition 11** A Iso-intensity manifold is an  $n$ -dimensional manifold in the  $(\mathbf{x}; t)$  scale space on which  $L(\mathbf{x}; t) = c$ ,  $c \in \mathbb{R}$ .

## 5.2.1 Deep Structure in Gaussian Scale Space

### Catastrophe Theory

The behaviour of critical points as the (scale) parameter changes is described by catastrophe theory. As the parameter continuously changes, the critical points move along critical curves. If the determinant of the Hessian does not become zero, these critical points are called *Morse critical points*. In a typical image these points are extrema (minima and maxima) or saddles. *The Morse lemma* states that the topology of a neighbourhood of a Morse critical point can essentially be described by a second order polynomial. At isolated points on a critical curve the determinant of the Hessian may become zero. These points are called *non-Morse points*. As described by *Thom's theorem* [238, 239], neighbourhoods of such points need  $m^{\text{th}}$ -order polynomial, where  $m > 2$ . These polynomials are called the *catastrophe germs*. If an image is slightly perturbed, the Morse critical points may undergo a small displacement, but qualitatively nothing happens to them. A non-Morse point, however, will change. It will split into a non-Morse point that can be described by a polynomial of lower order and a number of Morse critical points, or solely into Morse critical points. This event is called *morsification*. Thom's theorem provides a list of elementary catastrophes with canonical formulas<sup>1</sup> for the catastrophe germs and the perturbations. The Thom splitting lemma states that *canonical coordinates* exist in which these events can be described. In general, these "curved" coordinates don't coincide with the user-defined (usually Cartesian) coordinates, but are used for notational convenience. In Gaussian scale space the only generic events are *annihilations* and *creations* of a pair of Morse points: an extremum and a saddle in the 2D case. All other events can be split into a combination of one of these events and one "in which nothing happens". See Damon [45] for a proof. Canonical descriptions of these events are given by the following formulae:

$$f^A(\mathbf{x}; t) \stackrel{\text{def}}{=} x_1^3 + 6x_1 t + Q(x_2, \dots, x_n; t) \quad (5.1)$$

$$f^C(\mathbf{x}; t) \stackrel{\text{def}}{=} x_1^3 - 6x_1(x_2^2 + t) + Q(x_2, \dots, x_n; t), \quad (5.2)$$

where for all  $a_i \neq 0$ ,  $Q$  is defined by

$$Q(x_2, \dots, x_n; t) \stackrel{\text{def}}{=} \sum_{i=2}^n a_i (x_i^2 + 2t)$$

with  $\sum_{i=2}^n a_i \neq 0$  and  $a_i \neq 0$ ,  $2 \leq i \leq n$ . Note that Eq. (5.1) and Eq. (5.2), describing annihilation and creation respectively, satisfy the diffusion equation

$$\frac{\partial L}{\partial t} = \Delta L. \quad (5.3)$$

It can be verified that the form  $f^A(x_1, \mathbf{y}; t)$ , with  $\mathbf{y} = (x_2, \dots, x_n)$ , corresponds to an annihilation at the origin via the critical path  $(\sqrt{-2t}, \mathbf{0}; t)$ ,  $t \leq 0$ , and  $f^C(x_1, \mathbf{y}; t)$  to a creation via the critical path  $(\sqrt{2t}, \mathbf{0}; t)$ ,  $t \geq 0$ .

Note that creations are generic. They are not sometimes temporarily created, nor false extrema, nor pathological cases, although it is true that they are not as frequently encountered as annihilations.

In 1-D images only annihilations occur. Then Eq. (5.1) becomes  $f^A(x; t) \stackrel{\text{def}}{=} x^3 + 6xt$ . See e.g. Lindeberg [174] for a proof.

<sup>1</sup>Notation due to Gilmore [91]. Also the terminology *normal forms* is used in the literature, e.g. by Poston and Steward [212].

### Extremum Principle and Iso-Intensity Manifolds

A consequence of the Gaussian scale space representation is the strong smoothing property, usually mentioned for its *non-enhancement of local extrema*. It corresponds to the *extremum principle* for parabolic differential equations:

If at a certain scale  $t_0 > 0$  a point  $\mathbf{x}_0$  is a local maximum (minimum) of the function  $L(\mathbf{x}; t_0)$ , then the Laplacean  $\Delta L(\mathbf{x}_0; t_0)$  at this point is negative (positive). This means that  $\partial_t L(\mathbf{x}_0; t_0)$  is strictly negative (positive).

In other words, small local variations will be suppressed. See *e.g.* Lindeberg [174] or Weickert [245] for more details.

As a result, the structure of iso-intensity manifolds in scale space close to an extremum is dome-shaped: At some scale an extremum, *e.g.* a maximum, is encapsulated by iso-intensity manifolds (isophotes in 2D), topologically equivalent to spheres (circles in 2D). The intensity of each of these manifolds is smaller than that of the maximum. Due to the extremum principle the intensity of the maximum decreases with increasing scale. At a certain scale the intensity of the maximum will equal the intensity of some manifold. Alternatively, the shape of the intersection of the image at increasing scales and the iso-intensity manifold shrinks until it coincides at certain scale with the maximum and then disappears. In 2D this can easily be visualised by a set of circles contracting to the maximum at increasing scale: that is, the iso-intensity manifold is dome-shaped. The top of the dome corresponds to the disappearance of the iso-intensity manifold around this extremum. See Figure 5.1 for an example of various iso-intensity manifolds.

Since the image at sufficiently large scale contains only one extremum (see [182]), the evolution of extrema induces a family of iso-intensity domes, nested like onion peels.

#### 5.2.2 Scale Space Critical Points

Since scale provides an extra dimension to the initial image, interesting features are to be expected from the critical points of the scale space image as defined by Definition 7. In this and the following sections we present novel theory regarding these points.

The scale space critical points are defined as the points in scale space with zero gradient and zero Laplacean:

$$\begin{cases} \nabla L(\mathbf{x}; t) = \mathbf{0} \\ \Delta L(\mathbf{x}; t) = 0 \end{cases}$$

since  $\partial_t L(\mathbf{x}; t) \stackrel{\text{def}}{=} \Delta L(\mathbf{x}; t)$ . The type of these scale space critical points is determined by the eigenvalues of the matrix of second order derivatives in scale space,  $\mathcal{H}$ . We call this matrix the *extended Hessian*:

$$\mathcal{H} = \begin{pmatrix} H & \Delta \nabla L \\ (\Delta \nabla L)^T & \Delta \Delta L \end{pmatrix}. \quad (5.4)$$

Here  $H$  is the (spatial) Hessian. All derivatives are evaluated at the location of the scale space critical point of interest. Points are maxima (minima) if all eigenvalues are negative (positive). If at least two eigenvalues have a different sign, the point is a saddle.  $\mathcal{H}$  has the following properties:

- Since the matrix  $\mathcal{H}$  is symmetric all eigenvalues are real.
- At scale space critical points  $\text{tr } H \equiv \Delta L = 0$ , so  $\text{tr } \mathcal{H} = \Delta \Delta L$ .
- $\det \mathcal{H} = \det H \Delta \Delta L - \left( (\Delta \nabla L)^T \tilde{H} \Delta \nabla L \right)$ , where  $\tilde{H} \stackrel{\text{def}}{=} \det H \cdot H^{-1}$ , the transposed co-factor matrix of  $H$ . In fact, this matrix is always well-defined, since its components are homogeneous polynomial combinations of the components of  $H$  of degree  $n - 1$ , see [72, 154]. So at catastrophe points  $\tilde{H}$  is generically non-zero, although  $\det H = 0$ . At these points  $\det \mathcal{H}$  reduces to  $-\left( (\Delta \nabla L)^T \tilde{H} \Delta \nabla L \right)$ , which is equal to the generically non-zero invariant  $-\Delta L_i \Delta L_j \tilde{H}_{ij}$  (summation convention applies).
- The determinant of  $\mathcal{H}$  can also be written as

$$\det \mathcal{H} = \left( (\Delta \nabla L)^T; \Delta \Delta L \right) \cdot \begin{pmatrix} -\tilde{H} \Delta \nabla L \\ \det H \end{pmatrix}$$

Here the component  $\left( (\Delta \nabla L)^T; \Delta \Delta L \right)$  is the normal vector of the plane with constant Laplacean. The component  $\left( -\tilde{H} \Delta \nabla L; \det H \right)^T$  denotes the (scale space) tangent of the critical curve in scale space at the spatial critical points. It is always finite in value, even at catastrophe points. See Florack and Kuijper [72, 154] for more details.

- Scale space critical points are always scale space saddle points. See Theorem 3.

**Theorem 3** *The matrix  $\mathcal{H}$  has both positive and negative eigenvalues at scale space critical points.*

**Proof of theorem 3** *Let the point  $(\mathbf{x}_0; t_0)$  be a scale space critical point of the function  $L(\mathbf{x}; t)$ . Then  $(\mathbf{x}_0; t_0)$  is also a spatial critical point of the function  $L(\mathbf{x}; t_0)$  at scale  $t_0$ . If  $(\mathbf{x}_0; t_0)$  is a scale space extremum of  $L(\mathbf{x}; t)$ , it is also a spatial extremum of  $L(\mathbf{x}; t_0)$ . However, the extremum principle (section 5.2.1) states that the Laplacean of a spatial extremum is non-zero, leading to the contradiction that  $(\mathbf{x}_0; t_0)$  cannot be a scale space critical point. Therefore  $(\mathbf{x}_0; t_0)$  is a scale space saddle point. Consequently,  $\mathcal{H}$  has both positive and negative eigenvalues at scale space critical points.  $\square$*

As a consequence, critical points in scale space ( $\nabla L = 0$  and  $\Delta L = 0$ ) are *always* saddle points. These scale space saddle points form a subset of the spatial saddles, *viz.* those with vanishing Laplacean.

This property of scale space critical points follows directly from the notion of causality, that states that isophotes in scale space only disappear and never appear (no spurious detail).

The only spatial critical point traversing the scale space saddle is the spatial saddle. Since the manifold  $\nabla L = 0$  intersects the manifold  $\Delta L = 0$  transversally, the intensity of this spatial saddle has an extremum at the scale space saddle. Therefore, its intensity first increases and then decreases, or vice versa. This is exactly the behaviour Lifshitz and Pizer observed, see [168]. We elaborate on this behaviour in section 5.2.3 and go into details in the appendix.

### 5.2.3 Properties of Critical Curves in Scale Space

According to Definition 10, in scale space each critical curve contains branches representing spatial critical points. Branches are connected at catastrophe points, where two spatial critical points are annihilated or created. These two spatial critical points differ with respect to the sign of one eigenvalue of the Hessian, that becomes zero at the catastrophe. Of all other eigenvalues the number of positive and negative signs is equal. Note that a critical curve can contain several catastrophe points if  $n > 1$ .

In two-dimensional images the two branches connected at catastrophe points necessarily are a saddle and an extremum branch, in one-dimensional images they are a maximum and a minimum branch. In higher dimensions interactions become more complicated, since catastrophes of saddles of different type are also possible. For writing convenience we will use the terminology appropriate for 2D images: saddle and extremum (minimum, maximum) branches to distinguish between the two types of spatial critical points involved at the catastrophe, but results remain valid for other dimensions.

It is known from catastrophe theory that each branch of the critical curve is bounded with respect to scale: at some scale the spatial critical points annihilate. Spatial critical points are either present from the initial scale or they are created at a certain (catastrophe) point in scale space. If the coarsest scale is taken large enough only one extremum remains. Then the scale space image contains one critical curve bounded by the coarsest scale.

Apart from catastrophe points a second type of points exhibits special behaviour, *viz.* scale space saddles.

#### Scale Space Saddles

On an extremum branch the intensities are damped continuously while increasing scale. Each minimum (maximum) intensity therefore increases (decreases) monotonically towards the intensity at the annihilation point. At certain spatial and scale distance from the annihilation, the intensity of corresponding saddle will generally tend to move towards the intensity of extremum, *i.e.* it decreases (increases) to the intensity of minimum (maximum). So the signs of the Laplacean of both spatial critical points at that scale will be opposite. At the catastrophe point, however, they necessarily have the same sign and both points approach the intensity of the annihilation in a decreasing (increasing) fashion.

This was observed by Griffin, who pointed out that at a catastrophe the saddle and the extremum necessarily have the same sign of the Laplacean. He distinguished between ridge and trough saddles. Saddles may change from “ridge” (negative Laplacean) to “trough” (positive Laplacean) or vice versa with increasing scale and generically occur as “balanced” saddle (zero Laplacean) [95, 98].

Therefore, at the saddle-branch of the critical curves, the saddle will generically pass a point at which the Laplacean equals zero: a scale space saddle. Since the sign of the Laplacean changes while passing the scale space saddle, the intensity on the saddle branch has a local extremum.

#### Parametrisation

A parametrisation of a critical curve leads to a 1D-function of the intensity of the spatial critical points.

**Definition 12** *Let  $(\mathbf{x}(s); t(s))$  be a parametrisation of  $(\mathbf{x}; t)$ , such that  $\nabla L(\mathbf{x}(s); t(s)) = 0$ , *i.e.*  $(\mathbf{x}(s); t(s))$  defines a critical curve. Then the intensity of the parametrised curve  $P(s)$  is defined by  $L(\mathbf{x}(s); t(s))$  for a compact range  $s \in [s_{\min}; s_{\max}]$ .*

Note that  $P(s)$  can be a combination of several connected parts  $P_i(s_i)$ , each defined on a compact interval  $[s_{i,\min}; s_{i,\max}]$ . Two parts  $P_i(s_i), P_j(s_j)$  are connected at a catastrophe point given by either  $s_{i,\min} = s_{j,\min}$  OR  $s_{i,\max} = s_{j,\max}$ .

The local extrema of  $P(s)$  have the following property:

**Theorem 4** For  $n-D$  images,  $n > 1$ ,  $P(s)$  has its critical points at the scale space saddle(s) and the catastrophe point(s). They are extrema.

**Theorem 5** If, for 1D images (signals), the critical point of  $P(s)$  is located at the interior of  $[s_{\min}; s_{\max}]$ , it is a point of inflection.

**Proof of theorem 4** The critical points of  $P(s)$  are defined by  $\partial_s P(s) = 0$ . According to definition 12, the left part of this equation equals the total differentiation of  $L(\mathbf{x}(s); t(s))$  with respect to  $s$ , defined by

$$\frac{dL(\mathbf{x}(s); t(s))}{ds} = \nabla L(\mathbf{x}(s); t(s)) \cdot \mathbf{x}_s(s) + \Delta L(\mathbf{x}(s); t(s)) \cdot t_s(s). \quad (5.5)$$

Here

$$\mathbf{x}_s(s) \stackrel{\text{def}}{=} \frac{d\mathbf{x}}{ds}, \quad t_s(s) \stackrel{\text{def}}{=} \frac{dt}{ds}.$$

Since  $\nabla L(\mathbf{x}(s); t(s)) = 0$ , the critical points of Eq. (5.5) are given by  $\Delta L(\mathbf{x}(s); t(s)) \cdot t_s(s) = 0$ . The scale space saddles are defined as the spatial critical points where  $\Delta L(\mathbf{x}(s); t(s)) = 0$ . The catastrophes take place at the location where the saddle and the extremum “meet” in scale space, i.e. where the parametrisation of scale has its local extrema. These points are given by  $t_s(s) = 0$ .

The critical points of  $P(s)$  are extrema, since at the catastrophe point the Laplacean is non-zero for  $n-D$  images,  $n > 1$ .  $\square$

**Proof of theorem 5** For 1D images the zero-Laplacean and the catastrophe point coincide, so if the critical point lies in the interior of  $[s_{\min}; s_{\max}]$ , the solution of  $t_s(s) = 0$  equals that of  $\Delta L = 0$ .  $\square$

Although these results holds for any parametrisation of the critical curves, in practice the intensities of spatial critical points are obtained at the calculated scales of the scale space. In other words, they are measured as a function of scale. Then  $t = s$ , so  $t_s = 1$  and  $P(s)$  is obtained as the union of parts  $P_i(s_i)$  containing the branches of critical points. Each branch is defined on an open interval  $s_1 < s < s_2$ , where  $s_1$  is either the initial or the creation scale, and  $s_2$  is the annihilation scale of the spatial critical point. The branches are connected at the catastrophe points, emphasising that the detection and use of creations is essential to build accurate critical paths.

In the appendix we clarify these theorems using generic events in scale space.

### Number of Scale Space Saddles

As argued in section 5.2.3, we may generally assume that the intensity at the annihilation of an extremum-saddle pair lies between the intensities of both spatial critical points at a certain scale below the annihilation scale. Then the spatial critical points have opposite signs of Laplacean and the saddle passes a scale space saddle with increasing scale. The number of scale space saddles on a saddle branch of a



critical curve is, however, undetermined and the saddle branch of a critical curve can contain zero, one, or multiple scale space saddles.

This was also observed by Lindeberg [170, 174] who investigated the locations of Laplacean zero-crossings in combination with the (annihilation of) critical points concluding that in two and higher dimensions there is no absolute relation between locations of the Laplacean zero-crossing curves and the local extrema of a signal. Intuitively the case without scale space saddles can be made clear by imagining an image of an extremum and a saddle with (already) the same sign of Laplacean. Multiple scale space saddles on a saddle branch are caused by changing structure in the image nearby the saddle point.

Examples of this varying number of scale space saddles on a single branch can be found in section 5.4.2.

### 5.2.4 The Structure of Iso-Intensity Manifolds

The iso-intensity manifolds of a 2D image are formed by the isophotes. These isophotes generally are Jordan curves, *i.e.* non-intersecting curves. If they don't end on the boundary they are closed, *e.g.* the isophotes around an extremum. There exist a finite number of non-Jordan curves. These curves do intersect themselves in the (spatial) saddle points of the image. Generically these curves have but one point of self-intersection. Consequently, the image is separated into regions in which all isophotes are Jordan curves by the isophotes through the saddle points. This separation can be extended to arbitrary dimension.

The extension to scale space images leads to the necessity of scale space saddle points, as defined in the previous section. The iso-intensity manifolds through these points form the natural separation of parts of the scale space image. Each spatial extremum can be assigned to a spatial saddle by means of an extremum-saddle catastrophe, and consequently it can be assigned to the scale space saddle corresponding to the spatial saddle, if the saddle branch contains one, see section 5.3.1 for more details. Each spatial extremum is encircled by iso-intensity manifolds of which the one through the scale space saddle forms the "critical" manifold. That is: all iso-intensity manifolds beneath the critical manifold form a closed segment in scale space.

**Definition 13** *A scale space segment is defined as a part of a scale space image that is bounded by the dome part of the iso-intensity manifold through a scale space saddle; the top of the dome is the spatial extremum to which the scale space saddle has been assigned.*

There are four essentially different types of iso-intensity manifolds shown in Figure 5.1 and explained hereafter:

- Iso-intensity manifolds are dome-shaped and don't intersect themselves. Each dome has its open ends towards finer scale. The top of the dome lies on the extremum branch of the critical curve. Consequently, these domes encapsulate a bounded region in scale space. The dome doesn't intersect nor touch the saddle branch, see Figure 5.1a.
- The iso-intensity manifold through a scale space saddle consists of two parts, separated by the scale space saddle. One part is dome-shaped around the spatial extremum connected to the scale space saddle by the critical curve. At the scale space saddle this manifold touches another having the same intensity, see Figure 5.1b.

- Iso-intensity manifolds with intensities between the scale space saddle and the catastrophe point are still dome-shaped around the spatial extremum, but have a “hole in the roof” around the scale space saddle. Consequently, the maximum scale at which the iso-intensity manifold occurs is not determined by the spatial extremum, see Figure 5.1c. The saddle branch is intersected twice by the iso-intensity manifold. In fact, the manifold transforms from dome-shaped to horseshoe as described in the next item.
- The iso-intensity manifold through a catastrophe point has a horseshoe shape, as is known from catastrophe theory. It touches the critical curve at the catastrophe point, see Figure 5.1d.

As a dual expression it follows that starting from the initial image, spatial extrema on an extremum branch of a critical curve form the top of a dome-shaped iso-intensity manifold in scale space that doesn't intersect itself and is present at all scales beneath the scale at which the spatial extremum occurs, until its intensity equals that of a scale space saddle on the saddle branch of the critical curve. Increasing scale, *i.e.* tracking the extremum further on the extremum branch, the iso-intensity manifold through the spatial extremum transforms to a horseshoe shape at the annihilation. In case of a minimum (maximum) there are only pure domes at intensities smaller (larger) than the intensity of the scale space saddle.

### 5.3 Scale Space Hierarchy and Pre-Segmentation

In the previous section we have given a theoretical framework in which iso-intensity manifolds defined scale space segments. The manifolds through scale space saddles can be regarded as separatrices of these segments. By definition, each of the scale space segments contains at least one extremum. If a segment contains multiple extrema, it obviously contains subsegments. Consequently, the set of scale space saddles and their iso-intensity manifolds induce both a hierarchy and a segmentation of the scale space image. These two properties are discussed in detail in the following subsections.

#### 5.3.1 Scale Space Hierarchy

A natural hierarchy results as scale space segments are defined by the regions encapsulated by the iso-intensity manifolds through the scale space saddles. This hierarchy avoids problems arising when defining a straight-forward and non-multiscale hierarchy of an image based solely on the nesting of iso-intensity contours through the spatial saddle points in the initial image. Although this nesting defines a hierarchy at some scale, it is not scale independent. Generically, spatial saddles have different intensities in the initial image since they are Morse-saddles. When scale is increased the nesting can change: At some scale levels intensities of saddles become equal. Then, for example, the isophote through a saddle contains another saddle and encircles three extrema. They form the so-called Maxwell set. Increasing scale, the nesting of the saddles swaps, see *e.g.* Lindeberg [174].

Since scale space saddles generically have different intensities, a unique scale space hierarchy is found using the nesting of the scale space saddle, as described by the following algorithm:

**Scale Space** With the input of an  $n$ -D image, build a scale space consisting of  $k+1$  levels,  $t = 0, 1, \dots, k$

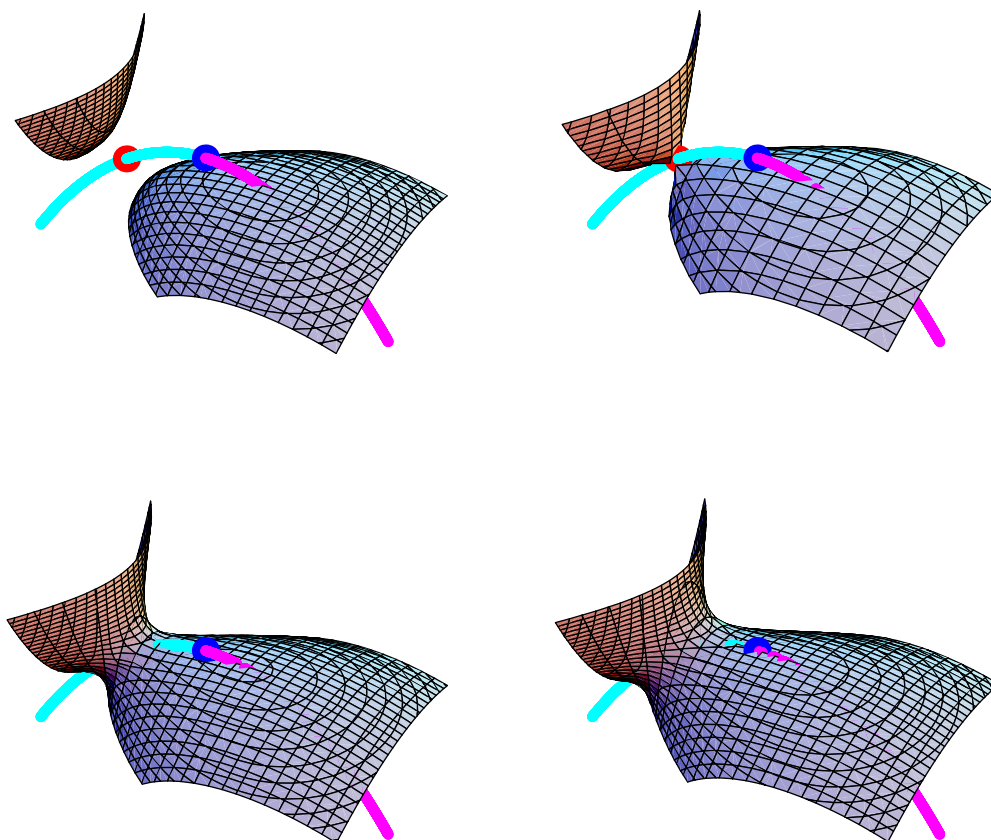


Figure 5.1: Intersections of 2D iso-intensity surfaces and the critical curve. Top left: Dome-shaped – one intersection. Top right: Through the scale space saddle, two touching manifolds – two intersections. Bottom left: Dome-with-hole: intensities between the scale space saddle and the catastrophe point – three intersections. Bottom right: Horseshoe surface through the catastrophe point – two intersections.

**Extremum and Saddle Stacks** Find the extrema and the saddle points at each level  $t$  together with their intensities and put them in two separate stacks.

**Extremum and Saddle Branches** Link each critical point location at level  $t$  to its corresponding location at level  $t + 1$ ,  $t = 0, \dots, k - 1$  and vice versa, as long as this successive location is found. This results in doubly linked lists of critical points in each stack.

**Connected Critical Paths** For each list in the extremum stack find a list in the saddle stack and combine them pairwise to critical curve lists by means of these catastrophe points.

**Scale Space Saddles** Find the scale space saddles and their intensities along each critical curve, *i.e.* find the intensity extrema of each saddle list.

**Hierarchical Tree** Sort the extremum branches containing the catastrophe points from appearance at coarse to fine scales and construct the hierarchy tree starting at highest scale. While descending in scale, each successive catastrophe denotes a critical curve with a scale space saddle and thus defines a new segment of the hierarchy tree as a sub-segment of an existing segment. That is, one branch of the tree is split into two branches in a unique way.

In the following sections these items will be explained and illustrated.

## Scale Space

Input is a discrete image of arbitrary size and dimension. Only for the sake of illustration we consider the one- and two-dimensional cases. Images of higher dimension are comparable to the two-dimensional ones, albeit that they allow saddle-saddle pairs at catastrophes. These pairs, however, behave equivalently to saddle-extremum pairs.

A scale space image is obtained by convolving the input image with a normalised Gaussian filter of variable size. The intermediate levels are sampled logarithmically, see *e.g.* [65, 102, 106, 139, 145, 174, 197, 233].

### Extremum and Saddle Stacks

Each level in scale space is a blurred image. Its spatial critical points can be calculated by various methods, *e.g.* zero-crossings of the derivatives, winding-numbers (see [130]), or neighbourhood-relations. The latter has several implementations. For 2-D images Bloms method [21, 24] may be preferred. This method uses a hexagonal lattice based scheme, in which the intensity of each point is compared to its 6 neighbours. The advantage of this scheme is that it finds all the saddle points and “respects” the Euler number. Common pixel-based methods like the 4- and 8-neighbourhood schemes sometimes miss saddles or cluster them. However, the generalisation of Bloms method to higher dimensions is non-trivial.

Critical point locations and their intensities are stored in two stacks, one containing the saddles and one containing the extrema.

### Extremum and Saddle Branches

Since critical points can be annihilated and created, they inherit both movement in increasing scale direction and spatial drift. This scale space movement can be calculated accurately by means of derivatives up to third order, see *e.g.* [72, 154] and gives the expected location of the spatial critical point at the next scale.

So to each spatial critical point  $\mathbf{x}_{i,t}$  at level  $t$  its expected location  $\mathbf{x}_{i,t+1}^e$  at level  $t + 1$  is assigned. To link spatial critical points at two subsequent levels, the point sets  $\mathbf{x}_{i,t}$  and  $\mathbf{x}_{i,t+1}^e$  are compared to the critical points  $\mathbf{x}_{j,t+1}$  at the next level. We define the distance matrices  $d_{i,j}^1$  and  $d_{i,j}^2$  by

$$\begin{cases} d_{i,j}^1 &= \|\mathbf{x}_{i,t} - \mathbf{x}_{j,t+1}\|, \\ d_{i,j}^2 &= \|\mathbf{x}_{i,t+1}^e - \mathbf{x}_{j,t+1}\|, \end{cases}$$

and set  $d_{i,j} = \min(d_{i,j}^1, d_{i,j}^2)$ . Next, we take  $\min_{i,j} d_{i,j}$ , establishing a link, and remove the row and column containing this value. The linking continues until either all points at level  $t + 1$  are linked (and the matrix  $d$  has zero rank), or  $\min d_{i,j}$  exceeds scale. The intensities of the points at both levels can be used for verification.

The outcome of this procedure are two stacks each containing doubly linked lists. The head of each list corresponds with the creation of the critical point (or the initial scale), its tail with the annihilation.

### Connected Critical Paths

Since the annihilation of an extremum involves a saddle, each tail of an extremum list at a certain scale  $t$  corresponds to a tail of some saddle list at the same scale  $t$ . The same holds for creations in relation to the heads of the lists. The intensities can be used for verification.

Note that at catastrophes the spatial drift becomes undetermined since  $\det H = 0$ . Then the movement of a critical point can still be accurately predicted, see [72, 154].

Relating saddle and extremum lists results in chains of extremum-saddle sets, *viz.* critical curves.

### Scale Space Saddles

Scale space saddles have the property that they are the local extrema of the parametrised intensity-curve, obtained by taking the intensity along the saddle branches as function of scale, as argued in section 5.2. They are easily found by a list-operation on the saddle lists. Saddle lists can have zero or multiple extrema with respect to intensity.

If no extrema are found then the Laplaceans of the extremum and the saddle have either the same or the opposite sign at all scales on which their are found. The former signals that there was no scale space saddle in the range of used scales. One might say that it is located at a scale that is smaller than the scale of the first image of the scale space stack. To identify a segment with the extremum, the intensity of the saddle in that first image can be taken. The latter case represents a scale space saddle located closer to the catastrophe point than resolutions allows to be measured. Then the saddle at the coarsest scale is assigned as scale space saddle.

If multiple scale space saddles are found within one saddle list, the one with maximum (minimum) intensity in case of a minimum (maximum) is chosen.

Since each extremum list is linked to a saddle list, each extremum is linked to a scale space saddle containing the global intensity extremum in the saddle list. Equivalently, the iso-intensity manifold through the scale space saddle encapsulates the corresponding extremum.

### Hierarchical Tree

The annihilations –and consequently each extremum branch– are sorted from coarse to fine scale. Each scale space saddle defines an iso-intensity manifold around an extremum: the part of the image encapsulated by this manifold is a segment of the image at that scale. Segments may have sub-segments, defined by scale space saddles within the segment.

At the coarsest scale only one extremum remains. Since it has no corresponding saddle branch containing a scale space saddle, it doesn't have an a priori critical dome. Without the presence of a saddle the iso-intensity manifolds through an extremum is obviously dome-shaped. Therefore the iso-intensity manifold of the remaining extremum can be chosen having the intensity of the extremum at the coarsest scale. Since the heat equation under suitable boundary conditions (*e.g.* periodic or reflecting ones) is energy preserving, it preserves the average grey value of the image. It is then known that the input image converges to an image of constant value equalling the average value of the input image. Consequently the value of the iso-intensity manifold of the remaining extremum can be set to this value.

The hierarchy tree contains as nodes the locations of the annihilations in scale space, together with their corresponding scale space saddles and their intensities. The branch to the parent corresponds to the scale space segment in which the scale space saddle is located. The branches to the children of the tree are formed by the original segment and the new segment defined by the scale space saddle. The root of the tree is defined as the one remaining extremum.

### 5.3.2 Segmentation

A natural segmentation of *scale space* is thus obtained by the iso-intensity manifolds of the scale space saddles with their corresponding extrema. Consequently, a *spatial* segmentation, or rather “pre-segmentation”, of the image at any scale  $t$  is found by the intersection of the scale space segmentation and the image at this fixed scale  $t$ . A full (partial) pre-segmentation of the initial image is found by taking into account the intensities of all (a subset of all) scale space saddles. The word “pre-segmentation” is used to distinguish between the proposed separation of the image into topologically different parts and the commonly user-defined (and user-verified) segmentations. The latter introduce by definition prior knowledge and are therefore definitely different from our proposed pre-segmentation.

At a partial segmentation each selection of scale space saddles defines segments of the image within some grey-level range in the part of the image enclosed by the iso-intensity manifold. Knowledge of the grey-level distribution of the image may then lead to a semantical choice of scale space saddles and their corresponding segments and thus using the pre-segmentation as a pre-stage for the “real” user-defined segmentation. This partial segmentation is easily obtained by elementary tree operations, *e.g.* selecting or deselecting subtrees, contracting nodes in the tree, etc.

Finally, to obtain a rough segmentation, that is a segmentation based on the large structures, only the upper part of the tree with large scales can be taken into account.



Figure 5.2: 1D signal at increasing scale: a) Initial signal b) After the first catastrophe, c) after the second catastrophe, d) and after the last catastrophe.

## 5.4 Applications

In this section we apply the algorithm as described in the previous section to a 1D signal and to two 2D images. We present the obtained hierarchy trees and show pre-segmentations. We also give an illustration of the effect of tree operations on the pre-segmentation.

### 5.4.1 1D Signals

As first example we use the part of a 1D signal shown in Figure 5.2a. As can be seen directly, it contains three minima and three maxima, so the scale space image contains three scale space saddles (equivalently: catastrophes, annihilations). The four topologically different appearances of this signal in scale space after successive catastrophes are shown in Figure 5.2a-d.

The scale space hierarchy tree is shown in Figure 5.3. At high scales there is only one segment  $S_0$ : the whole image from boundary to boundary, as shown on the top-right side of Figure 5.3. Decreasing scale, one reaches scale space saddle 3, from which point the image contains two segments:  $S_1$  and the complement of  $S_1$ : the parts that range from the boundaries to  $S_1$ . Continuing the descent one reaches scale space saddle 2, from which point segment  $S_1$  contains a subsegment, *viz.*  $S_2$ . Decreasing scale even more one ends up with scale space saddle 1, from which point a new segment  $S_3$  is obtained from the boundary part.

Interpreting Figure 5.3 the other way round one concludes that starting with the pre-segmentation where  $S_2 \subset S_1 \subset S_0$ ,  $S_3 \subset S_0$  at increasing scale firstly segment  $S_3$  vanishes at the boundary, secondly  $S_2$  is “gulped down” by  $S_1$ , and finally  $S_1$  disappears.

The notion of disappearing of structure at annihilation points gave rise to the gist that the essence of segmenting images should be based on catastrophe points instead of scale space points. This misinterpretation is caused by the coincidence of scale space saddles and catastrophe points in 1D.

### 5.4.2 2D Images

As 2D examples we firstly took an 81x81 artificial image, built up by the combination of four Gaussian blobs, see Figure 5.4a. Note that the four maxima induce one minimum. The simplicity of this image enables a quantitative check of the outcome. Subsequently we took a 2D slice from an artificial MR image shown in Figure 5.4b to illustrate the use and possibilities of the hierarchy tree. This image is taken from the *Brain Web* [40, 41, 163], web site <http://www.bic.mni.mcgill.ca/brainweb>.

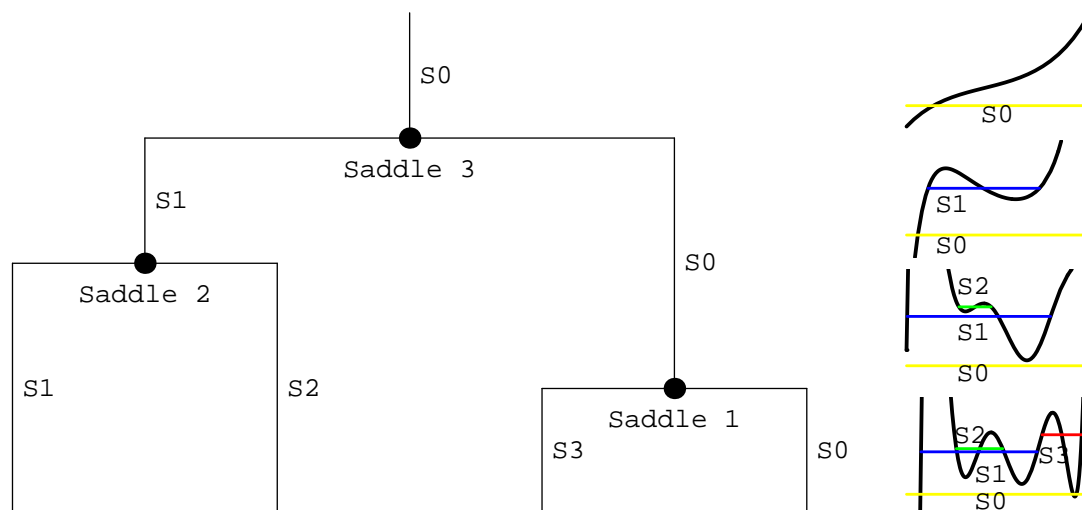


Figure 5.3: Left: Hierarchy tree of Figure 5.2a, at the top coarsest scale. The three “Saddles” denote the subsequent topological changes (catastrophes, annihilations) of the image as scale increases. The vertical branches denote the distinguished segments present at these scales. The stack of images at the right show the shape of the signal, changing at the three scale space saddle scales, and their pre-segmentations. Note that the lowest two are zoomed as to show clearly the distinct pre-segmentations.

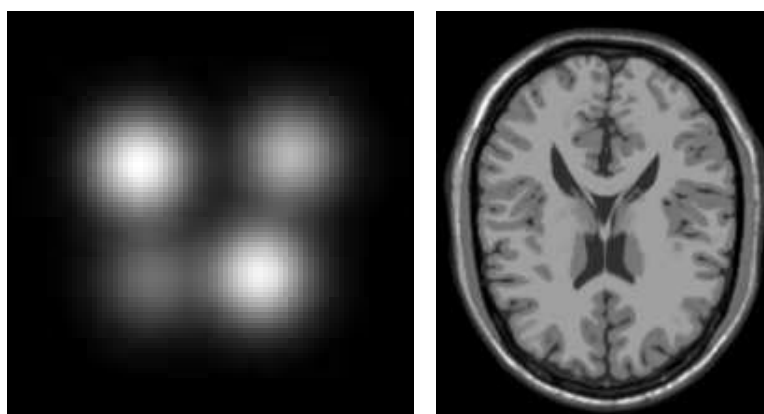


Figure 5.4: 2D test images Left: Artificial image built by combining four maxima and one minimum. Right: 181 x 217 artificial MR image.



### Artificial Image

The 81 x 81 artificial image contains five extrema. Since the image at (very) large scale contains only one blob, four extrema must be annihilated. To obtain the scale space hierarchy a scale space consisting of 113 levels was built. Levels were calculated at scales  $e^{i/32}$ ,  $i = 2, \dots, 114$  and at each level the spatial critical points were calculated. Figure 5.5 shows 15 levels of the stack at increasing scales together with the calculated spatial critical points.

Next, the spatial critical points of subsequent scales were linked resulting in the critical paths. Figure 5.6 shows the locations of spatial critical points in scale space. For visualisation purposes this 81x81x113 scale space was reduced to a 41x41x113 volume of interest space, since the critical points evolve in the middle of the image so a spatial border of 20 pixels was omitted. Dark grey points correspond to extrema, light grey points to saddle points. We note that at three isolated scales a pair of created and directly annihilated critical points were detected. The algorithm is able to detect these points and proposes the right linking.

The parametrised critical paths, *viz.* the intensities of the critical curves containing the branches of saddle and extremum branches, are shown in Figure 5.7. The top row shows the branches of the saddles (left) and the extrema (right). The extrema and saddle points were pairwise grouped by means of their catastrophe points. Annihilations occur at  $t = 48, 55, 66, 77$ , *i.e.* at scales 4.48, 5.58, 7.87, and 11.1. The four catastrophes are visible as the end of two branches of critical points. At these points saddle and extremum branches are connected forming the critical paths, see the bottom row of Figure 5.7. On the left all critical curves are shown, on the right one saddle-extremum pair is taken apart.

The scale space saddles are derived from the saddle branches. It can be seen that the upper three saddle branches shown in Figure 5.7, although containing multiple local extrema with respect to the intensity, have a global maximum, *viz.* the scale space saddle of interest. The fourth saddle branch is monotonically increasing, just as its corresponding minimum. Therefore the intensity of the spatial saddle at the first level is chosen as value for the minimum encapsulating manifold.

Finally, an unambiguous hierarchy based on the catastrophe points and the scale space saddles, just as in the 1D case, can be made. The presence of 5 extrema results in 5 inner regions  $S_i$ ,  $i = 1, \dots, 5$  and a boundary region  $S_0$ . The first region is defined by the remaining extremum. The scale space dome defined by this maximum is the iso-intensity manifold valued by the intensity of the extremum at coarsest scale. Since the diffusion equation is energy preserving, it thus preserves the grey value. Consequently, the value of the remaining extremum converges (down, in this case of a maximum) to the average intensity of the initial image. This convergence can also be seen in Figure 5.7b. The projection of this segment  $S_1$  and its dual  $S_0$  onto the initial image are shown in Figure 5.8a.

To find the next segment, scale is decreased until the second extremum appears. From the fourth row of Figure 5.5 it can be seen that this segment  $S_2$  is located at the top left part of the image. The value of the iso-intensity manifold is obtained from the scale space saddle of the spatial saddle corresponding to this extremum. The intersection of this manifold with the initial image is shown in Figure 5.8b. The other segments are found in the same way, resulting in the pre-segmentation of the image as shown in Figure 5.8f.

This image, although it follows from a well-defined mathematical concept, might be counterintuitive in view of the assumed absence of a small closed region around the extremum of segment  $S_1$ . From Figures 5.4a and 5.7b it is clear that this extremum has almost the same intensity as the extremum of segment  $S_2$ , so one might expect the size of segment  $S_1$  to be approximately the same as  $S_2$ . However,

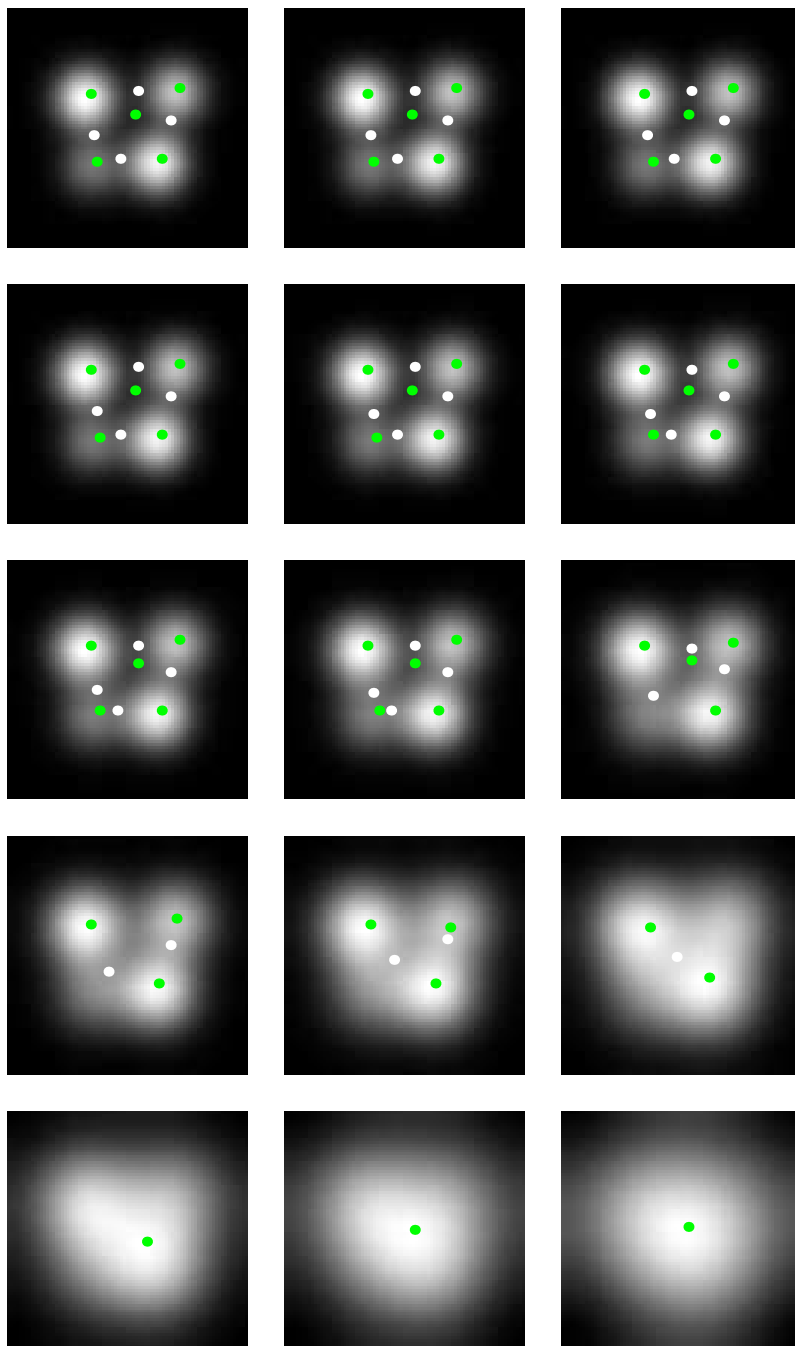


Figure 5.5: Images from the scale space stack of Figure 5.4a. Scale increases from left to right, top to bottom. Dark dots denote extrema, bright dots saddle points.

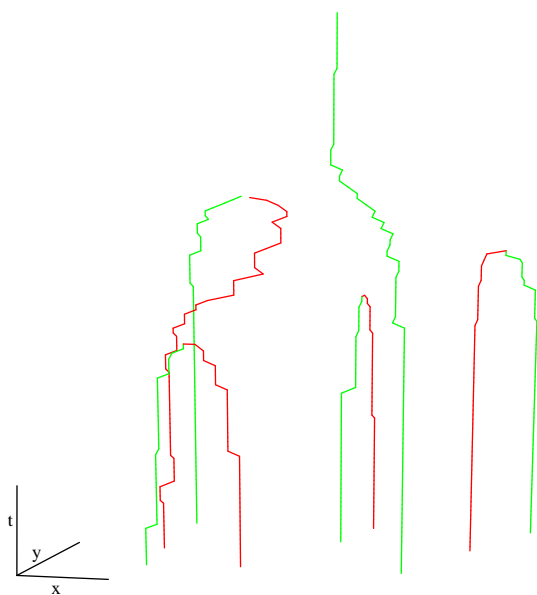


Figure 5.6: Spatial critical points of Figure 5.4a in  $(x, y; t)$  scale space. Dark grey points correspond to extrema, light grey points to saddle points.

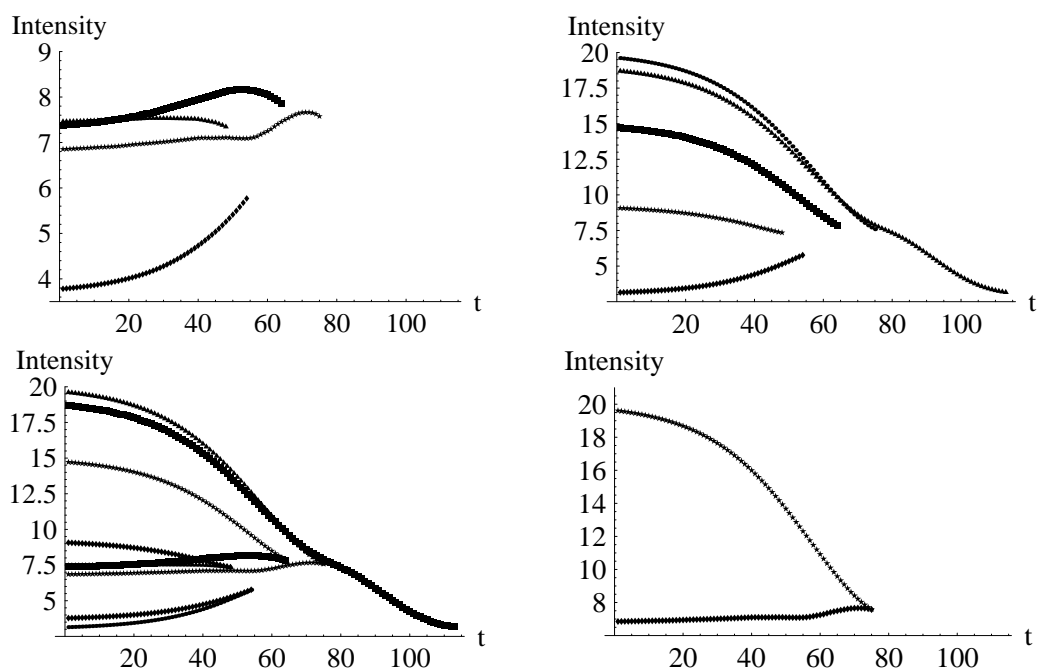


Figure 5.7: Intensities of the critical paths shown in Figure 5.6 parametrised by scale. Top left: Intensities of all saddle points. Top right: Intensities of all extrema. Bottom left: Intensities of all critical points. Bottom right: Intensities of one specific saddle-extremum pair.

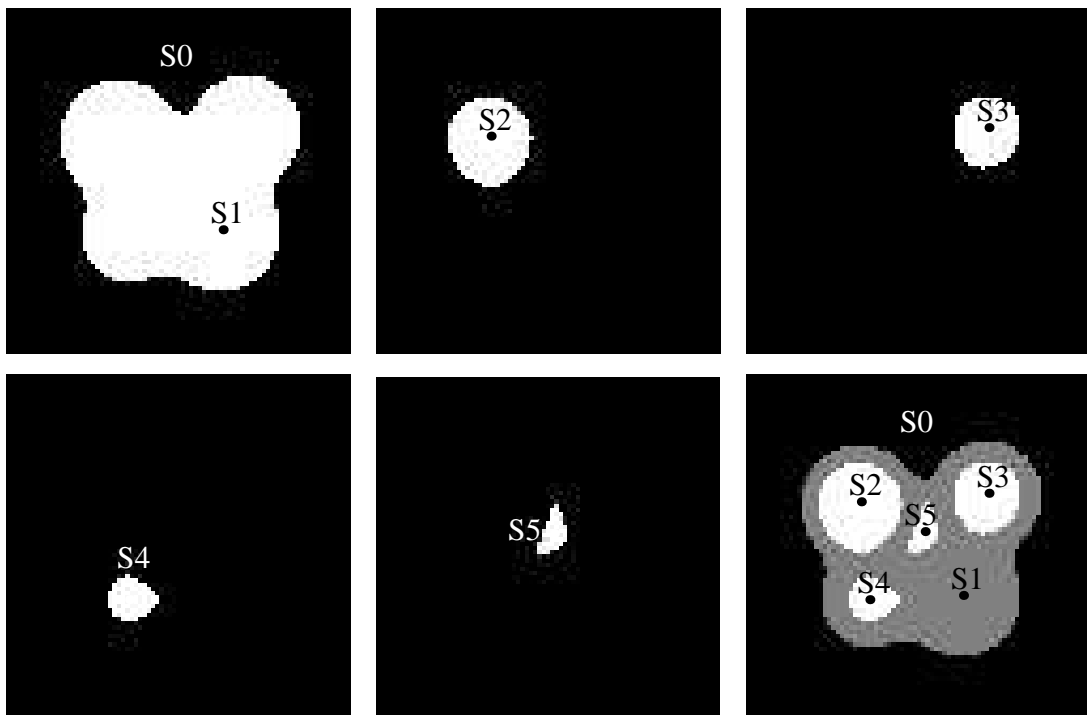


Figure 5.8: Segments of Figure 5.4a as defined by the catastrophe points and the scale space saddles. a: Segments  $S_1$  and  $S_0$  projected to the initial image. b: Segment  $S_2$ . c: Segment  $S_3$ . d: Segment  $S_4$ . e: Segment  $S_5$ . f: Pre-segmentation of the initial image.

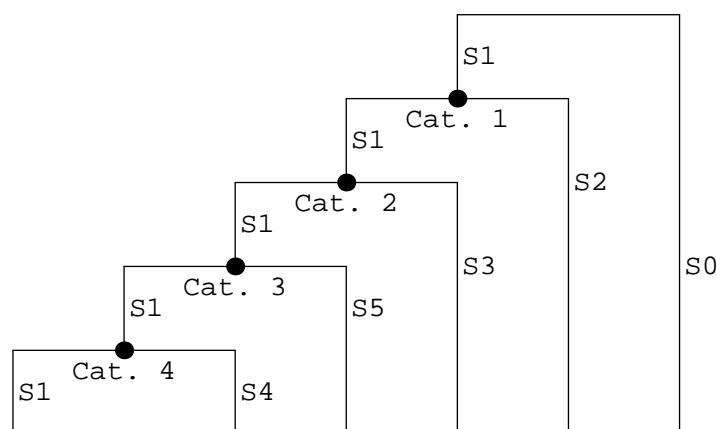


Figure 5.9: Hierarchy tree of Figure 5.4a. Segments are labelled corresponding to Figure 5.8. Segments  $S_2, \dots, S_5$  are subsegments of segment  $S_1$ , but annihilate in the sequence  $S_4, S_5, S_3, S_2$  at increasing scale.

the domes defined by the scale space saddles are nested, so essentially  $S_2 \subset S_1$  and from Figure 5.7 it is clear which saddle-extremum pair annihilates. Although the correct annihilating extrema can be found, it may be desirable – based on prior knowledge of the image and / or of human perceptive characteristics – to add this extra iso-intensity manifold and thus extra segment. In the next section we give an example.

Furthermore, the hierarchy tree associated with this pre-segmentation is given by the successive annihilations in scale space, shown in Figure 5.9. The nesting of segments is given by  $(S_2, S_3, S_4, S_5) \subset S_1$  and the whole image is given by  $S_0 \cup S_1$

### MR Image

Having a hierarchical description tree of the image, one can disregard parts of the tree. Combined with knowledge of the image one can thus obtain a pre-segmentation useful for *e.g.* further segmentation. Figure 5.4b shows a 2D slice from a simulated MR brain image.

This input image has 812 extrema and consequently at least 813 separate regions. Obviously, most of these are only defined on a small range of scales. In order to investigate the large structures of this 2D image, we focused on the part of the scale space from scales 8.37 to 33.1, exponentially sampled by 89 scales. The image on scale 8.37, which can be seen in Figure 5.11a, contains seven extrema of which six annihilate in the range unto scale 33.1. The parametrised critical paths in this scale range are shown in Figure 5.10a, the saddle branches are taken apart in Figure 5.10b.

The seven extrema define the eight segments of Figure 5.11b in a similar fashion as in the previous subsection. This pre-segmentation of Figure 5.11a contains only four levels. The four segments  $S_1, S_3, S_4$ , and  $S_5$  correspond to the four maxima located within the most white part of the image. Segment  $S_2$  and its subsegments  $S_6$  and  $S_7$  correspond to the three minima in the interior. The hierarchical structure of this image is shown in Figure 5.12. To visualise the role of Segment  $S_1$  compared to the other maxima – the part of the tree with catastrophes 2,3, and 4 – the critical intensity of segment  $S_3$  (the adjoined segment by catastrophe 2) was assigned to it. The pre-segmentation with this extra segment is shown in

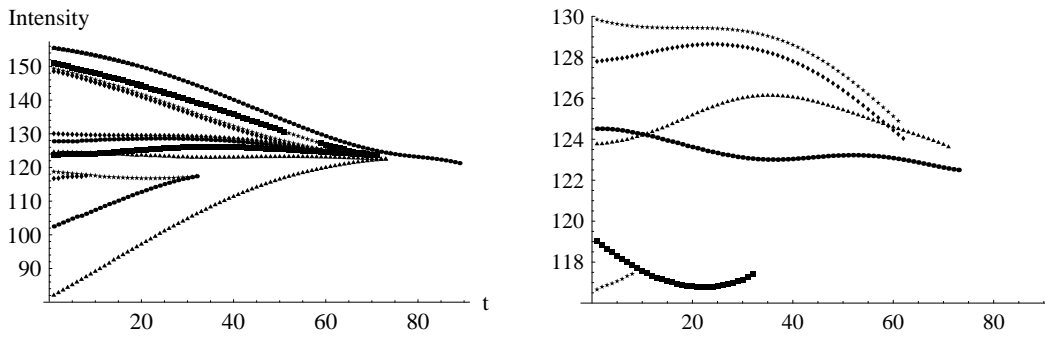


Figure 5.10: Parametrised intensities of the critical points of the scale space of Figure 5.11a; 89 scales exponentially sampled from 8.37 to 33.1 Left: All 15 critical points. Right: Intensities of the six spatial saddles.

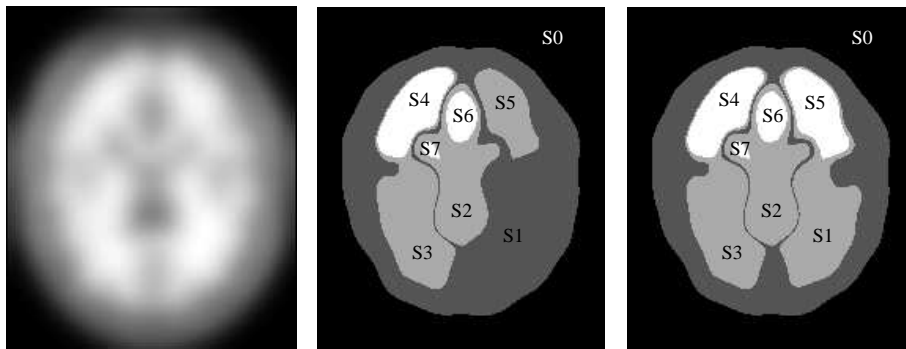


Figure 5.11: a) MR Image of Figure 5.4b on scale 8.39. b) Segments of the 7 extrema of a. c) Idem, with the iso-intensity manifold of  $S_1$  chosen equally to  $S_3$ .

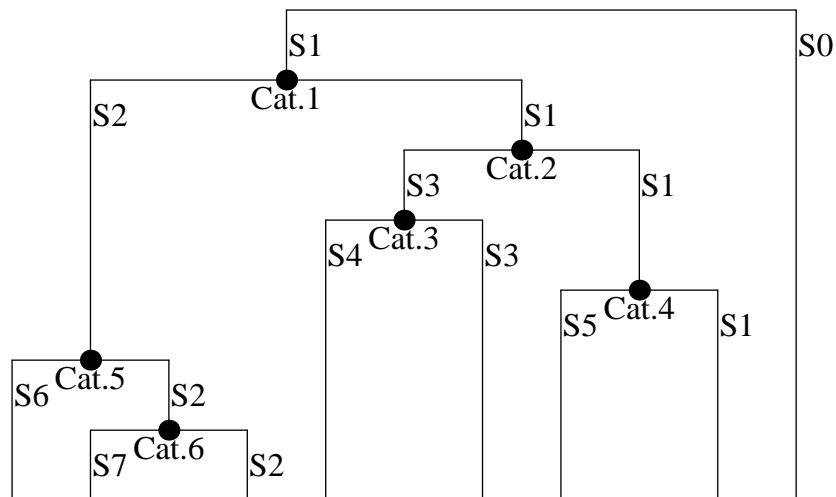


Figure 5.12: Hierarchy of Figure 5.11a.

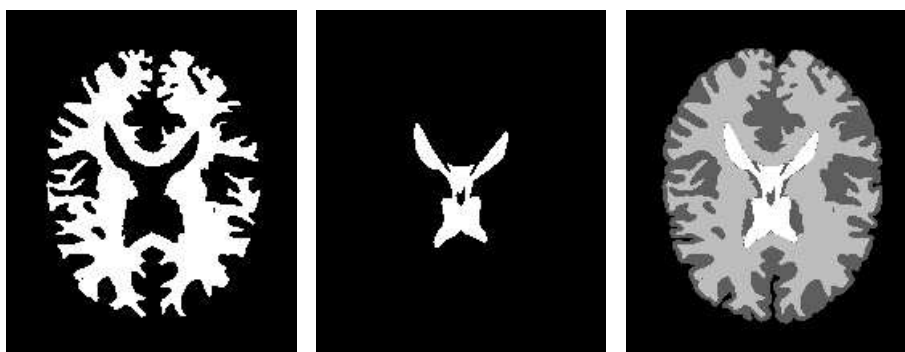


Figure 5.13: Intersection of the initial image, Figure 5.4a, with various scale space parts (see text). a) The bright region. b) The dark region. c) Hierarchy simplified to four parts.

Figure 5.11c.

As an (other) example of a tree operation on Figure 5.12, recall that the four segments  $S_1$ ,  $S_3$ ,  $S_4$ , and  $S_5$  correspond to the four maxima located within the most white part of Figure 5.11a. We can therefore simplify the tree by clustering these four segments to one region of interest, “the bright region”. The iso-intensity manifolds have the intensity of the scale space saddle defining segment  $S_3$ . Similarly, Segment  $S_2$  and its subsegments  $S_6$  and  $S_7$  correspond to the three minima in the interior of Figure 5.11a, the dark region in the middle, and can be clustered to one region, “the dark region”.

The part in scale space bounded by the intensity of the scale space saddles is found by a 3D region growing algorithm. The intersection of the simplified bright and dark region with the initial MR image, Figure 5.4b, are shown in Figure 5.13a-b. The pre-segmentation of the initial image with respect to these two parts together with the segments  $S_0$  and  $S_1$  is shown in Figure 5.13c.

With the simulated MRI (again shown in Figure 5.14a), also the probabilistic distributions of the white matter (Figure 5.14b) and the gray matter (Figure 5.14c) are given as ground-truth images with values ranging from 0 to 255.

Comparing Figures 5.13a and 5.14b shown that the intensity defining the scale space segment of the bright region is a good estimator of the threshold value to the white matter. However, this region is connected whereas the white matter distribution also contains isolated regions. To overcome this difference, we compare the given distributions the initial image thresholded on the values of the scale space saddles.

Figure 5.14d shows a direct intersection of the original image, Figure 5.14a, with all the iso-intensity manifolds equalling the intensities of the 7 extrema of the parametrised critical curves. So the range of values is reduced from  $0, \dots, 255$  in the initial image to  $0, \dots, 8$ .

The original image thresholded on the intensity defining segment  $S_3$  is shown in Figure 5.14e. The difference with Figure 5.13a yields four isolated regions, three in the middle and one in the bottom-right part of the image.

Furthermore, the gray matter can be estimated by subtraction of the bright and the dark regions, as Figure 5.13c indicates. The original image thresholded on the values of these bright and dark regions is shown in Figure 5.14f.

To compare the Figures 5.14b-c with the Figures 5.14e-f we used the similarity measure of two

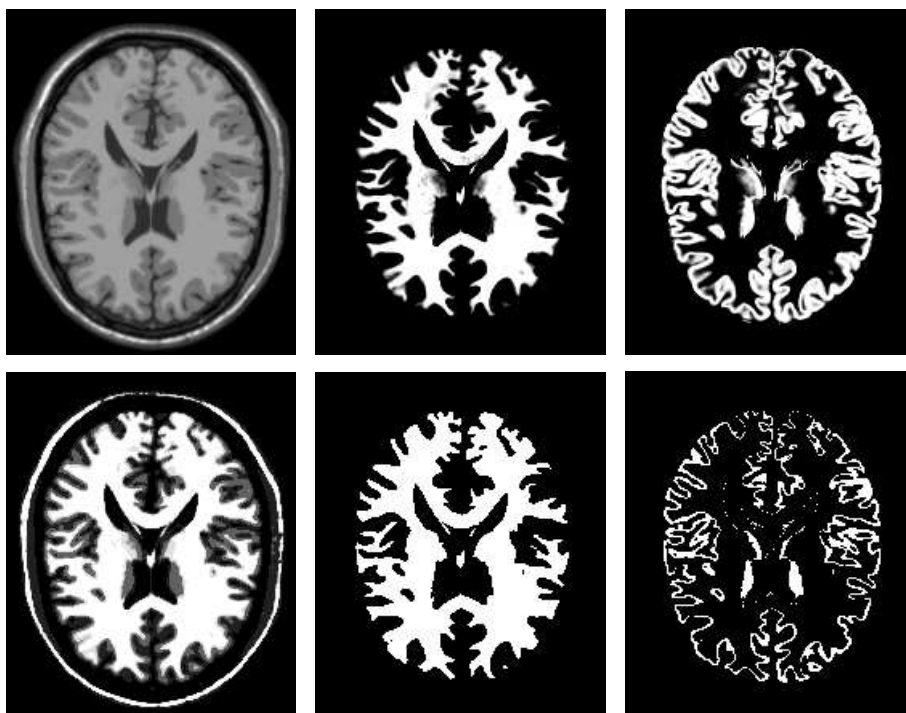


Figure 5.14: Top row: a) Simulated MR brain image, Figure 5.4b. b) Ground-truth distribution of white matter. c) Ground-truth distribution of grey matter. Bottom row: d) Segmentation by the isophotes with the value of the 7 extrema. e) Segment thresholded on the value of the bright region. f) Segment thresholded on the values of the bright and dark regions.



segments  $A$  and  $B$  defined by  $2\frac{A \cap B}{A+B}$ . Since the Figures 5.14b-c are probabilistic segmentations, they are made binary by thresholding them on the value 128. Then the similarity of the Figures 5.14b and 5.14e is 96.6% and of the Figures 5.14c and 5.14f is 68.1%. The similarity of the unions of Figures 5.14b+c and of Figures 5.14e+f is 89.9%. The error is mainly caused by pixels included only in the segmentation of the ground truth. In other words, Figures 5.14e and 5.14f give an underestimation of the probabilistic distributions. The regions found by the tree simplification may be used as an initialisation of a post-processing step to obtain a more accurate segmentation based on the geometry of the image. The latter is obviously not present in the hierarchy tree.

## 5.5 Conclusions and Discussion

We developed a method to calculate the hierarchical structure of an arbitrary input image. The method is based on the scale space image of the input image and the critical paths within it. The latter exist of branches of spatial extrema and spatial saddle points. The range of scales at which these branches exist follow from their catastrophe points in scale space. These points essentially describe annihilations or creations of pairs of spatial critical points. To each spatial extremum an iso-intensity manifold is assigned. The value of this manifold equals that of the global intensity extremum of the saddle branch that is connected by the annihilation with the extremum branch containing the spatial extremum. This global intensity extremum is located at either the initial scale or at a scale space saddle, a critical point in scale space. The iso-intensity manifold encapsulates the extremum in scale space. The manifolds through the extrema are nested and non-intersecting and thus form a hierarchy.

In contrast to what has been described in the literature we showed that these manifolds necessarily should be chosen such that they go through the scale space saddle instead of the annihilation point.

As application, this structure can be visualised as a pre-segmentation by the intersection of the iso-intensity manifolds with the image at a specified scale or with the input image. The word “pre-segmentation” is chosen, since it is not a task-specified segmentation, but only a division of the image in several topologically defined parts without any a priori knowledge about the contents of the image itself. It may be thus used as an initial segmentation for further post-processing. Other applications may include *e.g.* clustering and data compression.

The proposed algorithm has two main advantages. Firstly, it has a severe mathematical underpinning which encourages and facilitates future improvements, and admits reproducible, predictable, and provable segmentation results. Secondly, it has the potential to include semantics enabling an intelligent choice of the nodes, either by deterministic, statistic or probabilistic means.

Experimental results based on artificial images and simulated MRI with respect to the hierarchy and pre-segmentation were given. They clarified the theory and showed results that correspond to a fair size to both the mathematical and the intuitive forecast.

## 5.6 Appendix: Critical Curves and Manifolds

We clarify the theory presented in section 5.2 by discussing the appearance of scale space saddles at the generic catastrophe event in scale space describing an annihilation. This event, called a Fold catastrophe, is known from catastrophe theory (see *e.g.* [6, 8, 29, 81, 91, 184, 212, 238, 239]) and applied to and

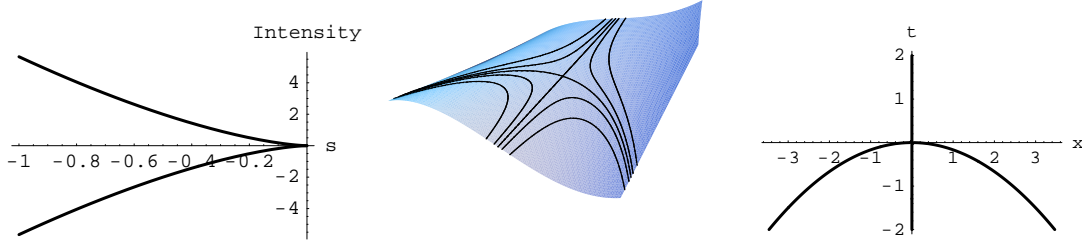


Figure 5.15: a) Parametrised intensity of a fold catastrophe in 1D with respect to scale. b)  $(x, t, L(x; t))$  scale space surface of the fold catastrophe with iso-intensity curves  $L(x; t) = c$ . c) Segments of b), defined by the scale space saddle intensity  $L(x; t) = 0$ : for  $t < 0$  four segments exist, for  $t > 0$  two remain.

used in scale space (see *e.g.* [45, 46, 47, 72, 126, 128, 129, 130, 131, 154]). Firstly, an example on one-dimensional images is given, because scale space saddles coincide with the catastrophe points. Secondly, the results on a multi-dimensional image is discussed.

### 1D Images

In 1D images the iso-intensity manifolds (or separatrices) are given by the isophotes through the catastrophe points, since these points are identical to the scale space saddles:  $H = L_{xx}$  and  $L_t = \Delta L = L_{xx}$ . The extended Hessian, Eq. (5.4), reads

$$\mathcal{H} = \begin{pmatrix} 0 & L_{xxx} \\ L_{xxx} & L_{xxxx} \end{pmatrix}.$$

It is generically non-zero at scale space saddles and  $\det \mathcal{H} = -L_{xxx}^2 < 0$ . The generic annihilation is described by

$$L(x; t) = x^3 + 6xt$$

and has a scale space saddle if both derivatives are zero, that is,  $L_x = 3x^2 + 6t = 0$  and  $L_t = 6x = 0$ . So it is located at the origin with intensity equal to zero. The parametrisation of the critical curve with respect to the scale  $t$  is  $(x(s); t(s)) = (\pm\sqrt{-2s}; s)$ ,  $s \leq 0$  and the parametrised intensity reads  $P(s) = \pm 4s\sqrt{-2s}$ ,  $s \leq 0$ , see Figure 5.15a. This parametrisation has its local extremum at  $s = 0$ , the right boundary of the interval on which the branches are defined. An alternative parametrisation of the critical curve, based on the position of the critical points, reads  $(x(s); t(s)) = (s; -\frac{1}{2}s^2)$ ,  $\forall s$ . Then  $P_1(s) = -2s^3$  and its critical point  $s = 0$  is a point of inflection.

The dome defined by the scale space saddle is given by the isophotes  $L(x; t) = 0$  through the origin, so  $(x; t) = (0; t)$  and  $(x; t) = (x; -\frac{1}{6}x^2)$ . Figure 5.15b shows isophotes in the  $(x, t, L(x; t))$ -space, where the isophote  $L = 0$  gives the annihilation point with the separatrices. The separation curves in the  $(x; t)$ -plane are shown in Figure 5.15c.

At the catastrophe point the isophotes of the scale space saddle form a pitchfork. Due to the causality principle it has 3 branches downwards and only one upward, *i.e.* at the scale space saddle four separate regions change to two separate regions. Locally the isophotes are described by  $L(x; t) = L_{xt}(\frac{1}{6}x^3 +$

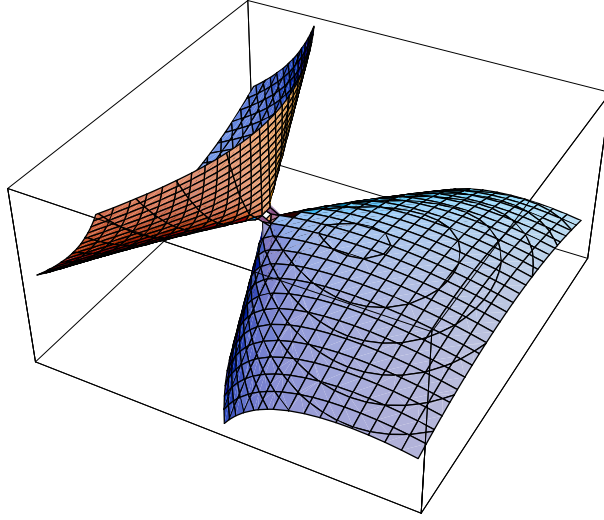


Figure 5.16: 2D Surface trough a scale space saddle; see text for further details.

$xt) \stackrel{\text{def}}{=} 0$ , so the horizontal traversing branches of the scale space saddle isophote necessarily have negatively oriented branches by  $t = -\frac{1}{6}x^2$ .

#### ***n*-D Images, $n > 1$**

In higher dimensions the structure is more complicated, since the scale space saddle does not coincide with the catastrophe point. For  $n$ -D images,  $n > 1$ , it suffices to investigate scale space critical points in 2D, see *e.g.* [45, 46, 47, 91, 212, 238, 239].

If we assume  $L_{yy} = -L_{xx}$  as to satisfy  $\Delta L = 0$ , the extended Hessian, Eq. (5.4), becomes

$$\mathcal{H} = \begin{pmatrix} L_{xx} & L_{xy} & L_{xt} \\ L_{xy} & -L_{xx} & L_{yt} \\ L_{xt} & L_{yt} & L_{tt} \end{pmatrix}.$$

The determinant is  $-L_{tt}(L_{xx}^2 + L_{xy}^2) + L_{xx}(L_{xt}^2 - L_{yt}^2) + 2L_{xt}L_{xy}L_{yt}$  and the trace simplifies to  $L_{tt}$ , which are both generically non-zero.

The annihilation germ reads

$$L(x, y; t) = x^3 + 6xt + \alpha(y^2 + 2t), \quad (5.6)$$

where  $\alpha = \pm 1$ . Positive sign describes a saddle – minimum annihilation, negative sign a saddle – maximum one. Without loss of generality we take  $\alpha = 1$ . Then  $L_x = 3x^2 + 6t$ ,  $L_y = 2y$ ,  $L_t = 6x + 2$ , and  $\det H = 12x$ , so the catastrophe takes place at the origin with intensity equal to zero and the scale space saddle is located at  $(x, y; t) = (-\frac{1}{3}, 0; -\frac{1}{18})$  with intensity  $-\frac{1}{27}$ . The surface  $L(x, y; t) = -\frac{1}{27}$  is shown in Figure 5.16. It has a local maximum at  $(x, y; t) = (\frac{1}{6}, 0; -\frac{1}{72})$ : the top of the extremum dome.

The iso-intensity surface through the scale space saddle can be visualised by two surfaces touching each other at the scale space saddle. One part of the surface is related to the corresponding extremum of

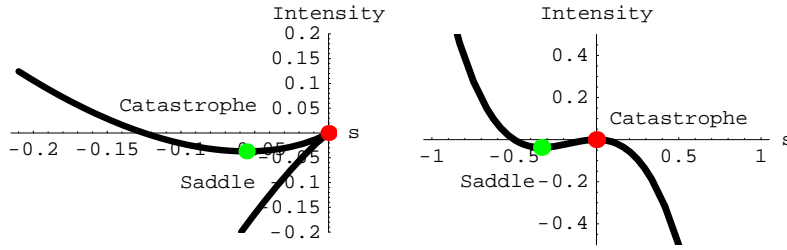


Figure 5.17: Intensity of the critical curve at fold catastrophe in 2D, parametrised by a) the  $t$ -coordinate and b) the  $x$ -coordinate. Both show at the origin an annihilation, at the minimum the scale space saddle.

the saddle. The other part encircles another – currently unknown – segment of the image. The surface belonging to the extremum forms a dome. The critical curve intersects this surface twice. The saddle branch has an intersection at the scale space saddle, the extremum branch at the top of the dome.

The parametrisation of the critical curve with respect to  $t$  (that is: a parametrisation of the branches of the critical curve) is given by  $(x(s), y(s); t(s)) = (\pm\sqrt{-2s}, 0; s)$ ,  $s \leq 0$ .

The intensity of the critical curve (shown in Figure 5.17a) then reads  $P(s) = 2s \pm 4s\sqrt{-2s}$ ,  $s \leq 0$ , with  $\partial_s t(s) = 1$  and  $\partial_s P(s) = 2 \pm 6\sqrt{-2s} = \Delta L \cdot t_s(s)$ . The critical points of  $P(s)$  are given by the scale space saddle, located at  $s = -\frac{1}{18}$ , and the catastrophe, located at  $s = 0$ , the boundary of the interval on which the branches are defined. These points are visible in Figure 5.17a as the local minimum of the parametrisation curve and the connection point of the two curves (a local maximum). The upper branch represents the spatial saddle, the lower one the minimum.

This image led Lifshitz and Pizer [168] to the observation that the intensity of the saddle point decreased even below the annihilation intensity resulting in theoretically problematic linking due to the escape of non-extremum paths from the extremal region they originate in.

This is, however, a generic property of scale space images and shows in an elegant way the necessity of limiting the extremal region by the critical iso-intensity manifold formed by the scale space saddle intensity.

An alternative parametrisation of the critical curve is given by  $s = x$ , so  $(x(s), y(s); t(s)) = (s, 0; -\frac{1}{2}s^2)$ , that is: a parametrisation of both branches of the critical curve simultaneously, based on the spatial position of the critical points. Then the intensity of the critical curve is given by  $P_1(s) = -2s^3 - s^2$ . Now  $\partial_s t(s) = -s$  and  $\partial_s P_1(s) = -6s^2 - 2s = (6s + 2)(-s)$  and the latter is still equivalent to  $\Delta L \cdot t_s(s)$ . The critical points of  $P_1(s)$  are given by  $s = 0$ , the catastrophe point, and at  $s = -\frac{1}{3}$ , the scale space saddle. These points are visible in Figure 5.17b as the extrema of the parametrisation curve. The branch  $s < 0$  represents the saddle point, the branch  $s > 0$  the minimum.

---

# The Application of Catastrophe Theory

---

Insofar as mathematics is about reality, it is not certain, and insofar as it is certain, it is not about reality.

---

ALBERT EINSTEIN

**abstract** The understanding of the behaviour of critical points under the influence of blurring opens the ability of investigation of the deep structure of Gaussian scale space images. The mathematical framework of catastrophe theory can be used to describe the various different types of events that can occur. For that purpose we investigate the generic and non-generic annihilations of critical points, as well as the creation of them. We show how this knowledge can be exploited in a scale space hierarchy tree for the purpose of pre-segmentation. We clarify the theory with an artificial image and a simulated MR image.

## 6.1 Introduction

The presence of structures of various sizes in an image demands almost automatically a collection of image analysis tools that is capable of dealing with multiple scales simultaneously. Various types of multi-scale paradigms have been developed [220]. They can be divided into two groups: linear and non-linear scale spaces.

### 6.1.1 Scale Space

The concept of (linear) scale space has been introduced in the Western world by Witkin [249] and Koenderink [139]. They showed that the natural way to represent an image at finite resolution is by convolving

it with a Gaussian of various bandwidths, thus obtaining a smoothed image at a scale determined by the bandwidth. This approach has led to the formulation of various invariant expressions – expressions that are independent of the coordinates – that capture certain features in an image at distinct levels of scale [53, 65, 76, 77, 78, 79, 80].

Under convolution with a Gaussian features are blurred and their locations change as a function of scale, as long as they remain well-defined. To avoid this as much as possible, non-linear scale spaces have been introduced, in which *e.g.* the blurring on parts with a high gradient (*i.e.* edges) is much smaller than in the rest of the image [75, 211, 245].

Multi-scale approaches are nowadays becoming more and more common and are being integrated with methods using PDEs, variational approaches and mathematical morphology [1, 27, 68, 73, 102, 106, 122, 193, 197].

### 6.1.2 Deep Structure

We focus on linear Gaussian scale space. This has the advantage that each scale level only requires the choice of an appropriate scale; and that the image intensity at that level follows linearly from any previous level. It is therefore possible to trace the evolution of certain image entities over scale. The exploitation of various scales simultaneously has been referred to as *deep structure* by Koenderink [139]. It pertains to information of the change of the image from highly detailed – including noise – to highly smoothed. Furthermore, it may be expected that large structures “live” longer than small structures (a reason that Gaussian blur is used to suppress noise). The image together with its blurred version was called “primal sketch” by Lindeberg [170, 171, 174]. Since multi-scale information can be ordered, one obtains a hierarchy representing the subsequent simplification of the image with increasing scale. In one dimensional images this has been done by several authors [124, 128, 129, 244], but higher dimensional images are more complicated as we will discuss below.

### 6.1.3 Related Work

An essentially unsolved problem in the investigation of deep structure is how to establish meaningful links across scales. This linking can be region-wise, that is: all points that belong to a certain region are identified with that region and are connected to a similar region at a larger scale, *cf.* multi-scale watershed segmentation [82, 122, 204, 205, 207]. A disadvantage is that one firstly needs to define these regions.

Another way is to link points if they satisfy some constraint. Vincken *et al.* [152, 240, 242] built the so-called *hyperstack*, based on a linear scale space, but with linking essentially based on the “affection” between two potentially corresponding points. It appeared that this line of approach also worked well if non-linear scale spaces were used. A drawback of the hyperstack is the counter-intuitively linking in a fine-to-coarse direction.

A well-defined and user-independent strategy is obtained by linking points that satisfy a topological constraint. This approach has been used in 2-D images by various authors [99, 168, 230]. They linked extrema, but noticed that sometimes new extrema occurred, disrupting a good linking.

This creation of new extrema in scale space has been studied in detail by Damon [45, 46, 47], proving that these creations are generic in images of dimension larger than one. That means that they are not some kind of artifact, introduced by noise or numerical errors, but that they are to be expected in any typical case. This was somewhat counterintuitive, since blurring seemed to imply that structure could

only disappear, thus suggesting that only annihilations could occur. Damon, however, showed that both annihilations and creations are generic catastrophes. Whereas Damons results were stated theoretically, application of these results were reported in *e.g.* [98, 154, 168, 170].

The main consequence is that in order to be able to use the topological approach one necessarily needs to take into account these creation events. This has been done in previous work by Kuijper *et al.* [157, 161, 162].

Apart from the aforementioned catastrophe points (annihilations and creations) there is a second type of topologically interesting points in scale space, *viz.* scale space critical points. These are spatial critical points with vanishing scale derivative. This implies a zero Laplacean in linear scale space. Although Laplacean zero-crossings are widely investigated (the “Laplacean of Gaussian” as edge-detector), the combination with zero gradient has only been mentioned occasionally, *e.g.* [98, 144, 168].

Several authors investigated the shape of iso-intensity manifolds [98, 113, 139] in scale space. Obviously, at annihilations some structure disappears. However, these points are not the only special points in relation to the iso-intensity manifolds as we showed in [157]. In contrast, in [157] we proved that the *critical points in scale space* also form special points as these define so-called *critical iso-intensity manifolds*, *i.e.* iso-intensity manifolds with self-intersection encapsulating an extremum, see Section 6.2.4.

Scale space critical points, together with annihilations and creations allow us to build a hierarchical structure that can be used to obtain a so-called pre-segmentation: a partitioning of the image in which the nesting of iso-intensity manifolds becomes visible.

#### 6.1.4 Aim

In the aforementioned articles [157, 161, 162] we also showed that it is sometimes desirable to use higher order (and thus non-generic) catastrophes to describe the change of structure. It has a direct relation to the hierarchy tree and the pre-segmentation, in the sense that two or more regions can be endowed with the same critical iso-intensity manifold. In this chapter we describe these catastrophes in scale space and show the implications for both the hierarchy tree and the pre-segmentation.

In section 6.2 theory on Gaussian scale space, catastrophe theory and a brief outline of the hierarchy tree is given. Catastrophes in scale space in generic coordinates and their effects on the hierarchy are discussed in section 6.3. We give some applications in section 6.4 and end with a summary and discussion in section 6.5.

## 6.2 Theory

In [157] we presented a uniquely defined hierarchical structure describing a scale space image. In section 6.2.4 we shortly outline the basic steps. In order to understand the essential elements, we define a Gaussian scale space in section 6.2.1. The structure depends on the evolution of spatial critical points as the scale changes. The locations of these points in scale space form one dimensional manifolds, the so-called critical curves, containing two types of special points. The first type is formed by the scale space saddles, discussed in section 6.2.2. The second type are the catastrophe points, presented in section 6.2.3.

### 6.2.1 Gaussian Scale Space

**Definition 14**  $L(\mathbf{x})$  denotes an arbitrary  $n$ -dimensional image. We will refer to this image as the initial image.

**Definition 15**  $L(\mathbf{x}; t)$  denotes the  $(n + 1)$ -dimensional Gaussian scale space image of  $L(\mathbf{x})$ .

The Gaussian scale space image is obtained by convolution of an initial image with a normalised Gaussian kernel of zero mean and standard deviation  $\sqrt{2t}$ :

$$L(\mathbf{x}; t) = G(\mathbf{x}; t) \otimes L(\mathbf{x}) = \int \frac{1}{\sqrt{4\pi t}^n} e^{-\frac{|\mathbf{x}-\mathbf{y}|^2}{4t}} L(\mathbf{y}) d\mathbf{y} .$$

Consequently,  $L(\mathbf{x}; t)$  satisfies the diffusion equation:

$$\partial_t L(\mathbf{x}; t) = \sum_{i=1}^n \frac{\partial^2}{\partial x_i^2} L(\mathbf{x}; t) \stackrel{\text{def}}{=} \Delta L(\mathbf{x}; t) . \quad (6.1)$$

Here  $\Delta L(\mathbf{x}; t)$  denotes the Laplacean. Differentiation is now well-defined, since derivatives of the image up to arbitrary order at any scale are obtained using

$$\frac{\partial}{\partial x_i} L(\mathbf{x}; t) = \frac{\partial}{\partial x_i} (G(\mathbf{x}; t) \otimes L(\mathbf{x})) = \left( \frac{\partial}{\partial x_i} G(\mathbf{x}; t) \right) \otimes L(\mathbf{x}) .$$

That is, an arbitrary derivative of the image is obtained by the convolution of the initial image with the corresponding derivative of a Gaussian.

**Definition 16** *Spatial critical points, i.e. saddles and extrema (maxima or minima), at a certain scale  $t_0$  are defined as the points at fixed scale  $t_0$  where the spatial gradient vanishes:  $\frac{\partial}{\partial x_i} L(\mathbf{x}; t_0) = 0 \forall i$ , that is,  $\nabla L(\mathbf{x}; t_0) = 0$ . We will refer to these points as spatial critical points to distinguish them from scale space critical points, see Definition 19.*

The type of a spatial critical point is given by the eigenvalues of the Hessian  $H$ , the matrix with the second order spatial derivatives, evaluated at its location.

**Definition 17** *The Hessian matrix at a certain scale  $t_0$  is defined by  $H \stackrel{\text{def}}{=} \nabla \nabla^T L(\mathbf{x}; t_0)$ , where each element of  $H$  is given by*

$$H_{i,j} = \frac{\partial^2}{\partial x_i \partial x_j} L(\mathbf{x}; t) .$$

The trace of the Hessian equals the Laplacean. For non-degenerate critical points at maxima (minima) all eigenvalues of the Hessian are negative (positive). At a spatial saddle point  $H$  has both negative and positive eigenvalues.

Since  $L(\mathbf{x}; t)$  is a smooth function in  $(\mathbf{x}; t)$ -space, spatial critical points are part of a one dimensional manifold in scale space by virtue of the implicit function theorem.

**Definition 18** *A critical curve is a one-dimensional manifold in scale space on which  $\nabla L(\mathbf{x}; t) = 0$ .*

Consequently, the intersection of all critical curves in scale space with a plane of certain fixed scale  $t_0$  yields the spatial critical points of the image at that scale.



### 6.2.2 Scale Space Saddles

**Definition 19** The scale space saddles of  $L(\mathbf{x}; t)$  are defined as the points where both the spatial gradient and the scale derivative vanish:  $\nabla L(\mathbf{x}; t) = 0$  and  $\Delta L(\mathbf{x}; t) = 0$ .

In Definition 19 we used Eq. (6.1). Note that it describes the critical points of  $L(\mathbf{x}; t)$  in scale space. In [157] it is proven that these points are indeed always saddle points, a result of the well-known maximum principle.

**Definition 20** The extended Hessian  $\mathcal{H}$  of  $L(\mathbf{x}; t)$  is matrix of second order derivatives in scale space defined by

$$\mathcal{H} = \begin{pmatrix} \nabla \nabla^T L & \Delta \nabla L \\ (\Delta \nabla L)^T & \Delta \Delta L \end{pmatrix}.$$

Here  $\nabla \nabla^T L$  is the Hessian.

Note that the elements of  $\mathcal{H}$  are purely spatial derivatives. Again, this is possible by virtue of the diffusion equation, Eq. (6.1).

The fact that scale space critical points are always saddles implies that the extended Hessian has both positive and negative eigenvalues at scale space critical points. Furthermore, in [157] we have proven that if the intensity of the spatial saddle points on a critical curve is parametrised by scale, scale space saddles are in fact the extrema of the parametrisation.

### 6.2.3 Catastrophe Theory

The spatial critical points of a function with non-zero eigenvalues of the Hessian are called *Morse critical points*. The *Morse Lemma* states that at these points the qualitative properties of the function are determined by the quadratic part of the Taylor expansion of this function. This part can be reduced to the *Morse canonical form* by a slick choice of coordinates.

If at a spatial critical point the Hessian degenerates, so that at least one of the eigenvalues is zero, the type of the spatial critical point is not defined.

**Definition 21** The catastrophe points of  $L(\mathbf{x}; t_0)$  are defined as the points where both the spatial gradient and the determinant of the Hessian vanish:  $\nabla L(\mathbf{x}; t_0) = 0$  and  $\det H(\mathbf{x}; t_0) = 0$ .

The term catastrophe was introduced by Thom [238, 239]. It denotes a (sudden) qualitative change in an object as the parameters on which this object depends change smoothly. This behaviour was already known by the terms perestroika, bifurcation and metamorphosis. The name catastrophe theory was suggested by Zeeman [255] to unify singularity theory, bifurcation theory and their applications and gained wide popularity. A thorough mathematical treatment on singularity theory can be found in the work of Arnol'd [5, 6, 7, 8, 9, 10]. More pragmatic introductions and applications are widely published, e.g. [29, 81, 91, 184, 212, 255].

The catastrophe points are also called *non-Morse critical points*, since a higher order Taylor expansion is essentially needed to describe the qualitative properties. Although the dimension of the variables is arbitrary, the *Thom Splitting Lemma* states that one can split up the function in a Morse and a non-Morse part. The latter consists of variables representing the  $k$  “bad” eigenvalues of the Hessian that

name	nickname	CG	PT
$A_2$	Fold	$x^3$	$\lambda_1 x$
$A_3^\pm$	Cusp	$\pm x^4$	$\lambda_1 x + \lambda_2 x^2$
$A_4$	Swallowtail	$x^5$	$\lambda_1 x + \lambda_2 x^2 + \lambda_3 x^3$
$A_5^\pm$	Butterfly	$\pm x^6$	$\lambda_1 x + \lambda_2 x^2 + \lambda_3 x^3 + \lambda_4 x^4$
$D_4^+$	Hyperbolic Umbilic	$x^2 y + y^3$	$\lambda_1 x + \lambda_2 y + \lambda_3 x^2$
$D_4^-$	Elliptic Umbilic	$x^2 y - y^3$	$\lambda_1 x + \lambda_2 y + \lambda_3 x^2$
$D_5^\pm$	Parabolic Umbilic	$x^2 y \pm y^4$	$\lambda_1 x + \lambda_2 y + \lambda_3 y^2 + \lambda_4 x^2$

Table 6.1: Description of non-Morse critical points for maximal 4 different perturbation parameters. Each contain a catastrophe germ (CG) and corresponding perturbation term (PT).

become zero. The Morse part contains the  $n - k$  remaining variables. Consequently, the Hessian contains a  $(n - k) \times (n - k)$  sub-matrix representing a Morse function. It therefore suffices to study the part of  $k$  variables. The canonical form of the function at the non-Morse critical point thus contains two parts: a Morse canonical form of  $n - k$  variables, in terms of the quadratic part of the Taylor series, and a non-Morse part. The latter can be put into canonical form called the *catastrophe germ*, which is obviously a polynomial of degree 3 or higher.

Since the Morse part does not change qualitatively under small perturbations, it is not necessary to further investigate this part. The non-Morse part, however, does change. Generally the non-Morse critical point will split into a non-Morse critical point, described by a polynomial of lower degree, and Morse critical points, or even exclusively into Morse critical points. This event is called a *morsification*. So the non-Morse part contains the catastrophe germ and a perturbation that controls the morsifications.

Then the general form of a Taylor expansion  $f(\mathbf{x})$  at a non-Morse critical point of an  $n$  dimensional function can be written as (*Thom's Theorem*):

$$f(\mathbf{x}; \lambda) = CG(x_1, \dots, x_k) + PT(x_1, \dots, x_k; \lambda_1, \dots, \lambda_l) + \sum_{i=k+1}^n \epsilon_i x_i^2, \quad (6.2)$$

where  $CG(x_1, \dots, x_k)$  denotes the catastrophe germ,  $PT(x_1, \dots, x_k; \lambda_1, \dots, \lambda_l)$  the perturbation germ with an  $l$ -dimensional space of parameters, and in the Morse part  $\epsilon_i = \pm 1$ . In Table 6.1 the germs of the generic families in  $l$  parameters, with  $l \leq 4$ , are listed. In 2D these form, together with  $A_1^\pm \stackrel{\text{def}}{=} \pm x^2 \pm y^2$  and taking  $D_4^+$  and  $D_4^-$  together as  $D_4^\pm$ , the so-called *Thom's seven*.

These germs are the starting point of the infinite set of so-called simple real singularities, whose catastrophe germs are given by the infinite series  $A_k^\pm \stackrel{\text{def}}{=} \pm x^{k+1}$ ,  $k \geq 1$  and  $D_k^\pm \stackrel{\text{def}}{=} x^2 y \pm y^{k-1}$ ,  $k \geq 4$ , and the three exceptional singularities  $E_6 \stackrel{\text{def}}{=} x^3 \pm y^4$ ,  $E_7 \stackrel{\text{def}}{=} x^3 + xy^3$ , and  $E_8 \stackrel{\text{def}}{=} x^3 + y^5$ . The germs  $A_k^+$  and  $A_k^-$  are equivalent for  $k = 1$  and  $k$  even.

### Catastrophes and Scale Space

In Definition 21, the number of equations defining the catastrophe point equals  $n + 1$  and therefore it is over-determined with respect to the  $n$  spatial variables. Consequently, catastrophe points are generically not found in typical images. In scale space, however, the number of variables equals  $n + 1$  and catastrophes occur as isolated points.

Although the list of catastrophes starts very simple, it is not trivial to apply it directly to scale space by assuming that scale is just one of the perturbation parameters.

For example, in one-dimensional images the Fold catastrophe reduces to  $x^3 + \lambda x$ . It describes the change from a situation with two critical points (a maximum and a minimum) for  $\lambda < 0$  to a situation without critical points for  $\lambda > 0$ . See *e.g.* Figure 6.1 in Section 6.3.1 for an example of such an annihilation sequence. This event can occur in two ways. The extrema are annihilated for increasing  $\lambda$ , but the opposite – creation of two extrema for decreasing  $\lambda$  – is also possible.

In scale space, however, there is an extra constraint: the germ has to satisfy the diffusion equation. Thus the catastrophe germ  $x^3$  implies an extra term  $6xt$ . On the other hand, the perturbation term is given by  $\lambda_1 x$ , so by taking  $\lambda = 6t$  scale plays the role of the perturbing parameter. This gives a directionality to the perturbation parameter, in the sense that the only remaining possibility for this  $A_2$ -catastrophe in one-dimensional images is an annihilation.

In higher dimensional images also the opposite – *i.e.* a Fold catastrophe describing the creation of a pair of critical points – is possible. Then the perturbation  $\lambda = -6t$  with increasing  $t$  requires an additional term of the form  $-6xy^2$  in order to satisfy the diffusion equation, see Definition 22.

The transfer of the catastrophe germs to scale space has been made by many authors, [45, 46, 47, 72, 126, 128, 129, 130, 131, 154, 157, 161, 162, 170, 174], among whom Damon's account is probably the most rigorous. He showed that the only generic morsifications in scale space are the aforementioned Fold catastrophes describing *annihilations* and *creations* of pairs of critical points. These two points have opposite sign of the determinant of the Hessian before annihilation and after creation. All other events are compounds of such events. It is however possible that one may not be able to distinguish these generic events, *e.g.* due to numerical limitations, coarse sampling, or (almost) symmetries in the image.

**Definition 22** *The scale space catastrophe germs are defined by*

$$\begin{aligned} f^A(\mathbf{x}; t) &\stackrel{\text{def}}{=} x_1^3 + 6x_1 t + Q(\mathbf{x}; t), \\ f^C(\mathbf{x}; t) &\stackrel{\text{def}}{=} x_1^3 - 6x_1 t - 6x_1 x_2^2 + Q(\mathbf{x}; t). \end{aligned}$$

*The quadratic term  $Q(\mathbf{x}; t)$  is defined*

$$Q(\mathbf{x}; t) \stackrel{\text{def}}{=} \sum_{i=2}^n \epsilon_i (x_i^2 + 2t),$$

*where  $\sum_{i=2}^n \epsilon_i \neq 0$  and  $\epsilon_i \neq 0 \forall i$ .*

Note that the scale space catastrophe germs  $f^A$  and  $f^C$ , and the quadratic term  $Q$  satisfy the diffusion equation. The germs  $f^A$  and  $f^C$  correspond to the two qualitatively different Fold catastrophes at the origin, an annihilation and a creation respectively. From Definition 22 it is obvious that annihilations occur in any dimension, but creations require at least 2 dimensions. Consequently, in 1D signals only annihilations occur. Furthermore, for images of arbitrary dimension it suffices to investigate the 2D case due to the Splitting Lemma.

### The Annihilation Germ

Spatial critical points at any scale  $t$  for  $f^A$  follow directly from  $\nabla f^A(\mathbf{x}; t) = 0$ :

$$\begin{cases} 3x_1^2 &= -6t \\ 2\epsilon_i x_i &= 0, \quad i \geq 2 \end{cases}$$

Then the critical curve is parametrised by  $(\pm\sqrt{-2t}, 0, \dots, 0; t), t \leq 0$ . At the origin a catastrophe takes place. The determinant of the Hessian is given by  $\det H = cx_1$ , with the constant  $c = 3 \cdot 2^n \prod_{i=2}^n \epsilon_i$ . So two critical points with opposite sign approach the origin as  $t$  increases to zero. Note that  $\text{tr } H = 6x_1 + \sum_{i=2}^n 2\epsilon_i$ , which is generically non-zero at catastrophe points. This explains the constraints on the  $\epsilon_i$  in Definition 22.

### The Creation Germ

The creation germ is a bit more complicated. Spatial critical points at any scale  $t$  for  $f^c$  follow from  $\nabla f^c(\mathbf{x}; t) = 0$ :

$$\begin{cases} 3x_1^2 - 6x_2^2 = 6t \\ 2x_2(\epsilon_2 - 6x_1) = 0 \\ 2\epsilon_i x_i = 0, \quad i \geq 3 \end{cases}$$

Since we look in the neighbourhood of the origin, we take  $x_2 = 0$ . Then the critical curve is parametrised by  $(\pm\sqrt{2t}, 0, \dots, 0; t), t \geq 0$ . At the origin a catastrophe takes place. The determinant of the Hessian is given by  $\det H = cx_1(\epsilon_2 - 6x_1) - 12cx_2^2$ , with the constant  $c = 3 \cdot 2^n \prod_{i=3}^n \epsilon_i$ , so two critical points with opposite sign leave the origin as  $t$  increases from zero. Note that this catastrophe is a Fold catastrophe since it describes the creation of two critical points, although there is a striking resemblance to the description of the Elliptic Umbilic catastrophe. Furthermore, the description of the catastrophe is essentially local: If  $t$  is taken too large, the (non-generic) degeneration of the Hessian at  $x_1 = \frac{1}{6}\epsilon_2$  has to be taken into account. We will elaborate on these items in Section 6.3.

### 6.2.4 Scale Space Hierarchy

From the previous section it follows that each critical curve in  $(\mathbf{x}; t)$ -space consists of separate branches, each of which is defined from a creation event to an annihilation event. We set  $\#_C$  the number of creation events on a critical path and  $\#_A$  the number of annihilation events. Since there exists a scale at which only one spatial critical point (an extremum) remains (see Loog et al. [182]), there is exactly one critical path with  $\#_A = \#_C$ , whereas all other critical paths have  $\#_A = \#_C + 1$ . That is, all but one critical paths are defined for a finite scale range.

One of the properties of scale space is non-enhancement of local extrema. Therefore, iso-intensity manifolds (isophotes in 2D) in the neighbourhood of a spatial extremum at a certain scale  $t_0$  move towards the spatial extremum at coarser scale until at some scale  $t_1$  the intensity of the extremum equals the intensity of the manifold. The iso-intensity surface in scale space forms a dome, with its top at the extremum at scale  $t_1$ . Since the intensity of the extremum is monotonically in- or decreasing (depending on whether it is a minimum or a maximum, respectively), all such domes are nested. Retrospectively, each extremum branch carries a series of nested domes, defining increasing regions around the extremum in the input image.

In [157] we have proven that these regions are uniquely related to one extremum as long as the intensity of the domes does not reach that of the so-called critical dome. The latter is formed by the iso-intensity manifold with its top at the extremum and containing a scale space saddle (see section 6.2.2) that is part of the same critical curve. An example of a critical dome and its related critical curve is shown in Figure 6.6 in Section 6.3.2.

In this way a hierarchy of regions of the input image is obtained, which can be regarded as a kind of pre-segmentation. It also results in a partition of the scale space itself. Details can be found in [157, 161, 162].

The crucial role is played by the scale space saddles and the catastrophe points. As long as only annihilation and creation events occur, the hierarchy is obtained straightforwardly. However, sometimes higher order catastrophes are needed to describe the local structure, *viz.* when two or more catastrophes happen to be almost incident and cannot be segregated due to coarse sampling, numerical imprecision, or (almost) symmetries in the image. In the next section we describe these higher order events.

### 6.3 Scale Space Catastrophes and Scale Space Saddles

In this section we discuss the appearance of catastrophe events in scale space and the effect on scale space saddles. Firstly, results on one-dimensional images are given, because in this particular case scale space saddles coincide with catastrophe points. Secondly, multi-dimensional images are discussed.

#### 6.3.1 1D Images

In 1D images the critical iso-intensity manifolds (or separatrices) are given by the isophotes through the catastrophe points, since these points are identical to the scale space saddles:  $H = L_{xx}$  and  $L_t = \Delta L = L_{xxx}$ . At such points the extended Hessian, Definition 20, reads

$$\mathcal{H} = \begin{pmatrix} 0 & L_{xxx} \\ L_{xxx} & L_{xxxx} \end{pmatrix}.$$

It is generically non-zero at scale space saddles and  $\det \mathcal{H} = -L_{xxx}^2 < 0$ . In one dimensional images only cuspid catastrophes (the  $A_k$ -type of Table 6.1) occur, of which we will discuss the Fold  $A_2$  and the Cusp  $A_3$ .

#### Fold Catastrophe

The generic annihilation is called a Fold and is defined by (see Definition 22 and further)

$$L(x; t) = x^3 + 6xt.$$

The only perturbation parameter is given by  $t$  after the identification  $\lambda_1 = 6t$ . The intensity for increasing scales is shown in Figure 6.1. It has a scale space saddle if both derivatives are zero, that is,

$$\begin{cases} L_x = 3x^2 + 6t = 0 \\ L_t = 6x = 0 \end{cases}$$

So it is located at the origin with intensity equal to zero. The determinant of the extended Hessian equals  $-36$ , indicating a saddle. A possible parametrisation of the critical curve is  $(x(s); t(s)) = (\pm\sqrt{-2s}; s)$ ,  $s \leq 0$  and the corresponding parametrised intensity reads  $P(s) = \pm 4s\sqrt{-2s}$ ,  $s \leq 0$ , see Figure 6.2a.

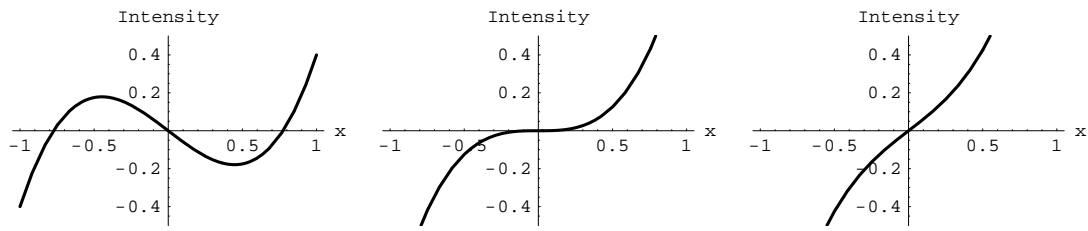


Figure 6.1: Fold catastrophe for increasing scales a)  $t=-1$ : Two extrema. b)  $t=0$ : Catastrophe at the origin. c)  $t=1$ : No extrema.

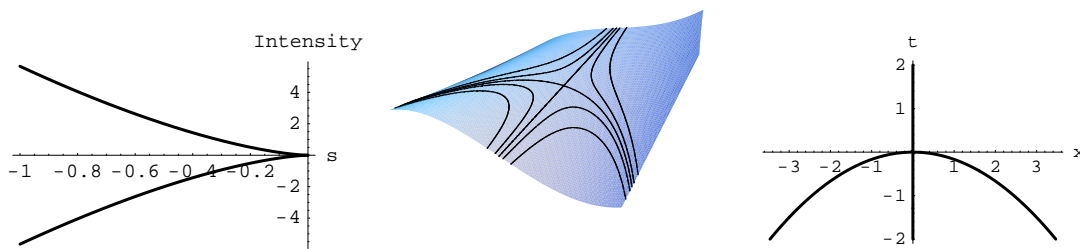


Figure 6.2: a) Parametrised intensity of the Fold catastrophe. b) 1+1D intensity scale space surface of the Fold catastrophe in  $(x, t, L(x; t))$  space. c) Segments of b), defined by the scale space saddle intensity.

The critical dome is given by the isophotes  $L(x; t) = 0$  through the origin, so  $(x; t) = (0; t)$  and  $(x; t) = (x; -\frac{1}{6}x^2)$ . Figure 6.2b shows isophotes  $L = constant$  in the  $(x; t, L(x; t))$ -space, where the self-intersection of  $L = 0$  gives the annihilation point. This isophote gives the separatrices of the different parts of the image. The separation curves in the  $(x; t)$ -plane are shown in Figure 6.2c. For  $t < 0$ , four regions exist, for  $t > 0$  two remain (compare to Figure 6.1a-c).

At the catastrophe point the isophotes of the scale space saddle form a pitchfork. Due to the causality principle it has 3 branches downwards and only one upward, *i.e.* at the scale space saddle four separate regions change to two separate regions. Locally the isophotes are described by  $L(x; t) = L_{xt}(\frac{1}{6}x^3 + xt) \stackrel{def}{=} 0$ , so the horizontally traversing branches of the scale space saddle isophote necessarily have branches given by  $t = -\frac{1}{6}x^2$ , describing the disappearance of two regions.

### Cusp Catastrophe

Although all catastrophes are generically described by fold catastrophes, one may encounter higher order catastrophes, *e.g.* due to numerical imprecision or symmetries in the signal, for instance when a set of two minima and one maximum change into one minimum, but one is not able to detect which minimum is annihilated.

The first higher order catastrophe describing such a situation is the Cusp catastrophe. The scale space representation of the catastrophe germ reads  $\pm(x^4 + 12x^2t + 12t^2)$ , the perturbation term was given by  $\lambda_1x + \lambda_2x^2$ , see Table 6.1. Obviously, scale can fulfil the role of the perturbation by  $\lambda_2$ . Therefore the

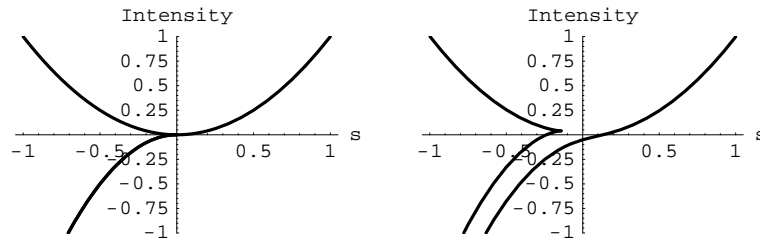


Figure 6.3: Parametrised intensity of the Cusp catastrophe a)  $\epsilon = 0$  b)  $0 < |\epsilon| \ll 1$

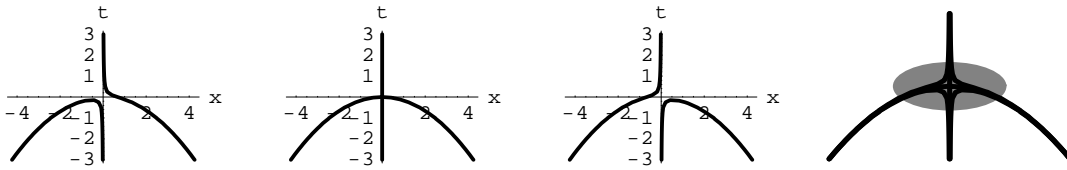


Figure 6.4: Critical paths in the  $(x; t)$ -plane. a)  $\epsilon < 0$  b)  $\epsilon = 0$  c)  $\epsilon > 0$  d) detection of the critical paths around the origin with uncertainty represented by the oval.

scale space form is given by

$$L(x; t) = \frac{1}{12}x^4 + x^2t + t^2 + \epsilon x,$$

where the two perturbation parameters are given by  $t$  for the second order term and  $\epsilon$  for the first order term. Scale space critical points are given by

$$\begin{cases} L_x = \frac{1}{3}x^3 + 2xt + \epsilon = 0 \\ L_t = x^2 + 2t = 0 \end{cases}$$

If  $\epsilon = 0$  the situation as sketched above occurs. The catastrophe takes place at the origin, where two minima and a maximum change into one minimum for increasing  $t$ . At the origin also  $L_{xxx} = 0$ , resulting in a zero eigenvalue of the extended Hessian. Note that this degeneration is automatically induced by the Cusp catastrophe. The parametrised intensity curves ( $L_1(0; s) = s^2, \forall s$  and  $L_2(\pm\sqrt{-6s}; s) = -2s^2, s \leq 0$ ) are shown in Figure 6.3a. Note that at the bottom left the two branches of the two minima with equal intensity, given by  $L_2$ , coincide. The case  $0 < |\epsilon| \ll 1$ , where a morsification has taken place, is visualised in Figure 6.3b. This Figure shows the remaining Fold catastrophe of a minimum and a maximum (compare to Figure 6.2a), and the unaffected other minimum.

It is this splitting that may not be discernible in practice, although it is the generic situation. Depending on the value and sign of  $\epsilon$  one can find the three different types of catastrophe shown in Figure 6.4a-c. With an uncertainty in the measurement they may coincide, as shown in Figure 6.4d, where the oval represents the possible measure uncertainty.

With the degeneration of the extended Hessian at the origin if  $\epsilon = 0$ , also the shape of the isophotes changes as shown in Figure 6.5. Since one eigenvalue is zero, the only remaining eigenvector is parallel to the  $x$ -axis. So there is no critical isophote in the  $t$ -direction, but both parts pass the origin horizontally. Consequently, three regions disappear. Furthermore the annihilating minimum cannot be distinguished from the remaining minimum.

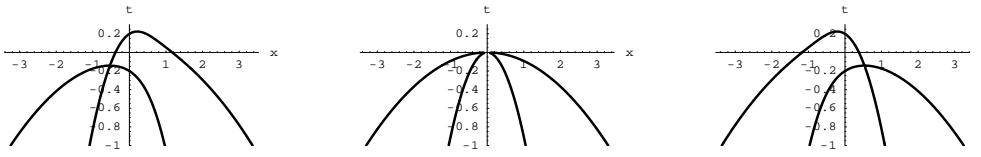


Figure 6.5: Critical isophotes in the  $(x; t)$ -plane. a)  $\epsilon < 0$  b)  $\epsilon = 0$  c)  $\epsilon > 0$

### Higher Order Cuspoids

One can easily verify that higher order Cuspoids,  $A_k$ ,  $k > 3$ , correspond to the annihilation of  $k$  regions simultaneously. Morsification per perturbation parameter leads to  $A_l$ ,  $l < k$  catastrophes, and a complete morsification yields only Fold catastrophes.

### 6.3.2 $n$ -D Images, $n > 1$

In higher dimensions the structure is more complicated, since generically scale space saddles do not coincide with catastrophe points. For  $n$ -D images,  $n > 1$ , it suffices to investigate scale space critical points in 2+1D, since the first seven elementary catastrophes can locally be written in 2 dimensions. Apart from the in one dimension determined cuspid catastrophes  $A_k$  causing annihilations, also umbilic catastrophes  $D_k$  occur, requiring 2 variables (see Table 6.1). The first two types are the hyperbolic  $D_4^+$  and the elliptic  $D_4^-$  umbilic catastrophes.

If we assume  $L_{yy} = -L_{xx}$  so that  $\Delta L = 0$ , the extended Hessian, Definition 20, becomes

$$\mathcal{H} = \begin{pmatrix} L_{xx} & L_{xy} & L_{xt} \\ L_{xy} & -L_{xx} & L_{yt} \\ L_{xt} & L_{yt} & L_{tt} \end{pmatrix}.$$

The determinant is  $-L_{tt}(L_{xx}^2 + L_{xy}^2) + L_{xx}(L_{xt}^2 - L_{yt}^2) + 2L_{xt}L_{xy}L_{yt}$  and the trace simplifies to  $L_{tt}$ . Both are generically non-zero.

In this section we subsequently describe the scale space representations in 2+1D of the cuspid catastrophes  $A_2$  and  $A_3$ , and the umbilic catastrophes  $D_4^+$  and  $D_4^-$ , together with their morsifications, the appearances of scale space saddles and the possibilities with respect to the degeneration of  $\mathcal{H}$ .

### Fold Catastrophe

The first type of catastrophes is given by the Fold catastrophe, which follows directly from Table 6.1 and Eq. (6.2) and was given in  $n$ -D in Section 6.2.3:

$$L(x, y; t) = x^3 + 6xt + \alpha(y^2 + 2t), \quad (6.3)$$



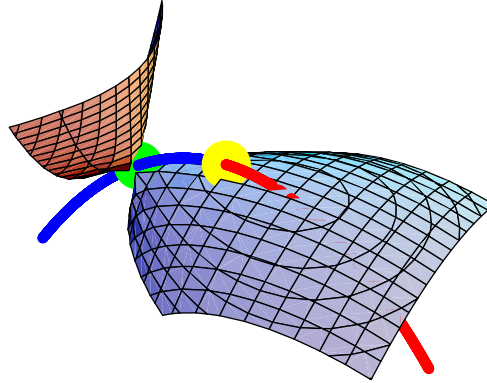


Figure 6.6: The critical curve contains a catastrophe point (bright dot) and a scale space saddle (dark dot). The iso-intensity surface through the scale space saddle contains two parts touching each other at the scale space saddle. One part is dome-shaped and intersects the critical curve at the top of the dome.

where  $\alpha = \pm 1$ . Positive sign describes a saddle – minimum annihilation, negative sign a saddle – maximum annihilation. Without loss of generality we take  $\alpha = 1$ . Then

$$\begin{cases} L_x = 3x^2 + 6t \\ L_y = 2y \\ L_t = 6x + 2 \\ \det H = 12x \\ \det \mathcal{H} = -72, \end{cases}$$

so the catastrophe takes place at the origin with intensity equal to zero and the scale space saddle is located at  $(x, y; t) = (-\frac{1}{3}, 0; -\frac{1}{18})$  with intensity  $-\frac{1}{27}$ . The surface  $L(x, y; t) = -\frac{1}{27}$  through the scale space saddle is shown in Figure 6.6. It has a local maximum at  $(x, y; t) = (\frac{1}{6}, 0; -\frac{1}{72})$ : the top of the extremum dome. Recall that the coordinates have no quantitative significance.

The iso-intensity surface through the scale space saddle can be visualised by two surfaces touching each other at the scale space saddle. One part of the surface is related to the extremum corresponding to the scale space saddle. The other part encircles some other segment of the image. The surface belonging to the extremum forms a dome. The critical curve intersects this surface twice. The saddle branch has an intersection at the scale space saddle, the extremum branch at the top of the dome, as shown in Figure 6.6.

A parametrisation of the two branches of the critical curve is given by

$$(x(s), y(s); t(s)) = (\pm\sqrt{-2s}, 0; s), \quad s \leq 0.$$

The intensity of the critical curve reads  $L(s) = 2s \pm 4s\sqrt{-2s}$ ,  $s \leq 0$  (with  $\partial_s t = 1$  and  $\partial_s L = \Delta L \cdot \partial_s t = 2 \pm 6\sqrt{-2s}$ ). The scale space saddle is located at  $s = -\frac{1}{18}$ , the catastrophe at the local

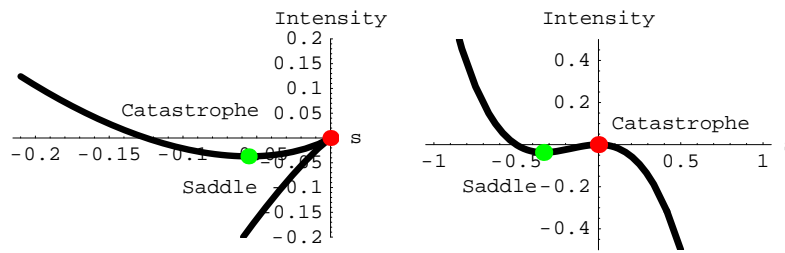


Figure 6.7: Intensity of the critical curve, parametrised by a) the x-coordinate and b) the t-coordinate. Both showing at the origin an annihilation, at the minimum the scale space saddle.

maximum, the connection of the two intensity-curves,  $s = 0$ . These points are visible in Figure 6.7a as the local minimum of the parametrisation curve and the connection point of the two curves, the upper branch representing the spatial saddle, the lower one the minimum.

Note that an alternative parametrisation of both branches of the critical curve simultaneously is given by  $(x(s), y(s); t(s)) = (s, 0; -\frac{1}{2}s^2)$ . Then the intensity of the critical curve is given by  $L(s) = -2s^3 - s^2$ . Now  $\partial_s t = -s$  and  $\partial_s L(s) = -6s^2 - 2s = (6s + 2)(-s)$  and the latter is still equivalent to  $\Delta L \cdot t_s$ . The catastrophe takes place at  $s = 0$ , the saddle at  $s = -\frac{1}{3}$ . These points are visible in Figure 6.7b as the extrema of the parametrisation curve. The branch  $s < 0$  represents the saddle point, the branch  $s > 0$  the minimum.

### Cusp Catastrophe

With the similar argumentation as in the one-dimensional case it is also interesting to investigate the behaviour around the next catastrophe event. The higher-dimensional cusp catastrophe in scale space follows directly from Table 6.1 and Eq. (6.2). It is the 2-D scale space extension of the catastrophe discussed in section 6.3.1 and is defined by

$$L(x, y; t) = \frac{1}{12}x^4 + x^2t + t^2 + \alpha(2t + y^2) + \epsilon x$$

where, again,  $\alpha = \pm 1$ . If  $\epsilon \neq 0$  a fold catastrophe results. Then

$$\begin{cases} L_x &= \frac{1}{3}x^3 + 2xt + \epsilon \\ L_y &= 2\alpha y \\ L_t &= x^2 + 2\alpha + 2t \\ \det H &= 2\alpha(x^2 + 2t) \\ \det \mathcal{H} &= 4\alpha(2t - x^2). \end{cases}$$

The critical curves in the  $(x; t)$ -plane at  $\epsilon = 0, y = 0$  are shown in Figure 6.8a. They form a so-called pitchfork bifurcation at the origin, the catastrophe point.

Critical points are on the curves given by  $(x(s), y(s); t(s)) = (0, 0; s)$  and  $(x(s), y(s); t(s)) = (\pm\sqrt{-6s}, 0; s), s \leq 0$ .

The intensities are given by  $L_1(s) = L(0, 0; s) = s^2 + 2\alpha s$  with its extremum at  $s = -\alpha$  and  $L_2(s) = L(\pm\sqrt{-6s}, 0; s) = -2s^2 + 2\alpha s, s \leq 0$ . The latter has an extremum at  $s = \frac{1}{2}\alpha$ . Since  $s \leq 0$ , these scale space saddles only occur if  $\alpha < 0$ . It is therefore essential to distinguish between the two signs of  $\alpha$ .

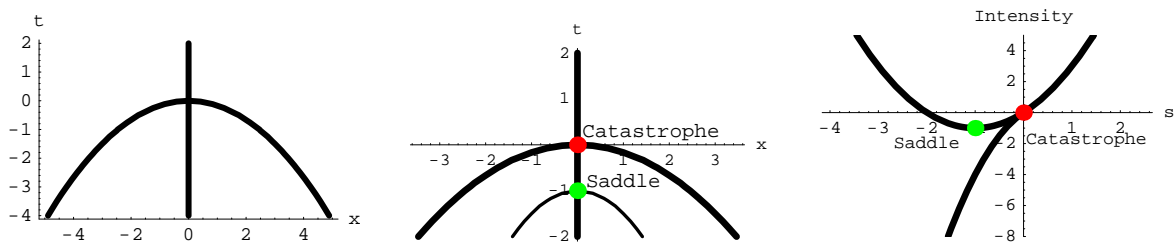


Figure 6.8: a) Critical paths. b) Critical paths with the zero-Laplacean curve (thin), the catastrophe point (dark) and the scale space saddle (bright) if  $\alpha > 0$ . c) Intensity of the critical paths. The part bottom-left represents two branches ending at the catastrophe point. The intensity takes a local minimum at the scale space saddle

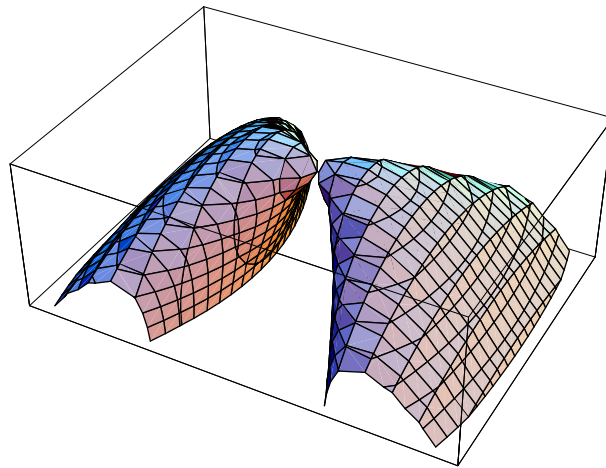


Figure 6.9: 2D Surface trough the scale space saddle at a Cusp catastrophe,  $\alpha > 0$ .

**The Case  $\alpha > 0$**  For positive  $\alpha$ , the curve  $(x, y; t) = (0, 0; s)$  contains saddles if  $t < 0$  and minima if  $t > 0$ . The other curve contains minima on both branches. At the origin a catastrophe occurs, at  $(x, y; t) = (0, 0, -\alpha)$  a scale space saddle, see Figure 6.8b. The intensities of the critical curves are shown in Figure 6.8c; The two branches of the minima for  $t < 0$  have equal intensity. The iso-intensity manifold in scale space forms a double dome since the two minima are indistinguishable, see Figure 6.9.

A small perturbation ( $0 < |\epsilon| \ll 1$ ) leads to a generic image containing a Fold catastrophe and thus a single cone. However, as argued in section 6.3.1 this perturbation may be too small to identify the annihilating minimum. We will use this degeneration in Section 6.4 to identify multiple regions with one scale space saddle.

**The Case  $\alpha < 0$**  If  $\alpha$  is negative, the curve  $(x, y; t) = (0, 0; s)$  contains a maximum if  $t < 0$  and a saddle if  $t > 0$ , while the curve  $(x, y; t) = (\pm\sqrt{-6s}, 0; s), s < 0$  contains saddles. Now 3 scale space saddles occur: at  $(x, y; t) = (0, 0, -\alpha)$  and  $(x, y; t) = (\pm\sqrt{-3\alpha}, 0; \frac{1}{2}\alpha)$ , see Figure 6.10a. The corresponding intensities are shown in Figure 6.10b, where again the intensities of the two saddle branches (and thus the scale space saddles) for  $t < 0$  coincide.

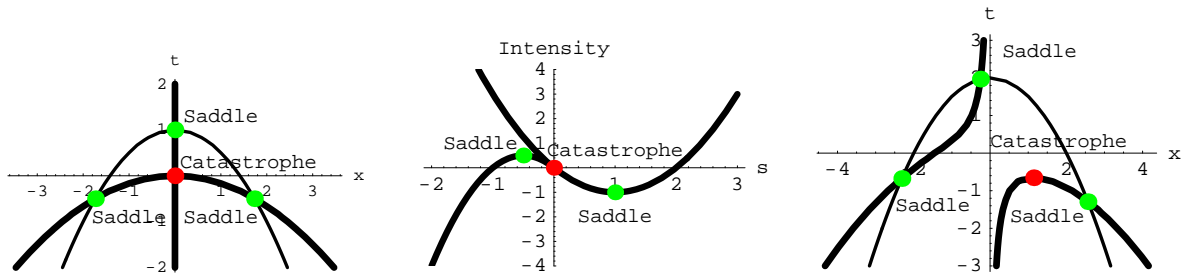


Figure 6.10: a) Critical paths (thick curves) with zero-Laplacean (thin curve), the catastrophe point (dark red) and scale space saddle (bright green points) if  $\alpha = -1$ . b) Intensity of the critical paths. The part bottom-left represents two branches ending at the catastrophe point. The intensity has local extrema at the scale space saddles. c) Critical paths (thick) with  $\alpha < 0$ ,  $9\epsilon^2 < -16\alpha^3$ , zero-Laplacean (thin), catastrophe point (dark red) and scale space saddles (bright green).

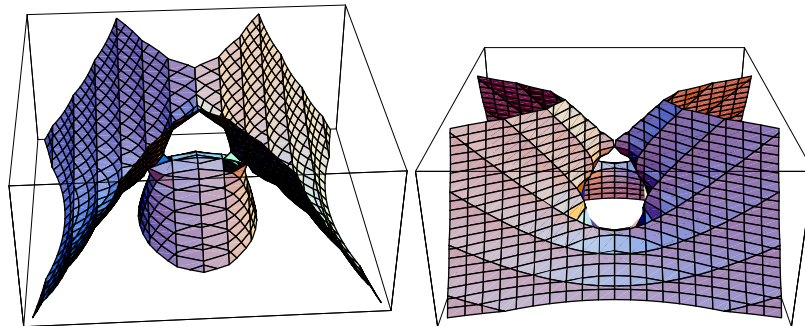


Figure 6.11: 2D iso-intensity manifold trough the scale space saddles a) at  $t = -\frac{1}{2}$  and b) at  $t = 1$

The iso-intensity surfaces through the scale space saddles are shown in Figure 6.11. The scale space saddles at  $t = \frac{1}{2}\alpha$  both encapsulate the maximum at the  $t$ -axis. The scale space saddle at  $t = -\alpha$  is *void*, *i.e.* it is not related to an extremum. This is clear from the fact that there is only one extremum present.

If a small perturbation ( $0 < |\epsilon| \ll 1$ ) is added the three scale space saddles remain present in the generic image. Their trajectories in the  $(x; t)$ -plane are shown in Figure 6.10c. Now a Fold catastrophe is apparent, but also a saddle branch containing two (void) scale space saddles, caused by the neighbourhood of the annihilating saddle-extremum pair.

**Degeneration of  $\det \mathcal{H}$**  The extended Hessian degenerates if its determinant vanishes, *i.e.* if  $4\alpha(2t - x^2) = 0$ . This implies  $2t = x^2$ . Then  $L_x = 0$  reduces to  $\frac{4}{3}x^3 + \epsilon = 0$ . For  $\epsilon = 0$  the degeneration takes place at the origin, that is, at the cusp catastrophe. But then  $x = 0, t = 0$  and  $L_t = 0$  implies  $\alpha = 0$ , which is non-generic. For other arbitrary values of  $\epsilon$ ,  $L_t = 0$  implies  $x^2 = -\alpha$ , so it is located at  $(x, y; t) = (-\text{sgn}(\epsilon)\sqrt{-\alpha}, 0, -\frac{1}{2}\alpha)$ , where  $\alpha < 0$  and  $9\epsilon^2 = -16\alpha^3$ .

This special value is located at the non-annihilating saddle branch where the two scale space saddle points coincide, *i.e.* where the saddle branch touches the zero-Laplacean. This case is non-generic, since the intersection of the critical curve and the hyper-plane  $\Delta L = 0$  at this value is not transverse. This

value describes the transition of the case with two void scale space saddles to the case without scale space saddles: For  $|\epsilon| < \frac{4}{3}\sqrt{-\alpha^3}$  two void scale space saddles occur on the non-annihilating saddle branch as shown in Figure 6.10c. For  $|\epsilon| > \frac{4}{3}\sqrt{-\alpha^3}$  none occur since the saddle branch does not intersect the zero-Laplacean. In other words: a Fold catastrophe *in scale space* occurs, regarding two scale space critical points (*i.e.* saddles) with different signs of  $\det \mathcal{H}$  and controlled by the perturbation parameter  $\epsilon$ .

### Hyperbolic Umbilic Catastrophe

The hyperbolic umbilic catastrophe germ is given by  $x^3 + xy^2$ . Its scale space addition is  $8xt$ . The perturbation term contains three terms:  $\lambda_1x + \lambda_2y + \lambda_3y^2$ . Obviously scale takes the role of  $\lambda_1$ . The scale space hyperbolic umbilic catastrophe germ with perturbation is thus defined by

$$L(x, y; t) = x^3 + xy^2 + 8xt + \alpha(y^2 + 2t) + \beta y$$

where the first three terms describe the scale space catastrophe germ. The set  $(\alpha, \beta)$  form the extra perturbation parameters. Then

$$\begin{cases} L_x &= 3x^2 + 8t + y^2 \\ L_y &= 2xy + 2\alpha y + \beta \\ L_t &= 8x + 2\alpha \\ \det H &= 12x(x + \alpha) - 4y^2 \\ \det \mathcal{H} &= -128(x + \alpha). \end{cases}$$

One can verify that at the combination  $(\alpha, \beta) = (0, 0)$  four critical points exist for each  $t < 0$ . At  $t = 0$  the four critical curves given by  $(x, y; t) = (\pm\sqrt{-\frac{8}{3}t}, 0; t)$  and  $(x, y; t) = (0, \pm\sqrt{-8t}; t)$  annihilate simultaneously at the origin (see *e.g.* Kalitzin [130]). This is non-generic, since this point is a scale space saddle and also  $\det \mathcal{H} = 0$ .

Morsification takes place in two steps. In the first step one perturbation parameter is non-zero. If  $\alpha \neq 0$  and  $\beta = 0$ , the annihilations are separated. At the origin a Fold catastrophe occurs with critical curves  $(x, y; t) = (-\sqrt{-\frac{8}{3}t}, 0; t)$ . On one of these curves both a scale space saddle at  $(x, y; t) = (-\frac{\alpha}{4}, 0; -\frac{3\alpha^2}{128})$ , and the other catastrophe at  $(x, y; t) = (-\alpha, 0; -\frac{3}{8}\alpha^2)$  are located. At the latter the critical curves  $(-\alpha, \pm\sqrt{-3\alpha^2 - 8t}; t), t < -\frac{3}{8}\alpha^2$  annihilate in a (non-generic!) Cusp catastrophe.

If  $\alpha = 0$  and  $\beta \neq 0$ , the double annihilation breaks up into two Fold annihilations with symmetric non-intersecting critical curves. A scale space saddle is not present.

Finally, if both  $\alpha$  and  $\beta$  are non-zero, this complete morsification results in the generic case with two critical curves, each of them containing a Fold annihilation. One the two critical curves contains a scale space saddle, located at  $(x, y; t) = (-\frac{1}{4}\alpha, -\frac{2\beta}{3\alpha}, -\frac{3\alpha^2}{128} - \frac{\beta^2}{18\alpha^2})$

The extended Hessian degenerates for  $x = -\alpha$ . Then it follows from  $L_t = 0$  that  $x = \alpha = 0$ , and from  $L_y$  that then also  $\beta = 0$ , which is a non-generic situation.

### Elliptic Umbilic Catastrophes

The elliptic umbilic catastrophe germ is given by  $x^3 - 6xy^2$ . Its scale space addition is  $-6xt$ . The perturbation term contains three terms:  $\lambda_1x + \lambda_2y + \lambda_3y^2$ . Obviously scale takes the role of  $\lambda_1$ . The

scale space elliptic umbilic catastrophe germ with perturbation is thus defined by

$$L(x, y; t) = x^3 - 6xy^2 - 6xt + \alpha(y^2 + 2t) + \beta y \quad (6.4)$$

where the first three terms describe the scale space catastrophe germ. The set  $(\alpha, \beta)$  form the extra perturbation parameters. Now

$$\left\{ \begin{array}{l} L_x = 3x^2 - 6t - 6y^2 \\ L_y = -12xy + 2\alpha y + \beta \\ L_t = -6x + 2\alpha \\ \det H = 12x(\alpha - 6x) - 144y^2 \\ \det \mathcal{H} = -72(\alpha - 6x). \end{array} \right.$$

The combination  $(\alpha, \beta) = (0, 0)$  gives two critical points for all  $t \neq 0$  on the critical curves  $(x, y; t) = (0, \pm\sqrt{-t}; t)$ ,  $t < 0$  and  $(x, y; t) = (\pm\sqrt{2t}, 0; t)$ ,  $t > 0$ . At the origin a so-called scatter event occurs: the critical curve changes from y-axis to x-axis with increasing  $t$ . Just as in the hyperbolic case, in fact two Fold catastrophes take place; in this case both an annihilation and a creation.

The morsification for  $\alpha = 0$ ,  $\beta \neq 0$  leads to the breaking into two critical curves without any catastrophe:  $\det H = 0$  implies  $x = y = 0$ , but then  $L_y = \beta \neq 0$ .

The morsification for  $\alpha \neq 0$ ,  $\beta = 0$  leads to only one catastrophe event at the origin: the Fold creation. The sign of  $\alpha$  determines whether the critical curve contains a maximum – saddle pair or a minimum – saddle pair. Without loss of generality we may choose  $\alpha = 1$ . For the moment we assume  $\beta = 0$  to compare this case with the Fold annihilation. Then the generic creation germ is defined as

$$L(x, y; t) = x^3 - 6xt - 6xy^2 + y^2 + 2t \quad (6.5)$$

The scale space saddle is located at  $(x, y; t) = (\frac{1}{3}, 0; \frac{1}{18})$  and its intensity is  $L(\frac{1}{3}, 0; \frac{1}{18}) = \frac{1}{27}$ . The surface  $L(x, y; t) = \frac{1}{27}$  has a local saddle at  $(x, y; t) = (-\frac{1}{6}, 0; \frac{1}{72})$ , see Figure 6.12. At creations newly created extremum domes cannot be present, which is obvious from the non-creation of new level-lines. Whereas annihilations of critical points lead to the annihilations of level-lines, creations of critical points are caused by the rearrangement of already existing level-lines.

This fact becomes clearer if we take a closer look at the structure of the critical curves. The critical curve containing the creation is given by  $(x, y; t) = (\pm\sqrt{2t}, 0; t)$ . The other critical curve given by  $(x, y; t) = (\frac{1}{6}, \pm\sqrt{\frac{1}{72} - t}; t)$  represents two branches connected at the second catastrophe, see Figure 6.13a. This point is located at  $(x, y; t) = (\frac{1}{6}, 0; \frac{1}{72})$ , is an element of both curves and obviously degenerates the extended Hessian. At this point two saddle points and the created extremum go through a Cusp catastrophe resulting in one saddle. Note that ignoring this catastrophe one would find a sudden change of the extremum into a saddle point while tracing the created critical points. Obviously this catastrophe is located between the creation catastrophe and the scale space saddle. The latter therefore does not invoke a critical dome around the created extremum.

The intensity of the creation pair is given by  $L(s) = 2s \pm 4s\sqrt{2s}$ ,  $s \geq 0$ , the intensity of the other pair by  $L(s) = \frac{1}{216} + s$ ,  $s \leq \frac{1}{72}$ . The intensities of both paths are shown in Figure 6.14a. A close-up around the catastrophe points is given in Figure 6.14b.

Note that the intensity curve at the bottom-left of Figure 6.14a-b contains two saddle branches with equal intensity. Figure 6.14b shows that at the catastrophe in the origin two curves are created. The

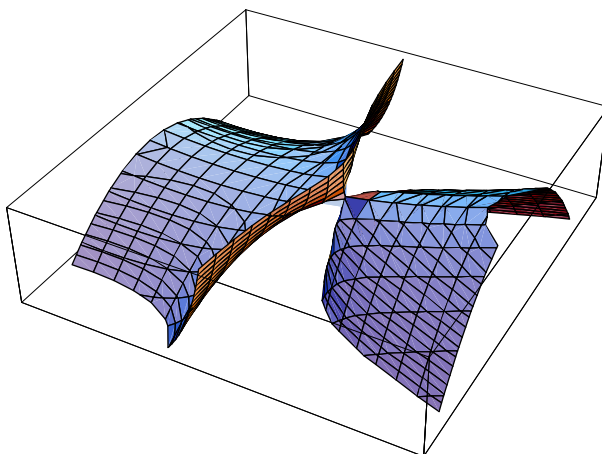


Figure 6.12: Iso-intensity surface of the scale space saddle of the creation germ.

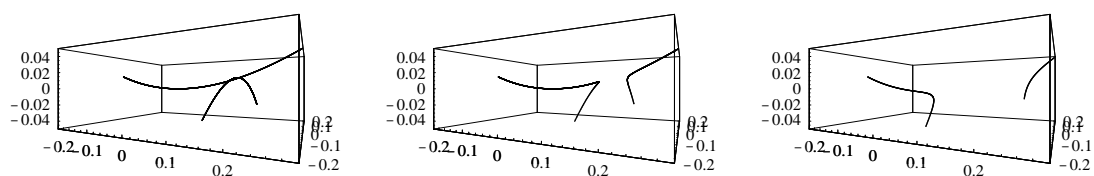


Figure 6.13: Critical curves of Eq. (6.4) with  $\alpha = 1$  in  $(x, y, t)$ -space. a)  $\beta = 0$ : Degeneration at the connection of the two critical paths b)  $0 < \|\beta\| < \frac{1}{32}\sqrt{6}$ : Morsification with two catastrophes on one of the critical curves. c)  $\|\beta\| > \frac{1}{32}\sqrt{6}$ : Morsification without catastrophes on the critical curves.

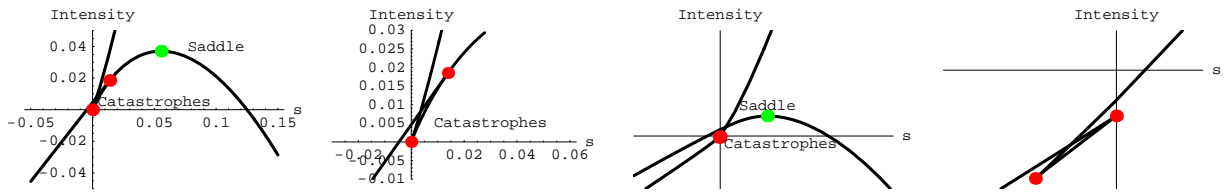


Figure 6.14: a) Intensities of critical paths,  $\beta = 0$ . b) Close-up at both catastrophes,  $\beta = 0$ . c) Intensities of critical paths,  $\beta = \frac{1}{24}\sqrt{2}$ . d) Close-up at both catastrophes,  $\beta = \frac{1}{24}\sqrt{2}$ .

saddle curve (the left curve) remains, the extremum one (the lower curve) is annihilated at the second catastrophe with one of the two saddle branches with equal intensity. The other saddle branch continues and contains a scale space saddle.

A complete morsification by taking  $0 < \|\beta\| \ll 1$  resolves the scatter. It can be shown that the Hessian has two real roots if and only if  $\|\beta\| < \frac{1}{32}\sqrt{6}$ . At these root points subsequently a creation and an annihilation event take place on a critical curve as shown in Figure 6.13b. If  $\|\beta\| > \frac{1}{32}\sqrt{6}$  the critical curve doesn't contain catastrophe points, see Figure 6.13c.

If we take  $\beta = \frac{1}{24}\sqrt{2}$  the creation is approximately at  $(0.013, -0.032; -0.00094)$  and the annihilation is at  $(x, y; t) = (1/12, -1/24\sqrt{2}; 0)$ . The intensity curves at this situation are visible in Figure 6.14c-d. Figure 6.14c shows that the two saddle curve have different intensities and do not coincide. One curve doesn't contain catastrophes, but only one scale space saddle. The other curve contains two catastrophes. A close-up around the catastrophes is shown in Figure 6.14d.

Due to this morsification the two critical curves do not intersect each other. Also in this perturbed system the minimum annihilates with one of the two saddles, while the other saddle remains unaffected. The scale space saddle remains on the non-catastrophe-involving curve. That is, the creation – annihilation couple and the corresponding saddle branch are not relevant for the scale space saddle and thus the scale space segmentation.

The iso-intensity surface of the scale space saddle due to the creation germ does not contain a dome-shaped surface connected to some other surface, but shows only two parts of the surface touching each other at a void scale space saddle, recall *e.g.* Figure 6.12.

### Higher Order Umbilics

One can verify that of the higher order Umbilic catastrophes,  $D_k^\pm$ ,  $k > 4$ , the  $D_k^+$  describe the various annihilations in two dimensions, the compound of (several) Fold catastrophes. The  $D_k^-$  introduce complicated scatter-like behaviour which also morsify into Fold catastrophes, but now a combination of both annihilations and creations.

### 6.3.3 Morsification Summary

All non-Fold catastrophes morsify to Fold catastrophes. The morsification gives insight in the structure around the catastrophe point regarding the critical curves and the scale space saddles. In one dimensional images, catastrophes and scale space saddles coincide. Therefore, at higher catastrophes the extended Hessian necessarily degenerates. These catastrophes, however, give insight in the case where more than



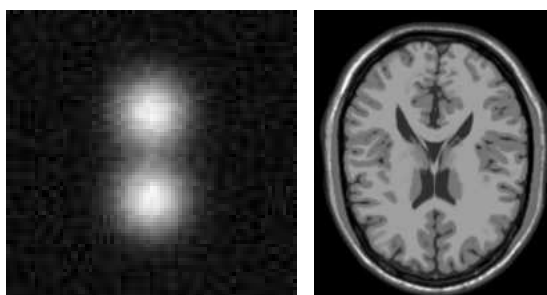


Figure 6.15: 2D test images a: Artificial image built by combining two identical blobs and additive noise. b: 181 x 217 artificial MR image.

two critical points are involved in a complicated annihilation or at several annihilations at almost the same scale space position, without having the ability of distinguish between the Fold pairs.

In higher dimensional images, the cuspid catastrophes (the  $A_k$ ) give the same insight, but also allow the assignment of a scale space saddle, and consequently a scale space segment, to more than one extremum. Furthermore the morsification of the Cusp catastrophe showed that it is generic to encounter scale space saddles that are not connected to some dome shaped iso-intensity manifold: the so-called void scale space saddles.

The morsified  $D_4^-$  catastrophe describes the creation of two critical points and the annihilation of one of them with another critical point. So while tracing the critical branches of a critical curve both an annihilation and a creation event are traversed.

## 6.4 Applications

In this section we give some examples to illustrate the theory presented in the previous sections. To show the effect of a cusp catastrophe in 2D, we firstly take a symmetric artificial image containing two Gaussian blobs and add noise to it. This will make the non-generic symmetric image generic, but in a sense “almost non-generic”. This image is shown in Figure 6.15a. Secondly, the effect is shown on the simulated MR image of Figure 6.15b. Note that also in this case an almost symmetric, thus non-generic, situation occurs. This image is taken from the web site <http://www.bic.mni.mcgill.ca/brainweb>.

### 6.4.1 Artificial Image

Of the noisy image of Figure 6.15a, a scale space image was built containing 41 scales ranging exponentially from  $e^{\frac{10}{8}}$  to  $e^{\frac{20}{8}}$ . The calculated critical paths are presented in Figure 6.16a. Ignoring the paths on the border, caused by the extrema in the noise, the paths in the middle of the image clearly show the pitchfork-like behaviour, typical of a non-generic Cusp catastrophe, recall Figure 6.4. Note that since the symmetric image is perturbed, instead of a cusp catastrophe a fold catastrophe occurs. The scale space saddle on the saddle branch and its intensity define a closed region around the lower maximum, see Figure 6.16b. For details on how the hierarchy and the segmentation is obtained, *cf.* the algorithm presented in [157]. However, if the noise were slightly different, one could evidently have found the region around the upper maximum instead. Knowing that the image should be symmetric and observing

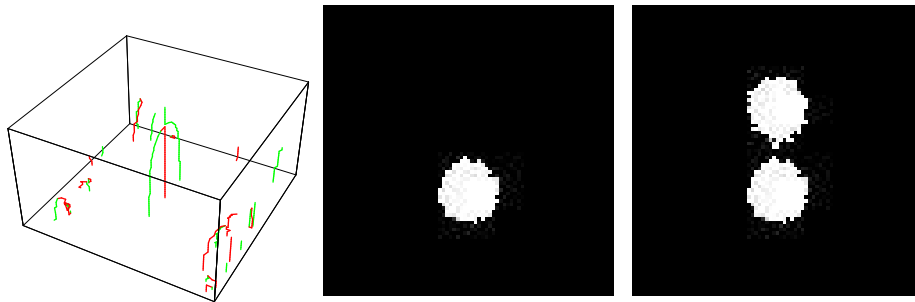


Figure 6.16: Example of a Cusp catastrophe: a: Critical paths in scale space. b: Segment according to a Fold catastrophe. c: Segment according to a Cusp catastrophe.

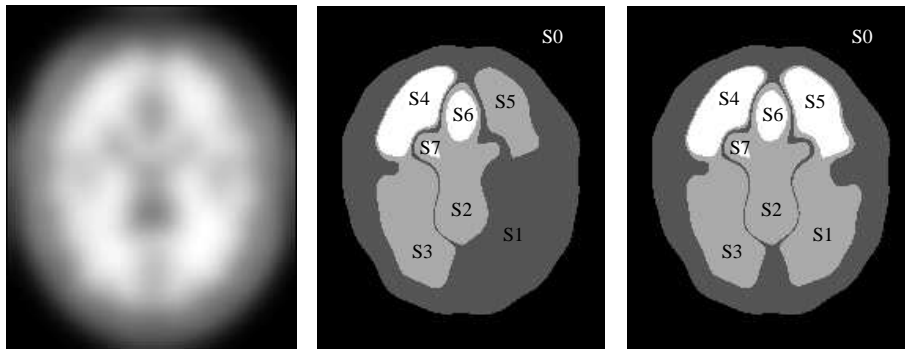


Figure 6.17: a) Image on scale 8.4 b) Segments of the 7 extrema of a, assuming that only generic catastrophes occur, which is the actual case in fact. c) Idem, with the iso-intensity manifold of  $S_1$  chosen equally to  $S_3$ , *i.e.* after changing the label of a generic event into a non-generic one.

that the critical paths indeed are pitchfork-like, it is thus desirable to label the catastrophe as a Cusp catastrophe. Then the scale space saddle (and its intensity) defines the two regions around both involved extrema, see Figure 6.16c. This image one would rather expect given Figure 6.15a.

## 6.4.2 Simulated MR Image

Subsequently, we took the 2D slice from an artificial MR image shown in Figure 6.15b. The scale space image at scale 8.37 with the large structures remaining is shown in Figure 6.17a. Now 7 extrema are found, defining a hierarchy of the regions around these extrema as shown in Figure 6.17b. In this case it is visually desirable to identify a region to segment  $S_1$  with more or less similar size as region  $S_3$ . This is done by assigning a Cusp catastrophe to the annihilation of the extremum of segment  $S_3$ , in which the extremum of segment  $S_1$  is also involved. Then the value of the scale space saddle defining segment  $S_3$  also defines an extra region around the extremum in segment  $S_1$ . This is shown in Figure 6.17c, reflecting the symmetry present in Figure 6.17a. We note that in this example several creation – annihilation events occurred, as described by the morsification of the  $D_4^-$  catastrophe.

## 6.5 Summary and Discussion

In this chapter we investigated the (deep) structure on various catastrophe events in Gaussian scale space. Although it is known that pairs of critical points are annihilated or created (the latter if the dimension of the image is 2 or higher), it is important to describe the local structure of the image around these events. The importance of this local description follows from its significance in building a scale space hierarchy. This algorithm depends on the critical curves, their catastrophe points and the space space saddle points. We therefore embedded the mathematically known catastrophes as presented in section 6.2 in the framework of linear scale space images.

Firstly, annihilations of extrema can occur in the presence of other extrema. In some cases it is not possible to identify the annihilating extremum due to numerical limitations, coarse sampling, or symmetries in the image. Then the event is described by a Cusp catastrophe instead of a Fold catastrophe. This description is sometimes desirable, *e.g.* if prior knowledge is present and one wishes to maintain the symmetry in the image. The scale space hierarchy can easily be adjusted to this extra information. We gave examples in section 6.4 on an artificial image and a simulated MR image. We discussed the  $A_3$  and the  $D_4^+$  for this purpose, but the higher order catastrophes in the sequences  $A_k, k > 3$  and  $D_k^+, k > 4$  can be dealt with in a similar fashion.

Secondly, the morsification of the  $D_4^-$  catastrophe was discussed, showing the successive appearance of a creation – annihilation event on a critical curve. This doesn't influence the hierarchical structure nor the pre-segmentation, but is only important with respect to the movement of the critical curve in scale space. We showed that this appearance heavily depends on the morsification parameters.

The theory described in this chapter extends the knowledge of the deep structure of Gaussian scale space. It embeds higher order catastrophes within the framework of a scale space hierarchy. It explains how these events can in principle be used for segmentation, interpreted and implemented, *e.g.* if prior knowledge is available.



---

## Modelling Non-Generic Events

---

Everything that you could possibly imagine, you will find that nature has been there before you.

---

JOHN BERRILL

**abstract** In order to investigate the deep structure of Gaussian scale space images, one needs to understand the behaviour of spatial critical points under the influence of blurring. We show how the mathematical framework of catastrophe theory can be used to describe and model the behaviour of critical point trajectories when various different types of generic events, *viz.* annihilations and creations of pairs of spatial critical points, (almost) coincide. Although such events are non-generic in mathematical sense, they are not unlikely to be encountered in practice. Furthermore the behaviour leads to the observation that fine-to-coarse tracking of critical points doesn't suffice, since trajectories can form closed loops in scale space. The modelling of the trajectories include these loops. We apply the theory to an artificial image and a simulated MR image and show the occurrence of the described behaviour.

### 7.1 Introduction

The presence of structures of various sizes in an image requires image analysis tools capable of dealing with multiple levels of resolution. Various multi-scale paradigms have been developed [220], giving rise to several new topics of interest. For instance, can specific properties at some scale be related to similar properties at other scales? And if so, what can be said about the way such properties change over scale.

### 7.1.1 Scale Space History

The introduction in the English image literature of the concept of the linear Gaussian scale space is due to Witkin [249] and Koenderink [139], showing that the natural way to represent an image at finite resolution is by convolving it with a Gaussian, thus obtaining a smoothed image at a scale determined by the bandwidth. Weickert et al. [247, 248] showed that the concept of scale space was introduced in Japan about twenty years earlier [119, 208]. Due to the fact that these papers were in Japanese, they remained unnoticed in the Western world. In their papers Weickert et al. give an overview of the several axioms leading to the paradigm of linear scale space. This approach has led to the formulation of various expressions that are independent of the coordinates and that capture certain features in an image at distinct levels of scale [53, 65, 76, 77, 78, 79, 80, 134]. Such invariant features are potential candidates that one would like to trace over scale and the topological changes of which one would like to investigate, e.g. splitting, merging, creation or vanishing. Nowadays, (properties of) scale spaces are widely used in image analysis, segmentation, clustering and statistical analysis [125, 106, 197, 136]. Introductions to scale space can be found in several books [65, 174, 233].

### 7.1.2 Deep Structure

Gaussian scale space has the advantage of linearity. As a consequence, the calculation of any scale level requires only the choice of the appropriate scale. Furthermore, the image intensity at any level follows linearly from any previous level. This enables one to trace the evolution of certain image entities, like spatial critical points, over scale. Koenderink referred to the exploitation of all scales simultaneously as *deep structure* [139]. It pertains to the dynamic change of the image from highly detailed to highly smoothed. It has been proven that in one dimensional images critical points can only vanish pairwise. Several authors have investigated these locations [17, 38, 124, 128, 129, 244, 257, 258, 259]. However, in higher dimensional images also pairwise creations of critical points can occur, as we will see below.

### 7.1.3 Related Work

A well-defined and user-independent method for establishing meaningful links across scales is obtained by linking points that satisfy some topological constraint, for example that maxima are linked to maxima, etc. This yields so-called critical curves. This extrema linking approach has been used in 2-D images by various authors [99, 168, 230]. However, they noticed that sometimes new extrema emerged, disrupting a good linking.

Damon studied this creation of new extrema in scale space in detail [45, 46, 47] and showed that both annihilations and creations of pairs of critical points are generic catastrophes. Furthermore, in [45] he gave a complete list of local perturbations of these generic events. Johansen [127] derived the same results by investigating the behaviour of critical curves in scale space. Griffin [96] investigated critical point events in an affine scale space.

Application of Damon's theoreticay results were reported in e.g. [98, 113, 154, 168, 170]. Kalitzin [130] gave artificial examples to show that the methodology of winding numbers (used for detecting critical and degenerated points) was able to detect more complicated catastrophes. Also the generic catastrophes for specified features in an image have been studied [56, 135, 204, 205, 206, 215, 216, 217].

The research on the generic events shown that in order to be able to use the topological approach of linking critical points, one necessarily needs to take into account both the annihilation and creation

events. This has been done in previous work by Kuijper *et al.* [156, 157, 158, 159, 160, 161, 162].

### 7.1.4 Aim

In images the location of critical points can be found up to the numerical precision of the image. The same holds for the location of catastrophe points in scale space. So although the appearance of catastrophe events can be uniquely separated in annihilations or creations of pairs of critical points, due to *e.g.* numerical limitations, (almost) symmetries in the image, or coarse sampling also indistinguishable compounds of these annihilation and creation events can be found in practise. In this way a couple of nearby generic events may well look like a single, non-generic one.

In this chapter we describe these so-called non-generic catastrophes in scale space. The investigation is based on the description of the evolution of critical points in scale space, called (scale space) critical curves, in the neighbourhood of the catastrophe point(s). The compounds of generic events can be modelled using descriptions of ‘‘Catastrophe Theory’’. Obviously, the models obey the property that assuming infinite precision, in non-generic compounds the generic events can be distinguished.

Furthermore we investigate the appearance of creations as described by these models in more detail and explain why they are, albeit generic, rarely found, probably the reason for current applications to simply ignore them.

The chapter is organised as follows: In section 7.2 relevant theory on Gaussian scale space and catastrophe theory is given, as well as the way to combine them. Non-generic catastrophe models in scale space in generic coordinates and their impact on the critical curves are discussed in section 7.3. We give some applications in section 7.4 and end with a summarising discussion in section 7.5.

## 7.2 Theory

We define a Gaussian scale space in section 7.2.1. The topological change as the scale varies, is called Catastrophe Theory. A summary of relevant theory is presented in section 7.2.2. The embedding of Catastrophe Theory in scale space and the generic events are discussed in section 7.2.3.

### 7.2.1 Gaussian Scale Space

**Definition 23**  $L(\mathbf{x})$  denotes an arbitrary  $n$ -dimensional image. We will refer to this image as the initial image.

**Definition 24**  $L(\mathbf{x}; t)$  denotes the  $(n + 1)$ -dimensional Gaussian scale space image of  $L(\mathbf{x})$ .

The Gaussian scale space image is obtained by convolution of an initial image with a normalised Gaussian kernel  $G(\mathbf{x}; t)$  of zero mean and standard deviation  $\sqrt{2t}$ :

$$L(\mathbf{x}; t) = (G * L)(\mathbf{x}; t) \stackrel{\text{def}}{=} \int \frac{1}{\sqrt{4\pi t}^n} e^{-\frac{|\mathbf{x}-\mathbf{y}|^2}{4t}} L(\mathbf{y}) d\mathbf{y} .$$

Differentiation is now well-defined. By using multi-index notation for  $\alpha = (\alpha_1, \dots, \alpha_{n+1})$ ,  $\alpha_k \in N$ , take  $|\alpha| = \sum_{k=1}^{n+1} \alpha_k$  and  $\partial^\alpha = \partial_1^{\alpha_1} \partial_2^{\alpha_2} \dots \partial_{n+1}^{\alpha_{n+1}}$ , and derivatives of the image up to arbitrary order  $|\alpha|$  at any scale  $t$  are given by

$$\partial^\alpha L = \partial^\alpha (G * L) = (\partial^\alpha G) * L.$$

That is, an arbitrary derivative of the image is obtained by the convolution of the initial image with the corresponding derivative of a Gaussian. Consequently,  $L(\mathbf{x}; t)$  satisfies the diffusion equation:

$$\partial_t L(\mathbf{x}; t) = \Delta L(\mathbf{x}; t). \quad (7.1)$$

Here  $\Delta L(\mathbf{x}; t)$  denotes the Laplacean.

**Definition 25** *Spatial critical points, i.e. saddles and extrema (maxima or minima), at a certain scale  $t_0$  are defined as the points at fixed scale  $t_0$  where the spatial gradient vanishes:  $\nabla L(\mathbf{x}; t_0) = 0$ . We will refer to these points as spatial critical points.*

The type of a spatial critical point is given by the eigenvalues of the Hessian  $H$ , the matrix with the second order spatial derivatives, evaluated at its location.

**Definition 26** *The Hessian matrix at a certain scale  $t_0$  is defined by  $H \stackrel{\text{def}}{=} \nabla \nabla^T L(\mathbf{x}; t_0)$ , where each element of  $H$  is given by*

$$H_{i,j} = \frac{\partial^2}{\partial x_i \partial x_j} L(\mathbf{x}; t).$$

The trace of the Hessian equals the Laplacean. For non-degenerate maxima (minima) all eigenvalues of the Hessian are negative (positive). At a spatial saddle point  $H$  has both negative and positive eigenvalues.

Since  $L(\mathbf{x}; t)$  is a smooth function in  $(\mathbf{x}; t)$ -space, spatial critical points are part of a one dimensional manifold in scale space by virtue of the implicit function theorem.

**Definition 27** *A critical curve is a one-dimensional manifold in scale space on which  $\nabla L(\mathbf{x}; t) = 0$ .*

Consequently, the intersection of all critical curves in scale space with a plane of certain fixed scale  $t_0$  yields the spatial critical points of the image at that scale.

## 7.2.2 Catastrophe Theory

The spatial critical points as defined above can be divided into two types, depending on the eigenvalues of the Hessian. If they are all non-zero, the spatial critical points are called *Morse critical points*. It is stated by the *Morse Lemma* that the quadratic part of the Taylor expansion at these points determine the qualitative properties. It can be reduced to the *Morse canonical form* if the coordinates are chosen properly.

At the second type, at least one of the eigenvalues of the Hessian equals zero. These points are called *non-Morse critical points* or *catastrophe points*. At these points obviously the Hessian degenerates. Since this situation requires  $n + 1$  equations for the  $n$  variables, one generically doesn't encounter these type of points. The situation is different if extra parameters are present. Then (some types of) catastrophes can occur. The essence of catastrophe points lies in the fact that at these points a discontinuous effect occurs due to a continuous change of some parameter(s).

The term catastrophe is due to Thom [238, 239]. A thorough mathematical treatment can be found in the work of Arnol'd [5, 6, 7, 8, 9, 10]. More pragmatic introductions and applications, "from the physical point of view", are widely published, e.g. [29, 81, 91, 184, 212, 251, 255].



The catastrophe points essentially need a Taylor expansion of order 3 or higher to describe the qualitative properties. Regardless the dimension of the variables, one can split up the function with  $k$  zero eigenvalues, into an  $(n - k)$ -dimensional Morse and a  $k$ -dimensional non-Morse part, as stated by the *Thom Splitting Lemma*. The Hessian then contains two distinct submatrices: an  $(n - k) \times (n - k)$  sub-matrix representing the Morse function, and a  $k \times k$  sub-matrix representing the non-Morse function. The  $(n - k)$ -dimensional Morse part of the expansion – the Morse canonical form – obviously does not change qualitatively under small perturbations. Further investigation of this part is therefore not necessary and it is enough to study the  $k$ -dimensional non-Morse part. It also can be put into a canonical form, called the *catastrophe germ*.

This catastrophe germ changes qualitatively under small perturbations. Let  $l$  be the number of different perturbation parameters that achieve the distinct perturbations. Then applying a perturbation germ containing  $k$  variables and  $l$  parameters will cause the non-Morse critical point to split. If all parameters are non-zero, it will result in solely Morse critical points, otherwise it will split up into a non-Morse critical point, described by a polynomial of a degree lower than before the split, and Morse critical points. This splitting-event is called *morsification*. Consequently, the non-Morse part contains the catastrophe germ and a perturbation germ that controls the morsifications.

Then the general form of a Taylor expansion  $f$  at a non-Morse critical point of an  $n$  dimensional function can be written as a combination of the non-Morse part, containing the catastrophe germ and a perturbation germ, and the quadratic Morse part, a result known as *Thom's Theorem*):

$$f(\mathbf{x}; \lambda) = CG(x_1, \dots, x_k) + PT(x_1, \dots, x_k; \lambda_1, \dots, \lambda_l) + \sum_{i=k+1}^n \epsilon_i x_i^2, \quad (7.2)$$

where  $CG(x_1, \dots, x_k)$  denotes the  $k$ -dimensional catastrophe germ and  $PT(x_1, \dots, x_k; \lambda_1, \dots, \lambda_l)$  the  $k$ -dimensional perturbation germ with an  $l$ -dimensional space of parameters. In the quadratic Morse part  $\epsilon_i = \pm 1$ .

For situations with at most two vanishing eigenvalues of the Hessian it suffices to investigate the known catastrophes in  $\mathbb{R}^2$ , the so-called simple real singularities in 2D, see Arnol'd [5, 6, 7, 8, 9, 10]. They have catastrophe germs given by the two infinite series

- $A_k^\pm \stackrel{\text{def}}{=} \pm x^{k+1}, k \geq 1$ . The germs  $A_k^+$  and  $A_k^-$  are equivalent for  $k = 1$  and  $k$  even,
- $D_k^\pm \stackrel{\text{def}}{=} x^2 y \pm y^{k-1}, k \geq 4$ , which we will rewrite to  $x^{k-1} \pm xy^2$  for notational convenience,

and furthermore three exceptional singularities occur:

- $E_6 \stackrel{\text{def}}{=} x^3 \pm y^4$ ,
- $E_7 \stackrel{\text{def}}{=} x^3 + xy^3$ , and
- $E_8 \stackrel{\text{def}}{=} x^3 + y^5$ .

### 7.2.3 Catastrophes and Scale Space

In an  $n$ -dimensional image, the number of equations defining the catastrophe point equals  $n + 1$ . Consequently, the set of equations is over determined and catastrophes are generically not to be encountered.

The  $(n + 1)$ -dimensional scale space contains an extra “parameter”, scale, so generically single catastrophes occur as isolated points. But it is not trivial to apply the list of catastrophes directly to scale space by assuming that scale is just one of the perturbation parameters. As Damon [45, 47] points out:

“There are significant problems in trying to directly apply Morse theory to solutions of the heat equation. First, it is not clear that generic solutions to the heat equation must be generic in the Morse sense. Second, standard models for Morse critical points and their annihilation and creation do not satisfy the heat equation. How must these models be modified? Third, there is the question of what constitutes generic behaviour. This depends on what notion of local equivalence one uses between solutions to the heat equation.”

**Example 4** *The catastrophe and perturbation germ of the  $A_2$  catastrophe are given by  $x^3 + \lambda x$ . It describes the change from a situation with two critical points for  $\lambda < 0$  to a situation without critical points for  $\lambda > 0$  in both directions: the extrema are annihilated for increasing  $\lambda$ , and created for decreasing  $\lambda$ .*

*Scale space, however, has an extra constraint: the germ has to satisfy the diffusion equation. Thus the catastrophe germ  $x^3$  implies an extra term  $6xt$ . On the other hand, the perturbation term is given by  $\lambda x$ , so by choosing  $\lambda = 6t$ , scale plays the role of the perturbing parameter. This “answers” the second problem. At the same time it may signal that the only remaining possibility for this adjusted  $A_2$ -catastrophe is an annihilation, since  $t$  is a directional parameter and can only increase. Since only Fold catastrophes depend on one control parameter, one thus comes to the wrong conclusion that only annihilations are generic in scale space, a commonly spread misunderstanding. This is a direct consequence of ignoring the third problem Damon stated. In  $n$ -dimensional images,  $n > 1$ , also the opposite – i.e. an  $A_2$  catastrophe describing the creation of a pair of critical points – is possible as we will see.*

Damon showed that the only generic morsifications in scale space are  $A_2$  catastrophes describing annihilations and creations of pairs of critical points [45, 46, 47]. Many authors have used and investigated these results [72, 126, 128, 129, 130, 131, 154, 157, 161, 162, 170, 174].

**Definition 28** *The scale space catastrophe germs are defined by*

$$\begin{aligned} f^A(\mathbf{x}; t) &\stackrel{\text{def}}{=} x_1^3 + 6x_1t + Q(\mathbf{x}; t), \\ f^C(\mathbf{x}; t) &\stackrel{\text{def}}{=} x_1^3 - 6x_1t - 6x_1x_2^2 + Q(\mathbf{x}; t). \end{aligned}$$

*The quadratic term  $Q(\mathbf{x}; t)$  is defined*

$$Q(\mathbf{x}; t) \stackrel{\text{def}}{=} \sum_{i=2}^n \epsilon_i (x_i^2 + 2t),$$

*where  $\sum_{i=2}^n \epsilon_i \neq 0$  and  $\epsilon_i \neq 0 \forall i$ .*

The scale space catastrophe germs  $f^A$  and  $f^C$ , and the quadratic term  $Q$  satisfy the diffusion equation. The germs describe the two qualitatively different  $A_2$  catastrophes at the origin,  $f^A$  an annihilation and  $f^C$  a creation. One can verify that annihilations occur in any dimension using Definition 28. In contrast, creations require at least 2 dimensions: the  $x_2$  involved is essential.

### The Annihilation Germ

The critical curve and the catastrophe point for the annihilation germ  $f^A$  follow from

$$\begin{cases} L_{x_1} &= 3x_1^2 + 6t \\ L_{x_i} &= 2\epsilon_i x_i, \quad i \geq 2 \\ \det H &= 3 \cdot 2^n \prod_{i=2}^n \epsilon_i x_1 \end{cases}$$

So the critical curve is parametrised by  $(\pm\sqrt{-2t}, 0, \dots, 0; t)$ ,  $t \leq 0$ . Two critical points with opposite sign approach the origin as  $t$  increases to zero and meet transversally to the Hessian zero-crossing in a catastrophe.

### The Creation Germ

For the creation germ  $f^C$  the critical curve and the catastrophe point follow from

$$\begin{cases} L_{x_1} &= 3x_1^2 - 6x_2^2 - 6t \\ L_{x_2} &= 2x_2(\epsilon_2 - 6x_1) \\ L_{x_i} &= 2\epsilon_i x_i, \quad i \geq 3 \\ \det H &= 3(x_1(\epsilon_2 - 6x_1) - 12x_2^2) 2^n \prod_{i=3}^n \epsilon_i \end{cases}$$

Since we look at a catastrophe in the neighbourhood of the origin, we must take  $x_2 = 0$  and disregard  $\epsilon_2 = 6x_1$ . Then the critical curve with a catastrophe at the origin is parametrised by  $(\pm\sqrt{2t}, 0, \dots, 0; t)$ ,  $t \geq 0$ , so two critical points with opposite sign leave the origin as  $t$  increases from zero, again transversally to the Hessian zero-crossing.

Two related remarks must be made

1. This germ only gives a *local* description of the catastrophe. If  $t$  is taken too large, the (non-generic) degeneration of the Hessian at  $x_1 = \frac{1}{6}\epsilon_2$  has to be taken into account.
2. This catastrophe – at the origin – is an  $A_2$  catastrophe, since it describes the creation of two critical points due to exactly one scale-“parameter”. One may notice, however, that the description of the creation germ is alike the description of the  $D_4^-$  catastrophe, which is given by  $x^3 - xy^2$ .

We will come back to these items in Section 7.3. The crux lies in the behaviour of critical curves due to the morsification of non-generic events.

### Non-Generic Events

Although two Fold events are the only generic events, one may sometimes not be able to distinguish compounds of generic events, *e.g.* due to numerical limitations, coarse sampling, or (almost) symmetries in the image.

**Example 5** *If at some scale three nearby critical points, e.g. two extrema and a saddle are present, but at the subsequent scale only one extremum, obviously one pair of critical points is annihilated. However, Figure 7.1 illustrates the case that one is not able to identify the annihilating extremum at the former scale. On the left the critical paths are shown, together with a grey area representing the uncertainty in determining the catastrophe location. On the right the non-generic model of this event is displayed.*

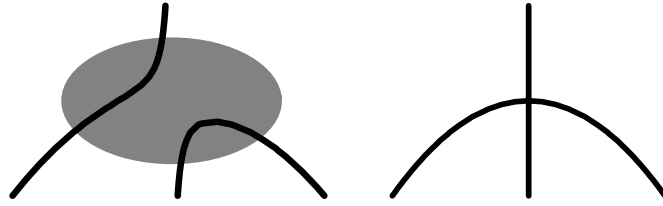


Figure 7.1: Left: Annihilation of two critical points in the neighbourhood of a third critical point. The grey area represents the uncertainty in determining the catastrophe. Right: Non-generic representation and model of this event.

This gives rise to the demand of using descriptions that model the behaviour of critical curves around non-generic catastrophes, as well as their perturbations. Obviously, the latter must lead to critical curves containing only the generic events.

### 7.3 Scale Space Catastrophe Models

In this section we describe how the following catastrophes (with nicknames and perturbation germs) can be used to model events in  $(2 + 1)$ -dimensional scale space. The catastrophes describe in canonical coordinates how critical curves pass the origin yielding compounds of annihilations and / or creations of pairs of critical points.

- $A_2$  Fold catastrophe:  $x^3 + \lambda_1 x \pm y^2$ .
- $A_3$  Cusp catastrophe:  $\pm x^4 + \lambda_1 x + \lambda_2 x^2 \pm y^2$ .
- $D_4^+$  Hyperbolic Umbilic catastrophe,  $x^3 + xy^2 + \lambda_1 x + \lambda_2 y + \lambda_3 y^2$ .
- $D_4^-$  Elliptic Umbilic catastrophe:  $x^3 - xy^2 + \lambda_1 x + \lambda_2 y + \lambda_3 y^2$ .
- $D_5^\pm$  Parabolic Umbilic catastrophe:  $x^4 \pm xy^2 + \lambda_1 x + \lambda_2 y + \lambda_3 y^2 + \lambda_4 x^2$ .
- $D_6^+$  Second Hyperbolic Umbilic catastrophe:  $x^5 + xy^2 + \lambda_1 x + \lambda_2 y + \lambda_3 x^2 + \lambda_4 y^2 + \lambda_5 x^3$ .
- $D_6^-$  Second Elliptic Umbilic catastrophe:  $x^5 - xy^2 + \lambda_1 x + \lambda_2 y + \lambda_3 x^2 + \lambda_4 y^2 + \lambda_5 x^3$ .

The  $\pm$  signs at the  $A_3$  and  $D_5$  denote “dual” possibilities with similar geometry.

The germs in this list will be adjusted such that they satisfy the heat equation. Furthermore, by choosing the perturbation terms non-zero and adjusting them in the same way, descriptions of critical curves in scale space will be obtained. These critical curves only contain the generic Fold annihilation(s) and/or creation(s).

Again we emphasise that this list not a complete list as can be found in [45], containing all the relevant mathematical details. However, the germs mentioned above are related to the perturbations of the generic annihilation and creation given in [45]. We will see that although most of these catastrophes are non-generic, they may still be relevant for modelling compounds of generic events that one is not capable of, or willing to, segregate as such. Recall, for example, Figure 7.1.

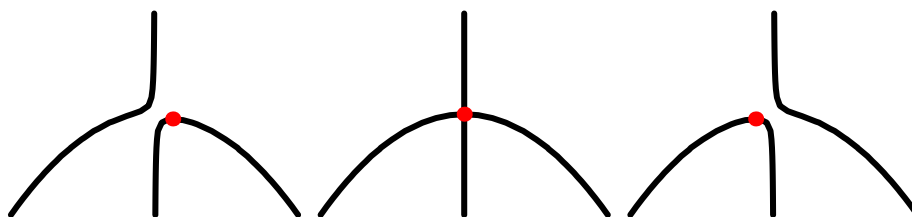


Figure 7.2: Critical paths of the Cusp catastrophe. The catastrophe is located at the dot. a)  $\lambda_1 = 1$ . b)  $\lambda_1 = 0$ . c)  $\lambda_1 = -1$ . Note that if the perturbation is very small, these three distinct cases may very well be confused.

### 7.3.1 $A_2$ Fold Catastrophe

The Fold catastrophe in scale space is given by

$$L(x, y; t) = x^3 + 6xt + \delta(y^2 + 2t),$$

where  $\delta = \pm 1$ . Critical curves and the catastrophe point follow from

$$\begin{cases} L_x = 3x^2 + 6t \\ L_y = 2\delta y \\ \det H = 12\delta x. \end{cases}$$

One can verify that at the origin a saddle and an extremum (a minimum if  $\delta = 1$ , a maximum if  $\delta = -1$ ) moving in the  $y = 0$  plane meet and annihilate while increasing the scale parameter  $t$ .

### 7.3.2 $A_3$ Cusp Catastrophe

The Cusp catastrophe germ is given by  $x^4$ . Its scale space addition is  $12x^2t + 12t^2$ . The perturbation term contains two terms:  $\lambda_1x + \lambda_2x^2$ . Obviously, scale can take the role of  $\lambda_2$ . Taking the dual Cusp gives the same geometry by changing the sign of  $\lambda_1$ , or by setting  $x = -x$ . The scale space Cusp catastrophe germ with perturbation is thus defined by

$$L(x, y; t) = x^4 + 12x^2t + 12t^2 + \lambda_1x + \delta(y^2 + 2t),$$

with  $\delta = \pm 1$ . Again, the critical curves and the catastrophe point follow from

$$\begin{cases} L_x = 4x^3 + 24xt + \lambda_1 \\ L_y = 2\delta y \\ \det H = 24\delta(x^2 + 2t). \end{cases}$$

Morsification by the perturbation  $\lambda_1 \neq 0$  yields one Fold catastrophe and one regular critical curve, see Figure 7.2a,c. The differences in behaviour depending on the sign of  $\delta$  is studied in detail in [156]. It suffices here to note that if  $\lambda_1 = 0$ , at the origin three critical points transform to one critical point while increasing scale, see Figure 7.2b.

One can verify that the  $A_k, k > 3$  catastrophes describes the (non-generic) simultaneous annihilations of critical points in one dimension under the influence of blurring, albeit in more complicated appearances.

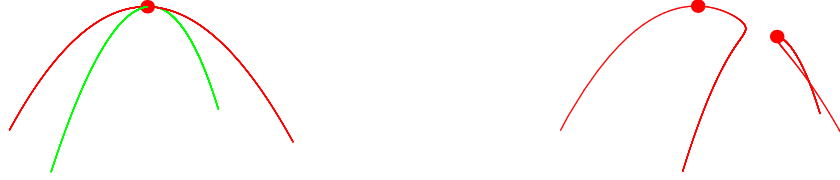


Figure 7.3: Critical paths of the  $D_4^+$ -catastrophe in  $(x, y; t)$ -space. a) Unperturbed. b) Perturbed. Again, if the perturbation is small we may not be able to tell which configuration is the actual one.

### 7.3.3 $D_4^\pm$ Umbilic Catastrophes

The  $D_4^\pm$  Umbilic catastrophe germs are given by  $x^3 + \delta xy^2$ , where  $\delta = \pm 1$ . The scale space addition is  $(6 + 2\delta)xt$ , yielding  $x^3 + xy^2 + 8xt$  for the Hyperbolic Umbilic catastrophe, and  $x^3 - xy^2 + 4xt$  for the Elliptic Umbilic catastrophe. The perturbation contains three terms:  $\lambda_1 x + \lambda_2 y + \lambda_3 y^2$ . Obviously, scale can take the role of  $\lambda_1$ .

#### $D_4^+$ Hyperbolic Umbilic Catastrophe

The scale space  $D_4^+$  Hyperbolic Umbilic catastrophe germ with perturbation is thus defined by

$$L(x, y; t) = x^3 + xy^2 + 8xt + \lambda_3(y^2 + 2t) + \lambda_2 y .$$

The critical curves and catastrophe points follow from

$$\begin{cases} L_x &= 3x^2 + 8t + y^2 \\ L_y &= 2xy + 2\lambda_3 y + \lambda_2 \\ \det H &= 12x(x + \lambda_3) - 4y^2 . \end{cases}$$

In the unperturbed situation four critical points exist for each  $t < 0$  on the  $x$ - and  $y$ -axes. At  $t = 0$  the four critical curves annihilate simultaneously at the origin, see Figure 7.3a. Taking perturbation into account, the curves are separated into two critical curves each containing a Fold catastrophe, see Figure 7.3b.

#### $D_4^-$ Elliptic Umbilic Catastrophes

The scale space elliptic Umbilic catastrophe germ with perturbation is given by

$$L(x, y; t) = x^3 - xy^2 + 4xt + \lambda_3(y^2 + 2t) + \lambda_2 y . \quad (7.3)$$

Again, the critical curves and the catastrophe points follow from

$$\begin{cases} L_x &= 6x^2 + 4t - y^2 \\ L_y &= -2xy + 2\lambda_3 y + \lambda_2 \\ \det H &= 12x(2\lambda_3 - 2x) - 4y^2 . \end{cases}$$

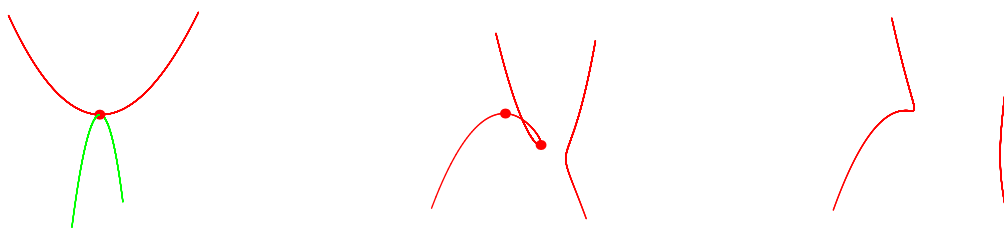


Figure 7.4: Critical paths of the  $D_4^-$ -catastrophe in  $(x, y; t)$ -space. a) Unperturbed. b) Small perturbation. c) Large perturbation.

The unperturbed equation gives two critical points for all  $t \neq 0$ . At the origin a so-called scatter event occurs: the critical curve changes from  $y$ -axis to  $x$ -axis with increasing  $t$ , see Figure 7.4. Just as in the hyperbolic case, in fact two Fold catastrophes take place; in this case both an annihilation and a creation. The morsification is shown in Figure 7.4b. The critical curve on the right does not contain catastrophe points. The critical curve on the left, however, contains two Fold catastrophe points: a creation and an annihilation. Both are studied in detail in [156]. A brief sketch was given in section 7.2, where we could set  $\lambda_2 = 0$ , since only the creation at the origin was investigated.

So while increasing scale one will find two critical points, suddenly two extra critical points appear, of which one annihilates with one of the already existing ones. Finally, one ends up with again two critical points. Clearly, if the samples in scale are taken too large, one could completely miss the subsequent catastrophes, see *e.g.* Figure 7.4c. The properties of the creations will be discussed in the next section.

### Creations

As we showed, a creation event occurs in case of a morsified elliptic Umbilic catastrophe. In most applications, however, creations are rarely found, giving rise to the (false) opinion that creations are caused by numerical errors and should be disregarded. The reason for their rare appearance lies in the specific requirements for the parameters in the (morsified) Umbilic catastrophe germ. Its general formulation is given by

$$L(x, y; t) = \frac{1}{6}L_{xxx}x^3 + \frac{1}{2}L_{xyy}xy^2 + L_{xt}xt + \frac{1}{2}L_{yy}(y^2 + 2t) + L_yy \quad (7.4)$$

In general, the spatial coefficients do *not* equal the derivatives evaluated in the coordinate system of the image. They follow from the alignment of the catastrophe in the plane defined by  $y = 0$  and can have arbitrary value. Furthermore, the diffusion equation implies  $L_{xt} \stackrel{\text{def}}{=} L_{xxx} + L_{xyy}$ . Then the scale space evolution of the critical curves follow from

$$\begin{cases} \partial_x L &= \frac{1}{2}L_{xxx}x^2 + L_{xt}t + \frac{1}{2}L_{xyy}y^2 \\ \partial_y L &= L_{xyy}xy + L_{yy}y + L_y \\ \det H &= L_{xxx}x(L_{xyy}x + L_{yy}) - L_{xyy}^2y^2. \end{cases}$$

Firstly we consider the case  $L_y = 0$ . Then Eq. (7.4) describes a Fold catastrophe (either annihilation or creation) at the origin, where the critical curve is positioned in the  $(x, t)$ -plane. A creation necessarily requires the constraint  $L_{xxx}L_{xt} < 0$  at the catastrophe point. This constraint is sufficient.

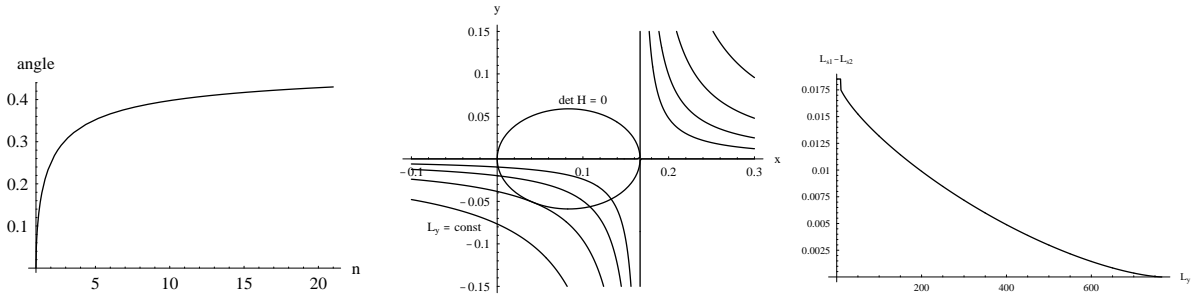


Figure 7.5: a) The fraction of the space of the third order derivatives in which creations can occur as a function of the dimension according Theorem 6. b) Intersections of the curves  $\det H = 0$  and  $\partial_y L = 0$  with different values for  $L_y$ . For the value given by Theorem 7 the curves touch. c) Difference in intensity between the creation and the annihilation event for  $L_y$  increasing from 0 to its critical value.

**Theorem 6** *At a catastrophe point in two spatial dimensions, if the third order derivatives of the general local form as given by Eq. (7.4) with  $L_y = 0$ , are uncorrelated, the number of creations has an a priori likelihood of  $1/4$  relative to the total number of catastrophes. In  $n$  dimensions it is  $\frac{1}{\pi} \arccos \frac{1}{\sqrt{n}}$ .*

**Proof of theorem 6** *The requirement  $L_{xxx}L_{xt} < 0$  can be rewritten to  $L_{xxx}(L_{xxx} + L_{xyy}) < 0$ . In the  $(L_{xxx}, L_{xyy})$ -space this constraint is satisfied by all point sets in the area spanned by the lines through the origin with direction vectors  $(1, 0)$  and  $(1, -1)$ , which is a quarter of the plane. For  $n-D$  this extends to the area  $L_{xxx}(L_{xxx} + L_{xy_1y_1} + \dots + L_{xy_{n-1}y_{n-1}}) < 0$  in  $(L_{xxx}, L_{xy_iy_i})$ -space, with  $\dim(\mathbf{y}) = n - 1$ . This representing two intersecting planes with normal vectors  $(1, 0, \dots, 0)$  and  $(1, -1, \dots, -1)$ . They make an angle of  $\phi$  radians, given by*

$$\cos \phi = \frac{(1, 0, \dots, 0) \cdot (1, -1, \dots, -1)}{|(1, 0, \dots, 0)| \cdot |(1, -1, \dots, -1)|} = \frac{1}{\sqrt{n}}$$

*Then the fraction of the space follows by taking twice this angle and dividing by the complete angle of  $2\pi$ , i.e.  $\frac{1}{\pi} \arccos \frac{1}{\sqrt{n}}$ .  $\square$*

Note that if  $n = 1$ , the fraction of the space where creations can occur is zero, for  $n = 2$  it is a quarter. The also interesting case  $n = 3$  yields a fraction that is slightly more than a quarter, whereas for  $n \rightarrow \infty$  the fraction converges to a half, see Figure 7.5a. That is: the higher the dimensions, the easier critical points can be created.

The reason that in practice in two dimensional images the number of creations observed is (much) smaller than a quarter, is caused by the role of the perturbation parameters. It is possible to give a tight bound to the perturbation of Equation (7.4) in terms of  $L_y$ :

**Theorem 7** *A creation and subsequent annihilation event occur in Equation (7.4) if and only if*

$$|L_y| \leq \frac{3}{16} L_{yy}^2 \sqrt{\frac{-3L_{xxx}}{L_{xyy}^3}} \quad (7.5)$$



**Proof of theorem 7** The catastrophes satisfy  $\partial_x L = \partial_y L = \det H = 0$ . Since the solution of the system

$$\begin{aligned} \partial_y L &= L_y + y(L_{yy} + L_{xyy}x) = 0 \\ \det H &= L_{xxx}x(L_{yy} + L_{xyy}x) - L_{xyy}^2 y^2 = 0 \end{aligned} \quad (7.6)$$

only contains spatial coordinates, their intersections define the spatial coordinates of the catastrophes. The catastrophe points form the local extrema of the critical curve in  $(x, y; t)$ -space, i.e. at these points the tangent vector has no scale component. If the curves given by Eq. (7.6) touch, there is only a point of inflection in the critical curve, i.e. the critical curve in  $(x, y; t)$ -space has a (Fold) catastrophe point. At this point of inflection, the spatial tangent vectors of the curves defined by Eq. (7.6) are equal.

Solving the system Eq. (7.6) with respect to  $y$  results in

$$y = -\frac{L_y}{L_{yy} + L_{xyy}x} = \pm \frac{1}{L_{xyy}} \sqrt{L_{xxx}x(L_{yy} + L_{xyy}x)}.$$

The equality of the tangent vectors at the point of inflection  $x_i, y_i$  yields

$$\frac{\partial}{\partial x} \left( -\frac{L_y}{L_{yy} + L_{xyy}x} \right) \Big|_{x_i, y_i} = \frac{\partial}{\partial x} \left( \pm \frac{1}{L_{xyy}} \sqrt{L_{xxx}x(L_{yy} + L_{xyy}x)} \right) \Big|_{x_i, y_i}$$

Solving both equalities results in

$$(x_i, y_i, L_y) = \left( -\frac{L_{yy}}{4L_{xyy}}, \pm \sqrt{\frac{-3L_{xxx}L_{yy}^2}{16L_{xyy}^3}}, \mp \frac{3L_{yy}^2}{16L_{xyy}} \sqrt{\frac{-3L_{xxx}}{L_{xyy}}} \right),$$

which gives the boundary values for  $L_y$ .  $\square$

Note that Eq. (7.5) has only real solutions if  $L_{xxx}L_{xyy} < 0$ , i.e. at the  $D_4^-$  (morsified) catastrophe. As a consequence of Theorem 7, creations only occur if the perturbation is small enough. Again, this perturbation occurs in the coordinate system, obtained by the alignment of the catastrophe in the plane defined by  $y = 0$ .

**Example 6** Taking  $L_{xxx} = 6, L_{xyy} = -12, L_{yy} = 2$  yielding  $L = x^3 - 6xy^2 - 6xt + y^2 + 2t + L_y$ , we obtain the “generic creation example” as given in section 7.2 with perturbation. Then Theorem 7 gives  $|L_y| \leq \frac{1}{32}\sqrt{6}$  as a – relatively small compared to the other derivative values– bound for the occurrence of a creation – annihilation couple. In Figure 7.5b the ellipse  $\det H = 0$  is plotted, together with the curves  $\partial_y L = 0$  for  $L_y = 0$  (resulting in two straight lines at  $y = 0$  and  $x = \frac{1}{6}$ , intersecting at  $(x, y) = (\frac{1}{6}, 0)$ ), and  $L_y = 2^{-i}\sqrt{6}, i = 4, \dots, 7$ . For  $i > 5$ , the perturbation is small enough and the intersection of  $\partial_y L = 0$  and  $\det H = 0$  contains two points. Thus a creation-annihilation is observed. If  $i = 5$ ,  $L_y$  has its critical value and the curves touch. For larger values the curves do not intersect each other.

Obviously the perturbation  $L_y$  can be larger if  $L_{yy}$  increases. If so, the structure becomes more elongated. It is known by various examples of creations given in literature that elongated structures play an important role. In fact, the quintessential property is scale anisotropy.

Another reason that creations are rarely found is that their lifetime is rather limited: with increasing  $t$  the created critical points annihilate. If the scale steps are taken too large, one simply misses the creation – annihilation couple. This may be regarded as a dual expression for the previous explanation. In the chosen coordinate system this can be calculated explicitly.

**Theorem 8** *The maximum lifetime of a creation given by Equation (7.4) is*

$$t_{lifetime} = \frac{-L_{xxx}L_{yy}^2}{2L_{xyy}^2(L_{xxx} + L_{xyy})}.$$

*The difference in intensity of the critical point that is created and subsequently annihilated is*

$$\frac{L_{xxx}(2L_{xxx} - L_{xyy})L_{yy}^3}{6L_{xyy}^3(L_{xxx} + L_{xyy})}.$$

**Proof of theorem 8** *Observe that the lifetime is bounded by the two intersections of  $\partial_y L = 0$  and  $\det H = 0$ , see Figure 7.5b. As  $|L_y|$  increases from zero, the two points move towards each other over the arch  $\det H = 0$  until they reach the value given by theorem 7 with lifetime equal to zero. The largest arch length is obtained for  $L_y = 0$ . Then the spatial coordinates are found by*

$$\partial_y L(x, y; t) = y(L_{xyy}x + L_{yy}) = 0$$

and

$$\det H = L_{xxx}x(L_{xyy}x + L_{yy}) - L_{xyy}^2y^2 = 0,$$

i.e.  $(x, y) = (0, 0)$  and  $(x, y) = (-\frac{L_{yy}}{L_{xyy}}, 0)$  The location in scale space is given by

$$\partial_x L(x, y; t) = \frac{1}{2}L_{xxx}x^2 - \frac{1}{2}L_{xyy}y^2 + L_{xt}t = 0.$$

Consequently, the first catastrophe takes place at the origin - since also  $t = 0$  - with zero intensity. The second one is located at

$$(x, y; t) = \left(-\frac{L_{yy}}{L_{xyy}}, 0; \frac{-L_{xxx}L_{yy}^2}{2L_{xyy}^2(L_{xxx} + L_{xyy})}\right)$$

with intensity

$$L_{cat} = \frac{L_{xxx}(2L_{xxx} - L_{xyy})L_{yy}^3}{6L_{xyy}^3(L_{xxx} + L_{xyy})}.$$

Then the latter is also the maximum difference in intensity.  $\square$

**Example 7** *To show the effect of the movement along the arch  $\det H = 0$ , see Figure 7.5c. Without loss of generality we took again  $L_{xxx} = 6, L_{xyy} = -12, L_{yy} = 2$ . Firstly, the two solutions to  $\nabla L = 0 \wedge \det H = 0$  were calculated as function of  $L_y$ . Secondly, the difference of the intensity of the solutions was calculated for 766 subsequent values of  $L_y, L_y \in [0, \dots, \frac{1}{32}\sqrt{6}]$ . It is clearly visible that the intensity decreases monotonously with an increase of  $L_y$ . For this example we find that the lifetime is  $\frac{1}{72}$ , the difference in intensity  $\frac{1}{18}$ .*

From the proof of Theorem 8 it is again apparent that  $L_{yy}$  plays an important role in enabling a (long)lasting creation. To observe this in more detail, note that the curve

$$\det H = 0 \Leftrightarrow L_{xxx}x(L_{xyy}x + L_{yy}) = L_{xyy}^2y^2$$

is an ellipse (see also Figure 7.5b). Replacing  $x$  by  $x - \frac{L_{yy}}{2L_{xyy}}$ , it is centred at the origin:

$$L_{xxx}\left(x - \frac{L_{yy}}{2L_{xyy}}\right)L_{xyy}\left(x + \frac{L_{yy}}{2L_{xyy}}\right) = L_{xyy}^2 y^2 .$$

And consequently

$$L_{xxx}L_{xyy}\left(x^2 - \frac{L_{yy}^2}{4L_{xyy}^2}\right) = L_{xyy}^2 y^2 .$$

Setting  $L_{xyy} = \frac{1}{b}$  and  $L_{xxx}L_{xyy} = -\frac{1}{a^2}$ , we find

$$\det H = 0 \Leftrightarrow x^2 + \frac{a^2}{b^2}y^2 = L_{yy}^2 \frac{b^2}{4} .$$

Assuming that we have a creation,  $a^2 > 0$ . The ellipse is enlarged with an increase of  $L_{yy}^2$ . Obviously, at the annihilations of the Hyperbolic Umbilic catastrophe  $a^2 < 0$ , so  $\det H = 0$  then describes a hyperbola.

### 7.3.4 $D_5^\pm$ Parabolic Umbilic Catastrophes

In the previous section we saw that the geometry significantly changed by taking either the term  $-xy^2$ , or the term  $+xy^2$ . Let us therefore, ignoring the perturbation terms  $\lambda_1$ ,  $\lambda_2$ , and  $\lambda_3$ , define the scale space Parabolic Umbilic catastrophe germ by

$$L(x, y; t) = \frac{1}{4!}x^4 + \frac{1}{2!}x^2t + \frac{1}{2!}t^2 + \delta\left(\frac{1}{2}xy^2 + xt\right) \quad (7.7)$$

where  $\delta = \pm 1$  and  $t$  is taking the role of  $\lambda_4$ . Its critical curves and catastrophes follow from

$$\begin{cases} L_x &= \frac{1}{6}x^3 + xt + \delta\left(t + \frac{1}{2}y^2\right) \\ L_y &= \delta xy \\ \det H &= \delta x\left(\frac{1}{2}x^2 + t\right) - y^2 \end{cases}$$

So two catastrophe points are located at the origin and a third at  $(x, y; t) = \left(-\frac{3}{2}\delta, 0; -\frac{9}{8}\delta^2\right)$ . The latter is a simple annihilation (a fold catastrophe), the former is a cusp catastrophe (three critical point change into one) for both values of  $\delta$ , see Figure 7.6a-b. Indeed the geometry of the  $D_5$  and its dual are not significantly different. Adding small perturbations by choosing the parameters  $\lambda_1$ ,  $\lambda_2$ , and  $\lambda_3$ , the morsified Cusp catastrophe remains, see Figure 7.6c-d. The critical curves at the Cusp breaks up into two curves, one with a Fold catastrophe, one without a catastrophe.

### 7.3.5 $D_6^\pm$ Second Umbilic Catastrophes

Ignoring the perturbation terms  $\lambda_1, \dots, \lambda_4$  for the moment, the scale space expression of the  $D_6^\pm$ -catastrophes are given by

$$L(x, y; t) = \frac{1}{5!}x^5 + \frac{1}{3!}x^3t + \frac{1}{2!}xt^2 + \delta\left(\frac{1}{2}xy^2 + xt\right), \quad (7.8)$$

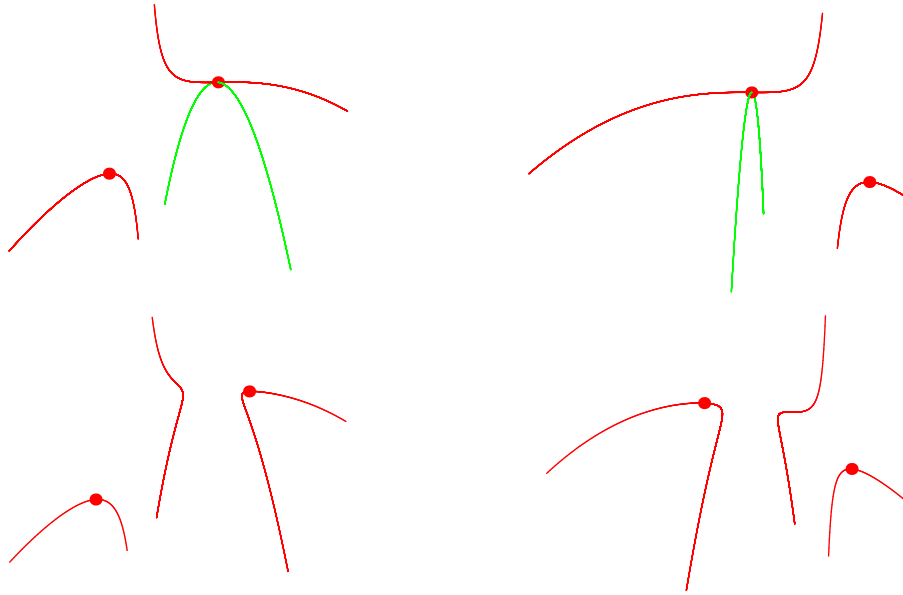


Figure 7.6: Critical paths of the  $D_5^\pm$ -catastrophe in the  $(x, y; t)$ -space. a) Unperturbed,  $\delta = -1$ . b) Unperturbed,  $\delta = 1$ . c) Perturbed,  $\delta = -1$ . d) Perturbed,  $\delta = 1$ .

where  $t$  is taking the role of  $\lambda_5$  and  $\delta = \pm 1$ . Its critical curves and catastrophes follow from

$$\begin{cases} L_x &= \frac{1}{4!}x^4 + \frac{1}{2}x^2t + \frac{1}{2}t^2 + \delta(t + \frac{1}{2}y^2) \\ L_y &= \delta xy \\ \det H &= \frac{1}{6}\delta x^2(x^2 + 6t) - y^2 \end{cases}$$

Setting  $y = 0$ , several catastrophes occur: At  $(x, y; t) = (\pm\sqrt{-6\delta}, 0; \delta)$  two Fold annihilations if  $\delta = -1$ , at the origin a creation and at  $(x, y; t) = (0, 0; -2\delta)$  again an annihilation, see Figure 7.7a for  $\delta = 1$  and Figure 7.7b for  $\delta = -1$ .

It is clear that the morsification by  $t$  of the  $D_6^+$  yields a  $D_4^-$  scatter followed (while increasing scale) by a  $D_4^+$  double annihilation at the origin. The  $D_6^-$  shows a  $D_4^-$  scatter at the origin, followed by again a  $D_4^+$  scatter at some higher scale. Both images show that a part of the critical curve forms a loop: The created critical points annihilate with each other.

So if the perturbations are small (or if the measurement contains some uncertainty), one might not be able to distinguish between the involved Fold catastrophes. However, the scale space representation causes a separation into two non-generic catastrophes already mentioned. Further morsification gives more insight in the way *critical curves* can behave.

By taking  $\lambda_1, \dots, \lambda_4 \neq 0$ , the generic critical curves shown in Figure 7.7c-d are obtained. The morsification of the  $D_6^+$  shows two critical curves behaving in an aesthetic way, combining the morsifications of the  $D_4^\pm$  catastrophes, *i.e.* containing Fold annihilations and creations. Both created critical points on the right critical curve in Figure 7.7c annihilate at some larger scale.

The morsification of the  $D_6^-$ , on the other hand, still shows the loop close to the origin. Consequently, in contrast to the elliptic Umbilic catastrophe, now *both created branches annihilate with each other*: the

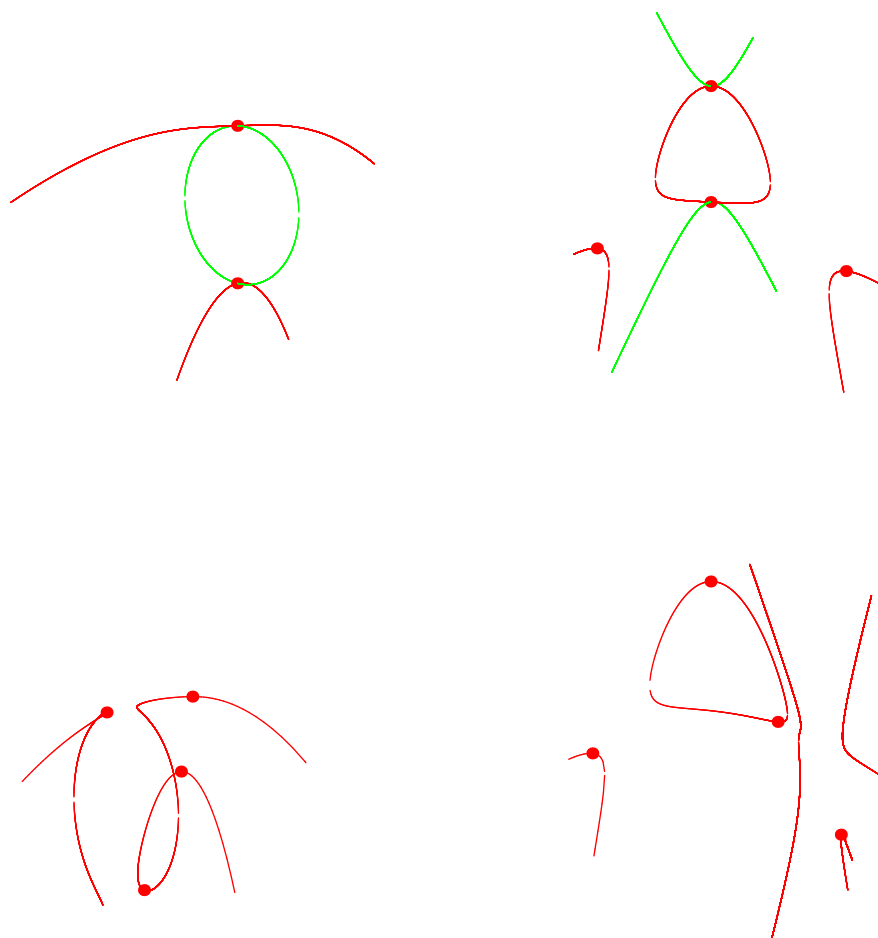


Figure 7.7: Critical paths of the  $D_6^\pm$ -catastrophe in  $(x, y; t)$ -space. a) Unperturbed,  $\delta = 1$ . b) Unperturbed,  $\delta = -1$ . c) Perturbed,  $\delta = 1$ . d) Perturbed,  $\delta = -1$ .

critical curve in the centre of Figure 7.7d is a closed loop in scale space.

### On Generic Loops

The perturbation term of the second Umbilic catastrophes in scale space is given by

$$\lambda_1 x + \lambda_2 y + \lambda_3(x^2 + 2t) + \lambda_4(y^2 + 2t).$$

If we assume that the image contains the catastrophe at the origin, we may set  $\lambda_1 = \lambda_2 = \lambda_3 = 0$ . Furthermore, if it contains an elongated structure at the creation,  $|\lambda_4| > 0$ . This perturbation causes the non-generic scatter event, visible in Figure 7.7b, to break up. While increasing  $|\lambda_4|$  the two parabolae in the  $x = 0$ -plane move along the critical loop, until they meet each other and change into two critical curves without a catastrophe, as shown in Figure 7.7d.

Setting  $\lambda_4 = 2L_{yy}$  we get

$$L(x, y; t) = L_{xtt}\left(\frac{1}{5!}x^5 + \frac{1}{6}x^3t + \frac{1}{2}xt^2\right) + L_x t(xt + \frac{1}{2}xy^2) + L_{yy}\left(\frac{1}{2}x^2 + t\right),$$

where  $L_{xtt} = L_{xxxxx}$  and  $L_{xt} = L_{xyy}$  in absence of other third and fifth order derivatives. Consequently,

$$\begin{cases} \partial_x L &= L_{xtt}\left(\frac{1}{4!}x^4 + \frac{1}{2}x^2t + \frac{1}{2}t^2\right) + L_{xt}\left(t + \frac{1}{2}y^2\right) \\ \partial_y L &= L_{xt}xy + L_{yy}y \\ \det H &= L_{xtt}\left(\frac{1}{6}x^3 + xt\right)(L_{xt}x + L_{yy}) - L_{xt}y^2 \end{cases}$$

One can verify that the solution  $x = -\frac{L_{yy}}{L_{xt}}$  of  $\partial_y L = 0$  describes the non-genericity on the loop if  $L_{yy}^2 \leq (-3 + \sqrt{3})\frac{L_{xt}^3}{L_{xtt}}$  by solving  $\partial_x L = 0$ , so  $L_{yy}$  needs to be large enough and  $L_{xtt}L_{xt} < 0$ , *i.e.* only the morsified  $D_6^-$  pertains its loop. Now at the origin the creation takes place. Note that there  $\partial_t L \neq 0$ . The successive annihilation follows from  $x = y = 0$  and  $\partial_x L = L_{xtt}\frac{1}{2}t^2 + L_{xt}t = 0$  and takes place at  $(x, y; t) = (0, 0; -\frac{2L_{xt}}{L_{xtt}})$ . So the lifetime of the scale space loop is  $t_l = -\frac{2L_{xt}}{L_{xtt}}$ . Furthermore, the difference in intensity between creation and annihilation yields  $L_{yy}t_l$ . The loop can therefore persist over a certain range of scales. We will come back to these parameter setting and coordinate choice in section 7.4.

### 7.3.6 Other Non-Generic Catastrophes

The catastrophes, their scale space formulation, and their morsifications, as treated in the previous sections, are only the beginning of an infinite set of possible descriptions on the behaviour of critical curves. Due to extreme local symmetries and inaccuracies – think of a large checkerboard pattern – one might encounter non-generic events to be described with higher order catastrophe models. These models follow straightforward from the route we described.

From the point of view of distinct appearances of critical curves, this expose suffices. Since the only possible generic catastrophes on critical curves are creations and annihilations of pairs of critical points, the possibilities are limited. Given an critical curve, it either originated from the initial image and the curve can contain several protuberances, *i.e.* sequences of successive creations and annihilations, or it didn't originate from the initial image and it forms a loop, perhaps also with protuberances. Both possibilities are described by the aforementioned catastrophe models. The scale space formulation of the “three exceptional catastrophes” don't yield any extra information, as one can verify.

### 7.3.7 Morsification Summary

All non-Fold catastrophes morsify to Fold catastrophes and Morse critical points. The morsification gives insight in the structure around the catastrophe point regarding the critical curves.

The morsification of the Umbilic catastrophes (the  $D_k$ ) show that the trajectories in scale space of the created critical points fall into several classes.

The morsified  $D_4^+$ -catastrophes describes two Fold annihilations. The morsified  $D_4^-$  catastrophe describes the creation of a pair of critical points and the annihilation of one of them with another critical point. So while tracing a critical branch of a critical curve both an annihilation and a creation event are traversed.

The morsified  $D_6^+$  catastrophe describes the creation of a pair of critical points and the annihilation of both of them with two other critical points. So while tracing a critical branch of a critical curve successively an annihilation, a creation and again an annihilation event are traversed.

The morsified  $D_6^-$ -catastrophe describes an *isolated* closed critical curve, appearing *ex nihilo* with two critical branches that disappear at some larger scale.

So the morsified  $D_4^-$  (and its extension, the  $D_6^+$ ) and  $D_6^-$ -catastrophes describe essentially different creation events. An important result lies on the area of tracing critical points. If one traces *only* critical points starting from the initial image, one will find the “ $D_4^-$ ” creations, since they emerge as the starting point of a part of a critical curve that annihilates with one of the initial critical points. However, one will miss the “ $D_6^-$ ” loops that occur somewhere in scale space, since they have no relation whatsoever to the critical points in the initial image. So fine-to-coarse tracing of critical points will not always yield the right result.

Note that the full morsification of the non-generic catastrophes always yields the generic Fold annihilations and creations and Morse critical points.

## 7.4 Applications

In this section we give some examples to illustrate the theory presented in the previous sections. We will focus on the critical curves emerging from a creation event. An example of desired symmetry in an image and consequently modelling by a Cusp catastrophe has been presented elsewhere [156].

Firstly, appearance of the morsified  $D_4^-$ -catastrophe on critical paths is shown using the artificial MR image of Figure 7.8a. This image is taken from the “Brain Web” [40, 41, 163], web site <http://www.bic.mni.mcgill.ca/brainweb>.

Secondly, an example of creation *ex nihilo*, the morsified  $D_6^-$ -catastrophe, is shown by means of the classic “bridge”-image of Figure 7.11a, and the aforementioned MR image.

### 7.4.1 $D_4^-$ Catastrophe

The artificial MR image of Figure 7.8a was used as initial image for the scale space image. For visualisation purposes, we restricted to the scale range 8.37 – 33.1. The image at scale 8.37 (with only the large structures remaining) is shown in Figure 7.8b. This image contains 7 extrema.

The scale space image in this scale range contains 161 logarithmically sampled scales. At all scales the spatial critical points were calculated and connected, forming the critical paths. Figure 7.9 shows these critical paths in the  $(x, y; t)$ -space. The bright curves represent the extrema, the dark ones the

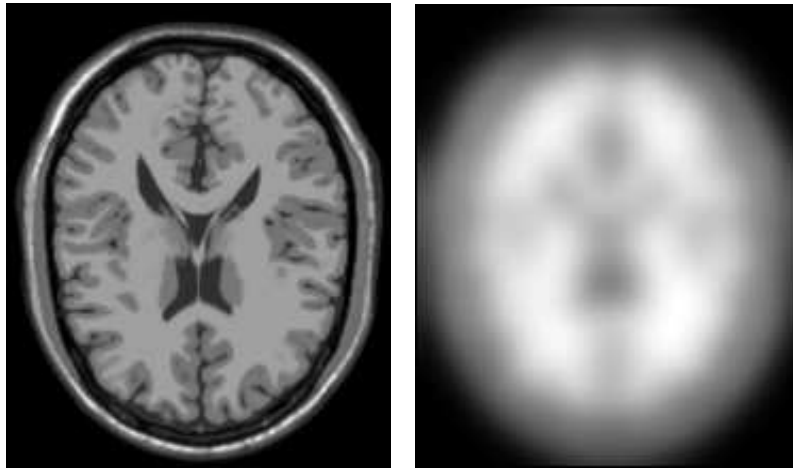


Figure 7.8: a) 181 x 217 artificial MR image. b) Image on scale 8.37

saddles. At the (approximate) catastrophe locations the curves are connected. Globally, the image shows annihilating pairs of critical points. Locally, however, the presence of extra branches of critical curves is visible.

A close-up of one of the critical paths is shown in Figure 7.10a. It clearly shows a critical curve containing two subsequent Fold annihilation – creation events. The critical curve evidently shows the appearance of an annihilation-creation-pair described by the  $D_4^-$  morsification. Note that the creation events would have been missed if the sampling was taking coarser, yielding one critical curve without protuberances in scale direction. Sampling without connecting critical paths yields the observation of temporarily created extrema (and saddles), *cf.* Simmons *et al.* [230].

#### 7.4.2 $D_6^-$ Catastrophe

Figure 7.11a shows the classical “bridge”-image: two mountains of different height (blobs with different intensity) connected by a small ramp and a deep valley between the mountains. This image was described by Lifshitz and Pizer [168] as possible initial image yielding a creation event in scale space.

- Firstly, there is only one maximum of the left blob. The right blob is not a maximum, since it is connected to the other blob by the ramp.
- Secondly, at some scale the ramp changes into a bridge with a deep dip in it due to the surrounding deep valleys: a maximum (right blob) – saddle (dip of the bridge) pair is created.
- Finally, at a large scale a saddle – extremum annihilation occurs.

If the saddle annihilates with the left extremum, it can be modelled by the  $D_4^-$  catastrophe, as in the previous section. However, as shown by Figure 7.11b, it can also annihilate with the newly created extremum. This figure shows the critical paths of the scale space image of 7.11a. The left string represents the extremum of the brightest blob, the loop represents the created and annihilated maximum-saddle pair.





Figure 7.9: Critical paths of the MR image in scale range 8.37 – 33.1.

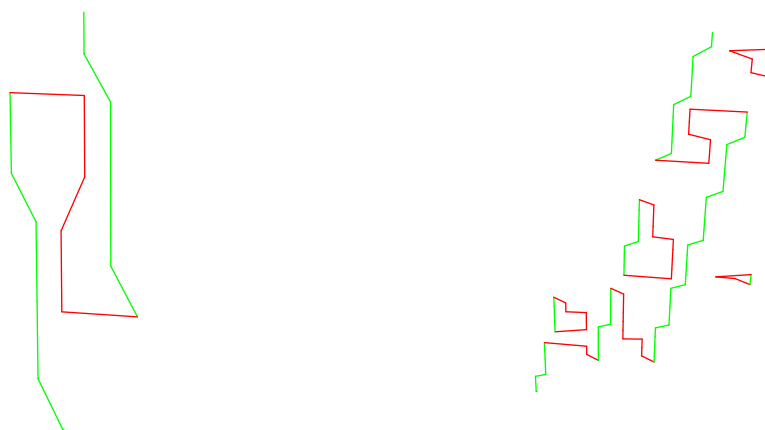


Figure 7.10: a) Close-up of one of the critical paths of the MR image, showing a subsequent annihilation – creation event. b) Close-up, showing subsequent annihilation – creation events and loop events.

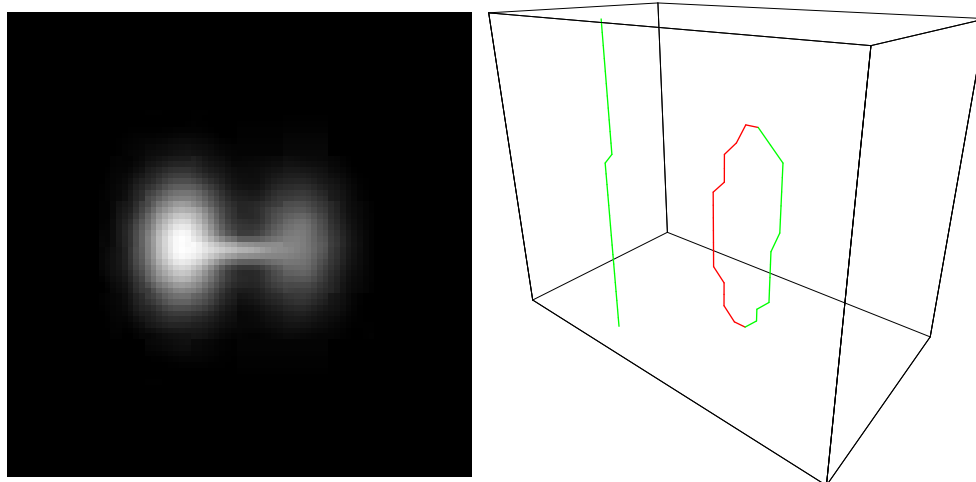


Figure 7.11: a) Artificial bridge image. b) Critical paths of the bridge image.

Since the structure is built up as discussed in section 7.3.5, the loop remains over a relatively large number of scales. Due to mirror symmetry we know that the  $x$ -direction is the one indeed corresponding to that used in the previous canonical models. Numerical calculations show a very strong response on the fraction  $\frac{L_{xyy}}{L_{xxxxx}}$  close to the scale space location of the creation, as predicted by the model as measure for the lifetime of the loop.

The same behaviour is observed at the MR scale space image. Figure 7.10b shows a close-up of one of the critical curves. Besides several aforementioned subsequent Fold annihilation – creation events along the critical curve, here clearly also several “loop events” occur.

## 7.5 Discussion

In this chapter we investigated the (deep) structure on various catastrophe events in Gaussian scale space. Although it is known that pairs of critical points are annihilated and created (the latter if the dimension of the image is 2 or higher), it is important to describe also the local structure of the image around the non-generic events. These events might be encountered in practical usage of scale spaces and the non-generic catastrophes can be used to model these occurrences. We therefore embedded catastrophes in scale space. Scale acts as one of the perturbation parameters. The morsification of the catastrophes yields generic Fold annihilations and creations of pairs of critical points.

The  $A_k$  series can be used to model (almost) simultaneous annihilations of pairs of critical points at a location (or indistinguishable region) in scale space. If  $k$  is even, it models the annihilation of  $k$  critical points, if  $k$  is odd, it models the collision of  $k$  critical points where  $k - 1$  annihilate and one remains.

For creations the  $D_k$  series can be used. Creations occur in different types. Critical paths in scale space can have protuberances, a subsequent occurrence of an annihilation and a creation. In scale space images this is visible by the creation of an extremum-saddle pair, of which one critical point annihilates at some higher scale with an already present critical point, while the other remains unaffected. It is also possible that critical paths form loops: the created pair annihilates at some higher scale. The possibility for both types to occur in practice was shown in the artificial MR image. This phenomena is known from physics, where it is used to describe the creation and successive annihilations of “virtual” elementary particles (and even the universe), see *e.g.* [4, 186, 191].

Furthermore we showed that the protuberances in the critical paths, expressed in canonical coordinates, occur only in case of a small local perturbation. In addition, creations are less likely to happen due to a special constraint on the combination of third order derivatives and local perturbation. We gave a dimension dependent expectation of this event and an upper bound for the perturbation in canonical coordinates.

The lifetime of a created pair is enlarged if the local structure is elongated. This was derived from the canonical formulation and visualised by the example of the bridge image in section 7.4.

Since the number of possible catastrophes is infinite, there is an infinite number of possible non-generic constellations in which (“infinite”) critical points are annihilated and created. We restricted ourselves to the situations in which at most 6 critical points annihilate and in which critical points are created, the latter divided into models representing protuberances and loops.

Finally, the calculations were based on the canonical coordinates. In general, it is not trivial to transform the local coordinate system to these nice formulated catastrophe germs. In that sense, the numerical values have no direct meaning. They do describe, however, the qualitative behaviour of the

critical curves close to the location of the catastrophes and can therefore be used to model the type of behaviour encountered in practical usage of a scale space. We gave examples of the appearances of this behaviour in section 7.4 based on an artificial MR image.

The theory described in this chapter extends the knowledge of the deep structure of Gaussian scale space, especially with respect to the behaviour of critical curves in the vicinity of creation events and the scale space lifetime of the created critical points. It emphasises the relevance of investigating the complete scale space image, instead of a series of images at different scales.

---

## Logical Filtering

---

Causality may be considered as a mode of perception by which we reduce our sense impressions to order.

---

NIELS BOHR

**abstract** Using a Gaussian scale space, one can use the extra dimension, *viz.* scale, for investigation of “built-in” properties of the image in scale space. We show that one of such induced properties is the nesting of special iso-intensity manifolds, that yield an implicit present hierarchy of the critical points and regions of their influence, in the original image. Its very nature allows one not only to segment the original image automatically, but also to apply “logical filters” to it, obtaining simplified images. We give an algorithm deriving this hierarchy and show its effectiveness on two different kinds of images, both with respect to segmentation and simplification.

### 8.1 Introduction

The paradigm of linear scale space has been introduced by Witkin [249] and Koenderink [139]. They noted that a single image contains objects or parts with various sizes. One way to exploit this fact is by observing the image with filters capturing these a priori unknown sizes, or scales. Assuming that these filters should be invariant with respect to location, scale and rotations and that they should be linear, one finds the set of Gaussian filters as a plausible solution.

From the field of distribution theory [224] it is known that these filters also allow one to take derivatives up to any order of non-continuous functions, solving the question of how to define proper derivatives of a discrete set (*e.g.* an image [65]) in a well-posed way.

Nowadays, Gaussian filters are widely used to calculate derivatives of images. However, in calculating these derivatives, one needs to specify the scale, or standard deviation, of the Gaussian. One way to avoid this, is by calculating the differential properties of interest at a range of scales [76] and selecting the one with the highest (or best) response according to some pre-defined criterion.

This approaches in some sense the concept of “deep structure”, defined by Koenderink as “investigation of the image at all scales simultaneously” [139]. In essence, this implies full investigation of the  $n$ -dimensional image in  $(n + 1)$ -dimensional scale space as opposed to a “slice-by-slice” approach.

Most of the research in scale space is focused on the selection of pre-defined invariants [77, 78, 107] at several scales with highest response (see e.g. [37, 176, 175, 177]). Some results have been obtained by examining the deep structure, e.g. in the behaviour of spatial critical points under blurring, using ideas from the field of catastrophe (or: singularity) theory [48, 72, 98, 132]. Alerted by outcome of results by Lifshitz and Pizer [168], Koenderink [144] mentioned the presence of spatial critical points in scale space with zero scale derivative and investigated their neighbourhood structure. In an earlier paper [157] we investigated the deep structure yielding a hierarchy tree representing the image, based on its spatial extrema at all scales, their disappearances with saddle points and the critical points in scale space found by tracing the spatial saddle points at all scales. This tree could be used to obtain a user-independent “pre-”segmentation of the image. In [160] we discussed the stability of the hierarchy tree and the ability to add a priori and a posteriori known symmetry to it, and showed the effect on the pre-segmentation.

In this paper we extend the results mentioned in [157] and explore the  $n + 1$  dimensional scale space with respect to its critical points and its iso-intensity manifolds. We show that the latter introduce a unique hierarchy which can be used as a so-called logical filter. Consequently, a unique partitioning of the scale space is obtained, which yields, if projected to the initial image, a partitioning of the image without prior knowledge.

## 8.2 Theory

The idea of logical filtering in scale space was introduced by Koenderink in [139]. In section 8.2.3 we will describe this idea. In order to understand the essential elements, we firstly define a Gaussian scale space in section 8.2.1 and the idea of the hierarchical structure in section 8.2.2. The structure depends on the evolution of spatial critical points as the scale changes. The locations of these points in scale space form one dimensional manifolds, the so-called critical curves, containing two types of special points, viz. scale space saddles and catastrophe points.

### 8.2.1 Gaussian Scale Space

**Definition 29**  $L(\mathbf{x})$  denotes an arbitrary  $n$  dimensional image. We will refer to this image as the initial image.  $L(\mathbf{x}; t)$  denotes the  $n + 1$  dimensional Gaussian scale space image of  $L(\mathbf{x})$ .

The isotropic Gaussian scale space image is obtained by convolution of an initial image with a normalised Gaussian kernel:

$$L(\mathbf{x}; t) \stackrel{\text{def}}{=} G_t \star L(\mathbf{x}) \stackrel{\text{def}}{=} \int \frac{1}{\sqrt{4\pi t}^n} e^{-\frac{|\mathbf{x}-\mathbf{y}|^2}{4t}} L(\mathbf{y}) d\mathbf{y}$$

$L(\mathbf{x}; t)$  satisfies the diffusion equation:

$$\partial_t L(\mathbf{x}; t) = \sum_{i=1}^n \frac{\partial^2}{\partial x_i^2} L(\mathbf{x}; t) \stackrel{\text{def}}{=} \Delta L(\mathbf{x}; t) \quad (8.1)$$

Here  $\Delta L(\mathbf{x}; t)$  denotes the Laplacean. Furthermore, differentiation is now well-defined, since any derivative of the image is given by the convolution of the image with the corresponding derivative of the Gaussian. The (discrete) initial image is now extended to a continuous scale space image,  $L(\mathbf{x}; t) \in \mathbb{R}^n \times \mathbb{R}^+$  with  $\lim_{t \downarrow 0} L(\mathbf{x}; t) = L(\mathbf{x})$ .

### Spatial critical points

**Definition 30** *Spatial critical points, i.e. saddles and extrema (maxima or minima), at a certain scale  $t_0$  are defined as the points at fixed scale  $t_0$  where the spatial derivatives vanish:  $\nabla L(\mathbf{x}; t_0) = 0$ . We will refer to these points as spatial critical points to distinguish them from scale space critical points, see Definition 34.*

The type of the spatial critical points is given by the eigenvalues of the Hessian  $H$ , the matrix with the second order spatial derivatives.

**Definition 31** *The Hessian matrix is defined by  $H \stackrel{\text{def}}{=} \nabla \nabla^T L(\mathbf{x}; t_0)$ , where each element of  $H$  is given by*

$$H_{i,j} = \frac{\partial^2}{\partial x_i \partial x_j} L(\mathbf{x}; t).$$

The trace of the Hessian equals the Laplacean. For maxima (minima) all eigenvalues of the Hessian are negative (positive). At a spatial saddle point  $H$  has both negative and positive eigenvalues.

Since  $L(\mathbf{x}; t)$  is a continuously differentiable (even smooth) function in the  $(\mathbf{x}; t)$ -space, spatial critical points are defined for any value  $t_0$  and, according to the implicit function theorem, constitute a one dimensional manifold in scale space.

**Definition 32** *A critical curve is a one dimensional manifold in  $(\mathbf{x}; t)$  (scale) space on which  $\nabla L(\mathbf{x}; t) = 0$ .*

Consequently, the intersection of all critical curves with an image at a certain scale  $t_0$  results in the spatial critical points of the images at scale  $t_0$ .

If at a spatial critical point the Hessian degenerates, that is: at least one of the eigenvalues is zero, the type of the spatial critical point cannot be determined using Definition 31.

**Definition 33** *The catastrophe points of  $L(\mathbf{x}; t)$  are defined as the points where both the spatial derivatives and determinant of the Hessian vanish:  $\nabla L(\mathbf{x}; t) = 0$  and  $\det H(\mathbf{x}; t) = 0$ .*

In scale space the catastrophe points are isolated points and form the top of critical curves in case of annihilations, and the starting point in case of a creation. The latter requires a spatial dimension of at least two.

### Scale Space Saddles

**Definition 34** The scale space saddles of  $L(\mathbf{x}; t)$  are defined as the points where both the spatial derivatives and scale derivative vanish:  $\nabla L(\mathbf{x}; t) = 0$  and  $\partial_t L(\mathbf{x}; t) = 0$ . Since for Gaussian scale spaces the diffusion equation holds, the latter equation equals  $\Delta L(\mathbf{x}; t) = 0$ .

Note that Definition 34 describes the critical points of  $L(\mathbf{x}; t)$  in scale space. In [158] it is proven that these points are always saddle points. This is a direct consequence of the notion of causality (or: the non-enhancement of local extrema, or: the prohibition of “spurious detail”, or: the maximum principle).

**Definition 35** The extended Hessian  $\mathcal{H}$  of  $L(\mathbf{x}; t)$  is matrix of the second order derivatives in scale space defined by

$$\mathcal{H} = \begin{pmatrix} \nabla \nabla^T L & \Delta \nabla L \\ (\Delta \nabla L)^T & \Delta \Delta L \end{pmatrix}. \quad (8.2)$$

where  $\nabla \nabla^T L$  is the Hessian.

Note that in Equation (8.2) the elements of  $\mathcal{H}$  are purely spatial derivatives. This is possible by employing of the diffusion equation, Equation (8.1).

The appearance of only saddles in scale space leads to the consequence that the extended Hessian has both positive and negative eigenvalues at scale space critical points. Furthermore, in [158] we have proven that if the intensity of the spatial saddle points is parametrised by scale, the scale space saddles form the extrema of the parametrised intensity along the critical curve.

### 8.2.2 Scale Space Hierarchy

From the previous section it follows that each critical curve in  $(\mathbf{x}; t)$ -space is formed by branches of critical points, where each branch is defined from a creation event or the initial scale to an annihilation event. We set  $\#_C$  the number of creation events on a critical path and  $\#_A$  the number of annihilation events. Since there exists a scale on which only one spatial critical point (an extremum) remains, there is one critical path with  $\#_A = \#_C$ , whereas all other critical paths have  $\#_A = \#_C + 1$ . That is, all but one critical paths are defined for a finite scale range. This widely accepted “folklore theorem” holds for  $L^1$ -integrable images that are non-negative and have finite compact support, see Loog *et al.* [182].

One of the properties of scale space is the non-enhancement of local extrema. Therefore, isophotes in the neighbourhood of an extremum at a certain scale  $t_0$  appear to move towards the extremum at coarser scale until at some scale  $t_1$  the intensity of the extremum equals the intensity of the isophote. The extension of an isophote into scale space is called iso-intensity manifold:

**Definition 36** A iso-intensity manifold  $I_c$ ,  $c \in R$ , is an  $n$ -dimensional manifold in  $(n + 1)$ -dimensional scale space satisfying  $L(\mathbf{x}; t) = c$ .

It is often implicitly understood that we consider connected components only. The iso-intensity surface in scale formed by these isophotes form a dome, with its top at the extremum.

Since the intensity of the extremum is monotonically in- or decreasing (regarding a minimum or a maximum, respectively), all these domes are nested. Retrospectively, each extremum branch carries a series of nested domes, defining increasing regions around the extremum in the input image. In [158]



we have proven that these regions are closed as long as the intensity of the domes does not equal that of the dome through (the extremum and) a scale space saddle (see section 8.2.1) on the saddle branch that is connected with the extremum branch in an annihilation event. In this way a hierarchy of regions of the input image is obtained, which can be regarded as a kind of pre-segmentation. It also results in a partitioning of the scale space itself.

### 8.2.3 Logical Filtering

Since the iso-intensity manifolds are nicely nested, they can be used to form logical filters, as pointed out by Koenderink [139]: The requirement that in two “successive” derived images, say  $L(\mathbf{x}; t)$  and  $L(\mathbf{x}; t + \delta t)$  (with  $\mathbf{x}$  variable), corresponding points have equal illuminance and are as close as possible, yields a simple rule of *projection* between images: the orbits of the projection are the integral curves of the vector field

$$\begin{pmatrix} \dot{\mathbf{x}} \\ \dot{t} \end{pmatrix} = \begin{pmatrix} \nabla L \Delta L \\ -\|\nabla L\|^2 \end{pmatrix}. \quad (8.3)$$

This follows from the fact that the point  $\mathbf{x} + d\mathbf{x}$  in the image at scale  $t + dt$  that is connected on a iso-intensity manifold to the point  $\mathbf{x}$  at scale  $t$ , must satisfy

$$0 = \delta L = \nabla L \cdot d\mathbf{x} + \partial_t L dt = \nabla L \cdot d\mathbf{x} + \Delta L dt. \quad (8.4)$$

Taking the direction of steepest decent, *i.e.* in the direction of  $\nabla L$ , we obtain

$$\frac{d\mathbf{x}}{dt} = -\frac{\Delta L}{\nabla L \cdot \nabla L} \cdot \nabla L$$

Noting that  $\nabla L \cdot \nabla L \geq 0$ , and that the singularities of the vector fields given by the Eqs. (8.3) and (8.4) coincide, namely if  $\nabla L = 0$ , the integral curves of the vector fields are the same.

Since the projection of a region of the image at some scale to the initial image cannot reach all points in the latter image, some regions are blanked out. These regions are described through the integral curves that pass through the extremum and those through the saddle that do reach the initial image. In Figure 8.6 one can see examples of iso-intensity manifolds formed by these integral curves. The region enclosed by each manifold cannot be reached. These regions are topologically equivalent to balls. Koenderink proposed to call these regions the “ranges” of the extrema, that can be taken to define the light and dark blobs defined by the extremum-saddle-point-pairs [139]. The ranges sweep out tube-like volumes, that are closed on one side. Constructing these ranges for all extrema, the image can be described as a superposition of light and dark blobs. A sub-family may be defined for each sub-image and the original family is just the superposition of the sub-families.

We will show that the top of the tube-like volumes are found by the integral curves that pass the scale space saddles. Firstly a further investigation of the vector field Eq. (8.3) is presented.

## 8.3 Properties of the Vector Field

The vector field given by Eq. (8.3) uniquely defines integral curves, except for those points where the gradient vanishes. To investigate the local behaviour of the vector field nearby critical points, a local

(Gaussian) Taylor expansion of  $L$  is used. As we will see, it suffices to take the ensemble of derivatives up to fourth order, the so-called *local jet of order 4* [77, 80]. Using the Einstein convention for repeated indices this reads

$$L^{(4)}(\mathbf{x}; t) = L_0 + L_i x^i + \frac{1}{2} L_{ij} x^i x^j + \Delta L t + \frac{1}{6} L_{ijk} x^i x^j x^k + \Delta L_i x^i t + \frac{1}{24} L_{ijkl} x^i x^j x^k x^l + \frac{1}{2} \Delta L_{ij} x^i x^j t + \frac{1}{2} \Delta \Delta L t^2. \quad (8.5)$$

Note that the local jet satisfies the Diffusion Equation. Locally the vector field given by Eq. (8.3) can be expressed by

$$\begin{pmatrix} \dot{\mathbf{x}} \\ \dot{t} \end{pmatrix} = \begin{pmatrix} v_0 \\ w_0 \end{pmatrix} + \begin{pmatrix} v_1 \\ w_1 \end{pmatrix} + \begin{pmatrix} v_2 \\ w_2 \end{pmatrix} + \dots \quad (8.6)$$

where the sub-indices denote the total order of the expansion in spatial variables. In terms of components we thus have

- $\begin{pmatrix} v_0^i \\ w_0 \end{pmatrix} = \begin{pmatrix} \Delta L L_i \\ -L_i^2 \end{pmatrix},$
- $\begin{pmatrix} v_1^i \\ w_1 \end{pmatrix} = \begin{pmatrix} (L_{ij} \Delta L + L_i \Delta L_j) x^j \\ -2L_i L_{ij} x^j \end{pmatrix},$
- $\begin{pmatrix} v_2^i \\ w_2 \end{pmatrix} = \begin{pmatrix} \frac{1}{2} (L_{ijk} \Delta L + 2L_{ij} \Delta L_k + L_i \Delta L_{jk}) x^j x^k + (\Delta L_i \Delta L + L_i \Delta \Delta L) t \\ -(L_{ik} L_{ij} + L_i L_{ijk}) x^j x^k - 2L_i \Delta L_i t \end{pmatrix},$
- and so on, with increasing complexity of the terms.

At spatial critical points  $L_i = 0$  reducing this expansion significantly. Then the zeroth order terms vanish

- $\begin{pmatrix} v_0^i \\ w_0 \end{pmatrix} = \begin{pmatrix} 0 \\ 0 \end{pmatrix},$
- $\begin{pmatrix} v_1^i \\ w_1 \end{pmatrix} = \begin{pmatrix} (L_{ij} \Delta L) x^j \\ 0 \end{pmatrix},$
- $\begin{pmatrix} v_2^i \\ w_2 \end{pmatrix} = \begin{pmatrix} \frac{1}{2} (L_{ijk} \Delta L + 2L_{ij} \Delta L_k) x^j x^k + (\Delta L_i \Delta L) t \\ -(L_{ik} L_{ij}) x^j x^k \end{pmatrix},$

and linear terms suffice. If also the Laplacean vanishes, a further reduction of terms is established:

- $\begin{pmatrix} v_0^i \\ w_0 \end{pmatrix} = \begin{pmatrix} 0 \\ 0 \end{pmatrix},$
- $\begin{pmatrix} v_1^i \\ w_1 \end{pmatrix} = \begin{pmatrix} 0 \\ 0 \end{pmatrix},$
- $\begin{pmatrix} v_2^i \\ w_2 \end{pmatrix} = \begin{pmatrix} (L_{ij} \Delta L_k) x^j x^k \\ -(L_{ij} L_{ik}) x^j x^k \end{pmatrix}.$

Consequently, a second order scheme is needed.

### 8.3.1 Local Environment

On a local environment of the vector field at critical points, reducing Eq. 8.6 to its first non-zero component, yields a linear system. Since  $w_1 = 0$ ,  $t$  is constant and can be disregarded. So a linear system with only spatial coordinates remains and its behaviour is given by the scale-independent vector field

$$\dot{\mathbf{x}}^i = L_{ij} \Delta L \mathbf{x}^j. \quad (8.7)$$

The matrix  $L_{ij} \Delta L$  in the linear system of Eq. 8.7 consists of two parts. The first term,  $L_{ij}$ , is equal to the Hessian matrix usually denoted by  $\mathbf{H}$ . The Laplacean term  $\Delta L$  reads, apart from the scale derivative of the image, also the trace of the Hessian, since  $\Delta L = L_{ii} = \text{tr}(\mathbf{H})$ . At the critical curve four possibilities can occur, see Figure 8.1:

1. Both the trace and the determinant of the Hessian are non-zero, *i.e.* the critical point is a Morse critical point;
2. The determinant of the Hessian is zero, *i.e.* a catastrophe takes place (annihilation or creation);
3. The trace of the Hessian is zero, *i.e.* a non-topological change of the saddle;
4. Both the trace and the determinant of the Hessian are zero.

The last possibility is only generic in one-dimensional images. In higher dimensions it will therefore be disregarded.

### 8.3.2 Morse Critical Points

At Morse critical points it is convenient to reformulate Eq. 8.7 to

$$\dot{\mathbf{x}} = \text{tr}(\mathbf{H}) \mathbf{H} \mathbf{x} = \widehat{\mathbf{H}} \mathbf{x}. \quad (8.8)$$

Note that the vector field given by Eq. 8.8 is a specially scaled extension of the usual vector field of  $L$  that is given by  $\dot{\mathbf{x}} = \mathbf{H} \mathbf{x}$ .

The characteristics of the  $\widehat{\mathbf{H}}$  vector field follows from its eigenvalues. Let  $(\lambda_i)$  be the set of eigenvectors of  $\mathbf{H}$ , sorted on value. Then the eigenvectors of  $\widehat{\mathbf{H}}$  are given by

$$\widehat{\lambda}_i = \sum_j \lambda_j \lambda_i, \quad (8.9)$$

where we used  $\text{tr}(\mathbf{H}) = \sum_j \lambda_j$ . Consequently, away from catastrophes, saddles remain saddles and extrema remain extrema. Then the following dependencies follow straightforwardly from Eq. (8.9):

$$\det \widehat{\mathbf{H}} = \text{tr}(\mathbf{H})^n \det \mathbf{H}, \quad (8.10)$$

$$\text{tr}(\widehat{\mathbf{H}}) = \text{tr}(\mathbf{H})^2, \quad (8.11)$$

where  $n$  is the dimension of  $\mathbf{x}$ .

Since the trace of the Hessian equals the sum of the eigenvectors, Eq. (8.11) shows that all eigenvalues of  $\widehat{\mathbf{H}}$  are positive definite. Consequently, the extrema of  $\widehat{\mathbf{H}}$  are always minima of the vector field, *i.e.* the

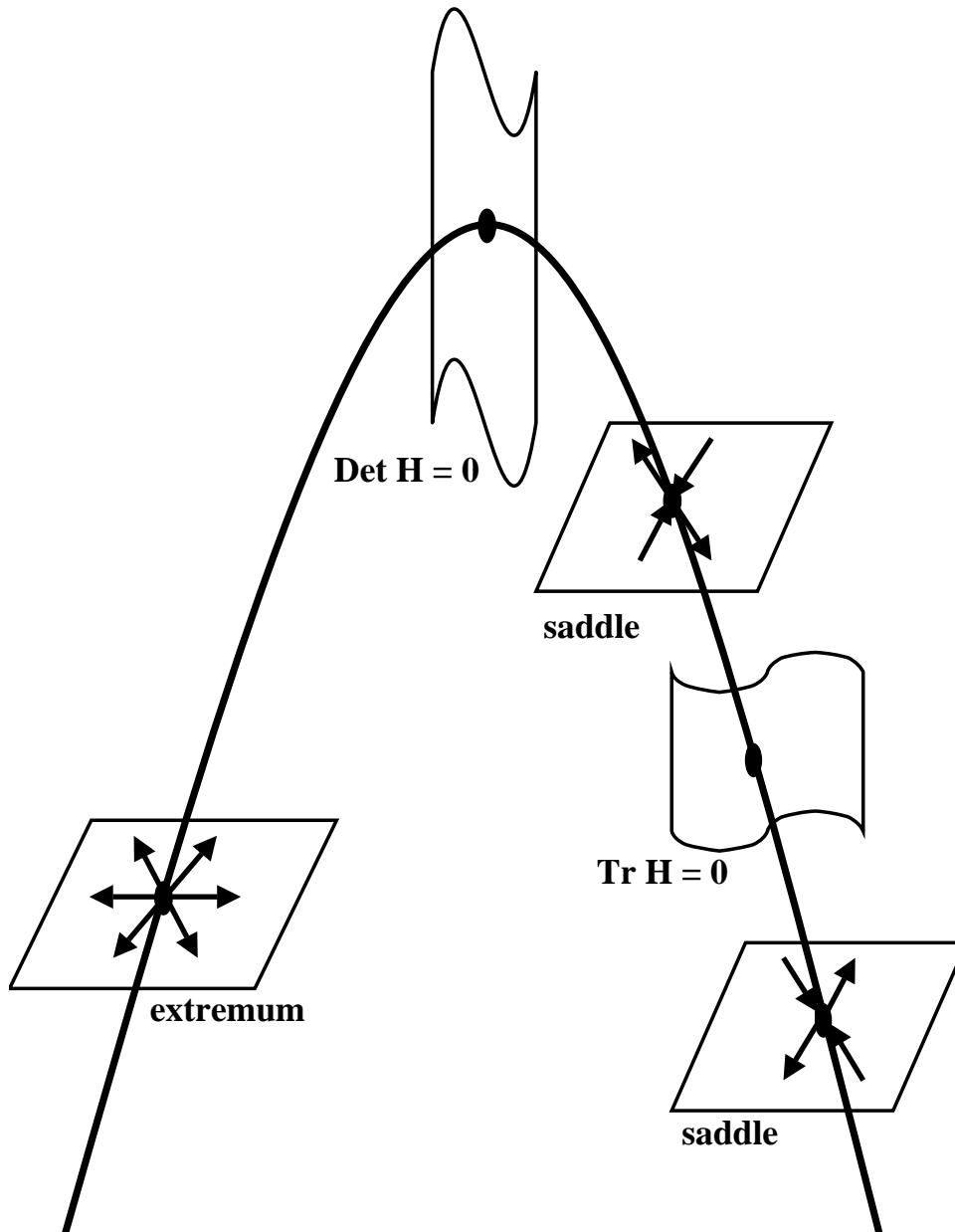


Figure 8.1: Possibilities of critical points in scale space on a critical curve, together with the local vector field. The left branch of the critical curve represents an extremum branch, the right one a saddle branch. Generically, critical points are somewhere on one of these branches (case 1). At the top, where  $\det \mathbf{H} = 0$ , a catastrophe takes place (case 2). The saddle point exhibits an extra degeneration, *viz.* where  $\text{tr} \mathbf{H} = 0$  (case 3). At this point the type of saddle changes. Only in one dimensional images the cases 2 and 3 coincide generically.

vectors point outward. Degenerations take place if  $\det \hat{\mathbf{H}} = 0$ . According to Eq. (8.10) this implies the degenerations of  $\mathbf{H}$  (the catastrophe points) or the zero-crossings of the trace of  $\mathbf{H}$ .

As a result, the  $\hat{\mathbf{H}}$  vector field has only minima and corresponding saddles. When we recall the full equation of the vector field, Eq. 8.3, it is clear that the scale component is negative at non-critical points. The flow lines infinitesimally close to the extrema move downward in scale.

### 8.3.3 Critical Points at Catastrophes

At catastrophes, Eq. 8.7 loses (generically) one degree of freedom, since the Hessian becomes singular, or, to put it differently, the determinant of  $\mathbf{H}$  equals zero.

The degeneration of  $\det \hat{\mathbf{H}}$  is only caused by the vanishing determinant of  $\mathbf{H}$ ; its trace will be non-zero iff  $n > 1$ . Since this is generically an event of co-dimension one, also the point where  $\det \hat{\mathbf{H}}$  vanishes has also co-dimension one. The trace of  $\hat{\mathbf{H}}$  at this point is always positive definite. The argumentation of the previous section can be repeated to conclude that a catastrophe due to  $\mathbf{H}$  causes a catastrophe in  $\hat{\mathbf{H}}$ . Again, while the  $\mathbf{H}$  vector field shows all sorts of catastrophes, the  $\hat{\mathbf{H}}$  vector field comprises only vector fields of catastrophes involving minima.

Consequently, at a catastrophe point the vector field of  $\hat{\mathbf{H}}$  is topologically equivalent to that of  $\mathbf{H}$  at a horseshoe surface.

### 8.3.4 Critical Points with Vanishing Laplacean

If the critical curve intersects the plane where the Laplacean of  $L$  is zero, the linear approximation Eq. 8.7 vanishes. A local vector field is found by examining the second order approximation of Eq. 8.6:

$$\begin{pmatrix} \dot{\mathbf{x}}^i \\ \dot{t} \end{pmatrix} = \begin{pmatrix} (L_{ij} \Delta L_k) x^j x^k \\ -(L_{ij} L_{ik}) x^j x^k \end{pmatrix}. \quad (8.12)$$

Although this expression is quite complicated, we still make the observation that a zero-Laplacean can only occur due to negative and positive eigenvalues of the Hessian, *i.e.* the critical point is always a saddle, albeit degenerate. Since the vector field involves the scale, see Eq. (8.12), the surface of zero-Laplacean will generically intersect the image transversally.

### 8.3.5 Non-Critical Points with Vanishing Laplacean

Although it may be clear from Eq. (8.3), it is emphasised that at non-critical points with zero Laplacean the vector field is non-degenerate, since it contains a non-zero scale component. If only spatial coordinates are investigated, the degeneracy is visible as a curve reversing the spatial orientation of the vectors.

### 8.3.6 Examples

#### One Dimensional Images

As already described, in one-dimensional images the determinant is equal to its trace. Therefore, at a catastrophe the critical curve also intersects the line where the Laplacean is zero. Since only annihilations occur, it suffices to investigate the generic annihilation in one dimension:

$$f(x, t) = x^3 + 6xt. \quad (8.13)$$

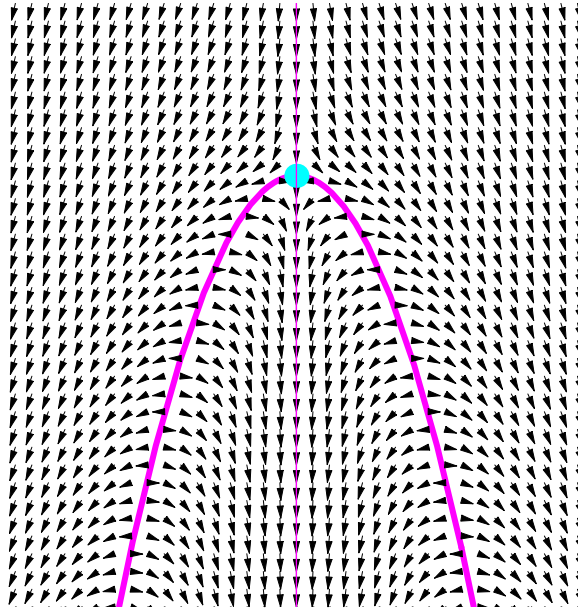


Figure 8.2: Vector field of a one dimensional scale space image around an annihilation at the origin, Eq. 8.13. The critical curve contains a catastrophe at the origin. The  $y$ -axis coincides with the zero Laplacean, reversing the spatial orientation of the vectors.

The corresponding vector field is plotted in Figure 8.2. The parabola is the critical curve, at its top (the origin), a minimum (the branch  $x > 0$ ) and a maximum annihilate. As argued in section 8.3.2, the  $\hat{\mathbf{H}}$ -vector fields of  $-f$  and  $f$  are topologically equivalent. The extrema in  $\mathbf{H}$ -vector field both become minima in the  $\hat{\mathbf{H}}$ -vector field, so the vector field is directing away from the critical points downwardly on both sides. The line where the Laplacean is zero, *i.e.* the line  $x = 0$ , acts as a mirror. This follows directly from section 8.3.5. For  $t < 0$  the zero-Laplacean is an attracting asymptote and for  $t > 0$  it is a diverging one. This is caused by the change of sign on traversing the critical curve at the origin.

### Two Dimensional Images

The generic annihilation in two dimensions is give by the function

$$f(x, t) = x^3 + 6xt + y^2 + 2t. \quad (8.14)$$

It contains an annihilation at the origin, and a scale space saddle at  $(-1/3, 0; -1/18)$ . The zero-Laplacean is given by the plane  $x = -1/3$ . Although this is non-generic, it suffices for our visualisation purposes.

**Spatial Components of the Vector Field** The vector field around Morse critical points (given by  $y = 0$  and  $x^2 = -2t$ ) for subsequent scale levels around the scale space saddle and the catastrophe point are shown in Figure 8.3 *for the spatial components*.

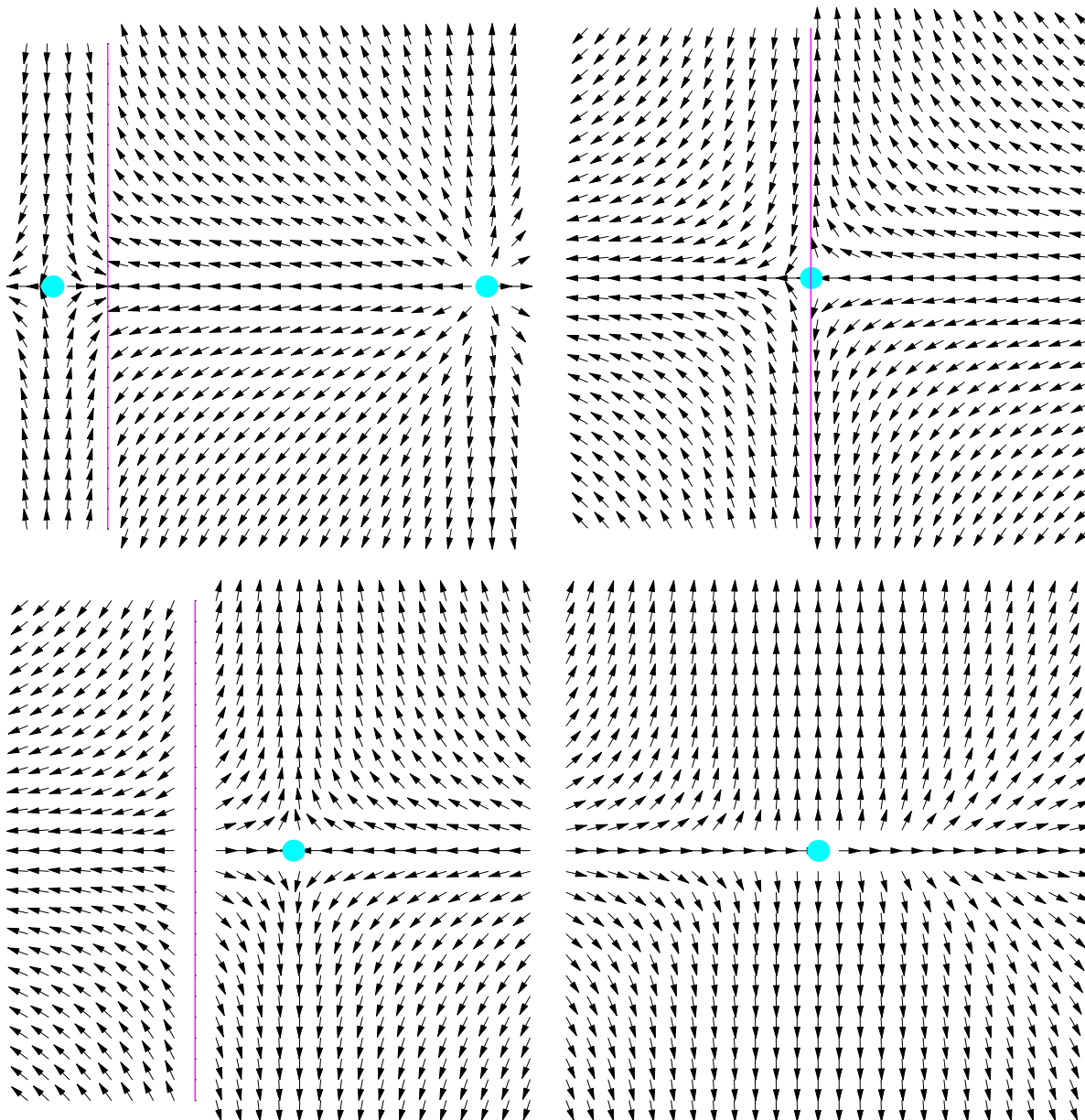


Figure 8.3: Vector field of the generic annihilation in two dimensions, Eq. 8.14, showing the *spatial* components for subsequent scale levels. The vertical line is the zero-Laplacean. Top-left: At  $t < -1/18$ . Top-right: At  $t = -1/18$ , around the scale space saddle. Bottom-left: At  $-1/18 < t < 0$ . Bottom-right: At  $t = 0$ , around the catastrophe point.

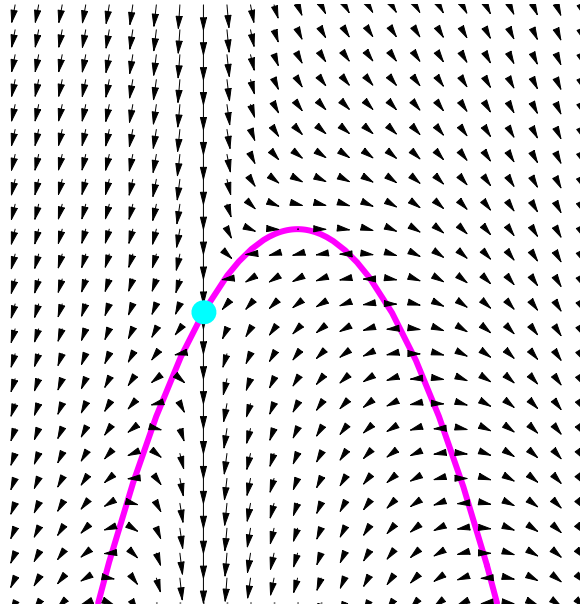


Figure 8.4: Vector field of the generic 2D annihilation, Eq. (8.14) in the  $(x;t)$  plane with  $t$  vertically, together with the critical curve and the scale space saddle. At the top of the curve the two critical points annihilate.

Firstly, the case for  $t < -1/18$  is shown in Figure 8.3 top-left. On the left a typical field around a saddle is visible, on the right the same for a minimum. Between the spatial critical points the zero-Laplacean is visible as a straight line, attracting and inverting the direction of the spatial vector components.

The situation around the scale space saddle ( $t = -1/18$ ) is shown in Figure 8.3 top-right, clearly showing the special second order behaviour.

The vector field for  $-1/18 < t < 0$ , *i.e.* between the scale space saddle and the catastrophe, is shown in Figure 8.3 bottom-left. Now the zero-Laplacean is diverging.

Finally, Figure 8.3 bottom-right shows the behaviour around the catastrophe, a combination of a saddle (on the left) and a minimum.

**A Spatial and a Scale Component of the Vector Field** Since the plane  $y = 0$  only acts as a mirror, the situation in the  $(x, t)$ -plane is shown in Figure 8.4, together with the critical curve and the scale space saddle. The fact that the scale space saddle doesn't coincide with the catastrophe point forces iso-intensity manifolds that intersect the critical curve between the scale space saddle and the catastrophe point, to intersect the critical curve a second time on the right.

Obviously iso-intensity manifolds through scale space saddles form the interesting ones. In the next section we will discuss the properties of the iso-intensity manifolds.



## 8.4 Deep Structure

In this section we investigate the nature of manifolds of co-dimension 1 in scale space, form  $(n + 1)$ -dimensional segments in scale space, give examples that also illustrate the definitions, and show how this route can be used to build the hierarchy embedded in the scale space image.

### 8.4.1 Manifolds and Segments

Recalling Definition 36, it follows directly from Koenderink's vector field, Eq. (8.3) that at the top of the tube-like structure the iso-intensity manifold  $I_c$  reduces to an extremum at that scale. From Loog's argument it follows that one extremum remains, so there exist a maximum end scale at which each  $I_c$  reduces to an extremum at that scale:

**Lemma 3** *Given a certain  $I_c$ , there exists exactly one point  $(\mathbf{x}, \sigma) \in (\mathbb{R}^n \times \mathbb{R})$  with  $L(\mathbf{x}, \sigma) \in I_c$  and  $\nabla L(\mathbf{x}, \sigma) = 0$  such that  $\forall \epsilon > 0 L(\mathbf{x}, \sigma + \epsilon) \notin I_c$ .*

**Proof of lemma 3** *Let  $(\mathbf{y}, \sigma) \in (\mathbb{R}^n \times \mathbb{R})$  and  $L(\mathbf{y}, \sigma) \in I_c$ . Then for all sets  $((\mathbf{x}, \sigma), (\mathbf{y}, \sigma))$ , the system  $\mathbf{x} \neq \mathbf{y} \wedge \nabla L(\mathbf{y}, \sigma) = 0 \wedge \nabla L(\mathbf{x}, \sigma) = 0 \wedge L(\mathbf{y}, \sigma) = c \wedge L(\mathbf{x}, \sigma) = c$  yields  $2n + 2$  equations with  $2n + 1$  variables, and is over-determined. So necessarily  $\mathbf{x} = \mathbf{y}$ .*

*Furthermore, let  $(P, S)$  be the set of points  $(\mathbf{y}_i, \sigma_{\mathbf{y}_i}) \in (\mathbb{R}^n \times \mathbb{R})$  satisfying  $\nabla L(\mathbf{y}_i, \sigma_{\mathbf{y}_i}) = 0 \wedge L(\mathbf{y}_i, \sigma_{\mathbf{y}_i}) \in I_c$ . Then  $\sigma_{\mathbf{y}_i} \neq \sigma_{\mathbf{y}_j}$  for  $i \neq j$ , and it suffices to take the point  $(\mathbf{y}_i, \sigma_{\mathbf{y}_i}) \in (P, S)$  with  $\sigma_{\mathbf{y}_i} = \max(S)$ .  $\square$*

Obviously, there may be multiple iso-intensity manifolds with the same intensity that are disjunct in the scale space image. So the first thing to do is to relate each iso-intensity manifold to a single extremum branch. Since a single iso-intensity manifold can contain multiple extrema, but has a unique one with the highest scale, it makes sense to uniquely assign it to that extremum.

**Definition 37** *A critical curve is built up of extremum and saddle branches, which are connected at catastrophe points. The set of all  $k$  extremum branches in the scale space image is given by  $(e_1 \dots e_k)$ .*

**Definition 38** *An extremum iso-intensity manifold  $I_c(e_i)$  is the iso-intensity manifold with as global top the extremum on extremum branch  $e_i$ .*

Examples of extremum iso-intensity manifolds are given in Figure 8.5, in which two critical curves are visualised by thick curves and five subsequent iso-intensity manifolds are drawn. It is clear that multiple types are present. To distinguish between extremum iso-intensity manifolds with multiple extrema on it, and those with only one, it is convenient to define a subset of the extremum iso-intensity manifolds:

**Definition 39** *An extremum manifold  $M_c(e_i)$  is an extremum iso-intensity manifold intersecting of all extremum branches only the extremum branch  $e_i$ .*

This type of extremum iso-intensity manifolds is shown in Figure 8.5a and 8.5e. A nesting of extremum iso-intensity manifolds is directly obtained, since the intensity of the extremum changes monotonically (either increases in case of a minimum, or decreases in case of a maximum). As a consequence,

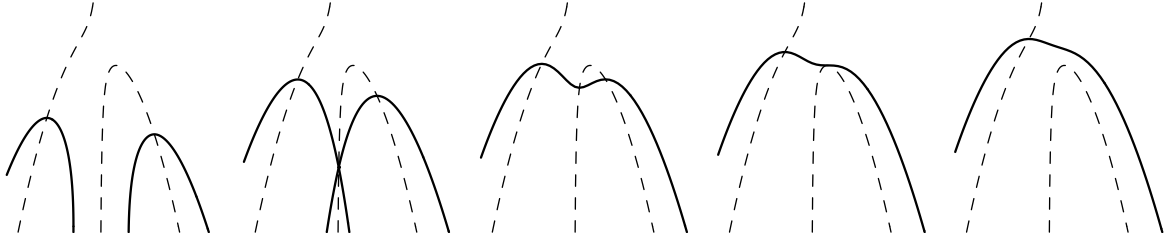


Figure 8.5: Critical curves (dashed curves, on the left one extremum branch  $e_1$ , on the right a saddle branch and extremum branch  $e_2$ , annihilating in the top point, see Definition 37) with subsequent iso-intensity manifolds (thick curves)  $c_1, \dots, c_5$ . a) Two distinct extremum iso-intensity manifolds, see Definition 38,  $I_{c_1}(e_1)$  and  $I_{c_1}(e_2)$  with their top of the cones at the extremum branch. At the same time they are both extremum manifolds, see Definition 39,  $M_{c_1}(e_1)$  and  $M_{c_1}(e_2)$ . b) The two touching extremum iso-intensity manifolds  $I_{c_2}(e_1)$  and  $I_{c_2}(e_2)$  are not extremum manifolds. They form the manifolds  $U_{c_2}(e_1)$  and  $U_{c_2}(e_2)$ , see Definition 40. c) The extremum iso-intensity manifold  $I_{c_3}(e_1)$  (with its top of the cone at the extremum branch  $e_1$ ) is not an extremum manifold, since it intersects  $e_2$ . d) The extremum iso-intensity manifold  $I_{c_4}(e_1)$  forms the manifold  $L_{c_4}(e_1)$ . It touches  $e_2$  at the annihilation point. e) The extremum iso-intensity manifold  $I_{c_5}(e_1)$  is again an extremum manifold  $M_{c_5}(e_1)$ .

each manifold exists for a scale interval  $[t_0, t_{\max}]$ . Recall that there is no creation of level lines, one of the (implicit) axioms leading to the diffusion equation. Consequently, each manifold transversally intersects the initial image, cf. Koenderink's "open end of the tube-like structure". The top of this structure is located at  $t_{\max}$ : by construction the spatial extremum on the branch  $i$  forms the top of the scale space dome.

Before turning to  $(n + 1)$ -dimensional segments, we first define to special types of extremum iso-intensity manifolds.

**Definition 40** An upper limiting manifold  $U_c(e_i)$  is an extremum iso-intensity manifold  $I_c(e_i)$ , such that  $I_{c+\delta\epsilon}(e_i) = M_{c+\delta\epsilon}(e_i)$ ,  $0 < \epsilon \ll 1$  and  $\delta = 1$  if  $e_i$  is a maximum and  $\delta = -1$  if  $e_i$  is a minimum, but  $I_c(e_i)$  is not an extremum manifold. If the maximum (minimum) branch  $e_i$  intersects  $n$  upper limiting manifolds, they are ordered on decreasing (increasing) intensity and labeled  $U_{c_j}(e_i)$  for  $j = 1, \dots, n$ .

A lower limiting manifold  $L_c(e_i)$  is an extremum iso-intensity manifold  $I_c(e_i)$ , such that  $I_{c+\delta\epsilon}(e_i) = M_{c+\delta\epsilon}(e_i)$ ,  $0 < \epsilon \ll 1$  and  $\delta = -1$  if  $e_i$  is a maximum and  $\delta = 1$  if  $e_i$  is a minimum, but  $I_c(e_i)$  is not an extremum manifold. If the maximum (minimum) branch  $e_i$  intersects  $n$  lower limiting manifolds, they are ordered on decreasing (increasing) intensity and labeled  $U_{c_j}(e_i)$  for  $j = 1, \dots, n$ .

An example is given in Figure 8.5. The extremum iso-intensity manifolds  $U_{c_2}(e_1)$  and  $U_{c_2}(e_2)$  are shown in Figure 8.5b. Manifolds below these two limiting manifolds (e.g. those in Figure 8.5a) are extremum manifolds. The extremum iso-intensity manifold  $L_{c_4}(e_1)$  is shown in Figure 8.5d. Manifolds above this limiting manifold (e.g. the one in Figure 8.5e) are extremum manifolds.

The next definitions construct  $(n + 1)$ -dimensional segments out of the  $n$ -dimensional iso-manifolds using the two limiting manifolds.

**Definition 41** The extremum segment  $E^1(e_i)$  is the volume in the scale space image under upper limiting manifold  $U_{c_1}(e_i)$ .

The extremum segment  $E^j(e_i)$ ,  $j > 1$ , is the volume in the scale space image under upper limiting manifold  $U_{c_j}(e_i)$  and above lower limiting manifold  $L_{c_{j-1}}(e_i)$ .

For  $0 < j < n$ ,  $I^j(e_1)$  is the scale space volume bounded by  $E^j(e_1)$  and  $E^{j+1}(e_1)$ .

In Figure 8.5, the extremum segments  $E^1(e_1)$  and  $E^1(e_2)$  are formed by the area beneath the manifolds  $U_{c_2}(e_1)$  and  $U_{c_2}(e_2)$ , respectively. Note that in Figure 8.5, if  $e_1$  would intersect at some intensity level  $c_6$  a second upper limiting manifold  $U_{c_6}(e_1)$ , the area between  $L_{c_4}(e_1)$  and  $U_{c_6}(e_1)$  would also form an extremum segment,  $E^2(e_2)$ . Then the area between  $L_{c_4}(e_1)$  and  $U_{c_2}(e_1)$  forms the scale space volume  $I^1(e_1)$ .

So this definition yields Koenderink's tubes, but not only them. Extremum branches may intersect multiple extremum segments: From the "extremum branch point of view", starting at the initial image the branch  $e_i$  firstly intersects extremum manifolds until for some intensity  $c$  the iso-intensity manifold  $I_c(e_i)$  contains a (scale space) saddle and becomes the union of two juxtaposed iso-intensity manifolds that intersect non-transversal. Note that at this point the manifold generated from  $e_i$  equals  $U_c(e_i)$ . Call the other part  $U_c(e_j)$ .

Continuing, two things can happen. The manifold  $U_c(e_i) \cup U_c(e_j)$  is either  $I_c(e_i)$  or  $I_c(e_j)$ . If the extremum branch  $e_i$  vanishes, *i.e.* it annihilates with the saddle branch containing the aforementioned saddle, the remaining part of the branch is no longer global top of a manifold, but part of the iso-intensity manifold  $I_c(e_j)$ . If it remains,  $e_j$  annihilates with intensity  $c_a$ , and the branch intersects the closed set of manifolds  $[I_c(e_i), \dots, I_{c_a}(e_i)]$  and additionally again extremum manifolds. Here  $I_{c_a}(e_i)$  equals  $L(e_i)$  for a second extremum segment, *cf.* Figure 8.5 and the branches  $e_1$  and  $e_2$ .

Note that there is no third possibility, since then the iso-intensity manifold through the saddle must contain two global extrema at the same scale. This was proven to be non-generic. This observations lead to the following definition.

**Definition 42** The scale space segment  $SSS(e_i)$  of an extremum branch  $e_i$  intersecting  $n$  extremum segments is

$$SSS(e_i) = \left( \bigcup_{j=0}^n U_{c_j}(e_i) \cup E^j(e_i) \right) \cup \left( \bigcup_{j=0}^{n-1} I^j(e_i) \right).$$

The critical manifold  $C(e_i)$  is the boundary of  $SSS(e_i)$ .

Recalling Figure 8.5, the right extremum branch  $e_2$  has one extremum segment, being the scale space segment, bounded by  $U_{c_2}(e_2) = C(e_2)$ . The left extremum branch has *no* scale space segment, since the second series of extremum manifolds starting above  $L_{c_4}(e_1)$  is unbound. Assuming again a second upper limiting manifold  $U_{c_6}(e_1)$  at intensity level  $c_6$ ,  $e_1$  intersects two extremum segments. Then  $U_{c_6}(e_1)$  forms the critical manifold  $C(e_1)$ . This manifold encapsulates  $C(e_2)$ . Then  $SSS(e_2) = E^1(e_1) \cup E^2(e_1) \cup I^1(e_2)$ , the complete area beneath the manifold  $U_{c_6}(e_1)$  and in this example  $SSS(e_2) \subset SSS(e_1)$ .

By definition,  $C(e_i)$  is  $U_{c_n}(e_i)$ , the supremum of the possible values  $c$  for which  $M_c(e_i)$  exists. Since all but one extremum in the initial image annihilate with spatial saddle points, all but one extremum branch define critical manifolds. The critical manifold contains one spatial saddle, that can be located either in scale space (and thus being a scale space saddle) or at the initial image. This saddle obviously relates the extremum branch to another extremum branch, namely the one to which it is secondary in the intensity hierarchy. It is convenient to denominate this remainder of the iso-intensity manifold.

**Definition 43** Let  $C(e_i) \subset I_c(e_k)$  and  $(\mathbf{x}; t)$  be the saddle on  $C(e_i)$ . Then the dual critical manifold  $D(e_i)$  is defined as

$$\begin{aligned} D(e_i) \cup C(e_i) &= I_c(e_i), \\ D(e_i) \cap C(e_i) &= (\mathbf{x}; t). \end{aligned}$$

Note that in this definition the critical curves  $e_k$  and  $e_i$  do *not* coincide. Recalling Figure 8.5,  $D(e_2)$  is formed by  $U_{c_2}(e_1)$ . In the following we will use this route to derive a unique algorithm deriving the hierarchy enclosed in the scale space image. Firstly, we will give some examples to clarify the definitions and notation.

### Example

Consider a part of the scale space image in which a catastrophe takes place, together with a second extremum in the neighbourhood. Furthermore, take the scale range such that also a scale space saddle is present. So this part contains two critical curves, of which one contains a catastrophe point and a scale space saddle. For simplicity we assume the two extrema are maxima. Reasoning for minima is alike. An example is given in Figure 8.6. Note that this image is the extension of Figure 8.5 with an extra dimension.

The dark lines show the critical curves in scale space. The right curve contains two branches of critical points, on the left spatial saddles, on the right spatial extrema ( $e_r$ ). The left curve contains an extremum curve without catastrophe points ( $e_l$ ).

- Figure 8.6a shows the case with some “large” intensity  $c_1$ . Both extremum branches intersect extremum manifolds,  $M_{c_1}(e_l)$  and  $M_{c_1}(e_r)$ .
- Decreasing the intensity, both manifolds intersect non-transversal, as shown in Figure 8.6b. Now the manifolds belonging to  $e_l$  and  $e_r$  have become  $U(e_l)$  and  $U(e_r)$ , respectively. The point of intersection is the scale space saddle. Since  $e_r$  is the vanishing extremum branch,  $U(e_r)$  is defined as the critical manifold  $C(e_r)$ , and  $U(e_l)$  is its dual  $D(e_l)$ . The parts enclose the extremum segments  $E(e_l)$  and  $E(e_r)$ , respectively. The volume enclosed by  $C(e_r)$ , *i.e.*  $E(e_r)$ , is the scale space segment  $SSS(e_r)$ .
- Decreasing intensity further, the manifold has  $e_l$  as its global top, as is visible in Figure 8.6c. Note that although  $e_r$  still exists, there is no extremum iso-intensity manifold assigned to it. However, its influence on  $e_l$  is that for this intensity  $e_l$  is only an extremum iso-intensity manifold, and not an extremum manifold: This manifold intersects both extremum branches; also the saddle branch is intersected twice.
- This situation remains until the intensity is decreased to that of the annihilation of the right extremum. From that intensity,  $e_l$  is again an extremum manifold, as shown in Figure 8.6d. So the annihilation intensity forms  $L(e_l)$  for a potential second extremum segment  $E^2(e_l)$ .

There is one scale space segment:  $SSS(e_r)$ . The left extremum branch doesn’t define a scale space segment, since there is – in this example – no limit to the manifolds  $M_c(e_l)$  for decreasing  $c$ . Only if it is assumed that this image is part of a larger image, an upper limiting manifold resulting in the segment  $E^2(e_l)$ , and a scale space segment  $SSS(e_l)$  may be found.

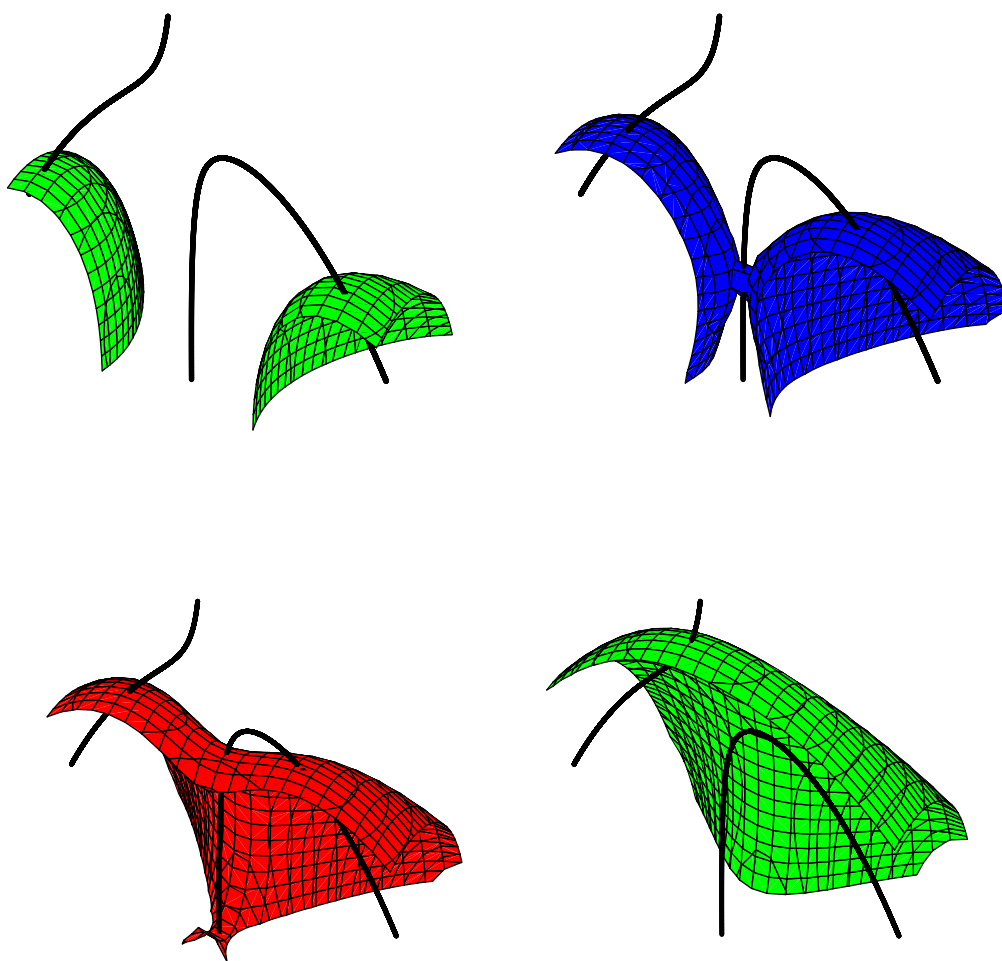


Figure 8.6: Subsequent iso-intensity manifolds and critical curves. Top-left: The extremum manifolds intersect the extremum branches, *cf.* Figure 8.5a. Top-right: The extremum iso-intensity manifolds touch at the scale space saddle, *cf.* Figure 8.5b. Bottom-left: The extremum iso-intensity manifold has its top on the left extremum branch, but intersects also the other extremum branch, *cf.* Figure 8.5c. Bottom-right: The extremum manifold intersects only the left extremum branch, *cf.* Figure 8.5e.

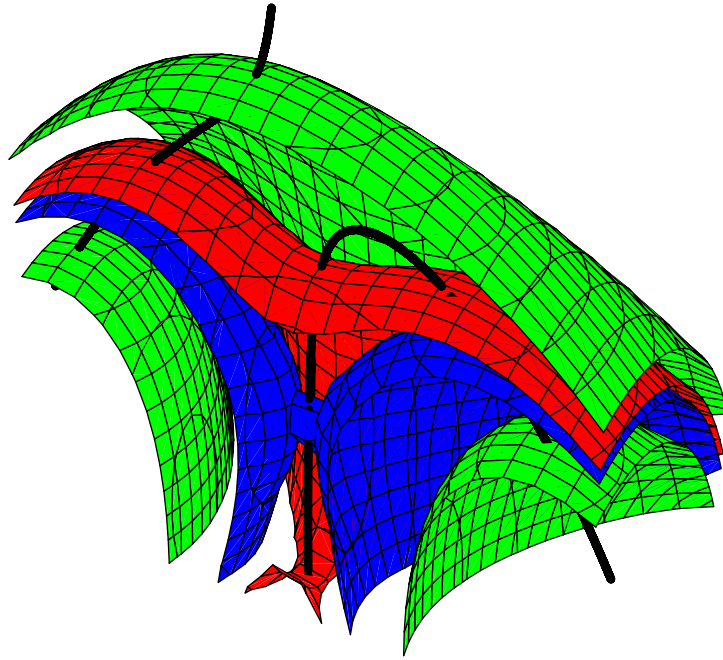


Figure 8.7: Nesting of iso-intensity manifolds and critical curves. See text for details.

It is clear that the left extremum branch contains two disjoint intensity intervals on which extremum manifolds are defined. The boundaries of these intervals are given by the intensities of the scale space saddle and the annihilation.

The nesting of the iso-intensity manifolds is shown in Figure 8.7.

### A More Complicated Example

A more complicated example involving two scale space saddles and two annihilations, is visualised in Figure 8.8, showing the hierarchy of the two manifolds induced by the intensities  $c_1$  and  $c_2$  of the scale space saddles.

Again the dark lines show critical curves, from left to right extremum 1, saddle 1, extremum 2, saddle 2, and extremum 3. Extremum 2 annihilates with saddle 2, extremum 3 annihilates with saddle 1. Extremum 1 remains.

In Figure 8.9 the two manifolds through the scale space saddles are shown separately. In the left image, the iso-intensity manifold around  $e_2$  and  $e_3$  is plotted:  $I_{c_1}(e_2) = I_{c_1}(e_3)$ . The left part of the

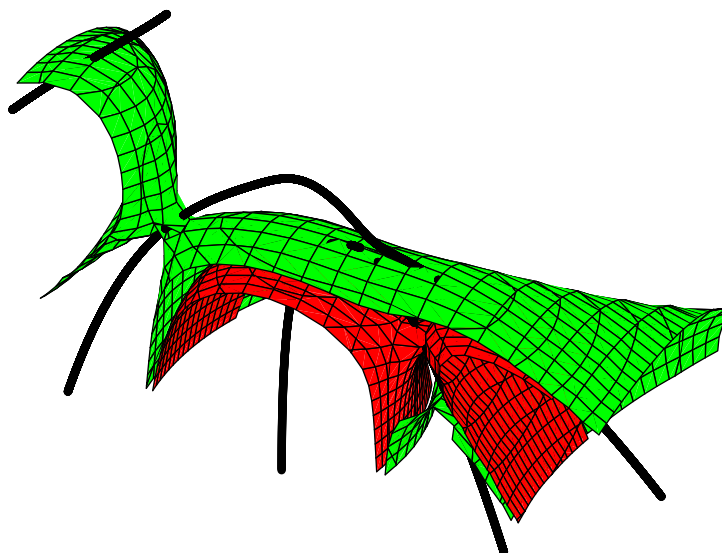


Figure 8.8: Iso-intensity manifolds and critical curves. See text for details.

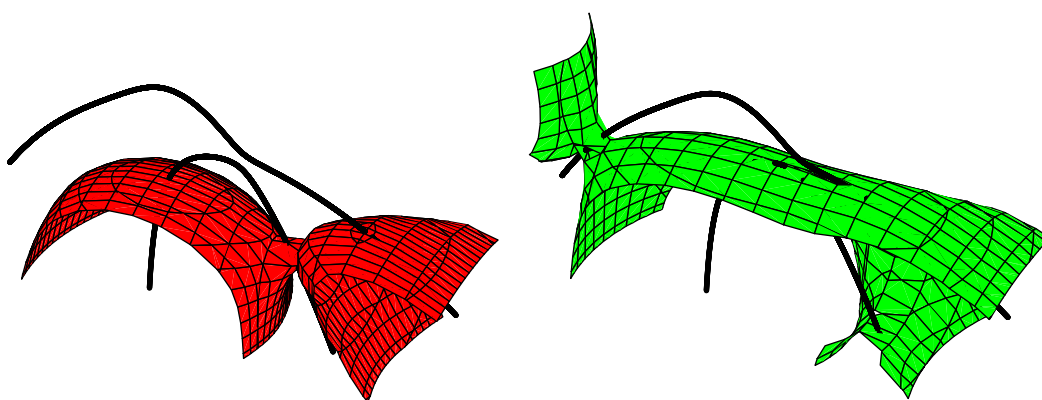


Figure 8.9: Iso intensity manifolds and critical curves. See text for details.

manifold equals  $C(e_2)$ , the right part  $D(e_2)$ . In contrast to the previous example, here also extremum  $e_3$  annihilates, inducing another critical manifold,  $C(e_3)$ , shown in the right image, together with the dual  $D(e_3)$ .

Now the critical manifold  $C(e_3)$  encapsulates  $I_{c_1}(e_2)$  and consequently both  $C(e_2)$  and  $D(e_2)$ . Therefore, it may (and in this case: does) split into two disconnected spatial regions if it is traced into negative scale direction due to the intersection of the saddle branch of saddle 2. Here the scale space segment  $SSS(e_3)$  exists of two connected “legs” encapsulating the extrema 2 and 3. The critical manifold  $C(e_3)$  forms the “trousers” with two open ends at the initial image.

### 8.4.2 Hierarchy Algorithm

The previously described hierarchy of manifolds entails a uniquely defined description of the image, based on the critical and dual manifolds. This description is obtained by executing the following steps (that are followed by an example based on the image of the previous section):

1. Initializing:
  - (a) Build a scale space.
  - (b) Find the critical points at each scale level.
  - (c) Construct the critical branches.
  - (d) Find the catastrophe points.
  - (e) Construct and label the critical curves, including the one remaining extremum.
  - (f) Find the scale space saddles.
2. Determining the manifolds
  - (a) For each annihilating extremum  $e_i$ , find its critical iso-intensity manifold  $C(e_i)$ .
  - (b) Construct the dual manifolds  $D(e_i)$ .
3. Label to each extremum branch the dual manifolds it intersects, sorted on intensity.
4. Build a tree:
  - (a) Start with the remaining extremum at the coarsest scale as root.
  - (b) Trace to finer scale until at some value it is labeled to a dual manifold.
  - (c) Split into two branches, one the branch containing the existent extremum and assigned to the dual manifold, the other containing the extremum assigned to the critical manifold.
  - (d) Continue for all branches / extrema until all extrema are added to the tree.
5. Bonus step: return a segmentation
  - (a) Based on the binary combinations of region belonging to each defined  $C(e_i)$ .
  - (b) Based on the binary combinations of region belonging to each defined  $C(e_i) \cup D(e_i)$ .



We note that step 1 has been exploited by the authors in [158]. The other steps follow straightforwardly from the previous exercise and examples. Regarding step 3, the intensities of all extrema either increase or decrease monotonically, and so do the dual manifolds that each intersects.

The tree that is obtained is a binary tree. All annihilating extremum branches intersect a critical manifold, and each critical manifold implies a dual manifold that intersects an extremum branch underneath its own critical manifold. Therefore, all extremum branches are linked in the tree.

The creation of pairs of critical points and their influence has been dealt with elsewhere by the authors. They are not of relevance to the iso-intensity hierarchy, since scale space implies non-creation of new level lines!

As a kind of bonus, one obtains a “knowledgeless” segmentation, solely based on the hierarchy tree. This can be the concatenation of the scale space segments, or one of the scale space segments together with their dual segments.

### Example – continued

Returning to the second example of the previous section, recall Figure 8.8.

1. Obviously, step 1 has been taken.
2. The algorithm yields in step 2a the two cones  $C(e_2)$  and  $C(e_3)$ . Step 2b yields the dual cones  $D(e_2)$  (intersecting  $e_3$ ) and  $D(e_3)$  (intersecting  $e_1$ ).
3. Step 3 gives the lists  $e_1 \rightarrow D(e_3)$ ,  $e_3 \rightarrow D(e_2)$ .
4. The tree is built by tracing down as root the remaining extremum,  $e_1$ . At some scale level it intersects  $D(e_3)$ , so a node is added and the tree splits into two branches  $e_1$  and  $e_3$ . Extremum  $e_1$  doesn't intersect any dual manifolds and doesn't split anymore. Extremum  $e_3$  intersects  $D(e_2)$ , so a node and a new branch ( $e_2$ ) is created.

Although the hierarchy dependency is obtained by the dual manifolds, we will use the critical manifolds for labeling the tree, since they identify a unique part of the scale space image to an extremum. The (binary) hierarchy tree can be collapsed into one single one-dimensional expression. The nodes of the tree are replaced by  $(e_i, e_j)_{C(e_j)}$ , stating that  $e_i$  is both parent and child, and  $e_j$  is child due to the fact that its dual manifold is assigned to  $e_i$ . So we have, starting at the root, firstly  $(e_1, e_3)_{C(e_3)}$ , and secondly the replacement of  $e_3$  by  $(e_2, e_3)_{C(e_2)}$ . Consequently, the tree reduces to

$$\left( e_1, (e_2, e_3)_{C(e_2)} \right)_{C(e_3)}$$

This is to be read as “extrema 2 and 3 are related by means of the intensity of the critical manifold of extremum 2. Extremum 2 annihilates and extremum 3 is (then) related to extremum 1 by means of the intensity of the critical manifold of extremum 3”. This parentheses formula can be extended at liberty.

### 8.4.3 Visualisation and Simplification

The binary tree can easily be visualised. One way to do this, is by only displaying the scale space segments at the initial image. This has been done by the authors in [158]. A disadvantage is that the

remaining extremum does not induce a scale space segment, and is thus not visible. Here we propose a visualisation strategy based on the critical manifolds together with their duals. Of both approaches we give examples.

As advantage of the latter method, now the remaining extremum is visualised. Also “more or less” symmetries appear, as we will see. Implementation is straightforward, by using a  $(n + 1)$ -dimensional region growing algorithm with as seed point the saddle point connecting the critical manifold and its dual.

Simplification of the structure, or “logical filtering”, is done by sweeping out parentheses from inside to outside. Equivalently one can sweep from the leaves of the tree inwardly. The closer to the root, the more significant parts of the image are represented. The “details” are stored in the leaves ([139]). Then, for instance, example 2 could be simplified as follows:

$$\left( e_1, (e_2, e_3)_{C(e_2)} \right)_{C(e_3)} \rightarrow (e_1, e_3)_{C(e_3)}$$

That is, Figure 8.8 is reduced to the Figure 8.9b.

Note that in this hierarchy the nodes connect regions regardless of scale. For example, a small region may vanish at fine scale, but at a small intensity value. If the dual manifold encapsulates a maximum as final parent, the top of this dual dome may be achieved at very coarse scale. If it encapsulates several extrema, the logically filtered image at the initial image shows several dual regions: these dual regions necessarily encapsulate these extrema, but do not need to be connected. Examples will pop up in more realistic images in the next section.

## 8.5 Results

The hierarchical algorithm and the possible application of logical filtering are investigated on two test images. As an artificial image allowing algebraic verification, firstly the 81 x 81 image is built by adding four blobs. This image is shown in Figure 8.10a. Secondly we used the artificial MR image Figure 8.14a, taken from the *Brain Web* [40, 41, 163], web site <http://www.bic.mni.mcgill.ca/brainweb>.

### 8.5.1 Blob Image

The scale space of this image was built by taking 113 scales,  $e^{i/32} i = 1, \dots, 113$ . The initial image contains five extrema and four saddles. One extremum, the minimum in the middle, is induced by the four extrema. Within the scale space, three scale space saddles were found: They connect cones around each vanishing extremum to the final remaining extremum. These three scale space saddles are located on saddle branches annihilating with the maximum branches. The saddle branch annihilating with the minimum branch does not contain a scale space saddle, so the value of the saddle at the initial image yields the intensity for the critical manifold encapsulating the minimum.

The labelling of the extrema and saddles is shown in Figure 8.10b. At coarsest scale, extremum  $e_4$  remains. It thus forms the root. It is found that only this extremum branch belongs to dual manifolds, yielding the hierarchy tree shown in Figure 8.11.

The Koenderink-parentheses-formula is

$$\left( e_5, \left( e_3, \left( e_1, (e_4, e_2)_{C(e_2)} \right)_{C(e_1)} \right)_{C(e_3)} \right)_{C(e_5)}$$

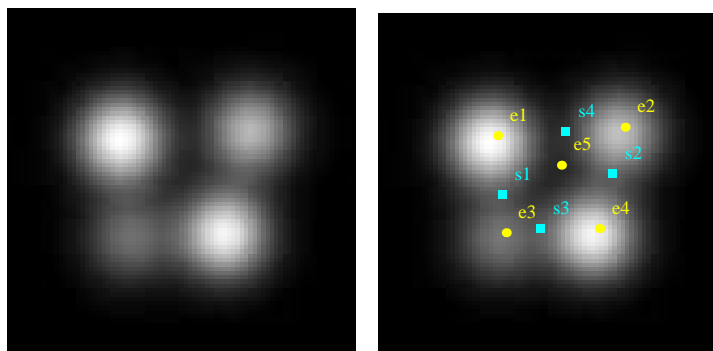


Figure 8.10: Left: Artificial image built by combining four maxima and one minimum. Right: Labelling of the critical points.

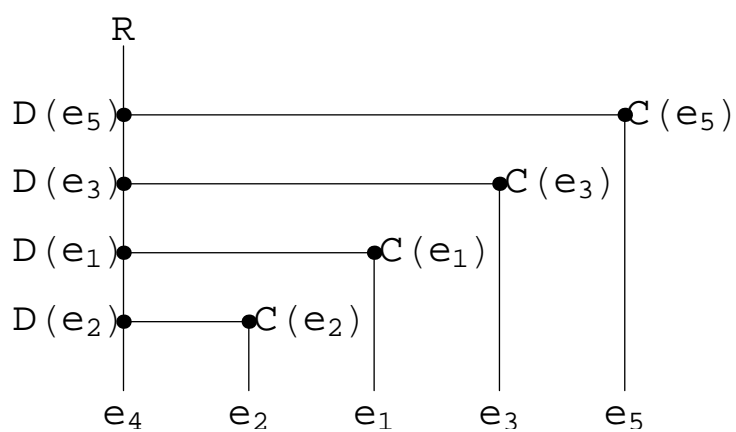


Figure 8.11: Hierarchy tree belonging to the artificial blob-image.

Logical filtering implies firstly removing the minimum  $e_5$ , the maximum  $e_3$  (the least brightest), and so on.

The area in the initial image belonging to the scale space segments, encapsulated by the critical manifolds, and those encapsulated by the dual manifolds, is shown in Figure 8.12. Each row shows the areas encapsulated by  $C(e_i)$ ,  $C(e_i) \cup D(e_i)$ , and  $D(e_i)$ , for  $i = 1, 2, 3$  for the first, second and third row, respectively. As can be seen,  $e_3$  yields a dual manifold containing three other extrema: the “critical intensity” of the scale space saddle is the lowest of all three scale space saddles. At increasing scale firstly  $D(e_2)$  is intersected, secondly  $D(e_1)$  and thirdly  $D(e_3)$ , as follows directly for the hierarchy tree of Figure 8.11.

Figure 8.13b shows the segmentation obtained when only the area of critical cones are plotted: the four regions belonging to the four annihilating extrema. Note that the minimum does not have a critical cone through a scale space saddle, but through the saddle at the initial image. Figure 8.13a extends Figure 8.13b by showing also the area of the dual manifolds. This elegantly shows the remaining blob  $e_4$ , but also the hierarchy: the area around  $e_3$  is less bright than that around  $e_1$ , which in turn is less bright than that around  $e_2$  and  $e_4$ . This effect is due to the number of encapsulating dual manifolds.

### 8.5.2 MR Image

The MR image, shown in Figure 8.14a, contains 812 extrema. For visualisation purposes we take as initial scale  $t = 8.39$ , yielding the image shown in Figure 8.14b.

This image contains 7 extrema, as labelled in the image. The scale space image in the scale range  $t \in (8.39, 33.1)$  is exponentially sampled by 89 scales. This yields the following annihilating couples:  $(e_1, s_3)$ ,  $(e_2, s_2)$ ,  $(e_3, s_4)$ ,  $(e_5, s_6)$ ,  $(e_6, s_1)$ , and  $(e_7, s_5)$ . On the saddle branches of the saddles  $s_1, s_2, s_3, s_5$  scale space saddles are found. The saddle branches  $s_4$  and  $s_6$  have their global extremal intensity at the initial scale (8.39). The intersections of the image at scale  $t = 8.39$  and the manifolds  $C(e_i)$  and  $D(e_i)$  for  $i \in [1, \dots, 7]$  (except, of course,  $e_4$ ) are shown in Figure 8.15, labelling from left to right, top to bottom. Note that the critical manifold and its dual can appear both juxtaposed and nested. The top row represents the regions belonging to the maxima in the initial image, the bottom row to the minima.

The labelling of extrema to dual manifolds gives the following sequences:

$$\begin{aligned} e_4 &\rightarrow \{D(e_6), D(e_2), D(e_3)\} \\ e_6 &\rightarrow \{D(e_7), D(e_5)\} \\ e_2 &\rightarrow \{D(e_1)\} \end{aligned}$$

The hierarchy tree belonging to it is shown in Figure 8.16.

The corresponding segmentation based on the binary combinations of region belonging to each defined  $C(e_i) \cup D(e_i)$ ,  $i \in [1, \dots, 7]$  is shown in Figure 8.17a. The close nesting of the intersection manifolds is visualised in Figure 8.17b. This suggests that for the sake of a “meaningful” segmentation, certain extrema are less important than others, or even redundant altogether. Taking into account all extrema may in some sense result in an “over-segmentation”.

One target for logical filtering could be identifying all minima regions and all maxima regions. For the tree this would imply removing the leaves  $e_5, e_7$  and  $e_1, e_2, e_3$ , respectively. The parentheses formulation is simplified from

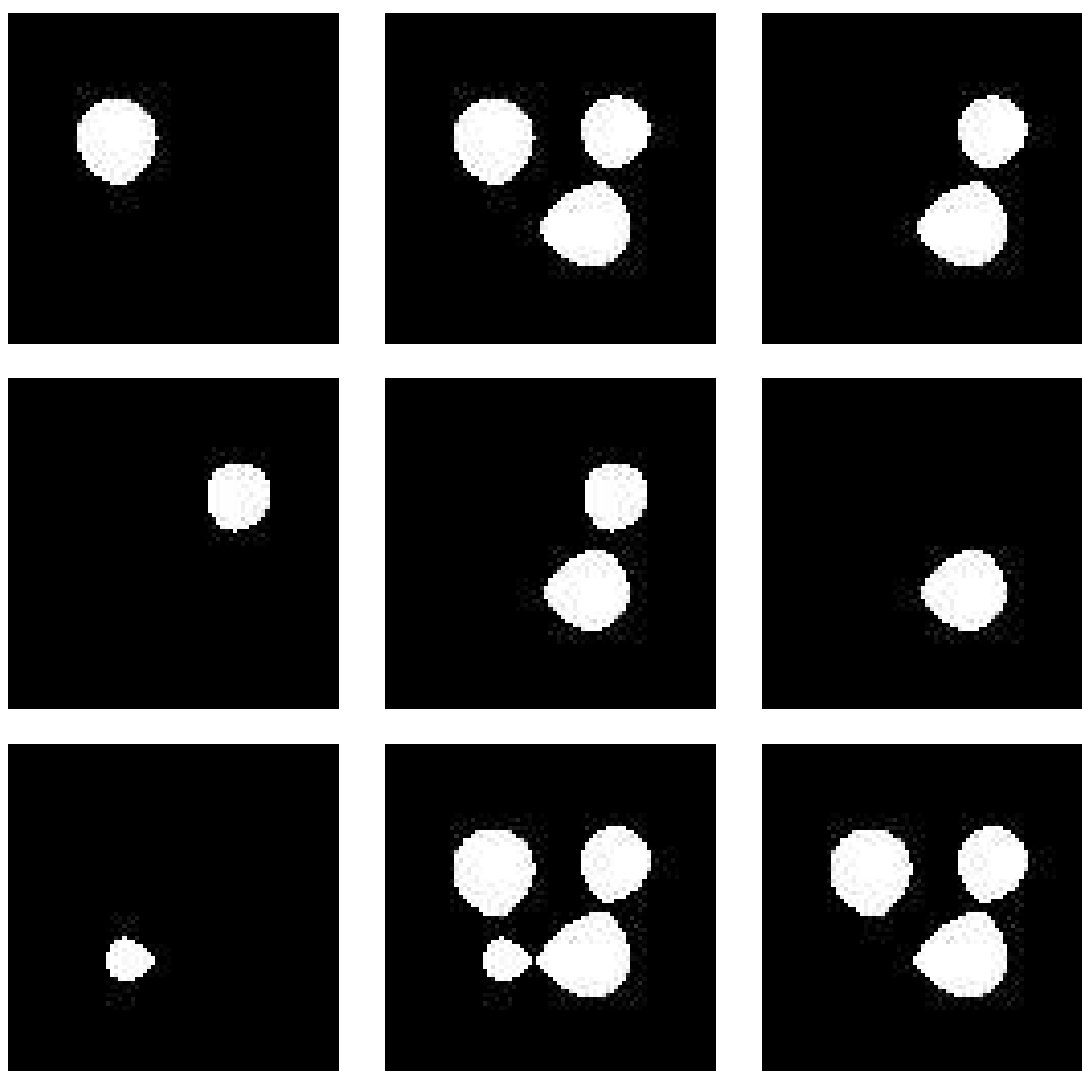


Figure 8.12: Each row: Regions at the initial image encapsulated by the following manifolds for  $i = 1$  (top row),  $i = 2$  (middle row), and  $i = 3$  (bottom row): Left:  $C(e_i)$ , Middle:  $C(e_i) \cup D(e_i)$ , Right:  $D(e_i)$ .

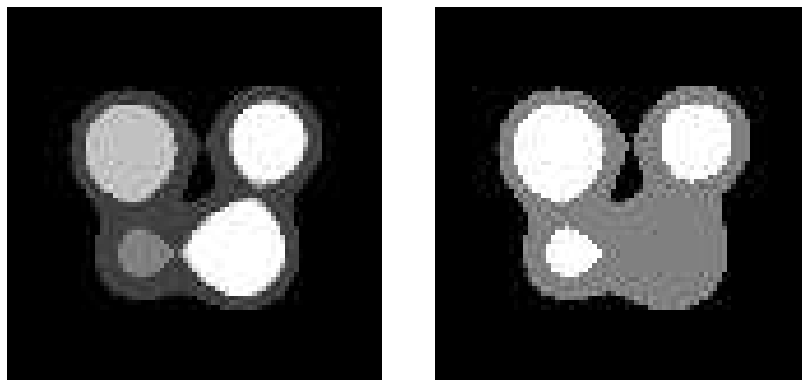


Figure 8.13: Left: Segmentation based on the binary combinations of region belonging to each defined  $C(e_i) \cup D(e_i), i \in [1, \dots, 5]$ . Right: Segmentation based on the binary combinations of region belonging to each defined  $C(e_i), i \in [1, \dots, 5]$ .

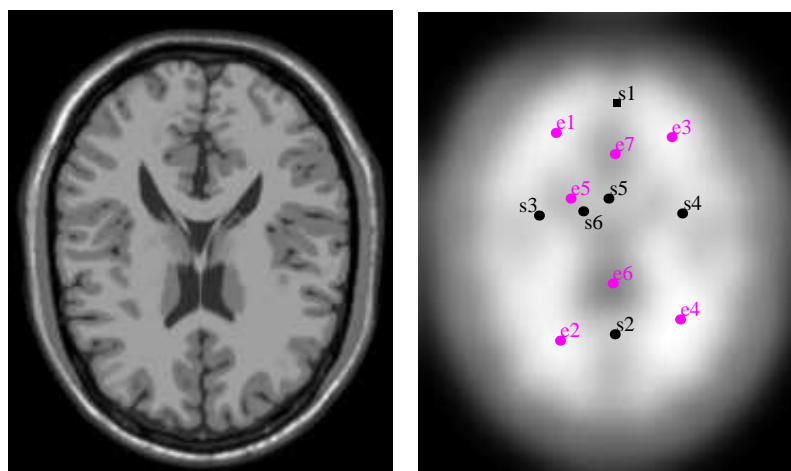


Figure 8.14: Left: 181 x 217 artificial MR image. Right: MR image at scale  $t = 8.37$ .



Figure 8.15: Contours of the critical and dual manifolds at the MR image at scale 8.39. Top row: Left)  $C(e_1)$  (lower contour) and  $D(e_1)$ . Middle)  $C(e_2)$  (left contour) and  $D(e_2)$ . Right)  $C(e_3)$  (upper part of the contour) and  $D(e_3)$ . Bottom row: Left)  $C(e_5)$  (top left part of the contour) and  $D(e_5)$ . Middle)  $C(e_6)$  (inner contour) and  $D(e_6)$ . Right)  $C(e_7)$  (small circle) and  $D(e_7)$ .

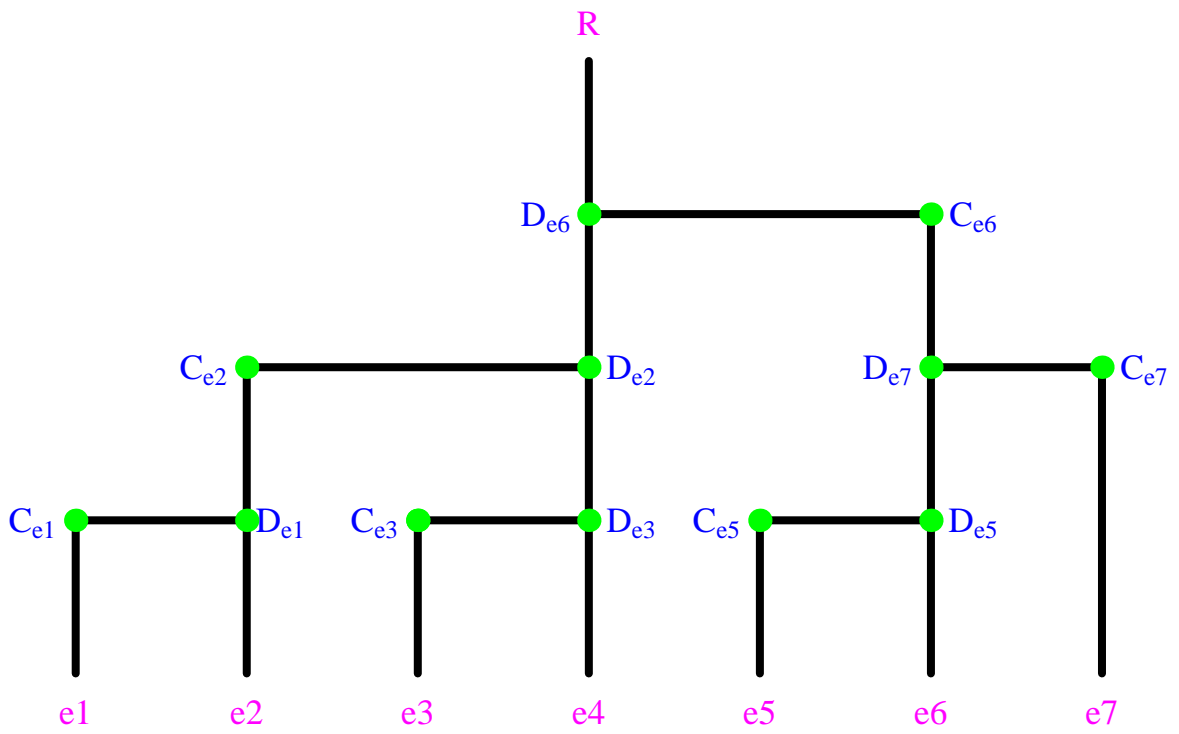


Figure 8.16: Hierarchy tree for the MR image.



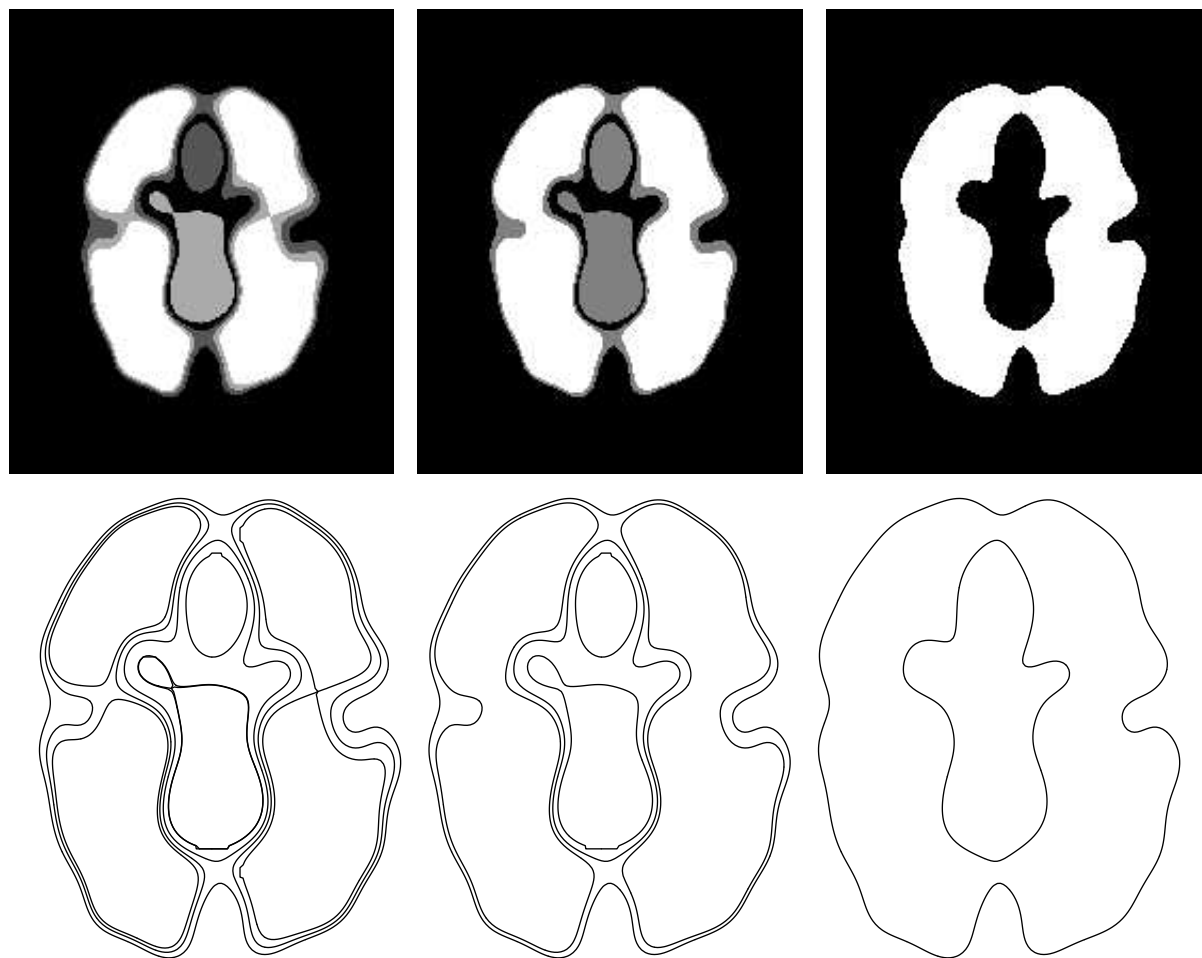


Figure 8.17: Example of logical filtering. Top row: Segmentation based on the binary combinations of region belonging to each defined  $C(e_i) \cup D(e_i)$ , from left tot right according to a) Eq. (8.15), b) Eq. (8.16), c) Eq. (8.17). Bottom row, d-f): Nesting of the corresponding contours as shown in the top row

$$\left( \left( (e_1, e_2)_{C(e_1)}, (e_3, e_4)_{C(e_3)} \right)_{C(e_2)}, \left( (e_5, e_6)_{C(e_5)}, e_7 \right)_{C(e_7)} \right)_{C(e_6)} \quad (8.15)$$

via (for example!)

$$\left( (e_2, e_4)_{C(e_2)}, (e_6, e_7)_{C(e_7)} \right)_{C(e_6)} \quad (8.16)$$

to

$$(e_4, e_6)_{C(e_6)} \quad (8.17)$$

This sequence of simplification is visualised in Figure 8.17. The top row shows the simplification of the binary combinations of regions belonging to selected manifolds, the bottom row shows the involved isophotes (intersections of the manifolds with the images at scale 8.37). The left couple of Figure 8.17 visualise Eq. (8.15). The first reduction of Eq. (8.16) is shown by the middle pair of images of Figure 8.17. The final simplification of Eq. (8.17) yields the right set of images in Figure 8.17. This illustrates the remark on “redundancy” quite neatly.

## 8.6 Summary and Discussion

In this chapter we investigated the deep structure of Gaussian scale space. A scale space image is obtained by convolution of an initial image with a normalised Gaussian with variable width, or scale. We showed that the critical curves, obtained when increasing scale, provide useful information for deriving a hierarchy structure that solely depends on intrinsic entities of the scale space.

Firstly, we investigated the mathematical properties of the vector field proposed by Koenderink. We showed that its characteristic behaviour is well-defined on all non-critical points. On Morse critical points a linear expansion suffices to derive the local vector field. It is *always* topologically equivalent to a vector field containing only minima (source nodes) and corresponding saddles. Non-Morse critical points are separated into two groups in  $n$ -D images,  $n > 1$ , namely those where the determinant of the Hessian vanishes (catastrophe points) and those where the Laplacean is zero (scale space saddles). The first group can easily be evaluated, the second group is more difficult to examine and the structure of iso-intensity contours through them gives more insight in the local structure around these points. In one dimensional images these groups coincide. It appears that the vector field proposed by Koenderink is a powerful tool in understanding the structure of an image at all levels of resolution simultaneously.

Secondly, we investigated the properties of the manifolds obtained by the integral curves of the vector field. We showed that to each extremum uniquely a scale space segment can be assigned. To this segment a natural extension can be made by means of its “dual” segment. Both segments have an manifold of co-dimension one as boundary with the same intensity. Their intersection contains one point, either a scale space saddle with the scale space image, or a spatial saddle point in the initial image. The maximum (or causality) principle guarantees that all iso-intensity manifolds in scale space behave proper, *i.e.* they are nicely nested and, they form surfaces that are closed above (at high scale) and have open ends in the initial image. No new manifolds are created upon coarsening.

The dual manifold, as boundary of the dual segment, provides the information needed for automatic building a (binary) hierarchy tree, that can be represented as a nested sequence (parentheses formulation) of related extrema and their linking saddle. This reduced representation of the image allows one to “filter

logically”. Parts of the tree, or sub-parentheses structures can be filtered out. It merely boils down to filter out certain preselected parts of the image.

We gave a theoretical expose to derive a self explanatory algorithm. This algorithm was applied to two test images, showing the usefulness of the conceptual ideas behind it.

Again we emphasise that the structure obtained is without any a priori information and is solely derived from the fact that convolution with a Gaussian (as test, or regularisation function in mathematical sense) is necessary in order to be able to perform well-defined continuous operations on a discrete image. The proposed hierarchy is thus induced by this mathematical concept.

As possible applications one can think of – besides of course user-independent segmentation and image simplification – image storage using compressed information, transmission by means of “significant data first”, image comparison, both searching in databases as stereo images, and so on.



---

## Bibliography

---

- [1] L. Alvarez and J. Morel. Morphological approach to multiscale analysis: From principles to equations. In *ter Haar Romeny, [102]*, pages 101–112, 1994.
- [2] D. A. Anderson, J. C. Tannehill, and R. H. Pletcher. *Computational Fluid Mechanics and Heat Transfer*. Hemisphere publishing corporation, 1984.
- [3] V. Anh, J. Y. Shi, and H. T. Tsui. Scaling theorems for zero crossings of bandlimited signals. *IEEE Transactions on Pattern Analysis and Machine Intelligence*, 18(3):309–320, 1996.
- [4] J. Argyris, C. Ciubotariu, and H.-G. Matuttis. Fractal space, cosmic strings and spontaneous symmetry breaking. *Chaos, Solitons and Fractals*, 12(1):1–48, January 2001.
- [5] V. I. Arnold, editor. *Geometrical Methods in the Theory of Ordinary Differential Equations*, volume 250 of *Grundlehren der mathematischen Wissenschaften: A Series of Comprehensive Studies in Mathematics*. Springer-Verlag, Berlin, 1983.
- [6] V. I. Arnold. *Catastrophe Theory*. Springer-Verlag, Berlin, 1984.
- [7] V. I. Arnold, editor. *Ordinary Differential Equations*. Springer-Verlag, Berlin, 1992.
- [8] V. I. Arnold, editor. *Dynamical Systems VI: Singularity Theory I*, volume 6 of *Encyclopaedia of Mathematical Sciences*. Springer-Verlag, Berlin, 1993.
- [9] V. I. Arnold, editor. *Dynamical Systems VIII: Singularity Theory II & Applications*, volume 39 of *Encyclopaedia of Mathematical Sciences*. Springer-Verlag, Berlin, 1993.
- [10] V. I. Arnold, editor. *Dynamical Systems V: Bifurcation Theory and Catastrophe Theory*, volume 5 of *Encyclopaedia of Mathematical Sciences*. Springer-Verlag, Berlin, 1994.
- [11] K. Åström and A. Heyden. Stochastic analysis of image acquisition, interpolation and scale-space smoothing. *Advances in applied probability*, 31(4):855–894, 1999.

- [12] J. Babaud, A. P. Witkin, M. Baudin, and R. O. Duda. Uniqueness of Gaussian kernel for scale-space filtering. *IEEE Transactions on Pattern Analysis and Machine Intelligence*, 8(1):26–33, 1986.
- [13] R. Banuelos and K. Burdzy. On the ‘hot spots’ conjecture of J. Rauch. *Journal of Functional Analysis*, 164:1–33, 1999.
- [14] R. Bass and K. Burdzy. Fiber brownian motion and the hot spots problem. *Duke Mathematical Journal*, 105:25–58, 2000.
- [15] G. K. Batchelor. *An Introduction to Fluid Dynamics*. Cambridge University Press, 1967.
- [16] F. Bergholm. Edge focusing. *IEEE Transactions on Pattern Analysis and Machine Intelligence*, 9:726–741, 1987.
- [17] K. Berkner. Resolution of singularities of convolutions with the Gaussian kernel. *Proc. Amer. Math. Soc.*, 127(2):409–415, 1999.
- [18] S. Biasotti, B. Falcidieno, and M. Spagnuolo. Extended Reeb graphs for surface understanding and description. In *G. Borgefors, I. Nyström, G. Sanniti di Baja (Eds.): Discrete Geometry for Computer Imagery 2000, Lecture Notes in Computer Science 1953*, pages 185–197, 2000.
- [19] S. Biasotti, B. Falcidieno, and M. Spagnuolo. Shape abstraction using computational topology techniques. In *Proceeding of the 7th workshop GEO-7, series on geometric modeling: fundamentals and applications, Parma, Italy*, pages 155–165, 2000.
- [20] J. Bijhold, A. Kuijper, and J.-H. Westhuis. Comparative study of image restoration techniques in forensic image processing. In *SPIE Proceedings Vol. 2942, Leonid I. Rudin, Simon K. Bramble (Eds.): Investigative Image Processing, Boston, MA, USA, 1996*, pages 10–21, 1997.
- [21] J. Blom. *Topological and Geometrical Aspects of Image Structure*. PhD thesis, Utrecht University, 1992.
- [22] J. Blom, J. J. Koenderink, B. M. ter Haar Romeny, and A. M. L. Kappers. Topological image-structure for a discrete image on a hexagonal lattice with finite intensity sampling. *J. of Vis. Comm. and Im. Repr.*, 1992.
- [23] J. Blom, J. J. Koenderink, B. M. ter Haar Romeny, and A. M. L. Kappers. Topological image-structure on a hexagonal lattice. *IEEE Transactions on Pattern Analysis and Machine Intelligence*, 1992.
- [24] J. Blom, B. M. ter Haar Romeny, A. Bel, and J. J. Koenderink. Spatial derivatives and the propagation of noise in Gaussian scale-space. *Journal of Visual Communication and Image Representation*, 4(1):1–13, March 1993.
- [25] R. van den Boomgaard. *Mathematical morphology: Extensions towards Computer Vision*. PhD thesis, University of Amsterdam, the Netherlands, 1992.

- [26] R. van den Boomgaard and L. Dorst. The morphological equivalent of Gaussian scale-space. In *Sporring et al. [233]*, pages 203–220, 1997.
- [27] R. van den Boomgaard and A. Smeulders. The morphological structure of images: The differential equations of morphological scale-space. *IEEE Transactions on Pattern Analysis and Machine Intelligence*, 16(11):1101–1113, 1994.
- [28] W. E. Boyce and R. C. DiPrima. *Elementary Differential Equations and Boundary Value Problems*. John Wiley and Sons, 1977.
- [29] J. W. Bruce and P. J. Giblin. *Curves and Singularities*. Cambridge University Press, 1984.
- [30] K. Burdzy and W. Werner. A counterexample to the hot spots conjecture. *Annals of Mathematics*, 149:309–317, 1999.
- [31] P. J. Burt and E. H. Adelson. The laplacian pyramid as a compact image code. *IEEE Transactions on Communications*, COM-31,4:532–540, 1983.
- [32] A. Cayley. On contour and slope lines. *Lond. Edin. Dublin Phil. Mag. and J. of Sci.*, 18(120):264–268, 1859.
- [33] P. Chaudhuri and J. S. Marron. Scale space view of curve estimation. *The annals of statistics*, 28(2):408–428, 2000.
- [34] I. Chavel and L. Karp. Movement of hot spots in riemannian manifolds. *Journal d'analyse Mathematique*, 55:271–286, 1990.
- [35] Y. Chen, B. C. Vemuri, and L. Wang. Image denoising and segmentation via nonlinear diffusion. *Computers and Mathematics with Applications*, 39(5-6):131–149, 2000.
- [36] S. Chinveeraphan, R. Takamatsu, and M. Sato. Understanding of ridge-valley lines on image-intensity surfaces in scale-space. In V. Hlavac and R. Sara, editors, *Computer Analysis of Images and Patterns*, pages 661–667. Springer, Berlin,, 1995.
- [37] O. Chomat, V. Colin de Verdiere, and J. L. Crowley. Recognizing goldfish? or local scale selection for recognition techniques. *Robotics and Autonomous Systems*, 35:191–200, 2001.
- [38] J. J. Clark. Singularity theory and phantom edges in scale space. *IEEE Transactions on Pattern Analysis and Machine Intelligence*, 10:720–727, 1988.
- [39] J. J. Clark. Authenticating edges produced by zero-crossing algorithms. *IEEE Transactions on Pattern Analysis and Machine Intelligence*, 11:43–57, 1989.
- [40] C. A. Cocosco, V. Kollokian, R. K.-S. Kwan, and A. C. Evans. Brainweb: Online interface to a 3D MRI simulated brain database. In *NeuroImage, vol.5, no.4, part 2/4, S425, 1997 – Proceedings of 3-rd International Conference on Functional Mapping of the Human Brain, Copenhagen, May, 1997*.

- [41] D. L. Collins, A. P. Zijdenbos, V. Kollokian, J. G. Sled, N. J. Kabani, C. J. Holmes, and A. C. Evans. Design and construction of a realistic digital brain phantom. *IEEE Transactions on Medical Imaging*, 17(3):463–468, 1998.
- [42] O. Coulon, I. Bloch, V. Frouin, and J.-F. Mangin. Multiscale measures in linear scale-space for characterizing cerebral functional activations in 3D pet difference images. In *Ter Haar Romeny et al, [106]*, pages 188–199, 1997.
- [43] O. Coulon, J.-F. Mangin, J.-B. Poline, M. Zilbovicius, D. Roumenov, Y. Samson, V. Frouin, and I. Bloch. Structural group analysis of functional activation maps. *Neuroimage*, 11(6):767–782, 2000.
- [44] E. B. Dam and M. Nielsen. Nonlinear diffusion schemes for interactive watershed segmentation. In *3rd MICCAI, Pittsburg, USA, Lecture Notes in Computer Science 1935*, pages 216–225, 2000.
- [45] J. Damon. Local Morse theory for solutions to the heat equation and Gaussian blurring. *Journal of Differential Equations*, 115(2):386–401, 1995.
- [46] J. Damon. Generic properties of solutions to partial differential equations. *Archive for Rational Mechanics and Analysis*, pages 353–403, 1997.
- [47] J. Damon. Local Morse theory for Gaussian blurred functions. In *Sporring et al. [233]*, pages 147–162, 1997.
- [48] J. Damon. Generic structure of two-dimensional images under Gaussian blurring. *SIAM Journal on Applied Mathematics*, 59(1):97–138, 1998.
- [49] J. Damon. Properties of ridges and cores for two-dimensional images. *Journal of Mathematical Imaging and Vision*, 10(2):163–174, 1999.
- [50] H. Dehghan. Zero-crossing contour construction for scale-space filtering. In *31st Asilomar Conference on Signals, Systems and Computers*, pages 1479–1483, 1998.
- [51] E. S. Deutsch. Thinning algorithms on rectangular, hexagonal, and triangular arrays. *Communications of the ACM*, 15(9):827–837, 1972.
- [52] R. Duits, L. M. J. Florack, J. de Graaf, and B. M. ter Haar Romeny. On the axioms of scale space theory, 2001. submitted.
- [53] J. Duncan and N. Ayache. Medical image analysis: Progress over two decades and the challenges ahead. *IEEE Transactions on Pattern Analysis and Machine Intelligence*, 22(1):85–105, 2000.
- [54] D. Eberly. A differential geometric approach to anisotropic diffusion. In *ter Haar Romeny, [102]*, pages 371–392, 1994.
- [55] D. Eberly. *Ridges in Image and Data Analysis*, volume 7 of *Computational Imaging and Vision Series*. Kluwer Academic Publishers, Dordrecht, The Netherlands, 1996.
- [56] D. Eberly, R. Gardner, B. Morse, S. Pizer, and C. Scharlach. Ridges for image analysis. *Journal of Mathematical Imaging and Vision*, 4(4):353–373, 1994.



- [57] D. Eberly and S. Pizer. Ridge flow models for image segmentation. In *SPIE Proceedings on Mathematical Methods in Medical Imaging II*, pages 54–64, 1994.
- [58] J. H. Elder. Are edges incomplete? *International Journal of Computer Vision*, 34(2):97–122, 1999.
- [59] J. H. Elder and S. W. Zucker. Local scale control for edge detection and blur estimation. *IEEE Transactions on Pattern Analysis and Machine Intelligence*, 20(7):699–716, 1998.
- [60] M. Fidrich. Iso-surface extraction in 4-D with applications related to scale space. In *Proceedings of DGCI'96, 6th International Conference on Discrete Geometry for Computer Imagery (Lyon, France, November 1996)*, pages 257–268, 1996. Lecture Notes in Computer Science 1176.
- [61] M. Fidrich. Iso-surface extraction in  $n$ -D applied to tracking feature curves across scale. *Image and Vision Computing*, 16(8):545–556, 1998.
- [62] M. Fidrich and J. Thirion. Stability of corner points in scale space: The effect of small nonrigid deformations. *Computer Vision and Image Understanding*, 72(1):72–83, 1998.
- [63] M. A. Fischler and O. Firschein. *Intelligence: the eye, the brain, and the computer*. Addison-Wesley Publishing Company, 1987.
- [64] L. M. J. Florack. Data, models, and images. Technical Report 96/13, Department of Computer Science, University of Copenhagen, 1996.
- [65] L. M. J. Florack. *Image Structure*, volume 10 of *Computational Imaging and Vision Series*. Kluwer Academic Publishers, Dordrecht, The Netherlands, 1997.
- [66] L. M. J. Florack. A geometric model for cortical magnification. In *S.-W. Lee, H.H. Buelthoff, T. Poggio (Eds.): Biologically Motivated Computer Vision 2000, Lecture Notes in Computer Science 1811*, pages 574–583, 2000.
- [67] L. M. J. Florack. Spatio-frequency trade-off scale for scale-space filtering. *IEEE Transactions on Pattern Analysis and Machine Intelligence*, 22(9):1050–1055, 2000.
- [68] L. M. J. Florack. Non-linear scale-spaces isomorphic to the linear case with applications to scalar, vector and multispectral images. *International Journal of Computer Vision*, 42(1/2):39–53, 2001.
- [69] L. M. J. Florack. Scale-space theories for scalar and vector images. In *Kerckhove [136]*, pages 193–204, 2001.
- [70] L. M. J. Florack. Visuele perceptie en digitale beeldverwerking. *Nieuw Archief voor Wiskunde*, 5/3(1):34–41, 2002. (in Dutch).
- [71] L. M. J. Florack and A. Kuijper. On the behaviour of critical points under Gaussian blurring. Technical Report UU-CS-1998-34, Utrecht University, 1998.
- [72] L. M. J. Florack and A. Kuijper. The topological structure of scale-space images. *Journal of Mathematical Imaging and Vision*, 12(1):65–80, February 2000.

- [73] L. M. J. Florack, R. Maas, and W. J. Niessen. Pseudo-linear scale space theory. *International Journal of Computer Vision*, 31(2/3):247–259, 1999.
- [74] L. M. J. Florack, W. J. Niessen, and M. Nielsen. The intrinsic structure of optic flow incorporating measurement duality. *International Journal of Computer Vision*, 27(3):263–286, 1998.
- [75] L. M. J. Florack, A. H. Salden, B. M. ter Haar Romeny, J. J. Koenderink, and M. A. Viergever. Nonlinear scale-space. *Image and Vision Computing*, 13(4):279–294, May 1995.
- [76] L. M. J. Florack, B. M. ter Haar Romeny, J. J. Koenderink, and M. A. Viergever. Scale and the differential structure of images. *Image and Vision Computing*, 10(6):376–388, July/August 1992.
- [77] L. M. J. Florack, B. M. ter Haar Romeny, J. J. Koenderink, and M. A. Viergever. Cartesian differential invariants in scale-space. *Journal of Mathematical Imaging and Vision*, 3(4):327–348, 1993.
- [78] L. M. J. Florack, B. M. ter Haar Romeny, J. J. Koenderink, and M. A. Viergever. General intensity transformations and differential invariants. *Journal of Mathematical Imaging and Vision*, 4(2):171–187, May 1994.
- [79] L. M. J. Florack, B. M. ter Haar Romeny, J. J. Koenderink, and M. A. Viergever. Linear scale-space. *Journal of Mathematical Imaging and Vision*, 4(4):325–351, 1994.
- [80] L. M. J. Florack, B. M. ter Haar Romeny, J. J. Koenderink, and M. A. Viergever. The Gaussian scale-space paradigm and the multiscale local jet. *International Journal of Computer Vision*, 18(1):61–75, April 1996.
- [81] A. T. Fomenko and T. L. Kunii. *Topological Modeling for Visualization*. Springer-Verlag, Tokyo, 1997.
- [82] J. M. Gauch. Image segmentation and analysis via multiscale gradient watershed hierarchies. *IEEE Transactions on Image Processing*, 8(1):69–79, January 1999.
- [83] J. M. Gauch and S. M. Pizer. Multiresolution analysis of ridges and valleys in grey-scale images. *IEEE Transactions on Pattern Analysis and Machine Intelligence*, 15(6), 1993.
- [84] J. M. Geusebroek. *Color and Geometrical Structure in Images*. PhD thesis, University of Amsterdam, 2000.
- [85] J.-M. Geusebroek, A. Dev, R. van den Boomgaard, A. W. M. Smeulders, F. Cornelissen, and H. Geerts. Color invariant edge detection. In *Nielsen et al. [197]*, pages 459–464, 1999.
- [86] J. M. Geusebroek, A. Dev, R. van den Boomgaard, A. W. M. Smeulders, F. Cornelissen, and H. Geerts. A scalespace approach to color invariance. In M. Boasson, J. A. Kaandorp, J. F. M. Tonino, and M. G. Vosselman, editors, *ASCI'99, Proceedings of the fifth annual conference of the Advanced School for Computing and Imaging*, pages 383–389. ASCI, 1999.
- [87] J.-M. Geusebroek, D. Koelma, A. W. M. Smeulders, and T. Gevers. Image retrieval and segmentation based on color invariants. In *IEEE Conference on Computer Vision and Pattern Recognition, 2000*, pages 784–785, 2000.

- [88] J.-M. Geusebroek, A. W. M. Smeulders, and R. van den Boomgaard. Measurement of color invariants. In *IEEE Conference on Computer Vision and Pattern Recognition, 2000*, pages 50–57, 2000.
- [89] J.-M. Geusebroek, R. van den Boomgaard, A. W. M. Smeulders, and A. Dev. Color and scale: The spatial structure of color images. In *European Conference on Computer Vision, 2000*, pages 331–341, 2000.
- [90] J. M. Geusebroek, R. van den Boomgaard, A. W. M. Smeulders, and H. Geerts. Color invariance. *IEEE Transactions on Pattern Analysis and Machine Intelligence*, 23(12):1338–1350, January 2001.
- [91] R. Gilmore. *Catastrophe Theory for Scientists and Engineers*. Dover, 1993. Originally published by John Wiley & Sons, New York, 1981.
- [92] B. van Ginneken and B. M. ter Haar Romeny. Applications of locally orderless images. In *Nielsen et al. [197]*, pages 10–21, 1999.
- [93] M. J. E. Golay. Hexagonal parallel pattern transformations. *IEEE Transactions on Pattern Analysis and Machine Intelligence*, 18:773–740, 1969.
- [94] C. N. de Graaf, K. L. Vincken, M. A. Viergever, J. J. Koenderink, F. J. R. Appelman, and O. Ying Lie. A hyperstack for the segmentation of 3D images. In D.A Ortendahl and J. Llacer, editors, *Information Processing in Medical Imaging*, pages 399–413. Wiley-Liss, New York, 1990.
- [95] L. D. Griffin. *Descriptions of Image Structure*. PhD thesis, University of London, 1995.
- [96] L. D. Griffin. Critical point events in affine scale-space. In *Sporring et al, [233]*, pages 165–180, 1997.
- [97] L. D. Griffin. Scale-imprecision space. *Image and Vision Computing*, 15:369–398, 1997.
- [98] L. D. Griffin and A. Colchester. Superficial and deep structure in linear diffusion scale space: Isophotes, critical points and separatrices. *Image and Vision Computing*, 13(7):543–557, September 1995.
- [99] L. D. Griffin, A. Colchester, and G. Robinson. Scale and segmentation of grey-level images using maximum gradient paths. *Image and Vision Computing*, 10(5):389–402, 1992.
- [100] L. D. Griffin, G. Robinson, and A. Colchester. Multi-scale hierarchical segmentation. In *Proceedings of British Machine Vision Conference*, pages 289–298, 1993.
- [101] D. Gurarie. *Symmetries and Laplacians: Introduction to Harmonic Analysis, Group Representations and Applications*. Elsevier science publishers, 1992.
- [102] B. M. ter Haar Romeny, editor. *Geometry-Driven Diffusion in Computer Vision*, volume 1 of *Computational Imaging and Vision Series*. Kluwer Academic Publishers, Dordrecht, 1994.
- [103] B. M. ter Haar Romeny. Applications of scale-space theory. In *Sporring et al, [233]*, pages 3–19, 1997.

- [104] B. M. ter Haar Romeny, editor. *Front end vision*. In press, 2002.
- [105] B. M. ter Haar Romeny and L. M. J. Florack. Front end vision: A multiscale geometry engine. In S.-W. Lee, H.H. Buelthoff, T. Poggio (Eds.): *Biologically Motivated Computer Vision 2000, Lecture Notes in Computer Science 1811*, pages 297–307, 2000.
- [106] B. M. ter Haar Romeny, L. M. J. Florack, J. J. Koenderink, and M. A. Viergever, editors. *Scale-Space Theory in Computer Vision: Proceedings of the First International Conference, Scale-Space'97, Utrecht, The Netherlands*, volume 1252 of *Lecture Notes in Computer Science*. Springer-Verlag, Berlin, July 1997.
- [107] B. M. ter Haar Romeny, L. M. J. Florack, A. H. Salden, and M. A. Viergever. Higher order differential structure of images. *Image and Vision Computing*, 12(6):317–325, 1994.
- [108] B. M. ter Haar Romeny, L. M.J. Florack, and M. Nielsen. Scale-time kernels and models. In *Kerckhove [136]*, pages 255–263, 2001.
- [109] B. M. ter Haar Romeny, J.-M. Geusebroek, P. Van Osta, R. van den Boomgaard, and J. J. Koenderink. Color differential structure. In *Kerckhove [136]*, pages 353–361, 2001.
- [110] B. M. ter Haar Romeny, B. Titulaer, S. Kalitzin, G. Scheffer, F. Broekmans, J. Staal, and E. te Velde. Computer assisted human follicle analysis for fertility prospects with 3D ultrasound. In *Proceedings International Conference on Information processing in Medical Imaging (IPMI99), Lecture Notes in Computer Science 1613*, pages 56–69, 1999.
- [111] R. Harvey, J. A. Bangham, and A. Bosson. Scale-space filters and their robustness. In *ter Haar Romeny et al. [106]*, pages 341–344, 1997.
- [112] R. Harvey, A. Bosson, and J. A. Bangham. The robustness of some scale-spaces. In *Proceedings British Machine Vision Conference*, pages Vol 1, pp 11–20, 1997.
- [113] R. D. Henkel. Segmentation in scale space. In *Computer Analysis of Images and Patterns. Lecture Notes in Computer Science, vol. 970. Springer-Verlag, pages 41-48*, 1995.
- [114] M. Henle. *A Combinatorial Introduction to Topology*. A Series of Books in Mathematical Sciences. W.H. freeman and Company, San Francisco, 1979.
- [115] Berthold Klaus Paul Horn. *Robot Vision*. MIT Press, Cambridge, MA, 1986.
- [116] D. H. Hubel. *Eye, Brain and Vision*, volume 22 of *Scientific American Library*. W. H. Freeman and Company, 1988.
- [117] R. Hummel, B. Kimia, and S. W. Zucker. Deblurring Gaussian blur. *Computer Vision, Graphics and Image Processing*, 38:66–80, 1987.
- [118] R. Hummel and R. Moniot. Reconstruction from zero-crossings in scale-space. *IEEE Transactions on Acoustic, Speech and Signal Processing*, 37(12):2111–2130, 1989.
- [119] T. Iijima. Basic theory of pattern normalization (for the case of a typical one dimensional pattern). *Bulletin of the Electrotechnical Laboratory*, 26:368– 388, 1962. (in Japanese).

- [120] T. Iijima and Y. Aoki. Derivation of an exact solution on a principal component analysis for a set of root visual patterns. *Systems and Computers in Japan*, 31(8):49–58, 2000.
- [121] P. T. Jackway. *Morphological scale-space with application to three-dimensional object recognition*. PhD thesis, Queensland University of Technology, Australia, 1994.
- [122] P. T. Jackway. Gradient watersheds in morphological scale-space. *IEEE Transactions on Image Processing*, 5(6):913–921, 1996.
- [123] S. Jimbo and S. Sakaguchi. Movement of hot spots over unbounded domains in  $\mathbb{R}^N$ . *Journal of Mathematical Analysis and Applications*, 182:810–835, 1999.
- [124] P. Johansen. On the classification of toppoints in scale space. *Mathematical Imaging and Vision*, 4(1):57–67, 1994.
- [125] P. Johansen, editor. *Proceedings of the Copenhagen Workshop on Gaussian Scale-Space Theory*, May 10–13 1996. Technical Rapport 96/19 ISSN 01078283.
- [126] P. Johansen. Local analysis of image scale space. In *Sporring et al. [233]*, pages 139–146, 1997.
- [127] P. Johansen. Local analysis of scale space. Technical Report 97/2, Department of Computer Science, University of Copenhagen, 1997.
- [128] P. Johansen, M. Nielsen, and O.F. Olsen. Branch points in one-dimensional Gaussian scale space. *Journal of Mathematical Imaging and Vision*, 13:193–203, 2000.
- [129] P. Johansen, S. Skelboe, K. Grue, and J. D. Andersen. Representing signals by their toppoints in scale space. In *Proceedings of the International Conference on Image Analysis and Pattern Recognition (Paris, France, October 1986)*, pages 215–217. IEEE Computer Society Press, 1986.
- [130] S. Kalitzin. Topological numbers and singularities. In *Sporring et al. [233]*, pages 181–190, 1997.
- [131] S. N. Kalitzin, B. M. ter Haar Romeny, A. H. Salden, P. F. M. Nacken, and M. A. Viergever. Topological numbers and singularities in scalar images. Scale-space evolution properties. *Journal of Mathematical Imaging and Vision*, 9(3):253–296, November 1998.
- [132] S. N. Kalitzin, B. M. ter Haar Romeny, and M. A. Viergever. On topological deep-structure segmentation. In *proceedings of ICIP'97, Santa Barbara*, volume II, pages 863–866, 1997.
- [133] S. N. Kalitzin, B. M. ter Haar Romeny, and M. A. Viergever. Invertible apertured orientation filters in image analysis. *International Journal of Computer Vision*, 31(2):145–158, 1999.
- [134] S. N. Kalitzin, J. Staal, B. M. ter Haar Romeny, and M. A. Viergever. A computational method for segmenting topological point-sets and application to image analysis. *IEEE Transactions on Pattern Analysis and Machine Intelligence*, 23(5):447–459, 2001.
- [135] R. S. Keller. *Generic Transitions of Relative Critical Sets in Parametrized Families with Applications to Image Analysis*. PhD thesis, University of North Carolina, 1999.

- [136] M. Kerckhove, editor. *Scale-Space and Morphology in Computer Vision*, volume 2106 of *Lecture Notes in Computer Science*. Springer -Verlag, Berlin Heidelberg, 2001.
- [137] Y. L. Kergosien. Generic sign systems in medical imaging. *IEEE Computer Graphics & Applications*, 11:46–65, September 1991.
- [138] B. Kimia and K. Siddiqi. Geometric heat equation and non-linear diffusion of shapes and images. *Computer Vision and Image Understanding*, 64(3):305–322, 1996.
- [139] J. J. Koenderink. The structure of images. *Biological Cybernetics*, 50:363–370, 1984.
- [140] J. J. Koenderink. The structure of the visual field. In W. Guttinger and G. Dangelmayr, editors, *The Physics of Structure Formation: Theory and Simulation. Proceedings of an International Symposium, Tübingen, Germany, October 27–November 2 1986*. Springer-Verlag, 1986.
- [141] J. J. Koenderink. Image structure. In M. A. Viergever and A. Todd-Pokropek, editors, *Mathematics and Computer Science in Medical Imaging, NATO ASI Series. F: Computer and Systems Sciences, Vol. 39*, pages 67–104. Springer-Verlag, 1987.
- [142] J. J. Koenderink. Operational significance of receptive field assemblies. *Biological Cybernetics*, 58:163–171, 1988.
- [143] J. J. Koenderink. Scale-time. *Biological Cybernetics*, 58:159–162, 1988.
- [144] J. J. Koenderink. A hitherto unnoticed singularity of scale-space. *IEEE Transactions on Pattern Analysis and Machine Intelligence*, 11(11):1222–1224, 1989.
- [145] J. J. Koenderink. *Solid Shape*. MIT Press, Cambridge, Massachusetts, 1990.
- [146] J. J. Koenderink and A. J. van Doorn. The structure of two-dimensional scalar fields with applications to vision. *Biological Cybernetics*, 33:151–158, 1979.
- [147] J. J. Koenderink and A. J. van Doorn. Dynamic shape. *Biological Cybernetics*, 53:383–396, 1986.
- [148] J. J. Koenderink and A. J. van Doorn. Representation of local geometry in the visual system. *Biological Cybernetics*, 55:367–375, 1987.
- [149] J. J. Koenderink and A. J. van Doorn. Receptive field families. *Biological Cybernetics*, 63:291–298, 1990.
- [150] J. J. Koenderink and A. J. Van Doorn. Blur and disorder. In *Nielsen et al. [197]*, pages 1–9, 1999.
- [151] J. J. Koenderink and A. J. Van Doorn. The structure of locally orderless images. *International Journal of Computer Vision*, 31(2/3):159–168, 1999.
- [152] A. Koster. *Linking Models for Multiscale Image Segmentation*. PhD thesis, Utrecht University, 1995.
- [153] A. S. E. Koster, K. L. Vincken, C. N. De Graaf, O. C. Zander, and M. A. Viergever. Heuristic linking models in multiscale image segmentation. *Computer Vision and Image Understanding*, 65(3):382–402, 1997.

- [154] A. Kuijper and L. M. J. Florack. Calculations on critical points under Gaussian blurring. In *Nielsen et al. [197]*, pages 318–329, 1999.
- [155] A. Kuijper and L. M. J. Florack. Calculations on critical points under Gaussian blurring. Technical Report UU-CS-1999-12, Department of Computer Science, Utrecht University, 1999.
- [156] A. Kuijper and L. M. J. Florack. The application of catastrophe theory to image analysis, 2001. submitted.
- [157] A. Kuijper and L. M. J. Florack. Hierarchical pre-segmentation without prior knowledge. In *Proceedings of the 8th International Conference on Computer Vision (Vancouver, Canada, July 9–12, 2001)*, pages 487–493, 2001.
- [158] A. Kuijper and L. M. J. Florack. Hierarchical pre-segmentation without prior knowledge. Technical Report UU-CS-2001-17, Department of Computer Science, Utrecht University, 2001.
- [159] A. Kuijper and L. M. J. Florack. The relevance of non-generic events in scale space. In *Proceedings of the 7th European Conference on Computer Vision (Copenhagen, Denmark, May 28–31, 2002), Part I, Lecture Notes in Computer Science, vol. 2350*, pages 190–204, 2002.
- [160] A. Kuijper and L. M. J. Florack. Understanding and modeling the evolution of critical points under Gaussian blurring. In *Proceedings of the 7th European Conference on Computer Vision (Copenhagen, Denmark, May 28–31, 2002), Part I, Lecture Notes in Computer Science, vol. 2350*, pages 143–157, 2002.
- [161] A. Kuijper, L. M. J. Florack, and M. A. Viergever. Scale space hierarchy. Technical Report UU-CS-2001-19, Department of Computer Science, Utrecht University, 2001.
- [162] A. Kuijper, L. M. J. Florack, and M. A. Viergever. Scale space hierarchy, 2001. accepted for publication.
- [163] R. K.-S. Kwan, A. C. Evans, and G. B. Pike. An extensible MRI simulator for post-processing evaluation. In *Visualization in Biomedical Computing (VBC'96). Lecture Notes in Computer Science, vol. 1131. Springer-Verlag, pages 135-140*, 1996.
- [164] C.-N. Lee, T. Poston, and A. Rosenfeld. Winding and Euler numbers for 2D and 3D digital images. *Computer Vision, Graphics and Image Processing: Graphical Models and Image Processing*, 53(11):522–537, 1991.
- [165] C.-N. Lee, T. Poston, and A. Rosenfeld. Holes and genus of 2D and 3D digital images. *Computer Vision, Graphics and Image Processing: Graphical Models and Image Processing*, 55(11):20–47, 1993.
- [166] H. Lester and S.R. Arridge. A survey of hierarchical non-linear medical image registration. *Pattern recognition*, 32(1):129–149, 1999.
- [167] Y. Leung, J.-S. Zhang, and Z.-B. Xu. Clustering by scale-space filtering. *IEEE Transactions on Pattern Analysis and Machine Intelligence*, 22(12):1396–1410, 2000.

- [168] L. M. Lifshitz and S. M. Pizer. A multiresolution hierarchical approach to image segmentation based on intensity extrema. *IEEE Transactions on Pattern Analysis and Machine Intelligence*, 12(6):529–540, 1990.
- [169] T. Lindeberg. On the behaviour in scale-space of local extrema and blobs. In P. Johansen and S. Olsen, editors, *Theory & Applications of Image Analysis, volume 2 of Series in Machine Perception and Artificial Intelligence*, pages 38–47. World Scientific, Singapore, 1992.
- [170] T. Lindeberg. Scale-space behaviour of local extrema and blobs. *Journal of Mathematical Imaging and Vision*, 1(1):65–99, 1992.
- [171] T. Lindeberg. Detecting salient blob-like image structures and their scales with a scale-space primal sketch: a method for focus-of-attention. *International Journal of Computer Vision*, 11(3):283–318, 1993.
- [172] T. Lindeberg. Discrete derivative approximations with scale-space properties: a basis for low-level feature extraction. *Journal of Mathematical Imaging and Vision*, 3(4):349–376, 1993.
- [173] T. Lindeberg. Effective scale: a natural unit for measuring scale-space lifetime. *IEEE Transactions on Pattern Analysis and Machine Intelligence*, 15(10):1068–1074, 1993.
- [174] T. Lindeberg. *Scale-Space Theory in Computer Vision*. The Kluwer International Series in Engineering and Computer Science. Kluwer Academic Publishers, 1994.
- [175] T. Lindeberg. Edge detection and ridge detection with automatic scale selection. *International Journal of Computer Vision*, 30(2):117–154, 1998.
- [176] T. Lindeberg. Feature detection with automatic scale selection. *International Journal of Computer Vision*, 30(2):79–116, 1998.
- [177] T. Lindeberg. A scale selection principle for estimating image deformations. *Image and Vision Computing*, 16:961–977, 1998.
- [178] T. Lindeberg and L. M. J. Florack. On the linear increase of receptive field size as a function of eccentricity. Technical Report ISRN KTH NA/P-92/29-SE, Department of Numerical Analysis and Computing Science, Royal Institute of Technology, S-100 44 Stockholm, Sweden, 1992.
- [179] T. Lindeberg and L. M. J. Florack. Foveal scale-space and the linear increase of receptive field size as a function of eccentricity. Technical Report ISRN KTH NA/P-94/27-SE, Department of Numerical Analysis and Computing Science, Royal Institute of Technology, S-100 44 Stockholm, Sweden, 1994.
- [180] T. Lindeberg, P. Lidberg, and P. E. Roland. Analysis of brain activation patterns using a 3-D scale-space primal sketch. *Human Brain Mapping*, 7(3):166–194, 1999.
- [181] B. F. Logan, Jr. Information in the zero crossings of bandpass signals. *Bell Systems Technical Journal*, 56(4):487–510, 1977.



- [182] M. Loog, J. J. Duistermaat, and L. M. J. Florack. On the behavior of spatial critical points under Gaussian blurring, a folklore theorem and scale-space constraints. In *Kerckhove [136]*, pages 183–192, 2001.
- [183] S. Louw, A. M. L. Kappers, and J. J. Koenderink. Haptic detection thresholds of Gaussian profiles over the whole range of spatial scales. *Experimental Brain Research*, 132:369–374, 2000.
- [184] Y.-C. Lu. *Singularity Theory and an Introduction to Catastrophe Theory*. Springer-Verlag, Berlin, second corrected printing edition, 1976.
- [185] D. Marr. *Vision*. W.H. Freeman and Company, San Francisco, 1982.
- [186] E. M. Maslov and A. G. Shagalov. Dynamics of first-order phase transitions in the  $\phi^4 - \phi^6$  model caused by the parametric instability of the metastable vacuum. *Physica D: Nonlinear Phenomena*, 152-153:769–778, 2001.
- [187] J. C. Maxwell. On hills and dales. *Lond. Edin. Dublin Phil. Mag. and J. of Sci.*, 40(269):421–425, 1870.
- [188] L. Middleton and J. Sivaswamy. Edge detection in a hexagonal-image processing framework. *Image and Vision Computing*, 19(14):1071–1081, 2001.
- [189] E. G. Miller. Alternative tilings for improved surface area estimates by local counting algorithms. *Computer Vision and Image Understanding*, 74(3):193–211, 1999.
- [190] J. Milnor. *Morse Theory*, volume 51 of *Annals of Mathematics Studies*. Princeton University Press, Princeton, third edition, 1969.
- [191] I. G. Moss. Heat kernel expansions for distributional backgrounds. *Physics Letters B*, 491(1-2):203–206, October 2000.
- [192] P. F. M. Nacken. *Image Analysis Methods Based on Hierarchies of Graphs and Multi-Scale Mathematical Morphology*. PhD thesis, University of Amsterdam, 1994.
- [193] E. Nakamura and N. Kehtarnavaz. Determining number of clusters and prototype locations via multi-scale clustering. *Pattern Recognition Letters*, 19(14):1265–1283, 1998.
- [194] M. Nielsen. *From Paradigm to Algorithms in Computer Vision*. PhD thesis, University of Copenhagen, Denmark, 1995.
- [195] M. Nielsen. Scale-space generators and functionals. In *Sporring et al. [233]*, pages 99–114, 1997.
- [196] M. Nielsen, L. M. J. Florack, and R. Deriche. Regularization, scale space, and edge detection filters. *Journal of Mathematical Imaging and Vision*, 7(4):291–307, October 1997.
- [197] M. Nielsen, P. Johansen, O. Fogh Olsen, and J. Weickert, editors. *Scale-Space Theories in Computer Vision*, volume 1682 of *Lecture Notes in Computer Science*. Springer -Verlag, Berlin Heidelberg, 1999.

- [198] M. Nielsen and M. Lillholm. What do features tell about images? In *Kerckhove [136]*, pages 39–50, 2001.
- [199] W. J. Niessen, J. S. Duncan, M. Nielsen, L. M. J. Florack, B. M. ter Haar Romeny, and M. A. Viergever. A multiscale approach to image sequence analysis. *Computer Vision and Image Understanding*, 65(2):259–268, February 1997 1997.
- [200] W. J. Niessen, K. L. Vincken, and M. A. Viergever. Comparison of multiscale representations for a linking-based image segmentation model. In *Proc. IEEE Workshop on Mathematical Methods in Biomedical Image Analysis*, pages 263–272, San Francisco, 1996.
- [201] W. J. Niessen, K. L. Vincken, J. Weickert, B. M. ter Haar Romeny, and M. A. Viergever. Multiscale segmentation of three-dimensional MR brain images. *International Journal of Computer Vision*, 31(2/3):185–202, 1999.
- [202] W. J. Niessen, K. L. Vincken, J. Weickert, and M. A. Viergever. Three-dimensional MR brain segmentation. In *ICCV*, pages 53–58. IEEE, 1998.
- [203] O. Fogh Olsen. Multi-scale segmentation of grey-scale images. Technical Report 96/30, Department of Computer Science, University of Copenhagen, November 1996.
- [204] O. Fogh Olsen. Multi-scale watershed segmentation. In *Sporring et al. [233]*, pages 191–200, 1997.
- [205] O. Fogh Olsen. *Generic Image Structure*. PhD thesis, University of Copenhagen, Denmark, 2000.
- [206] O. Fogh Olsen and M. Nielsen. Generic events for the gradient squared with application to multi-scale segmentation. In *Ter Haar Romeny et al, [106]*, pages 101–112, 1997.
- [207] O. Fogh Olsen and M. Nielsen. Multi-scale gradient magnitude watershed segmentation. In *ICIAP'97 - 9th International Conference on Image Analysis and Processing, volume 1310 of Lecture Notes in Computer Science*, pages 6–13, September 1997.
- [208] N. Otsu. *Mathematical Studies on Feature Extraction in Pattern Recognition*. PhD thesis, Electronical Laboratory, Ibaraki, Japan, 1981. (in Japanese).
- [209] X. M. Pardo, M. J. Carreira, A. Mosquera, and D. Cabello. A snake for CT image segmentation integrating region and edge information. *Image and Vision Computing*, 19(7):461–475, 2001.
- [210] M. Pelillo, K. Siddiqi, and S. Zucker. Matching hierarchical structures using association graphs. *IEEE Transactions on Pattern Analysis and Machine Intelligence*, 21(11):1105–1120, 1999.
- [211] P. Perona and J. Malik. Scale space and edge detection using anisotropic diffusion. *IEEE Transactions on Pattern Analysis and Machine Intelligence*, 12(7):629–639, 1990.
- [212] T. Poston and I. N. Stewart. *Catastrophe Theory and its Applications*. Pitman, London, 1978.
- [213] L. Remaki and M. Cheriet. Kcs–new kernel family with compact support in scale space: Formulation and impact. *IEEE Transactions on Image Processing*, 9(6):970–981, 2000.

- [214] Z. Reti. Deblurring images blurred by the discrete Gaussian. *Applied Mathematics Letters*, 8(4):29–35, 1995.
- [215] J. H. Rieger. Generic properties of edges and corners on smooth greyvalue surfaces. *Biological Cybernetics*, 66:497–502, 1992.
- [216] J. H. Rieger. Generic evolutions of edges on families of diffused greyvalue surfaces. *Journal of Mathematical Imaging and Vision*, 5:207–217, 1995.
- [217] J. H. Rieger. Topographical properties of generic images. *International Journal of Computer Vision*, 23(1):79–92, 1997.
- [218] M. Rosbacke, T. Lindeberg, E. Bjorkman, and P. E. Roland. Evaluation of using absolute versus relative base level when analyzing brain activation images using the scale-space primal sketch. *Medical Image Analysis*, 5(2):89–110, 2001.
- [219] D. Rotem and Y. Y. Zeevi. Image reconstruction from zero crossings. *IEEE Transactions on Acoustics, Speech, and Signal Processing*, 34(5):1269–1277, 1986.
- [220] A. H. Salden. *Dynamic Scale-Space Paradigms*. PhD thesis, Utrecht University, 1996.
- [221] A. H. Salden, B. M. ter Haar Romeny, and M. A. Viergever. Linear scale-space theory from physical properties. *Journal of Mathematical Imaging and Vision*, 9(2):103–140, September 1998.
- [222] A. H. Salden, B. M. ter Haar Romeny, and M. A. Viergever. A dynamic scale-space paradigm. *Journal of Mathematical Imaging and Vision*, 15(3):127–168, 2001.
- [223] P. M. Scheele. *Degeneratie - het einde van de evolutietheorie*. Buijten & Schipperheijn, Amsterdam, 1997. (in Dutch).
- [224] L. Schwartz. *Théorie des Distributions*, volume I, II of *Actualités scientifiques et industrielles; 1091, 1122*. Publications de l’Institut de Mathématique de l’Université de Strasbourg, Paris, 1950–1951.
- [225] S. Sengupta and S. C. Sahasrabudhe. Scale space displacement of zero-crossings of  $\nabla^2 g$  operated images for convex bodies and convex sets. *Signal Processing*, 47(3):279–285, December 1995.
- [226] Y. Shinagawa and T. L. Kunii. Constructing a Reeb graph automatically from cross sections. *IEEE Computer Graphics & Applications*, 11:44–51, November 1991.
- [227] Y. Shinagawa, T. L. Kunii, and Y. L. Kergosien. Surface coding based on Morse theory. *IEEE Computer Graphics & Applications*, 11:66–78, September 1991.
- [228] K. Siddiqi, B. B. Kimia, A. Tannenbaum, and S. W. Zucker. Shapes, shocks and wiggles. *Image and Vision Computing*, 17:365–373, 1999.
- [229] K. Siddiqi, A. Shokoufandeh, S. Dickinson, and S. Zucker. Shock graphs and shape matching. *International Journal of Computer Vision*, 30:1–22, 1999.

- [230] A. Simmons, S. R. Arridge, P. S. Tofts, and G. J. Barker. Application of the extremum stack to neurological MRI. *IEEE Transactions on Medical Imaging*, 17(3):371–382, June 1998.
- [231] M. Sonka, V. Hlavac, and R. Boyle. *Image Processing, Analysis, and Machine Vision*. International Thomson Computer Press, 1996.
- [232] M. Spivak. *Differential Geometry*, volume 1–5. Publish or Perish, 1975.
- [233] J. Sporring, M. Nielsen, L. M. J. Florack, and P. Johansen, editors. *Gaussian Scale-Space Theory*, volume 8 of *Computational Imaging and Vision Series*. Kluwer Academic Publishers, Dordrecht, second edition, 1997.
- [234] J. Staal, S. Kalitzin, B. M. ter Haar Romeny, and M. A. Viergever. Detection of critical structures in scale space. In *Nielsen et al. [197]*, pages 105–116, 1999.
- [235] G. Strang. *Linear Algebra and its Applications*. Academic Press, 1980.
- [236] G. J. Streekstra, R. Van Den Boomgaard, and A. W. M. Smeulders. Scale dependency of image derivatives for feature measurement in curvilinear structures. *International Journal of Computer Vision*, 42(3):177–189, 2001.
- [237] J. Suckling, M. J. Brammer, A. Lingford-Hughes, and E. T. Bullmore. Removal of extracerebral tissues in dual-echo magnetic resonance images via linear scale-space features. *Magnetic Resonance Imaging*, 17(2):247–256, 1999.
- [238] R. Thom. *Stabilité Structurelle et Morphogénèse*. Benjamin, New York, 1972.
- [239] R. Thom. *Structural Stability and Morphogenesis*. Benjamin-Addison Wesley, 1975. translated by D. H. Fowler.
- [240] K. L. Vincken. *Probabilistic Multiscale Image Segmentation by the Hyperstack*. PhD thesis, Utrecht University, 1995.
- [241] K. L. Vincken, C. N. de Graaf, A. S. E. Koster, M. A. Viergever, F. J. R. Appelman, and G. R. Timmens. Multiresolution segmentation of 3D images by the hyperstack. In *First Conference on Visualization in Biomedical Computing, Proc. VBC '90*, pages 115–122, Los Alamitos, CA, 1990. IEEE Computer Society Press.
- [242] K. L. Vincken, A. S. E. Koster, and M. A. Viergever. Probabilistic multiscale image segmentation. *IEEE Transactions on Pattern Analysis and Machine Intelligence*, 19(2):109–120, 1997.
- [243] K. L. Vincken, W. J. Niessen, and M. A. Viergever. Blurring strategies for image segmentation using a multiscale linking model. In *Proc. Computer Vision and Pattern Recognition*, pages 21–26, San Francisco, CA, 1996. IEEE Computer Society Press.
- [244] T. Wada and M. Sato. Scale-space tree and its hierarchy. In *ICPR90*, volume II, pages 103–108, 1990.
- [245] J. A. Weickert. *Anisotropic Diffusion in Image Processing*. Teubner, Stuttgart, 1998.

- [246] J. A. Weickert. Efficient image segmentation using partial differential equations and morphology. *Pattern Recognition*, 34(9):1813–1824, 2000.
- [247] J. A. Weickert, S. Ishikawa, and A. Imiya. On the history of Gaussian scale-space axiomatics. In *Sporring et al, [233]*, pages 45–59, 1997.
- [248] J. A. Weickert, S. Ishikawa, and A. Imiya. Linear scale-space has first been proposed in Japan. *Journal of Mathematical Imaging and Vision*, 10(3):237–252, 1999.
- [249] A. P. Witkin. Scale-space filtering. In *Proceedings of the Eighth International Joint Conference on Artificial Intelligence*, pages 1019–1022, 1983.
- [250] S. Wolfram, editor. *The Mathematica Book*. Wolfram Media / Cambridge University Press, Cambridge, third edition, 1996.
- [251] A. E. R. Woodcock and M. Davis, editors. *Catastrophe Theory*. Clarke, Irwin & Company Limited, 1978.
- [252] L. Wu and Z. Xie. Scaling theorems for zero-crossings. *IEEE Transactions on Pattern Analysis and Machine Intelligence*, 12(1):46–54, 1990.
- [253] A. L. Yuille and T. Poggio. Scaling theorems for zero crossings. *IEEE Transactions on Pattern Analysis and Machine Intelligence*, 8(1):15–25, 1986.
- [254] E. Zauderer. *Partial Differential Equations*. John Wiley and Sons, 1989.
- [255] E. C. Zeeman. *Catastrophe Theory: Selected Papers, 1972-1977*. Addison-Wesley Publishing Company, 1977.
- [256] S. Zeki. *A Vision of the Brain*. Blackwell scientific publications, 1993.
- [257] N. Zhao. *Feature Extraction of images by stable gaze tree*. PhD thesis, Dept. of Computer Science, Tokyo Inst. of Technology, Japan, 1985. (in Japanese).
- [258] N. Zhao and T. Iijima. A theory of feature extraction by the tree of stable view-points. *IECE Japan, Trans. D*, J68-D:1125–1132, 1985. (in Japanese).
- [259] N. Zhao and T. Iijima. Theory on the method of determination of view-point and field of vision during observation and measurement of figure. *IECE Japan, Trans. D*, J68-D:508–514, 1985. (in Japanese).



---

# Publications

---

## Articles:

- Chapter 4: L. M. J. Florack and A. Kuijper. The topological structure of scale-space images. *Journal of Mathematical Imaging and Vision*, 12(1):65–80, February 2000, combined with [154].
- Chapter 5: A. Kuijper, L. M. J. Florack, and M. A. Viergever. Scale space hierarchy. *Journal of Mathematical Imaging and Vision*, accepted, 2001.
- Chapter 6: A. Kuijper and L. M. J. Florack. The application of catastrophe theory to image analysis. Submitted, 2001.
- Chapter 7: A. Kuijper and L. M. J. Florack. The relevance of non-generic events in scale space models. Submitted, 2001.
- Chapter 8: A. Kuijper and L. M. J. Florack. Logical filtering in scale space. Submitted, 2002.

## Proceedings:

- J. Bijhold, A. Kuijper, and J.-H. Westhuis. Comparative study of image restoration techniques in forensic image processing. In *SPIE Proceedings Vol. 2942, Leonid I. Rudin, Simon K. Bramble (Eds.): Investigative Image Processing (Boston, MA, USA, 1996)*, pages 10–21, 1997.
- A. Kuijper and L. M. J. Florack. Calculations on critical points under gaussian blurring. In *M. Nielsen, P. Johansen, O. Fogh Olsen, and J. Weickert (Eds.): Proceedings of the second International Conference on Scale-Space Theories in Computer Vision (Corfu, Greece, September 1999). Lecture Notes in Computer Science, volume 1682. Springer -Verlag, Berlin Heidelberg*, pages 318–329, 1999.

- A. Kuijper and L. M. J. Florack. Hierarchical pre-segmentation without prior knowledge. In *Proceedings of the 8th International Conference on Computer Vision (Vancouver, Canada, July 9–12, 2001)*, pages 487–493, 2001.
- A. Kuijper and L. M. J. Florack. Understanding and modeling the evolution of critical points under Gaussian blurring. In A. Heyden, G. Sparr, M. Nielsen, and P. Johansen (Eds.): *Proceedings of the 7th European Conference on Computer Vision, Part I (Copenhagen, Denmark, May 28–31, 2002)*. *Lecture Notes in Computer Science, volume 2350*, Springer - Verlag, Berlin Heidelberg, pages 143–157, 2002.
- A. Kuijper and L. M. J. Florack. The relevance of non-generic events in scale space models. In A. Heyden, G. Sparr, M. Nielsen, and P. Johansen (Eds.): *Proceedings of the 7th European Conference on Computer Vision, Part I (Copenhagen, Denmark, May 28–31, 2002)*. *Lecture Notes in Computer Science, volume 2350*, Springer - Verlag, Berlin Heidelberg, pages 190–204, 2002.

### Technical reports:

- L. M. J. Florack and A. Kuijper. The topological structure of scale-space images. Technical Report UU-CS-1998-31, Utrecht University, 1998.
- L. M. J. Florack and A. Kuijper. On the behaviour of critical points under Gaussian blurring. Technical Report UU-CS-1998-34, Utrecht University, 1998.
- A. Kuijper and L. M. J. Florack. Calculations on critical points under gaussian blurring. Technical Report UU-CS-1999-12, Department of Computer Science, Utrecht University, 1999.
- A. Kuijper and L. M. J. Florack. Hierarchical pre-segmentation without prior knowledge. Technical Report UU-CS-2001-17, Department of Computer Science, Utrecht University, 2001.
- A. Kuijper, L. M. J. Florack, and M. A. Viergever. Scale space hierarchy. Technical Report UU-CS-2001-19, Department of Computer Science, Utrecht University, 2001.
- A. Kuijper and L. M. J. Florack. The application of catastrophe theory to image analysis. Technical Report UU-CS-2001-23, Department of Computer Science, Utrecht University, 2001.
- A. Kuijper and L. M. J. Florack. The application of catastrophe theory to medical image analysis. Technical Report UU-CS-2001-24, Department of Computer Science, Utrecht University, 2001.
- A. Kuijper and L. M. J. Florack. On the creations of critical points in scale space with application to medical image analysis. Technical Report UU-CS-2001-25, Department of Computer Science, Utrecht University, 2001.
- A. Kuijper and L. M. J. Florack. The relevance of non-generic events in scale space models. Technical Report UU-CS-2001-55, Department of Computer Science, Utrecht University, 2001.
- A. Kuijper and L. M. J. Florack. Logical filtering in scale space. Technical Report UU-CS-2002-018, Department of Computer Science, Utrecht University, 2002.



---

# Inleiding en Samenvatting

---

## Inleiding

In dit tijdperk van de computer komt een enorme hoeveelheid afbeeldingen voort uit computers<sup>1</sup>. Computers bieden grote voordelen voor afbeeldingen op het gebied van acquisitie, opslag, manipulatie, vermenigvuldiging, verzenden, etc.

## Beelden

In het algemeen weet de menselijke gebruiker zowel de inhoud van een beeld<sup>2</sup> als de betekenis. In deze vorm fungeren afbeeldingen alleen maar als *toegevoegde* informatie bij het geschreven verhaal. Het tegenovergestelde is echter ook mogelijk: de afbeelding kan het *subject* zijn dat verduidelijkt dient te worden. Het is een intrigerende vraag of het mogelijk is de computer data zodanig te manipuleren dat de inhoud, de bedoeling, duidelijker of meer expliciet wordt met een zo klein mogelijk aantal interacties tussen de mens en de computer. Om dit te bereiken moeten verschillende observaties in overweging worden genomen:

- Er is “iets” in de werkelijke wereld dat onderdeel is van het beeld, zoals personen, vliegtuigen, sterren of hersentumoren.
- “Het” is slechts digitaal aanwezig op de computer. Er zijn alleen maar “enen en nullen” die zo zijn gecombineerd dat “het” gevisualiseerd kan worden.
- Er moet “iets” gedaan worden met “het”, bijvoorbeeld het benadrukken of het eruit halen van belangrijke delen.

---

<sup>1</sup>Ook de afbeelding op de voorkant van dit proefschrift.

<sup>2</sup>In het vervolg gebruik ik het woord ‘beeld’ in plaats van afbeelding als vertaling van ‘image’.

- Datgene wat er gedaan is, moet in een betekenisvolle en reproduceerbare manier gedaan zijn. Het is niet zo moeilijk met beelden te spelen, delen te wissen en snorretjes te tekenen, maar het moge duidelijk zijn dat dat niet de bedoeling is.
- De uitkomst van de hetgeen gedaan is, dient op een zinvolle manier gepresenteerd te worden.

De lezer voele zich natuurlijk vrij extra eisen toe te voegen.

Beeldacquisitie en de analyse van computer data die “iets” voorstelt, kortweg *beeldanalyse*, kennen interactie met verschillende wetenschappelijke disciplines, die variëren van wiskunde, via (bijvoorbeeld) biologie en informatica, tot natuurkunde. Zo vond in het begin van de beeldanalyse het meeste onderzoek plaats op signalen, zoals radar en sonar, door de elektrotechnische gemeenschap. Tegenwoordig is daarentegen medische beeldbewerking het onderwerp van een groot deel van het onderzoek.

### Beeldacquisitie

Hoe situaties in het werkelijke leven worden vastgelegd door “observatie machines” als digitale camera’s, MR scanners of telescopen, kan beschreven worden met *fysische “wetten”*. Deze wetten zijn regels die opgelegd worden door de intrinsieke eigenschappen van de observatie machine. In het algemeen hebben ze totaal geen a-priori relatie met de situatie in het werkelijke leven zelf. We kunnen dus wel afbeeldingen van alles en nog wat maken, maar de manier waarop het beeld wordt verkregen, is ongerelateerd aan de *buiten* wereld.

De initiële beelden, ook wel ruwe data genoemd, zijn echter verkregen door de observatie machine en ze hangen dus sterk af van de keuzes van de parameters *binnen* in de observatie machine. Een close-up opname bijvoorbeeld, kan niet worden omgezet in een panorama opname. Hetzelfde geldt voor het omgekeerde, als dezelfde resolutie gewenst is. Ook de uitkomst van een MR scan bevat extra informatie, zoals “T1” of “T2” gewogen, hetgeen informatie geeft over de manier waarop de meting is verricht. Dit houdt niet alleen in dat fysica aan de basis van beelden ligt, maar zorgt tevens voor een verlies aan informatie, in de zin dat de verkregen data slechts *gedeeltelijk* de situaties in het werkelijke leven voorstellen. Als de parameters in de observatie machine goed gekozen zijn, is dat niet zo erg, hoewel het de beperktheid van verdere resultaten aangeeft. Als we een close-up willen, moeten we daar gewoon van tevoren op inspelen. Een andere type verlies ligt in de wens de data op een *georganiseerde, digitale* manier te verkrijgen. Op die manier is er de mogelijkheid de data geschikt te maken voor opslag, berekeningen en representatie op een computer. Hoewel alle observatie machines hun fysische grenzen hebben (fotokorrels, dichtheid van fotonen, magnetische spin), wordt meestal een vaste, bepaalde resolutie gekozen, zodat de data handelbare afmetingen heeft. De situaties van het werkelijke leven worden dus gereduceerd tot een verzameling van losse metingen die netjes geordend zijn op een bepaald raster.

### Beeldanalyse

In vele gevallen is de volgende stap iets *doen* met de data: ze zijn immer verkregen met een bepaald doel. Ze is de uitkomst van een beeldacquisitie procedure en op hun beurt weer de invoer van een beeldanalyse taak. Gedeeltes van de data kunnen dus meer relevante informatie bevatten dan andere delen en dienen ontstoord, benadrukt of eruit gehaald worden, zoals: nieuwe melkwegstelsels, zwarte gaten of planeten met de mogelijkheid van leven in astronomische data; hersentumoren, slagaderlijke zwellingen of zwakke botten in medische beelden; kentekenplaten of mogelijke verdachten in forensische data,

etc. Hier komt duidelijk veel menselijk inzicht en interpretatievermogen om de hoek kijken. Wiskundige modellen die gebaseerd zijn op de veronderstelde verstoring in het beeld, op de intrinsieke eigenschappen van de interessante objecten, of op bijvoorbeeld biologische of medische kennis, worden voorgesteld en geïmplementeerd in computer algoritmen. De uitkomst wordt gevalideerd en gebruikt – of niet. In het laatste geval wordt het model aangepast, geïmplementeerd, etc. Hier wordt iets opmerkelijks duidelijk. De validatie kan aangeven of een model goed of slecht is – binnen het raamwerk van de aannames –, maar de verwerping of het gebruik van het resultaat is vaak gebaseerd op de mens die interpreterend naar de uitkomsten kijkt. Het oordeel is duidelijk gebaseerd op een visuele inspectie van de gegenereerde gegevens, op grond van de kundigheid en ervaring van de interpreterende mens. Wil een model het goed doen, dan moet het een zekere coherentie hebben met het menselijk visuele en interpretatievermogen. Een andere manier om dat te verwoorden, is dat het model het menselijk visuele en interpretatievermogen op één of andere manier dient te simuleren. Daarom is er binnen beeldanalyse ook een rol weggelegd voor (neuro-)biologie, dat onderzoekt welke mechanismen betrokken zijn bij kijken, het transporteren van data naar de hersenen en het interpreteren van deze data (en het vervolgens weer terugkoppelen naar de ogen).

### Meer en Meer Data

De exponentiele groei van computer faciliteiten in de laatste tientallen jaren heeft geleid tot een geweldige groei in data, zowel door de observaties – het verkrijgen van beelden – als door de voorgestelde modellen – de beeldanalyse taken. Aan de invoerkant kunnen verschillende redenen worden gevonden:

- Het aantal acquisities groeide.
- Het formaat van een acquisitie groeide.
- De acquisities werden gecompliceerder.

Dit was duidelijk het gevolg van de groter wordende opslag capaciteit. Binnen de medische beeldanalyse kan men denken aan een groeiend aantal MR beelden, met een factor 2, 4 of meer gedetailleerd, en de overgang van twee naar drie dimensionale beelden, en zelfs naar tijdreeksen ervan. Aan de uitkomsten kant vond ook een groei plaats. Rekening legt een zware voorwaarde op mogelijke algoritmen. Als een gevolg daarvan waren de algoritmes in de begintijd van de beeldanalyse eenvoudig en vaak gebaseerd op éénstaps *filters*, enkelvoudige operaties op een twee dimensionaal beeld op een rechthoekig raster. Men kan daarbij denken aan *randdetectie* en aan *ruisreductie*.

De stijgende CPU snelheid leidde tot een stijgend *aantal* voorgestelde wiskundige modellen en een stijgende *complexiteit* ervan. In plaats van éénstaps filters waren meerstaps filters nodig om de voorgestelde modellen te representeren: een opeenvolging van dezelfde ingewikkelde operatie op een beeld levert de uitkomst. De modellen beschrijven een gewenste situatie van het beeld, gegeven een aantal randvoorwaarden, zoals de eis van zowel randdetectie als ruis onderdrukking.

Ook ontstonden nieuwe taken gebaseerd op beeld *herkenning* binnen deze enorme hoeveelheid beschikbare beelden. Bijvoorbeeld: “Vind een afbeelding van Rembrandt’s Thuiskomst van de Verloren Zoon op internet”, of: “Gegeven een afbeelding van een naald, vind z’n plaats (of vind soortgelijke afbeeldingen) in een beeld database, een (hooi)berg van afbeeldingen.” Dit soort taken leidde tot de ontwikkeling van digitale beeldbeheer systemen, ook wel “afbeeldingopslag en -communicatie systemen” genoemd. Ze zijn bijvoorbeeld in opkomst in klinische en radiologische omgevingen.

Een andere nieuwe taak is beelden *vergelijken*: beschrijven twee beelden hetzelfde op een voorgeschreven manier? En bij stereo beelden: kunnen we de drie dimensionale situatie zo goed mogelijk reconstrueren gegeven de twee beelden van het linker- en rechteroog (of camera).

### Over Bomen en een Bos

Deze explosieve groei van data aan de invoer- en de uitvoerkant vereist duidelijke en transparante wiskundige methoden die ze reguleren en wildgroei voorkomen: alles is mogelijk, maar niet alles is nuttig. Sterker nog, wiskundige modellen en algoritmen hebben de neiging te functioneren als “zwarte dozen”, waarvan de uitkomsten met een paar parameters geregeld kunnen worden. Verschillende problemen doken op. Om er een paar te noemen:

- Het is niet altijd duidelijk wat voor soort gedrag verwacht kan worden als bepaalde modellen toegepast worden.
- De keuzes bij het vaststellen van de parameterwaardes hangen af van de persoon die met de beelden werkt en de relatie tussen de keuzes en de uitkomst is niet duidelijk.
- Het is soms niet duidelijk wat de parameters “voorstellen”, of wat een combinatie ervan inhoudt.
- Een kleine verandering in de parameters leidt soms tot grote veranderingen in het uiteindelijke beeld.
- De ruwe data bestaat uiteraard uit een discrete verzameling van getallen. Het is dus niet triviaal om continue wiskundige modellen erop toe te passen.

De eerste drie punten benoemen de *ad hoc natuur*, het vierde punt laat de zogeheten *slechte gesteldheid* zien en het laatste item duidt een *conceptueel probleem* aan. De laatste tijd is het aantal wiskundigen dat geïnteresseerd is in beeldanalyse sterk gegroeid, omdat bovengenoemde problemen verklaard kunnen worden door de gebruikte modellen wiskundig te onderzoeken. Beeldanalyse blijkt een veelbelovend toepassingsgebied van de wiskunde te zijn, zelfs als gebruik gemaakt wordt van sterk abstracte theorieën die voor niet-wiskundigen totaal niet duidelijk zijn.

### De Combinatie is Meer dan de Som der Delen

Samenvattend: binnen het gebied van de beeldanalyse is de combinatie van natuurkunde, elektrotechniek, wiskunde, (neuro-)biologie en informatica, samen met kennis van toepassingsgebieden van specifieke beeldanalyse taken, noodzakelijk om zinvolle resultaten te bereiken. De lezer kan wel raden dat dit gigantische wetenschapsgebied onmogelijk in één proefschrift omvat kan worden.

### Samenvatting van dit Proefschrift

In dit proefschrift beperk ik mij tot de wiskunde rond de ruwe data, het initiële beeld, dat digitaal opgeslagen is. Hoe de beelden verkregen zijn, is voor kennisgeving aangenomen en verder niet relevant. Het is ook niet bekend wat ze voorstellen of welke speciale objecten er aanwezig zouden kunnen zijn. Als een gevolg daarvan is validatie van de resultaten met betrekking tot een hooggespecificeerde taak, zoals

segmentatie, *niet* van toepassing, omdat ik eenvoudigweg veronderstel dat er geen hooggespecificeerde taak is. De validatie vindt plaats op een ander vlak. De *methoden* en *modellen* die gebruikt en afgeleid worden, dienen een “betekenis” te hebben. De uitkomst dient dus voorspelbaar en begrijpbaar zijn op grond van de methoden en modellen. Men kan dit een laaggespecificeerde taak noemen die gebaseerd is op de data en niet op de afbeelding.

De volgende paragrafen beschrijven in het kort de hoofdstukken van dit proefschrift. Omdat de hoofdstukken als artikelen (zullen) verschijnen, vindt er enige overlapping plaats in de beschrijving van schaalruimte en catastrofe theorie in de “introductie” en “theorie” delen van de verschillende hoofdstukken. Om deze hoofdstukken leesbaar te houden, is hierin geen verandering gebracht.

## Hoofdstuk 2

Hoofdstuk 2 bespreekt meer gedetailleerd het laatste probleem dat hierboven genoemd is, over het verschil tussen discrete data en continue modellen. Dit verschil is wiskundig opgelost door Schwartz’ “Distributie Theorie”. Een fysische benadering, gebaseerd op het “Pi Theorema”, komt neer op het idee om de noodzakelijke parameter *schaal* te introduceren. Of beter: om die te ont-dekken. De punten in een beeld zijn erdoor gerelateerd en kunnen alleen daardoor geïnterpreteerd en gebruikt worden. Onder bepaalde aannames, zoals dat “er niets van het beeld bekend is”, worden er oplossingen gevonden die aan de wiskundige voorwaarden voldoen. Omdat er geen a-priori te prefereren schaal is, kunnen (en moeten) alle mogelijke schalen gebruikt worden. Het beeld wordt daarom uitgebreid met een extra dimensie, schaal, en dit nieuwe beeld vormt een *schaalruimte*.

Een van de eerdergenoemde oplossingen houdt in dat het oorspronkelijke beeld geconvolveerd wordt met een Gaussisch profiel, waarvan de breedte gerelateerd is aan de schaal. Deze schaalruimte heet daarom *Gaussische schaalruimte*. Tegelijkertijd is dit profiel de algemene oplossing van de zogenoemde *Diffusie Vergelijking*, of *Warmte Vergelijking* als schaal wordt opgevat als tijdparameter. Deze vergelijking beschrijft de verspreiding van warmte over tijd als een homogene plaat in het begin op verschillende plekken wordt verwarmd. Zoals men kan voorstellen heeft de plaat aan het einde (als we “oneindig” lang wachten) een constante temperatuur. Hetzelfde geldt voor het schaalruimte beeld: op een “oneindig” grote schaal heeft het beeld een constante waarde. Het vergroten van schaal leidt dus tot vervaging. Een belangrijke eigenschap is lineariteit, waardoor deze schaalruimte een *lineaire schaalruimte* is.

Vanuit het oogpunt van de eindgebruiker die slechts let op de individuele beelden, zal het toepassen van een schaalruimte de hoeveelheid ruis wel verminderen, maar ook alles vervagen, waardoor het onbruikbaar kan worden voor bijvoorbeeld segmentatie taken. Het gebruiken van alle schalen is daarentegen redundant. Daarom wordt ook wel de omgekeerde route genomen: met de diffusie vergelijking als uitgangspunt kan het nut voor beeldanalyse onderzocht worden. Men kan dus ook niet-lineaire versies ervan bestuderen. Taakspecifieke informatie kan gebruikt worden bij het modelleren, waardoor deze aanpak *geometrisch gedreven diffusie* wordt genoemd. Een stap verder is het gebruik van elke partiële differentiaal vergelijking (PDE), hetgeen de oneindige reeks van de PDE-benaderingen oplevert. Zoals al eerder opgemerkt, geldt voor deze benaderingen dat ze met de data “iets doen met een bepaalde bedoeling”.

Naar de lineaire diffusie vergelijking terugkerend, komt de vraag op wat de relevantie met betrekking tot *biologisch modelleren* van (onderdelen van) het visuele systeem is. Het blijkt dat in de eerste momenten van het visuele systeem, als licht in het oog valt en visuele stimuli naar de hersenen getransporteerd worden, zowel Laplaceaanse profielen als vervaging optreedt. Dit geeft de mogelijkheid aan

om een Gaussische schaalruimte te gebruiken als model voor dit stadium van zien. De schaalruimte kan gevisualiseerd worden door een stapel gesimplificeerde versies van het beeld. Gedurende de simplificatie verdwijnen gebieden in een opeenvolgende manier. Theoretisch kan dus een *hiërarchische structuur* worden gevonden: er zijn gebieden binnen gebieden.

Een kort overzicht van enige resultaten van onderzoek van *Gaussische schaalruimte* met betrekking tot beeldanalyse en de intrinsieke eigenschappen van de laatste jaren besluiten dit hoofdstuk. Lezers die reeds bekend zijn met (Gaussische) schaalruimte, kunnen dit hoofdstuk overslaan. In de volgende hoofdstukken veronderstel ik bekendheid met het schaalruimte concept.

### Een Diepe Gedachte over Diepe Structuur

Weten dat schaal belangrijk is en dat het nemen van een enkele schaal niet geschikt is, is één ding. Het bevat nog niet de notie van schaalruimte. De relevantie ligt in het onderzoek van Gaussische schaalruimte *zelf*, dat wil zeggen, alle schalen tegelijk. Dit wordt de *diepe structuur* van Gaussische schaalruimte genoemd. Het is de taak om te onderzoeken – en hopelijk te begrijpen — wat er gebeurt tussen twee verschillende schalen en welke mechanismen optreden als de schaal geleidelijk wordt veranderd. Dat is het onderwerp van dit proefschrift.

Hiervoor beschouw ik het beeld als een hoogtefunctie. Ik beperk mij tot de meest basale eigenschappen van deze functie: de kritieke punten en enige deelverzamelingen van punten met dezelfde waarde. Deze punten geven een adequate beschrijving van een beeld, denk bijvoorbeeld aan een twee dimensionaal beeld met zijn kritieke punten (minima, maxima en zadels) en de isofoten door de zadels. Deze laatste omsluiten gebieden in het beeld.

### Hoofdstuk 3

Op dit punt ontmoet men nog steeds problemen bij het toepassen van wiskundige handelingen (het vinden van kritieke punten) op een discreet raster. In hoofdstuk 3, een kort intermezzo, leg ik de problemen uit die voortkomen uit de keuze voor een *rechthoekig* raster: De horizontale en verticale nabuurrelaties en de uitbereiding ervan naar de dubbele diagonale nabuurrelaties, geven wiskundige en praktische problemen. Een *zeshoekig* raster lost het probleem op. Tevens is het in het menselijk gezichtsvermogen aanwezig. Ik zal dit gebruiken door het rechthoekige raster als zeshoekig te beschouwen.

### Hoofdstuk 4

Nu het mogelijk is kritieke punten te detecteren, is het tijd ze over schaal te *volgen*. Een belangrijk resultaat dat uit het wiskundige gebied van singulariteiten komt, laat zien dat bij vergrotende schaal spatiële kritieke punten allen in paren kunnen verdwijnen (annihilatie). In twee (en hogere) dimensies kunnen zulke paren ook ontstaan (creatie). Als we dus naar een serie vervagende beelden kijken, zien we het aantal kritieke punten veranderen. De locaties in schaalruimte waar deze annihilaties en creaties plaats vinden, worden *catastrofepunten* genoemd. In hoofdstuk 4 wordt de beweging van spatiële kritieke punten onderzocht. In een enkel beeld op een bepaalde schaal liggen kritieke punten in het algemeen “tussen de raster punten” (sub-pixel) en alleen de omliggende punten worden gevonden. Idealiter wordt de beweging gevonden door gebruik te maken van de tangent vector aan het schaalruimte kritieke pad waarover ze bewegen. In het discrete geval kan de beweging worden geschat met behulp van storingsrekening.

Dit levert vectoren in schaalruimte op, die met sub-pixel precisie wijzen naar de locatie van het kritieke punt op een grotere schaal. Wordt ook schaal informatie gebruikt dan kan de locatie preciezer worden berekend. De zaak wordt gecompliceerd als catastrofepunten betrokken zijn. Dan is de formulering die gebruikt wordt voor kritieke punten niet langer geldig en een ingewikkelder expressie is noodzakelijk. Deze wordt dan ook gegeven.

Alle expressies worden gegeven in een willekeurig coördinaten systeem, de *co-variante formulering*. Dit is een belangrijke notie, daar alle theoretische resultaten in zogenoemde *canonieke coördinaten* worden gegeven. Deze coördinaten zijn zo gekozen, dat het stelsel eenvoudig en simpel te beschrijven en te begrijpen is. In de werkelijkheid komt men echter zo een situatie bijna nooit tegen, omdat het coördinaten systeem meestal van te voren vastgesteld is en niet aangepast is aan de lokale configuratie van het beeld. Elke catastrofe is daarentegen wel weer lokaal op zo een eenvoudige wijze te beschrijven. De determinant van de matrix die in de expressie voor het vinden van catastrofepunten voorkomt, is tegelijkertijd een indicator of het catastrofepunt een annihilatie of een creatie is. Experimenten laten zien dat de fractie van de ruimte waar creaties “toegestaan” zijn door het teken van deze determinant, relatief klein is. Dit sluit aan bij de intuïtie dat er meer annihilaties zijn te verwachten dan creaties, omdat op één na alle extrema annihileren. Voorbeelden van de theorie worden gegeven op twee dimensionale beelden.

## Hoofdstuk 5

In hoofdstuk 5 worden deze resultaten gebruikt om kritieke curven in schaalruimte te maken. De spatiale kritieke punten van het beeld worden voor toenemende schaal berekend en aan elkaar gekoppeld, waardoor ze kritieke takken van extrema en zadelpunten vormen. De takken worden in de catastrofepunten aan elkaar gekoppeld, waarmee de kritieke curven worden gevormd. In het schaalruimte beeld zijn catastrofepunten reguliere punten. Ik laat zien dat de enige kritieke punten in schaalruimte *schaalruimte zadelpunten* zijn, welke liggen op de zadeltakken. Als de intensiteit van de kritieke punten over schaal wordt gevolgd, dan dalen maxima monotoon en stijgen minima monotoon. Zadeltakken kunnen daarentegen lokale extrema met betrekking tot de intensiteit hebben. Ik laat zien dat deze lokale extrema plaats vinden in de schaalruimte zadels.

Gebruik makend van het feit dat extrema onderdrukt worden dankzij de diffusie vergelijking, wordt bereikt dat oppervlakken met gelijke intensiteit in schaalruimte een koepelvorm hebben als ze een extremumtak snijden. Als het oppervlak geen zadeltak snijdt, omsluit het een gesloten gebied in schaalruimte, waarbij de top samenvalt met het snijpunt van de extremumtak en het oppervlak. Elke extremumtak snijdt een oppervlak dat een zadel bevat. Dit is ofwel een spatiëel zadel in het oorspronkelijke beeld, of een schaalruimte zadel. Dit *kritieke oppervlak* vormt de grens van een serie van om elkaar vallende gesloten gebieden. Aan alle annihilerende extrema kan zo een kritiek gebied worden toegekend.

Door deze nestende eigenschap van Gaussische schaalruimte volgt een hiërarchische procedure recht toe, rechtaan. De gebieden definiëren een “*pre-segmentatie*” van het oorspronkelijke beeld. Deze speciale segmentatie wordt verkregen zonder enige kennis van het beeld, in tegenstelling tot de gebruikelijke definitie van een willekeurige segmentatie. Het is een “complete” segmentatie in de zin dat alle structurele (topologische) betekenisvolle segmenten betrokken zijn. In de praktijk is het typisch een “oversegmentatie”, omdat het gehele beeld opgedeeld is, terwijl verschillende pre-segmenten typisch tot een “semantisch” segment zullen behoren, bijvoorbeeld een enkel weefsel type in een MR beeld. Gesteld wordt daarentegen – hierin ligt de ware betekenis – dat een pre-segmentatie nooit een “ondersegmentatie” is, omdat het opdelen van een pre-segment niet gerechtvaardigd wordt van de kant van de data.

Natuurlijk kan een ervaren gebruiker met behulp van externe kennis toch een opdeling opleggen.

Merk op dat de pre-segmentatie alleen wordt verkregen doordat een Gaussische schaalruimte volgt uit de noodzakelijkheid van schaal. Ik geef voorbeelden van de beschreven procedure en resultaten.

## Hoofdstuk 6

De eerdergenoemde procedure gebruikt *generieke* catastrofes: gebeurtenissen met precies twee kritieke punten. Soms is het nodig te veronderstellen dat ook *niet-generieke* gebeurtenissen voorkomen, als meerdere kritieke punten samenkomen. Dit is het geval als van drie kritieke punten er één over blijft, maar men is niet in staat het annihilerende paar te identificeren. Soms wil men die identificatie niet maken, bijvoorbeeld als het beeld lokaal symmetrisch is. De uitbereiding van het hiërarchische algoritme dat in staat is om met dit speciale geval om te gaan, wordt gegeven in hoofdstuk 6. Het grote voordeel is dat het de hiërarchische boomstructuur *stabiliseert*. Meerdere symmetrieën – denk aan een schaakbord – kunnen op een soortgelijke manier geïmplementeerd worden.

Ik bespreek tevens de *irrelevantie* van de creatie van kritieke punten met betrekking tot de boomstructuur en de pre-segmentatie. Vanuit het idee van de kritieke curven is dit duidelijk, omdat ze slechts uitstulpingen van de kritieke curve in schaalruimte vormen. Tenslotte laat het modelleren van lokale symmetrie zien dat een *zadeltak* *meerdere* schaalruimte zadels kan bevatten. Omdat het kritieke gebied dat aan een extremum is toegekend, bereikt wordt door het eerste oppervlak dat een zadel bevat, is er slechts één van relevant. In het geval van een minimum betreft het het schaalruimte zadel met de laagste intensiteit, in het geval van een maximum is het degene met de hoogste intensiteit.

Testen laten de toepassing van deze theorie zien.

## Hoofdstuk 7

In de vorige paragraaf noemde ik dat creaties “*slechts uitstulpingen van de kritieke curve in schaalruimte vormen*”. Dit vraagt om een meer gedetailleerde uitleg. Daarvoor wordt een belangrijk resultaat uit “Catastrofe Theorie” gebruikt, namelijk een lijst met polynomen die catastrofes en hun moeilijkheid beschrijft. Dat laatste wordt zichtbaar in het aantal parameters dat nodig is een catastrofepunt te verwijderen. Als schaal wordt opgevat als een parameter, is het duidelijk dat de gebruikelijke catastrofe in schaalruimte één parameter vereist. De catastrofes die in het vorige deel werden genoemd, hebben meerdere parameters nodig, bijvoorbeeld om de lokale symmetrie te verstoren. In hoofdstuk 7 onderzoek ik de lijst en pas die zó aan, dat de polynomen aan de diffusie vergelijking voldoen en dus schaalruimte polynomen worden. De aanpassing van polynomen met meerdere parameters leidt tot één speciale parameter, namelijk schaal. Ik laat zien dat met deze aanpassing *non-generieke gebeurtenissen* in schaalruimte gemodelleerd kunnen worden. Dat houdt niet alleen de meervoudige annihilaties in het geval van symmetrieën in, maar ook een beschrijving van de uitstulpingen van de kritieke curven.

Als de polynomen in de spatiële variabelen en een schaal parameter worden beschouwd, leveren ze een modellering van de kritieke curven zelf. Hier komen twee opmerkelijke zaken aan het licht. Allereerst zijn de uitstulpingen *niet* erg stabiel: een kleine verstoring doet ze geen kwaad, maar een iets grotere verwijdert ze van de kritieke curve. Dit is precies volgens intuïtie – bij het vervagen verdwijnen dingen, dus creaties zijn niet echt te verwachten. Maar wiskundig was ervan al bewezen dat het *lokaal* onjuist was voor kritieke punten. Ten tweede kunnen kritieke curven ook voorkomen als *gesloten lussen*, op een bepaalde schaal gecreëerd en op een grotere schaal geannihileerd. Deze curven zal men compleet



missen als alleen de kritieke curven volgt die in het originele beeld starten. Berekeningen aan beelden laten inderdaad het voorspelde gedrag voor de kritieke curven zien.

## Hoofdstuk 8

Het is nu tijd om terug te keren naar de hiërarchische structuur. In hoofdstuk 5 beschrijf ik de aanwezigheid van koepels in het schaalruimte beeld, maar er is meer over te zeggen. Zoals al genoemd omvatten de kritieke oppervlakken een hele reeks oppervlakken en bevatten ze een zadel, soms een schaalruimte zadel, soms een spatiëel zadel – in dat geval in het originele beeld. In hoofdstuk 8 onderzoek ik het andere deel van het oppervlak dat door het zadel gaat. Dit komt er eenvoudigweg op neer de structuur van de *oppervlakken met gelijke intensiteit* in schaalruimte en hun “uienschil”-structuur te onderzoeken. In een gewoon twee dimensionaal beeld zijn de isofoten genest, cirkelen rondom een extremum en snijden zichzelf in zadelpunten. Een curve door een zadel bevat dus twee delen. Voor schaalruimte beelden geldt iets soortgelijks. Een deel is reeds bekend, namelijk de kritieke koepel. De prangende vraag is wat voor informatie er in het *andere* deel bevat is.

Ik onderzoek het gedrag van de oppervlakken en laat zien dat als het andere deel van het oppervlak dat de kritieke koepel bevat, wordt meegenomen, op een elegante manier een eenduidige, op intensiteit gebaseerde schaalruimte hiërarchie wordt verkregen, die degene genoemd in hoofdstuk 5 omvat, maar veel *robuuster* is. De hiërarchie kan gevisualiseerd worden door een binaire boomstructuur, een structuur waarin elke knoop een ouder en twee kinderen heeft. Een van de kinderen is de koepel uit hoofdstuk 5, het andere kind is equivalent aan de ouder. Ze kan zelfs gereduceerd worden tot een verzameling van in elkaar vallende onderdelen, waarin elke knoop wordt gerepresenteerd door een paar haken. Binnen de haken staan de kinderen en de haken worden gelabeld met het kind dat de koepel bevat. Dit stelt men tegelijkertijd in staat een “*logisch filter*” te gebruiken: Kinderen in de boomstructuur die minder significant zijn, kunnen weggeveegd worden door de kleine takken te snoeien. En vanaf de andere kant bekeken: de meest significante schaalruimte delen zijn de sterkste, dikste (of grootste) takken. Men verkrijgt dus een structuur van het schaalruimte beeld dat impliciet aanwezig is, maar nog wel eruit gehaald moest worden.

## Conclusie

Dit brengt ons bij het einde van het proefschrift. De belangrijkste bijdrage is dat het het onderzoek van de diepe structuur van Gaussische schaalruimte start. In de verschillende hoofdstukken geeft het nieuwe inzichten in het gedrag van spatiële kritieke punten onder de invloed van de schaal parameter, hetgeen kritieke curven met niet alleen generieke catastrofepunten, maar ook schaalruimte zadelpunten oplevert. Het modelleren van niet-generieke catastrofes geeft inzicht in de structuur van kritieke curven, zoals de aanwezigheid van kritieke curven die gesloten lussen vormen.

Een ander nieuw inzicht ligt in de oppervlakken met gelijke intensiteit in schaal ruimte. Een geschikte selectie ervan, gedeeltelijk gebaseerd op die door de schaalruimte zadels, delen het schaalruimte beeld – en dus het originele beeld – uniek in “gebieden van invloed”, geregeld door de extrema. Men krijgt dus gratis een hiërarchie van het beeld en de mogelijkheid tot een onvoorwaardelijke “pre-segmentatie”.

Verder zijn ook onvoorwaardelijke beeldanalyse taken mogelijk, zoals registratie, codering, compressie, clusteren, vereenvoudiging, transmissie en vergelijking – om er enige te noemen. Het sleutel

woord in al deze toepassingen is *onvoorwaardelijk*. De toepassingen volgen eenvoudigweg uit het feit dat een unieke gedefiniëerde hiërarchie beschikbaar is.

Dit is *volslagen verschillend* van elke gebruikergedefinieerde taak, hetgeen meestal het geval is. De hiërarchie is (impliciet) reeds aanwezig in *de diepe structuur van Gaussische schaalruimte beelden*.

---

## Dankwoord

---

Na zo'n vier jaar onderzoek is het goed om ook eens terug te kijken naar alles wat er gepasseerd is. Bijna automatisch komt er een lange reeks van namen naar boven die op een of andere manier geliëerd is aan de totstandkoming van dit proefschrift. Daarbij allereerst mijn dank aan u, lezer, voor de moeite dit proefschrift open te slaan en ten minste dit gedeelte te lezen. Ik hoop dat u ook de rest de moeite van het lezen waard vindt, en dat u tenminste een idee hebt gekregen van de dingen waarmee ik mij de afgelopen jaren heb bezig gehouden.

Er zijn een aantal mensen die ik bijzonder dankbaar ben. Mensen die mij geholpen hebben dit proefschrift in deze vorm gestalte te geven.

Allereerst natuurlijk mijn promotor, Prof. Max Viergever, die mij het vertrouwen gaf lekker aan de gang te gaan. Maar tegelijkertijd hield je het globale overzicht goed in het oog als ik me te eenzijdig in de details wilde verdiepen, en hielp je me de richting van artikelen en dit proefschrift in de gaten te houden.

Mijn copromotor Luc Florack is essentieel geweest voor mijn gedachtevorming. Alle inhoudelijke discussies en brainstorm sessies waren bijzonder vruchtbaar – hoewel dat soms pas wat later bleek – en tegelijkertijd af te toe bijzonder vermoeiend. Toen ik na vier jaar mijn projectomschrijving onder ogen kreeg, bleek die precies te voldoen aan hetgeen er uiteindelijk uit kwam. Daarnaast heb ik je nogal eens “gebruikt” als corrector Engels: elke stukje tekst dat ik gegenereerd had, werd uitgebreid “gescrutinized”. Aangezien vooral het laatste jaar een enorme stapel artikelen uit de printer vloeide, was dat hard werken.

De “M.” van Prof. Bart M. ter Haar Romeny staat vast voor Mathematica. Bart, voor de uitwerking van de theorie maakte ik dankbaar gebruik van je inzichten in Mathematica, hetgeen (veel) snelle codes opleverde. Daarnaast leidde je de inspirerende TGV-bijeenkomsten. Het laatste jaar misschien uit eigenbelang, omdat we mooi je boek konden bespreken. Het gevolg was wel dat daardoor jouw boek (wat) dikker, en het onderwerp van mijn proefschrift inzichtelijker werd. Daarnaast dank ik je voor het willen plaatsnemen in de leescommissie.

Prof. Mark Overmars, dank je voor het lezen van dit proefschrift. Je nam een niet-geometrische AiO in je groep op. Gelukkig is dat tegenwoordig niet meer zo'n vreemde situatie en heeft beeldanalyse de laatste 4 jaar een duidelijker plaats binnen het instituut gekregen. Het zou me echter wel veel plezier

doen iets van het fundamentele beeldonderzoek terug te vinden op de GIVE-webpagina's.

Prof. Dirk Siersma dank ik eveneens voor het lezen van dit werk. Daarnaast heb ik veel geleerd van inhoudelijke gesprekken over het onderzoek, specifiek met betrekking tot de singulariteiten. Daarnaast dank ik je voor het meedenken over de patenteerbare mogelijkheden ervan.

I thank Prof. Joachim Weickert for his effort to read this thesis, as well as for his comments and recommendations with respect to chapters of this thesis in an early stage. With pleasure I could use your book and the various Japanese papers – fortunately with their translations!

I also thank Prof. Peter Johansen for taking time to read this thesis. Your research on one dimensional scale space images has been an inspiration for my research. Your (board) contribution to the scale space community in Denmark has also given a boost in scale space literature.

That gives me the opportunity for thanking the 'scale space' people in Denmark at DIKU and IT-C, especially Ole Fogh Olsen en Mads Nielsen. We had inspiring conversations in Utrecht, Copenhagen, and on Corfu.

Jim Damon gave me lots of new insights in the possible applications of catastrophe theory in scale space, due to his articles, course, and the discussions we had on genericity as well as modelling non-generic events.

Jan Koenderink heeft min of meer aan de wieg gestaan van de Utrechtse scale space groep door de "ont-dekking" van scale space. Door het eenvoudigweg voorstellen om de diepe structuur te onderzoeken was de weg voor dit proefschrift gebaad. Kortom: zonder jou was dit proefschrift er niet geweest.

Het voordeel van promovendus-zijn is dat je vooral geen eigen kamer krijgt, maar lekker gezellig met zoveel mensen op een kamer wordt gestouwd. Het heeft een leuke tijd opgeleverd met een aantal (ex-)kamerogenoten. Steven van Dijk gaf de nuttige en nodige L<sup>A</sup>T<sub>E</sub>X en computer hints en tips. De discussies over degeneraties [223], zij het in een andere context dan in dit proefschrift, waren me bijzonder aangenaam. Door Tycho Strijk heb ik geleerd om aan het volume van mijn muziek te denken. Marleen de Bruijne zat even voor me en was toen plotseling overal en nergens in het AZU. Gelukkig bevalt het je daar goed! Zeger Knops was eindelijk een aan het ISI verbonden kamergenoot met de nodige nuttige kennis over Windows, XP, netserver, Napster-klonen, AVI, DivX en wat dies meer zij. Toen Arend de Grootte eenmaal op A221 zat, was hij alweer bijna weg. Gelukkig scheen het niet aan je kamergenoten gelegen te hebben. Grigore Ovidiu zorgde voor de nodige reflectie over alle dingen waarin wij Nederlanders eigenlijk wel raar zijn.

Vaak interessant en boeiend waren de gesprekken binnen het ISI, al dan niet binnen overlegclubjes met obscure namens zoals RSV, IP, TGV en BVD, met mede (sommige inmiddels ex-) promovendi Joes, Wiro, Bram, Ingrid, Marco, Marleen (weer!), Miriam, Kees, en allen die er nog meer rondlopen. De mede-promovendi en staf binnen Informatica hebben mij verbazingwekkend genoeg willen aanhoren op colloquia. De gesprekken – al dan niet met taart – in de koffiekamer waren eveneens waardevol, zij het niet zozeer op het gebied van mijn onderzoek. Veel dank ben ik verschuldigd aan mensen op het secretariaat voor het regelen van allerlei voor mij te moeilijke zaken, in de bibliotheek voor het regelen van vage artikelen en al dan niet vakinhoudelijke boeken, en van systeembeheer voor het beantwoorden van allerlei bijna triviale vragen, het oplossen van fouten mijnerzijds en backuppen van bestanden.

Op een gegeven moment was er sprake van een deel van het onderzoek te patenteren. Hoewel het, toen het puntje bij het paaltje kwam, toch niet door kon gaan om een mij nog steeds duistere reden, was het een enerverende belevenis en toch leuk om meegemaakt te hebben. Ik wil dan ook iedereen bedanken die zich heeft inzet om mij te helpen op dit voor mij toen onbekende octrooi-pad.

Mijn voorkeur voor de wiskundige kant van beeldanalyse stamt uit 1995, toen Prof. Brenny van

Groesen en Frits van Beckum in Enschede, en Jurrien Bijhold in Rijswijk mijn ogen openden voor dit prachtige toepassingsgebied van de wiskunde.

Mijn ex-collega's van ELTRA, Rob Elverding, Hans Versteegt en Thea Wienholts hebben gezorgd voor een geweldige sfeer in een fantastisch bedrijf. Ik heb er veel geleerd en voel me nog steeds een beetje verbonden met het hele circus rondom het automatisch verwerken van parkeerbonnen. Als ik "ze" rond zie lopen om foutparkeerders te bekeuren met zo'n computer, dan denk ik nog steeds in termen van "mijn computer". Dat zegt genoeg over het plezier dat we samen gehad hebben.

Het schrijven van een proefschrift en het doen van onderzoek is wetenschappelijk vorming. Tegelijkertijd is het ook een stuk persoonlijke en maatschappelijke ontwikkeling. Daarvoor wil ik alle vrienden in mijn persoonlijke omgeving en de kerkelijke gemeente van Ede bedanken. Ik zou vele namen kunnen noemen. Veel dank ben ik verschuldigd aan Margreet, Christianne en Miranda, die mij op velerlei wijzen verdiepte levenswijsheid gegeven hebben.

Uit m'n Enschedeese (stad in Twente met 16 letters) RSK<sup>3</sup> tijd wil ik speciaal Wilhelm en Jannie & Martijn bedanken voor alle goede momenten en zinvolle gesprekken.

Natuurlijk dank ik ook mijn familie en schoonfamilie. Bijvoorbeeld voor alle ondersteuning en begrip en vooral geduld als ik weer eens probeerde uit te leggen wat ik nou precies aan het doen was. Al snel werd dat "wat ik ongeveer aan het doen was", en uiteindelijk "wat je zou kunnen doen met wat ik aan het doen was". Ik hoop dat ik jullie overtuigd heb dat ik hiermee echt niet alleen wiskundeleraar kan worden.

Ik wil Helma, mijn zus, bedanken voor het -onbewust- aandragen van het idee voor de voorkant van het proefschrift. Dat de appel niet ver van de boom valt, blijkt uit onze gezamenlijke interesse in ruimtelijke topologie, zij het dat jouw specialiteit meer aan de artistieke visualisatiekant ligt, terwijl die van mij meer theoretisch is!

Veel dank ben ik verschuldigd aan mijn ouders, die mij in liefde hebben grootgebracht en mij gesteund hebben in mijn keuzes. Nou lagen die voor de hand en erg vervelend waren ze niet, maar jullie gaven mij wel alle ruimte om mijn eigen weg te zoeken en te gaan. Ik weet dat jullie nu trots zijn. Ik hoop wel dat het gepaste trots is. Dit boekje is een mijlpaal, maar daarvan zijn er zoveel. Ik heb slechts de mij gegeven talenten mogen ontwikkelen.

Van alle mensen die ik dankbaar ben, neemt Alieke de belangrijkste plaats in. Het was moeilijk voor je toen ik toch nog, na twee jaar "gewoon werk" AiO werd. Een halvering van het salaris, weg van vaste baan en op naar een onzekere toekomst. Het angstbeeld van promovendi in onze vriendenkring die op de meest onmogelijke tijden aan hun onderzoek werkten, stond je helder voor ogen. De ruime mate van vrijheid in tijd- en locatieplanning ("zal ik vandaag thuis of in Utrecht werken?") bleek gelukkig zeer aangenaam te zijn.

Het laatste jaar werd opgevrolijkt door onze zoon Micha. Op een of andere manier wist (weet) je nachtelijke escapades en verplichte verschoningen te vergezellen van bijzonder veel plezier. 's Nachts hoofdzakelijk vaak van jouw kant, trouwens. Je was tegelijkertijd de grote aanjager voor mijn schrijf-tijd. Misschien voelde ik ineens de verantwoordelijkheid op m'n schouders drukken. Wie zal het zeggen...

Tenslotte. Het schrijven van een proefschrift is slechts het neerleggen van een periode van specialisatie van je werk. Zo bezien is het weinig bijzonder. Op een moment van terugkijken verbaast het mij desalniettemin dat het met mij zover gekomen is. Ik kan, en wil, daarom niet anders dan mijn hemelse Vader danken met geheel mijn hart, geheel mijn ziel en geheel mijn verstand.

---

<sup>3</sup>voor je leven!



---

## Curriculum Vitae

---

Arjan Kuijper werd op 23 december 1970 in Alkmaar geboren. Hij bracht zijn middelbare schooltijd door op de Christelijke Scholengemeenschap Jan Arentsz te Alkmaar en behaalde daar in 1989 het VWO diploma.

Vervolgens begon hij met de studie Toegepaste Wiskunde aan de Universiteit Twente. Naast allerlei nevenactiviteiten gelukte het hem in 1994 een stage te doen aan de Åbo Akademi in Turku, Finland. Hij verrichte in 1995 zijn afstudeeronderzoek binnen de afstudeerrichting Toegepaste Analyse met als specialisatie Dynamische Systemen. Het onderzoek vond plaats aan het Gerechtelijk Laboratorium van het Ministerie van Justitie, dat tegenwoordig Nederlands Forensisch Instituut wordt genoemd. Het onderzoek betrof een analytische en praktische vergelijking van twee beeldbewerkingmethoden die gebruikt kunnen worden door het Laboratorium in gerechtelijk onderzoek.

Na zijn afstuderen begon hij – eerst op uitzendbasis, maar al snel op vaste basis – als systeemanalist bij ELTRA Parkeergroep, een bedrijf dat marktleider was en is op het gebied van de geautomatiseerde parkeercontrole. Daarvoor levert het handcomputers, onderhoudt ze en biedt bijbehorende software aan. Al snel droeg hij zorg voor alle software en gaf daarnaast instructie en (on-line) hulp.

Aangezien de wetenschap bleef roepen, keerde hij in oktober 1997 terug naar de universiteit. In Utrecht werd hij Assistent in Opleiding aan de faculteit Wiskunde en Informatica. Hoewel gestationeerd binnen het Informatica Instituut (tegenwoordig: Instituut voor Informatica en Informatiekunde), was hij tevens betrokken bij het Image Sciences Institute en de onderzoeksschool ImagO binnen het Academisch Ziekenhuis Utrecht, dat ook al een nieuwe naam heeft gekregen, namelijk Universitair Medisch Centrum Utrecht. Het onderzoek vond wederom plaats op het gebied van de beeldanalyse. De resultaten zijn beschreven in dit proefschrift.

Aansluitend werd hij post-doc op het project “Coreregistratie van 3D beelden”, eveneens aan het Instituut voor Informatica en Informatiekunde van de Universiteit Utrecht.

Arjan Kuijper is getrouwd met Alieke Schulenburg. Ze hebben sinds 8 juli 2001 een zoon, Micha.

